PHD

The effect of transient overloads on the stress-rupture of glass fibre reinforced polymers

Rawles, J. D.

Award date:
1990

Awarding institution:
University of Bath

The Effect of Transient Overloads on the Stress-rupture of Glass Fibre Reinforced Polymers.

submitted by J.D.Rawles

for the degree of Ph.D.

of the University of Bath.

1990

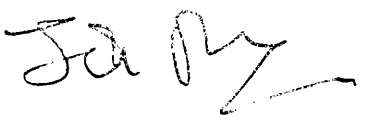

ProQuest LLC
789 East Eisenhower Parkway
P.O. Box 1346
Ann Arbor, MI 48106-1346

Abstract.

Power station cooling water (CW) system components may be subject to water hammer events during their thirty year service life. The immediate and long term effects of such events on glass fibre reinforced polymer (GFRP) structures were hitherto unknown. This study investigates these effects and considers how well design codes address the problem of water hammer.

A sequence of model water hammer events were applied to coupons of glass reinforced polyester and vinyl ester laminates ("overloaded" coupons). Damage studies revealed transverse resin cracking but no fibre fractures. The effect of stress/time profile on damage was investigated. CW systems operating from a constant head reservoir were modelled by stress-rupture tests in an aqueous environment at 40°C. Stress-rupture lifetime of overloaded coupons was found to be reduced in comparison to virgin coupons. CW systems operating from a coastal reservoir were simulated by applying a sinusoidal load regime, with an R-ratio of 0.67, at a frequency of 23.15μHz, to overloaded coupons in an aqueous environment at 40°C. The results were then compared with those from the stress-rupture tests.

Genuine water hammer events were also applied to a model component. Glass reinforced polyester pipes of 151mm diameter were subjected to ten water hammer events of the type occurring in a CW system ("overloaded" pipes). Axial cracking resulted. Stress-rupture testing was carried out on virgin and overloaded pipes in an aqueous environment at 40°C. The lifetime of overloaded pipes was reduced in comparison to virgin pipes. This was attributed to enhanced stress-corrosion cracking at sites of water hammer induced cracking.

Stress-rupture results for material tested in pipe and coupon form were compared. At a given stress level, longer lifetimes were exhibited by pipe material. This indicated that designing from coupon data might lead to costly over-design.

Design codes were then reviewed in the light of the above experimental results.

Acknowledgements.

The author is indebted to Mr M.G. Phillips of Bath University School of Materials Science for his advice, support and supervision throughout the project. Thanks, also, to Dr. R.C. Wyatt (CEGB-Powergen) and Dr. J.A. Roscow (Nuclear Electric plc) for their supervision and encouragement. The financial support of the SERC and the CEGB is gratefully acknowledged.

CONTENTS.

CHAPTER 5.
Damage development and failure in polyester/glass composites.

CHAPTER 6.
Summary of published work and plan of the investigation.

PART 2.

COUPON TESTING PROGRAMME.

CHAPTER 7.
Materials and testing.

CHAPTER 8.
Results.

CHAPTER 9.
Discussion of results.

PART 3.

PIPE TESTING PROGRAMME.

CHAPTER 10.
Experimental.

PREFACE.

Objectives and scope of project.

Glass fibre reinforced polymer materials are employed in electricity generating power station cooling water (CW) systems. They provide "safe-life" components in aqueous environments where metallic structures require financially costly replacement and repair due to corrosion damage. At present Central Electricity Generating Board (CEGB) stuctures are designed in accordance with BS 4994, British Standard Specification for "Design and construction of vessels and tanks in reinforced plastics"[1]. The complex load profile of a CW system is not adequately considered in this code and may result in either inefficient, and therefore costly, or unsafe design. Both such scenarios detract from the otherwise very attractive concept of a maintenance free component with a safe-life of thirty years and have slowed the advance in the use of glass fibre reinforced polymers (GFRP) in industrial applications. In an attempt to improve the efficiency, safety and economic attraction of the design of GFRP, the CEGB have commissioned several research programmes to investigate the long term behaviour of GFRP, specifically under CW system service conditions. Previous studies based on coupon type test pieces have considered service loads due to constant pressure, tidal variations in water pressure and plant outages for maintenance.

The work reported in this thesis had three broad objectives.

(1) To study the effects of transient overloads.

(2) To compare real and simulated transient overloads.

(3) To compare coupon and component behaviour in accelerated tests.

All objectives were approached with a view to improving the quality of design information.

CHAPTER 1

1.0 Introduction: GFRP in power station cooling water plant.

Electricity generating stations require vast quantities of water for the operation of their cooling systems. As a result power stations are frequently situated in coastal locations facilitating the use of sea water as the coolant. The material used in the construction of the piping system is therefore subject to an aggressive environment of sea water at up to 40°C internally, in addition to sea spray and saline rain externally.

Conventionally, pipework, waterboxes and other peripheral structures have been fabricated in cast iron or mild steel. Corrosion is a major problem with direct maintenance or replacement of corroded structures proving costly over the thirty year lifetime of the plant. Corrosion products can also be a problem, causing fouling of the condenser tubes for example. Clearly a more corrosion resistant material is desirable and GFRP is an obvious candidate.

The Central Electricity Generating Board (CEGB) has been experimenting with GFRP structures in cooling water systems since 1958[2]. Early successes include an expansion bellows installed in 1964 at Poole power station, with three similar structures presently providing problem free service. A

condenser return-end waterbox also provided satisfactory service at Portsmouth power station from 1966 to 1977.

Some problems have been encountered however. A return end water box fabricated for installation at East Yelland power station in 1958 split during early trials. This was due to incorrect design with the GFRP structure closely ressembling its cast iron predecessor, despite the vast difference in the Youngs modulus of the two materials. Amendments to the design, more suitable to the mechanical properties of GFRP, resulted in a structure providing over 20 years of satisfactory service. Another design inadequacy was highlighted by a GFRP condenser door failure at Pembroke power station. In this instance the sudden closure of a failing cast iron valve resulted in a "water hammer" pressure pulse which ruptured the GFRP door. Subsequent analysis revealed "under design" of the door. Improved design of the door suggested that a structure of identical weight but six times stronger than the failed door was feasible.

The brief examples cited above demonstrate that GFRP can be successfully employed in the cooling water system under consideration. The failures experienced do however illustrate that structural design needs to cater specifically for the mechanical properties of GFRP, and that precise operating loads need to be considered. In one

example described above a failure resulted from a water hammer pulse, an event which may occur several times during the lifetime of a power station cooling water system. Water hammer pulses do not always result in component failure and it is the objective of this thesis to determine the effect of sub-critical water hammer events upon the long term mechanical properties of GFRP thus aiding the safe, efficient and economical design of cooling water systems fabricated in GFRP.

1.1 Service conditions of cooling water system pipes and structures.

In a coastal power station the cooling water system components are subjected to three types of load, static, sinusoidal, and transient. Plant outages also result in an unload cycle when the entire system is depressurised for maintenance. The so-called static load is associated with the hydrostatic pressure of the liquid coolant which results in a hoop stress in the pipe wall. The material from which the pipe is fabricated is therefore subject to a tensile stress related to the pressure of the fluid it contains.

At coastal power stations coolant (sea water) pressure also varies sinusoidally due to fluctuations in the height of the tide. The maximum pressure, corresponding to high tide, is experienced twice a day and consequently the pipe wall is subjected to a low frequency sinusoidal load superimposed on

the existing static load. The fluctuation in load due to this tidal effect is equivalent to ±20% of the static load. This could be considered to be a sinusoidal load variation, with an R ratio of 0.67, at a frequency of 23.15μHz.

Sudden overloads, or transients as they are more commonly known are the third component of the loading profile. The cause, nature and magnitude of such overloads vary and the entire phenomenon is discussed in chapter 4.

Apart from the load profile other important service conditions include environment, specifically sea or river water at temperatures varying from ambient coastal to 40°C after performing its cooling function, and component design lifetime of 30 years.

1.2 Outline of the investigation.

The principal aims of the project were to;

(1) model a transient overload of the type occurring in service in power station CW systems and apply it to coupon type test pieces fabricated from material modelling that found in service.

(2) determine the immediate effect of this overload on the material by; (i) damage investigation and, (ii) investigation of residual short term mechanical properties such as ultimate tensile strength and elastic modulus.

(3) determine the the long term effect of overload events on material behaviour by testing previously overloaded coupons to failure under constant load (stress-rupture).

(4) apply a load regime simulating the variation in water pressure due to tidal variations to overloaded coupons, thereby elucidating any long term effect peculiar to low frequency cyclic fatigue load regimes.

(5) design and fabricate a model of a real structure (a pipe) found in service in a CW system from material similar to that presently in service.

(6) determine the time to failure of pipes designed in (5) over a range of constant internal pressures (stress-rupture).

(7) apply "real" hydromechanical water hammer events simulating CW system service transient overloads to the pipes fabricated in (5).

(8) determine the long term effect of the water hammer event (overload) described in (7) by stress-rupture tests on overloaded pipes and comparing the times to failure of these with the virgin pipes tested in (6).

(9) compare the simulated overload event applied to coupon test pieces with the genuine water hammer thus considering whether the model event reflects a genuine event, and if such models are useful in accumulating design data.

(10) compare virgin coupon stress-rupture results from previous work with the stress-rupture tests on virgin pipes fabricated from identical material to obtain an indication

of the relevance of coupon tests to the design and behaviour of real structures.
(11) discuss the various design codes in the light of the findings from (8) and (10).

1.3 Organisation of thesis.

Although the pipe and coupon testing programmes could stand alone as separate lines of research, both programmes follow very similar themes, use almost identical materials, and have much common terminology. It is also a major aim for the two programmes to be complementary and provide comparisons. To accommodate the multiple aims of the project this thesis is separated into four parts reporting coupon experimentation in Part 2, pipe testing in Part 3 and finally comparing the two in part 4. The general composition is as follows;

Part 1 is a critical review of existing design codes and the previous research upon which design codes are loosely based. Experimental results related to the load profile and conditions in a CW system covering stress-rupture, cyclic fatigue, multiaxial stress systems and environmental factors are reported and discussed. The phenomenon of transient overloads and the limited amount of experimental information which may give some idea of their effect on GFRP is then discussed. Mechanisms of failure and modes of damage development in GFRP are presented in chapter 5. Finally the

status of published research is summarised and the plan of the experimentation briefly outlined.

Part 2 is devoted to the coupon testing programme describing fabrication, overload model development, mechanical testing and damage investigation. The results are discussed in isolation from the pipe testing as many comparisons can be made, and conclusions drawn, without the added complication of considering the pipe testing programme.

Part 3 concentrates on the pipe testing work alone. This allows a clear account of design, overload application and the stress-rupture programme.

In Part 4 the two main components of the experimental programme, coupon and pipe tests, are brought together. In both cases similar load regimes are applied to almost identical materials. The results are compared and the relevance of coupon testing to the behaviour of real structures is discussed. Finally the implications for design and the significance of design codes are considered.

PART 1

REVIEW OF PREVIOUS WORK

CHAPTER 2

Design codes and their experimental basis.

2.0 Design guidelines for GFRP pressure vessels.

At present the design code applicable to the structures required in a CW system is specified by British Standard BS 4994. This standard dictates the design and construction of vessels and tanks in reinforced plastics incorporating the effects of load profile, environment, time under load and method of manufacture in one design factor, K as determined by equation 1. Dividing the ultimate tensile unit strength (UTUS) of a laminate by K gives the permitted load per unit width, per unit mass of reinforcement.

$$K = 3 \times k_1 \times k_2 \times k_3 \times k_4 \times k_5 \quad \text{(EQUATION 1)}.$$

The multiple of three is designated to allow for the reduction in material strength caused by long term loading. Each of the sub-factors also has a specific designation;

k_1 relates to manufacturing method (1.5 for hand lay-up).

k_2 accounts for the chemical nature of the environment (2.0).

k_3 relates to temperature (1.0).

k_4 relates to cyclic loading (1.4).

k_5 relates to the curing procedure (1.1)

The figures in brackets give the values prescribed by BS 4994 for each of the sub-factors appropriate to the operating conditions experienced in a power station CW system. Applying equation 1 results in a design factor of 13.86 for coastal CW systems and 9.9 for systems with a constant pressure reservoir.

The design criteria outlined in BS 4994 are subject to several criticisms;

(i) The factor for cyclic loading, k_4, is determined from a graph of factor, k_4, as a function of number of cycles. The frequency at which tests were carried out in the compilation of this data is not given, but will almost certainly be higher than the 2 cycles per day resulting from tidal forces. The applicability of data obtained at high frequencies to a situation at lower frequencies is questionable.

(ii) The standard also takes no account of any interaction between a static load and a superimposed cyclic load.

(iii) The factor k_2 relates to the loss in strength of an unstressed GFRP laminate when exposed to the operating conditions for the design lifetime of the component. Neither aqueous or saline environments are considered specifically and the standard requires the designer to have knowledge of material performance over the component lifetime in order to calculate the sub-factor.

(iv) Sudden overloads are not considered. The only method of accounting for such events would be to consider the overload magnitude as a design stress leading to vastly inefficient and uneconomic component design and manufacture.

Evidently BS 4994 does not address the specific design needs of the operating conditions of a power station CW system. Although the K factor calculated from BS 4994 appears large and conservative, the criticisms highlighted above indicate that design may be incorrect, leading to component failure prior to its design life.

The comparable American Society for Testing and Materials (ASTM) standard, entitled "Obtaining hydrostatic design basis for reinforced thermosetting resin pipe and fittings"[3], approaches design on a far more experimental

basis. Separate procedures are outlined to design for both cyclic and constant internal pressures with references to other standards for specific test methods. A minimum of 18 pipes are tested at various hoop stress levels and a linear regression of $\log_{10}$ hoop stress versus $\log_{10}$ time to failure established. Extrapolation of this line to 100,000 hours (11.41 years) defines the "long-term hydrostatic strength", a parameter which presumably provides some comparison between materials.

The standard has some merits when compared with BS 4994, namely;

(i) There is a clear experimental basis to design for cyclic and constant internal pressures.

(ii) Design can be based upon experiments on the exact material and temperature of the service component.

(iii) Clear test procedures are defined.

However, defining the "long-term hydrostatic strength" is meaningless and leaves the designer with no other option than to extrapolate to the service life of the component and apply an "ad-hoc" safety factor. No justification of the use of a log/log plot is given although much published data are commonly plotted on log/linear axes. The acceptable minimum duration and range of tests is defined as "over two or more logarithmic decades of time (hours)" which allows design in accordance with the code based upon experimentation with a duration of less than 1000 hours. Considering stresses, and

not unit loads, is also inapropriate when dealing with composite materials as the amount of reinforcement may be more important than the laminate thickness. In common with the British standard no provision is made for transient overloads in the design methodology.

Applying either standard to CW system components is difficult and in response to this an extensive design code has been compiled by the CEGB[4]. The code is based upon CEGB experience and various British standards, but particularly BS 4994. The design factor, K is calculated in accordance with BS 4994 and experimental data is presented demonstrating the K factor to be conservative in comparison to extrapolated stress-rupture data from tests on coupon type test pieces. Unlike BS 4994 or ASTM D-2992 the code does address the possible effect of transient overloads. The conclusion was drawn that such load events would have an insignificant effect on component behaviour. The basis for this assertion was four-fold;

(i) Transient overloads are very rapid loading rate events and considerable experimental evidence (see section 4.3) exists demonstrating that the ultimate strength of GFRP are enhanced at high rates of load application.

(ii) The time at the enhanced (overload) load will be very small in comparison to the component design life and hence will result in an insignificant overall lifetime reduction.

(iii) Significant damage resulting from transient overloads is often a consequence of reflected stress waves. GFRP materials attenuate acoustic (stress) waves more rapidly than steel, thereby reducing damage.
(iv) GFRP have a low elastic modulus in comparison to steel and hence have a greater capacity to absorb elastic energy.

Points (i) and (ii) rely on the assumption that sub-critical loads will be basically insignificant. No consideration is given to the damage state following such a load event, or the subsequent interaction of any damage with the environment.

Although points (iii) and (iv) are valid suggesting that GFRP will sustain less impact damage than steel no assessment of post-overload performance is given.

The criticisms highlighted above demonstrate that safe and efficient design require experimental data directly applicable to the unit and service conditions under consideration. The comparison between experimental data and the design factor calculted from BS 4994 reported in the CEGB code suggests that BS 4994 provides a safe design basis for CW system components providing no transient overloads occur. Clearly transient overloads still require experimental investigation.

Although the design codes discussed above are open to criticism, there is considerable research upon which they were based. In this chapter studies relevant to the effect of the environment and constant load conditions are considered, demonstrating some of the difficulties faced in evolving a design code for the long term service of GFRP in an aqueous environment.

2.1 Effect of aqueous environments on GFRP.

In CEGB applications GFRP are subject to aqueous environments and simultaneous stress. Much published information is available in this field with some authors concerned with qualitative damage assessment, others with short term mechanical property degradation, and some purely with stress-rupture. In an attempt to separate the lines of research carried out the effect of an aqueous environment is first considered followed by the effects of combining this with an applied stress. These are then drawn together and the overall effect on short term mechanical properties assessed. The wealth of stress-rupture studies are then discussed separately.

2.2 Aqueous environment without an applied stress.

Degradation of glass fibre reinforced polymers in aqueous environments has been widely recognised for some time. The mechanism of degradation may involve fibres, matrix materials and the fibre-matrix interface. Glass fibres are

themselves very sensitive to moisture. It has been demonstrated that tensile strength decreases with both increasing humidity and time of exposure to a humid environment[5].

The scale of effect of any environment on the reinforcement depends upon the effectiveness of the barrier provided by the gel coat (if it exists), the matrix and any surface treatment to which the fibre has been subjected. Polymeric materials however, do not prevent water diffusing through to the reinforcing fibres and are also subject to degradation in an aqueous environment. This degradation can be physical in form, manifesting itself as cracks or result from chemical breakdown. In polyester resins the most widely reported chemically degradative processes are the hydrolytic scission of the ester groups, and the dissolution of low molecular weight components of the resin, commonly known as leaching.

Cracks were observed by Ashbee, Frank and Wyatt[6] in cast polyester resin samples following immersion in hot distilled water. The disc shaped cracks resulted merely from the hot, aqueous environment with no external force applied. Following an elegant set of experiments Ashby et al. demonstrated that the most likely explanation of the pressure causing the cracks was an osmotic effect and hence such cracking is sometimes known as osmotic cracking.

Despite a reasonable understanding of the individual physical and chemical processes occurring little idea has so far been presented upon their mutual interaction or relative importance. This has been investigated in recent years by Abeysinghe, Edwards, Pritchard and Swampillai[7]. They concluded that the degradation of cast polyester resins begins with water uptake and is followed by swelling and the leaching of non chemically bound substances. Hydrolysis will be occurring at this stage and is greatly promoted by the osmotically induced cracks which provide new surfaces for the hydrolysis reaction. Abeysinghe et al. demonstrated this by chemical analysis of residues retrieved from the crack surfaces which proved to be products of the hydrolysis reaction.

In composites such as E-glass polyester similar damage to that described above for cast resins has also been witnessed. Ashbee and Wyatt[8] continued their work on cast resins with a study of polyester reinforced with randomly oriented uncoated chopped glass fibres. As with their previous study specimens were immersed in water at various temperatures with no external stress applied. At 20°C interfacial failure between fibre and resin (debonding) initiated after about 20 minutes, with the fibre becoming totally debonded from the encapsulating polymer after

approximately 1.75 hours. At higher temperatures debonding, not surprisingly, occurred more rapidly.

Other samples were also prepared but with coated chopped glass fibres. The coating was a coupling agent designed to improve fibre-matrix interfacial adhesion. These samples were then subjected to the same tests as the samples with the uncoated fibres. Significantly different results were obtained, with no debonding detected after 10 months in the 20°C environment. Hot water immersion did eventually lead to interfacial failure but after far longer times than for the specimens reinforced with pristine, untreated fibres. In this case debonding was initiated by the formation of discontinuous bubble like regions at the fibre-matrix interfaces. Ashbee and Wyatt demonstrated that these bubbles were pressurised osmotically, the osmotic pressure arising from the dissolution of some of the glass fibre constituents.

Cracks oriented radially to the reinforcing fibres were also evident in association with discontinuously debonded regions, but their growth ceased after some 20 hours immersion in boiling water. One would however expect such cracks to create new surfaces for hydrolysis in accordance with the theory proposed by Abeysinghe et al. above. Water soluble hydrolysis reaction products would then increase the osmotic potential, cause an internal pressure rise and

further crack growth. The cessation of crack growth reported by Ashbee et al. contradicts this theory. It is however plausible that in a test situation the small amount of water used would rapidly become contaminated with leached materials and thus reduce the osmotic potential between the bubble region and the surrounding water.

Once the fibre has completely debonded from the surrounding matrix relative longitudinal movement between fibre and resin is permitted. As a consequence the fibre end acts as an indenter resulting in conically shaped cracks when the resin shrinks after significant leaching.

Exposure to water and moderate temperature evidently result in physical and chemical degradation of composite materials with the reduced load transfer between matrix and reinforcement resulting from resin cracking and debonding inhibiting the mechanical performance of the material.

2.3 Applied stress and an aqueous environment.

The addition of an external stress to a component in an aqueous environment further complicates lifetime prediction. If any synergism existed between the applied external stress and the water induced damage a material would be expected to degrade more rapidly in the more demanding stressed situation. Pritchard and Taneja[9] compared stressed and unstressed glass chopped strand mat (CSM) reinforced

polyester laminates immersed in water baths at temperatures between 35 and 80°C. In the unstressed specimens features similar to those reported above such as interfacial failure, associated disc cracks and disc cracks in the resin bulk were observed. Some surface cracking was also experienced at water immersion temperatures of 80°C.

Pitchard and Taneja then applied constant strain, tensile loads to the laminates. Strains of up to 0.3% neither visibly accelerated the amount of damage observed nor produced any different damage types. Pritchard and Taneja suggest that evidence for the lack of effect of stress is provided by the position of the interfacial failures. In both stressed and unstressed tests these were confined to the surface regions suggesting that debonding only occurs in regions of water permeation. At first this appears a reasonable conclusion but is rather contradicted by data from an earlier study by Pritchard and Taneja[10] demonstrating that water permeation is greatly increased by the application of strain. Such results would suggest that high strain would expose the fibre-matrix interfaces further from the specimen surfaces to water and lead to debonding at a greater depth in a stressed sample.

Whilst Pritchard and Taneja give some account of the extent (i.e. depth) to which fibre resin interfacial failure was observed no idea of the rate of degradation or the effects

of applied external stress upon it are given. This is however rectified in later research by the same authors[11]. In this study the time of the first appearance of debonding was noted. Comparisons between tests with stress alone and water alone illustrate that a combination of the two result in a more rapid appearance of the first debond. The debonds were still however confined to the surface exposed to the water.

The stresses and consequent strains applied in these experiments are low and thus may explain the apparent insignificance of stress upon water associated damage. The test durations with a maximum of 2000 hours are relatively short and further degradation might be observed after longer periods where the effect of stress enhanced water permeation might become apparent.

2.4 The effect of aqueous environments upon the mechanical properties of glass fibre reinforced composites.

The two previous sections have demonstrated the degradative nature of an aqueous environment without giving any idea of the quantitative effect on the mechanical properties of the material. Several authors[12,13] have reported a degradation in the strength and modulus of composite materials immersed in an aqueous environment. In all cases failure is attributed to a combination of the deterioration of resin, reinforcement and interfacial adhesion.

Ellis and Found[14] however discovered that tensile breaking strength and the corresponding elongation can be enhanced by water absorption. Following immersion in distilled water at 51°C for forty days both debonding and resin cracking were evident in chopped strand glass mat reinforced polyester laminates. It would be expected that these features would reduce load transfer between resin and reinforcement as well as general material integrity. Subsequent tensile strength tests however resulted in a failure stress 30% greater than the value obtained for dry test specimens.

Ellis and Found tentatively attributed this enhancement in mechanical properties to an increase in resin extensibility due to sorbed water. This is a plausible explanation. Water absorption leads to matrix swelling which results in greater polymer chain separation and reduction in intermolecular attraction. This greater polymer chain mobility therefore has a plasticising effect on the resin permitting greater elongation prior to failure.

This effect has not been dominant in other similar research where water absorption has a deleterious effect on the mechanical properties of the material. One possible explanation of this apparent anomaly lay in the duration of immersion in the aqueous medium. Ellis and Found tested specimens after 40 days exposure to distilled water.

Although test pieces became saturated during this period chemical attack on the resin, fibre and interface may only be in their early stages and resin plasticisation due to absorbed water dominates. Such an effect would not be expected in a woven roving or unidirectionally reinforced laminate as the ultimate failure strength depends upon the amount of reinforcement in the direction of loading, irrespective of any resin plasticisation effect.

The nature of the aqueous medium, duration of exposure, temperature, resin and reinforcement geometry are all important parameters in the behaviour of composite mechanical properties in aqueous environments. Many researchers suggest that some relationship exists between the amount of water absorbed and the degradation in mechanical properties. Springer, Sanders and Tung[15] demonstrated this to be the case using a glass reinforced sheet moulding compound (SMC). They found that at high temperatures more water was absorbed more rapidly with correspondingly greater decreases in tensile strength and modulus. They could not however define a unique relationship despite concluding that some correlation existed.

Pritchard and Speake[16] also attempted to define this correlation between the mass of water absorbed and mechanical property changes. In many simple diffusion processes Ficks' law is applicable. This predicts that the

mass of water absorbed increases linearly with the square root of time, until an equilibrium plateau is reached. Crosslinked unsaturated polyesters are more complicated, with chemical degradation resulting in the loss of organic matter. Pritchard and Speake compensated for this weight loss and demonstrated residual mechanical properties to be functions of the true water content. Empirical relationships were then obtained between mechanical properties and water content. After extrapolating kinetic data from tests temperatures of between 30°C and 100°C to 15°C they obtained an empirical expression to predict laminate properties for a period of 25 years. Data from tests lasting 3 years gave good agreement with this empirical expression.

2.5 Stress-rupture of GFRP.

One part of the cooling system service conditions which requires special consideration is the anticipated plant lifetime of 30 years. The very object of fabricating structures in GFRP is to produce components which require little or no maintenance and exhibit a lifetime exceeding the life of the power station. Some consideration of the long term performance of GFRP is therefore necessary. Apart from plant "outages" for maintenance, which are very costly and therefore infrequent, the pipe wall material is permanently loaded.

The properties of GFRP are highly time dependent and creep occurs at much lower temperatures than in steel. For example, a GFRP coupon might support a load corresponding to 80% of its quasi-static dry strength for a few hours with a load 40% of the quasi-static strength being supported for approximately a month. Evidently performing constant load, stress-rupture tests is straightforward, but conducting tests equivalent to the 30 year lifetime of the power station is highly impractical. This problem has motivated various researchers to attempt to rationalise the stress-rupture behaviour of GFRP and to form predictive methods whereby short term data can be used to predict material behaviour at much longer lifetimes.

2.6 Predictions from stress-rupture data.

It is very common to present stress-rupture data for GFRP by plotting stress on a linear scale as ordinate as a function of time to failure on a logarithmic scale as the abscissa. Such an approach assumes a linear relationship of the form given in equation 2.

$$\sigma_f = A - B \log t_f \qquad \text{(EQUATION 2)}$$

σ_f represents the failure stress, t_f the time to failure with A and B constants. This simple approach is based upon an Arrhenius relationship of the type,

$$t_f = \tau_o \exp [(U_o - \gamma\sigma) / kT] \qquad (\text{EQUATION 3})$$

where t_f is the time to failure, τ_o the period of atomic vibrations, U_o the activation energy for bond rupture, γ a constant for the material, σ the applied stress, k Boltzmans constant and T the absolute temperature. This relationship was first proposed by Zhurkov[17] in work relating fracture to a thermally activated process based on the breaking of chemical bonds.

Several reports include data plotted in this manner with the work of Boller[18] one of the earliest. In his extensive study tensile, shear and flexural tests were carried out on a range of glass fibre reinforced polyester and epoxy materials with both air and aqueous environments considered. After 13.5 months Boller found that failure stresses had fallen to between 51% and 81% of the original dry quasi-static strength for the samples tested in air and 36% to 61% for those subjected to an aqueous environment. Linear extrapolation of these data would suggest stresses to failure after 30 years of between 21% and 52% for the water immersed samples.

Steel[19] also investigated glass reinforced polyester and epoxy laminates considering the additional factor of temperatures ranging from 4 to 48°C. Data were accumulated from tests on specimens immersed in air, water and paraffin

for up to 70 days. Extrapolation of the linear fits to the results of Steel estimates a flexural strength of 0% of the short term dry strength for a woven glass cloth polyester laminate in an aqueous environment at 20°C after 25 years.

Another extensive study was carried out by Bershtein and Glikman[20]. In tensile and pure bending tests of up to 13.5 months duration both varying environments (air, water and sea water) and temperature were applied to glass fibre reinforced polyester laminates. Linear extrapolation of a stress versus log time to failure plot again predicts a retained strength after 11 years less than 0% of the dry tensile strength of the material. The results of Dixon, Ramsey and Usher[21] are more optimistic however, predicting a tensile strength retention 30% of the short term value after 20 years immersion in water at room temperature.

Authors such as Cameron[22] claim that better straight line fits are obtained by plotting stress-rupture data on a log stress versus log time to failure basis. After superimposing his own results upon data from various other sources he attributes the creep-rupture behaviour of GFRP to the stress corrosion of the reinforcing fibres. Justification for this conclusion may be provided by the log stress/log time to failure relationship which is claimed to apply to the static fatigue (stress corrosion) of glass fibres in a moist environment.

Schumacher[23] also plots his data on a log stress/log time to failure basis. He reports tensile stress-rupture experiments lasting up to 13.5 months. Strength retentions of between 37.5 and 50% of the measured short term strength are predicted after 14 years for tests carried out at ambient temperatures in air. Other studies which select to present their results on a log/log basis include the work reported by Holland and Turner[24], and Menges and Schwartz[25].

Chiao, Lepper, Hetherington and Moore[26] suggested that creep-rupture data for composites could be represented by a power law relationship. Data from tests on unidirectional strands of S-glass impregnated with epoxy resin gave a close fit to equation 4.

$$\sigma = P + Q(t_m)^{-x} \qquad \text{(EQUATION 4)}$$

where;

σ = the applied stress.

t_m = the median lifetime of a large number of specimens.

P, Q and x are constants.

It is probable however, that these results reflect the fibre properties and bear little relevance to a composite laminate. The properties of a unidirectional laminate will

of course be vastly different from a multidirectional material.

A common method used in extrapolating data concerning unreinforced polymers is some form of "time-temperature superposition". Wright[27] applied this technique to tensile creep-rupture data for GFRP immersed in water at temperatures of 20, 40, 50 and 60°C. From the master curve obtained, he predicted that the stress bearing capability of the GFRP would have been reduced to 30% of its dry tensile strength after 30 years.

Although many workers have addressed the problem of stress-rupture lifetime prediction the literature discussed above is far from conclusive. Neither a clearly applicable mathematical method nor common predicted lifetimes from any one method are evident, with the scatter in results at a given load level providing a further complication. Comparisons of the results reported are further hampered by the different reinforcement geometries and resin types. It is also reasonable to assume that modern polymeric matrices would have a performance of a superior nature to those experimented upon by Bershtein and Glikman some thirty years ago.

Unlike metals there is a general lack of a well established data base relating to the mechanical properties of composite

materials. Many different composite combinations are possible thus necessitating experiments closely imitating service conditions in the absence of a rigorous predictive theory.

The CEGB have addressed this problem in recent years by instigating a program of stress-rupture testing on glass fibre reinforced isophthalic polyester composites, the material selected by the CEGB for use in cooling water systems. Initial tests conducted by the Rubber and Plastics Research Association (RAPRA)[28] were plotted on a stress/logtime basis. Linear extrapolation of data from test pieces subjected to an aqueous environment at 40°C indicated values of stress endurance approximately 10% of the measured tensile strength at ambient temperature in air. Work carried out at Bath University[29,30,31] produced similar results although a downturn in results was noticed at lifetimes in excess of 10^6s at 60°C and 10^7s at 40°C. Such data suggest that straight line regression analysis may be invalid although in the absence of data at longer lifetimes few other options are available.

CHAPTER 3

The effect of more complex loading patterns on the durability of GFRP.

3.1 The effect of tidal pressure variations and plant outages on component life.

The most appropriate experimental data pertaining to tidal variations in liquid coolant pressure are offered by cyclic fatigue studies. Many programmes of research have considered the effect of applying sinusoidal, saw-tooth and square-wave load profiles to GFRP. Most of these concentrate on the application of loads at frequencies above 1Hz, far higher than the 23.15μHz (two cycles per day) experienced in CW system service. Sims and Gladman[32] did consider the effect of frequency, testing GFRP under a saw-tooth load regime at a range of frequencies between 0.00247 and 50Hz. Lifetimes were compared on the basis of the number of cycles to failure. Interestingly, they found that the lifetimes of those coupons tested at the highest frequency were approximately one-hundred times greater than those tested at the lowest. This effect was attributed to a loading rate effect as it is well documented that GFRP demonstrate increasing failure strengths with increasing loading rate. To test this, data were then plotted as a proportion of the failure load measured at the rate of load application corresponding to the frequency of the fatigue load. This

normalisation procedure removed the apparent frequency effect. This study clearly bears relevance to the low frequency fatigue load to which CEGB CW systems are subjected, suggesting that design based on high frequency (i.e >1Hz) experiments may lead to optimistic predictions, unless this normalisation procedure relating frequency to loading rate is applied.

Evidently research into the fatigue behaviour of GFRP of the type in service in CEGB CW structures at frequencies less than 1Hz was necessary and this was carried out by Crowther[33] and further analysed and discussed by Crowther, Wyatt and Phillips[34]. The programme was specifically designed to address the effects of two components of a power station cooling water system load profile, namely, plant outages and tidal pressure variations. Glass/polyester laminates of the CEGB preferred reinforcement geometry were used with tests carried out in an aqueous environment at 40°C. Tidal variations in water pressure were modelled by a sinusoidal load variation with a period of two minutes (frequency=0.0083Hz) and a peak amplitude ±20% of the mean load. Results were plotted comparing times to failure at static loads with those from cyclic fatigue tests, taking the maximum load as the comparative load (see Figure 3.1). At high load levels the time to failure of purely statically loaded coupons was less than the coupons subjected to the fatigue regime. At low loads (<40%UTUS), however, the

fatigue loaded samples endured shorter lifetimes than those subjected to purely static loading.

This evidence of a life reducing dynamic fatigue effect at low frequencies and low load levels is relevant to CEGB CW systems operating from a coastal reservoir. The plot of these data is illustrated in Figure 3.1 and demonstrates that the difference in predictions from stress-rupture data and dynamic fatigue data is most pronounced below the 40% UTUS load level. This is of some importance as current CEGB structures are designed to operate at maximum loads as low as 10%UTUS.

Crowther also considered the effect of power station outages which result in the entire cooling water system being unloaded. These occur infrequently in the life of a power station with intervals between outages in excess of two months. Crowther used a square wave to model the effect of plant outages. Five different frequencies were selected allowing load to be maintained for between 0 and 33 minutes between unloading. In all cases the load/unload period lasted four seconds thereby maintaining a constant loading rate. The results revealed that at high frequencies, where the time at load was low, lifetime was governed by the number of cycles and not by the time at peak load. At low frequencies however, the material is at peak load for long periods in total and lifetimes were subject to load control.

Crowther proposed the existence of a boundary frequency above which failure is cycle controlled and below which it is load controlled. This boundary frequency was estimated at 1 cycle per 2 minutes. Power station outages are far more infrequent than this and hence component life will be dominated by the static load.

3.2 Multiaxial loads.

Whilst cyclic fatigue and load-up/load-down cycles discussed above are variations in the load/time profile, most industrial applications are also complicated by multiaxial stress systems. In structures such as pipes conditions can vary from a range of biaxial stresses to pure hoop stress, depending upon the stucture and its restraints. Designing for multiaxial stress system applications is the norm rather than the exception. As a result considerable attention has been given to this problem and many theories have been proposed to predict material strengths under complex load conditions. Such theories, referred to as failure criteria, are mathematical expressions of variables such as the material strengths and principal stresses under the service or test conditions of interest. They can be represented by plotting the in-plane stresses σ_1, σ_2 and σ_6 in cartesian space. The curve representing such a function is said to be a failure surface or failure envelope. A hypothetical surface is shown in Figure 3.2 to illustrate the concept. The area beneath the surface represents stress system

conditions under which the material is predicted not to have failed, the surface being the boundary to stress conditions causing material failure. Evidently a clear definition of failure is a necessity of applying this approach.

The derivation of strength predicting criteria can be two fold, either empirical or based on micromechanics. The micromechanics approach requires an understanding or prediction of the material failure modes and offers a rigorous analysis. Empirical criteria are more loosely based upon the broad concepts of how a material should behave. Having evolved such a criterion experimenters then evaluate it by running simple tests and attempt to verify it by further tests at different stress conditions. Commonly, experimentation will be deliberately confined to a stress condition where σ_6 is zero and a set or range of stress ratios (R ratios, where $R=\sigma_1/\sigma_2$) are explored. Of course this merely proves (or disproves) the applicabilty of the criterion at the stress conditions of the test.

Like much of the analysis applied to composite materials the origins of predicted material behaviour and hence empirical failure criteria are to be found in the theory applied to their isotropic counterparts. This may account for the limited success that has been achieved in applying failure criteria to composites. However, several failure criteria have been proposed for composite materials. Although this

thesis is not a study or critique of such theories, much experimentation was carried out by previous workers to test and adapt failure criteria. Such research provides some of the best information concerning the behaviour of GFRP under multiaxial load conditions and the most relevant is discussed below.

Many methods have been successfully devised for applying biaxial stresses to isotropic materials. However, only the off-axis tensile or compressive test, the thin walled cylinder test and the cruciform test are appropriate to GFRP. The off-axis tensile test can be readily performed with standard test machines on coupon test pieces. Several studies have been carried out using this simple test piece geometry. Amongst those Owen and Found[35] studied plain weave glass reinforced polyester resin laminates, comparing experimental values of quasi-static tensile strengths, compressive strengths and fatigue failure with predictions from nine different failure theories. Results from off-axis tests showed agreement with some portions of the theoretical failure surfaces. The general conclusion of this study sensibly observed that to predict material behaviour for other biaxial stress conditions would be fraught with difficulty as only a small region of the failure surface had been explored experimentally. Evidently off-axis tests can only provide a limited amount of information about the failure envelope.

The thin walled cylinder test is far more versatile and can, by a combination of axial load, internal pressurisation and torsion provide extensive exploration of failure surfaces. Several studies have been published applying multiaxial loads to glass fibre reinforced polyester composites. Owen, Griffiths and Found[36] carried out quasi-static (ie burst), static fatigue (stress-rupture) and cyclic fatigue tests on chopped strand mat reinforced polyester material fabricated into pipes of internal diameter 65mm. Applying principal stress ratios (R ratios) of between -1 and +1 the general shape of the failure surface was investigated. Surfaces were also plotted corresponding to the onset of debonding and resin cracking as well as constant life surfaces for fatigue data. The general shape of the failure surface was found to be a semi-circle, symmetrical about the σ_1 axis. Coupon and pipe fatigue tests were compared and coupons were found to exhibit longer lifetimes than pipes at a given stress level. This was attributed to the effect of the overlap in the chopped strand mat (CSM) pipe wall. Further experimentation on coupons, including sections modelling the joint in the CSM pipe wall, resulted in almost indistinguishable fatigue curves, proving the assertion that the overlap was detrimental.

Owen and Griffiths[37], and then Owen and Rice[38], continued this work with a programme testing plain weave and woven roving reinforced glass fabric polyester, materials very

similar to those in service in CEGB structures. Again both pipe and coupon tests were used although the programme centered on the pipe tests. Results for approximately 1200 tubes are reported allowing sensible comparisons with nine failure theories. Of those considered the Norris interaction[39] was the most successful. Reasonably, they concluded that whilst their volume of results offer a good agreement with the general shape of some of the proposed failure theories, as a basis for design, only service R ratios of the type modelled experimentally can be utilised.

The work of Owen and his co-workers provide data of direct relevance to CEGB power station CW system applications. Of most relevance are the R ratios, 0 and 0.5. R=0 corresponds to uniaxial tension for a coupon specimen and a pure hoop stress for pipes. This is very close to the situation in a piping system with frequent restraints and supports. R=0.5 relates to the type of load applied when pipes are pressurised internally with no end restraints. For static tests at R=0 coupon specimens performed poorly in comparison to their pipe counterparts. In agreement with Pagano and Whitney[40], Owen and Rice[38] attributed this to detrimental edge effects in the coupon test pieces. This observation has an important consequence for design, indicating that predictions from coupon testing may lead to pessimistic design of real structures.

Owen and Found also report that the results of burst and low cycle (short lifetime) fatigue tests offer a better correlation with the successful failure theories than the high cycle (longer lifetime) fatigue data. This effect may be a consequence of a difference between failure modes for short term tests as opposed to long term tests, indicating the possible problems of using a failure criterion which offers a good fit to readily obtainable short term test data to design long service life components.

Like many design and predictive techniques applied to composite materials the failure criterion type of method is open to much criticism. A particular failure surface can be plotted for certain R ratios for debonding, resin cracking and rupture. However, the origins of the criterion are usually empirical and take no account of damage micromechanisms or failure modes. Indeed the evidence above illustrates that even where a failure criterion is appropriate for a given material under one load profile, predictions for another similar profile cannot be made from that criterion.

Several studies of filament wound GFRP pipes have also been made including work on short term burst strength[41,42], stress-rupture[43,44] and cyclic fatigue[45]. In most cases the resin and reinforcement type and geometry differ from the current CEGB materials. Most of the work discussed above

highlights the need for research on the specific material and load conditions encountered in service. Furthermore an indication is given that coupon testing and pipe tests under nominally identical load conditions do not give the same results. Clearly some verification of the validity of using coupon test results in design is necessary.

CHAPTER 4.

Load transients and their effect on GFRP.

4.0 Transient overloads.

Whilst some overloads may occur due to accidental damage (during maintenance for example) the most significant overloads will occur due to sudden changes in the flow or pressure of the liquid coolant. In order to design experiments to simulate such overloads an understanding of the phenomenon of water hammer is essential.

4.1 The phenomenom of water hammer.[46-50]

The numerous controlling factors involved in a water transport system lead to frequent fluctuations in the pressure and flow of the working fluid. Equipment malfunctions can also rapidly alter the operating conditions of a system. Any alteration in the flow rate of the liquid requires an acceleration or deceleration of the fluid and hence requires a force to bring about this change in fluid velocity. In all cases this force manifests itself as a hydraulic pressure transient. The severity of the pressure change depends upon the rapidity of the change in flow rate and large pressures are usually referred to as water hammer. Specific events which cause water hammer include;

(i) Pump start up and shut down.

(ii) Pump power failure.

(iii) Valve motion.

(iv) Valve failure.

(v) Changes in valve settings, accidental or planned.

Although the cooling water system of a power station is complicated an understanding of water hammer can be obtained by considering the simple system illustrated in Figure 4.1.

The system consists of a reservoir, a single pipe of constant diameter and a valve at the downstream end. In this case the assumption is made that there is a negligible pressure drop along the pipe due to friction and hence all of the pressure due to the head of water in the reservoir occurs across the valve.

Initially (Figure 4.1) the water is flowing at a velocity, V_o with the valve open. At some instant in time the valve closes instantaneously. The flowing liquid has mass and velocity and therefore cannot be stopped instantaneously. Consequently the pipe wall expands permitting a small additional mass of fluid to be stored in the pipe. The remainder of the liquid mass is accommodated by compression of the liquid itself. As a result of this additional water storage a local pressure rise occurs as depicted in Figure 4.2.

Closing the valve has led to two events, a stoppage in fluid flow and a local pressure rise. Upstream however, pressure and flow have remained unaltered. The difference in conditions between the valve and the upstream region is unstable and very shortly after valve closure the pressure and flow disturbance created at the valve travels towards the reservoir at high speed. This travelling pressure disturbance, commonly called a wavefront, travels at the speed of sound (in the pipe wall material) and is just large enough to stop the fluid flow.

The condition of the system when the wavefront has reached the reservoir is illustrated in Figure 4.3. The time required to reach this condition is dependent upon the length of pipe between reservoir and valve (L) and the wavefront speed (a). Although pressure throughout the system is uniform at the elevated value and flow has been halted, the system is unstable because the pressure in the pipe is higher than that in the reservoir. Fluid therefore flows into the reservoir at a flow rate equal and opposite to the original flow, accompanied by a reduction in pressure to the level of pressure in the reservoir. The system is now in the condition depicted in Figure 4.4 where a reduced pressure wavefront is travelling towards the valve. Upstream of the wavefront flow towards the reservoir is established and pressure is at reservoir head.

Once the reduction pressure wavefront reaches the closed valve the conditions are as shown in Figure 4.5. Although the entire system is at a pressure equivalent to reservoir head flow is towards the reservoir. As fluid cannot travel through the closed valve the flow must stop leading to a sudden pressure drop at the valve as the fluid pulls away from it. Now a reduced pressure wavefront travels upstream towards the reservoir (see Figure 4.6).

When the wavefront arrives at the the reservoir the system is however still in an unbalanced condition. The reduced pressure level in the pipe at the reservoir causes flow back into the the pipe and the wavefront travels downstream back towards the closed valve. On the upstream side of the wavefront flow and pressure have returned to their original states and at the moment when the wavefront reaches the valve the system returns to the condition illustrated in Figure 4.1.

Evidently this process could continue indefinitely, repeating every 4L/a seconds, with the variation of pressure with time at the valve following the profile illustrated in Figure 4.7. In real systems energy dissipation due to frictional and viscous losses dampen out the oscillation of the wavefront between reservoir and valve, eventually bringing the system to rest. Systems with low energy losses

can, however, result in water hammer persisting for a long time.

By considering the change in fluid momentum resulting from valve closure, an expression for the head of pressure at the valve can be derived (see Appendix A). ΔH, the increase in pressure is given by;

$$\Delta H = -\delta V a/g \qquad \text{[EQUATION 5]}$$

Where, δV = change in fluid velocity.

a = velocity of pressure front.

g = acceleration due to gravity.

Equation 5 illustrates that the magnitude of the pressure rise resulting from valve closure, or any event causing an alteration in flow, is dependent upon the change in velocity. In a power station cooling water system the calculated maximum pressure rise would be approximately 26.3 bar (268m head) (see Appendix A).

4.2 Water hammer in piping systems with frictional losses.

In the frictionless pipe described above sudden valve closure causes the upstream flow to be brought to rest as the compression wave travels through the pipeline at acoustic speed. In a high friction pipe however, this may not be the case as the upsurge in pressure following valve closure may be smaller than the original hydraulic pressure. This is illustrated in Figure 4.8. The rise in pressure at the valve is related to the change in fluid velocity at that

point. As a result of frictional losses fluid velocity some distance from the reservoir is less than it would be for a frictionless system. Consequently, the potential surge travelling back towards the reservoir reaches a point where the hydrostatic pressure of the fluid is greater than the pressure upsurge. At this point the fluid flow is not brought to rest by the passage of the compression wave and the magnitude of the travelling pressure front is attenuated as it travels upstream.

Flow is therefore maintained towards the valve and additional fluid is stored. This effect is known as "line packing" and can result in pressures at the valve far larger than the initial pressure rise due to valve closure.

The duration of the pressure overload is also dependent upon the nature of the frictional losses. In a frictionless system an infinite number of overloads is conceivable, whereas the attenuating effect of frictional energy dissipation results in the oscillation of the wavefront coming to rest. A hypothetical profile of the pressure at the valve as a function of time for a simple system with friction is illustrated in Figure 4.9.

It is evident that the exact nature of a transient overload or water hammer event is highly dependent on both the event leading to it and the system in which it occurs. CEGB[51,52]

data on water hammer events suggest an overload profile of the type depicted in Figure 4.10, with a peak load possibly reaching a value six times the operating pressure of the fluid. Such an event subjects the pipe wall material to a high rate of load application. The response of the pipe wall material to tensile impact loads at high strain rates is therefore of great relevance here and is discussed in the following section.

4.3 The effect of strain rate upon the mechanical properties of composite materials.

The application of composite materials to dynamically loaded structures has resulted in considerable research into the behaviour of composites and their constituent components at different loading rates. In the following sections some of these studies are discussed with attention focussed on the effect of fibre type, reinforcement geometry and matrix resin on material behaviour.

4.3.1 Effect of fibre type.

Armenakas, Garg and Sciammarella[53] investigated the effect of strain rate and temperature upon the mechanical properties of S-glass fibres. At test temperatures of -15° and 10°C fibre strength decreased with increasing strain rate. At 65°C increasing strain rate to 8%/s produced an increase in the failure strength of approximately 10%. Despite providing some comparison in strain rates, 8%/s, the

maximum used in this study, is close to the quasi-static range and gives little idea of the effect of a truly dynamic event on a glass fibre. O'Neil, Dague and Kimmel[54] provide a more informative study. In tensile tests on glass fibres at a strain rate of 7000%/s, an increase in fracture strength of approximately 32% over that obtained at 2%/s was observed. Fracture strength also increased by approximately 25% at a strain rate of 1000%/s.

Several authors[55,56,57,58] report increases in ultimate strength, modulus, fracture energy and elongation at break for glass fibre composites at strain rates in the order of 100%/s when compared with data compiled in tests at quasi-static loading rates. At a strain rate of 1000%/s Harding and Welsh[59] report increases of 135% and 158% in modulus and tensile strength respectively.

Some authors have considered lower rates of load application. Rotem and Lifshitz[60] achieved a strain rate of 30%/s and recorded tensile strengths for glass fibre composites almost three times the quasi-static value. The dynamic modulus also increased by approximately 50%. Daniel and Liber[61] did not experience any change in mechanical properties of S-glass epoxy laminates tested at a strain rate of 18.8%/s. They sensibly proposed that strain rate effects in the 0° direction will be dominated by the strain rate sensitivity of the fibres. Logically they conclude from

their results that glass fibres do not exhibit any strain rate dependent mechanical properties. However, the strain rate sensitivity of glass fibres has been demonstrated by O'Neil et al. and is described above. It is therefore likely that had Daniel and Liber applied higher strain rates, changes in mechanical properties would have been observed. In tests on unidirectional glass/epoxy laminates Armenakas and Sciammarella[62] witnessed increased modulus, but reduced stress and strain at failure, in tests at a strain rate of at 500%/s. A very low glass content composite, with a fibre volume fraction of 9%, was used in this work. One would expect differences in the proportion of reinforcement to be reflected by the mechanical properties of the material and this is the most likely explanation of the anomaly between the results of the majority of reported literature (high fibre volume fraction), and Armenakas and Sciammarella.

Experimentation at high strain rates with fibres other than glass has also been reported. Harding and Welsh[59] considered unidirectional carbon and woven glass fibre reinforced polyester laminates. Despite achieving strain rates approaching 1000%/s no rate dependent properties were exhibited by the carbon reinforced material. In a later study[63] the same authors applied strain rates up to 800%/s to glass, carbon and kevlar reinforced polyester laminates. All reinforcement was in a woven form. Glass, carbon and

kevlar materials all exhibited increased modulus, breaking strength and elongation at break.

4.3.2 Effect of reinforcement geometry.

It is evident from the preceeding section that composites of glass, carbon and kevlar reinforcement can all exhibit some strain rate dependent behaviour. Both unidirectional and woven glass[64,65] fibre materials exhibit strain rate sensitivity in mechanical properties. However, only woven forms of carbon fibres behave in a similar fashion, indicating that the reinforcement geometry has an effect upon material behaviour at high strain rates.

Harding and Welsh[63] provide the best assessment of the effect of reinforcement geometry using glass and carbon reinforced polyester laminates. All samples were fabricated with woven reinforcement. The carbon fibre material exhibited an increased tensile strength at the highest strain rate (800%/s). The strain to failure at this strain rate, 1.59%, was appreciably larger than the 0.9% achieved with a unidirectional carbon laminate tested in a previous study[59]. The glass material exhibited substantial increases in tensile failure stress and modulus at the highest strain rate. The failure strain was also observed to increase with rate of load application. At the highest strain rate applied, three specimens failed at strains in excess of 9%

and one, tested at a strain rate of 1360%/s, attained a strain of 13% just prior to failure.

Strain rate sensitivity was also evident in the appearance of the glass reinforced specimens where a progressively larger damage zone and greater fibre pull-out were noted with increasing strain rate. At strain rates of approximately 1000%/s a change in fracture mode was reported with the specimen disintegrating into three separate pieces. The central portion remained relatively in tact with long fibre pull-outs on both sides.

The woven carbon fibre reinforced specimens exhibited the same type of failure at all strain rates with fibre pull-outs and fibre-matrix debonding adjacent to the fracture surface. In tests on unidirectional carbon fibre reinforced material the fracture surface exhibited little fibre pull-out and no rate dependency of mechanical properties were observed. This would suggest that the increased strain to failure in the woven laminates was a consequence of the reinforcement geometry. This is further borne out by the increased pull-out lengths and debonding adjacent to the fracture zone. If this is the case then one could envisage a situation where fibre-matrix debonding occurs facilitating greater extension of the fibres as the kinks in the fibre tows are straightened out. Once a fibre has straightened the material properties will be depend upon the rate dependency

of the fibre, which in the case of carbon appears to be insignificant. The reinforcement geometry therefore leads to a change in failure mode in comparison with the unidirectional material.

4.3.3 Effect of matrix resin.

High molecular weight polymers are also very sensitive to strain rate. Several authors[66-68] have demonstrated this to be the case although little work has been done on cast thermosetting resins similar to the polyester or vinyl ester used as the composite matrix in this study. McAbee and Chmura[69] tested both thermoplastic and thermosetting resin materials. In tests up to strain rates of 1500%/s the general trend in the results for the thermosetting materials illustrated increases in modulus and failure load with increasing strain rate. Most of the investigations of strain rate effects on the composite combinations discussed above use polyester or epoxy resins as the matrix material but no particular trends were evident.

Evidently the effect of strain rate on the mechanical properties of composite materials is very complicated. It is however clear that the type of reinforcement and its exact geometry greatly affect a composites mechanical properties at different strain rates. Particularly noteworthy were the experimental data indicating that woven mat glass reinforced polyester composites, similar to material in service in CEGB

CW systems, exhibit enhanced modulus and failure strength when tested at high loading rates.

4.4 The effect of preloads on composite materials.

The literature discussed above gives information concerning tests to failure. Little idea is given of the effect of a short duration, high strain rate, sub-critical overload of the type described in section 4.1. As water hammer events can occur at any point in the lifetime of a structure one way of modelling long term material behaviour following a water hammer event would be to consider the water hammer event as a tensile impact preload prior to normal, constant or cyclic loading. The effect of impact loads upon subsequent material behaviour has been widely studied. In most cases this is confined to falling weight type tests and not the tensile impact[70] which relates to a water hammer event. Of relevance here are studies of cyclic fatigue where a sequence of single amplitude and frequency fatigue loads are followed by a different load profile, sometimes referred to as block loading.

In one such study Bax[71] applied between 5 and 20 preloads to filament wound epoxy and polyester pipes prior to stress-rupture. As few as 6 preloads, with a magnitude approximately equivalent to 60% of the pipe burst strength, resulted in significant reductions in the time to failure under constant internal pressure. The cycle periods used, 12

minutes, are long in comparison to the milliseccond duration of a water hammer event. Hence, none of the enhanced mechanical properties associated with high strain rates would have been realised. It could be concluded from this evidence that the material survives preloads of a magnitude equivalent to the maximum envisaged in service (equivalent to 60% UTUS). One might then speculate that had the preloads been at a loading rate sufficient to induce enhanced mechanical properties, the subsequent lifetime might not have been reduced. However, one can only speculate how much damage would occur as a result of a preload and what its subsequent effect over the lifetime of the component or structure would be.

Jones et al.[72] considered the effect of applying a constant amplitude preload upon the subsequent fatigue beahaviour of 0°/90° GFRP coupons. Preload durations of up to 250 seconds were reported to have no discernible effect on the residual fatigue life (cycles) when compared with the fatigue life of virgin material.

The literature described offers only a few clues to the possible effects of transient load events. Experimentation is therefore necesary to model the short and long term effects of transient overloads such as water hammer events.

CHAPTER 5.

Damage development and failure in polyester/glass composites.

5.0 Failure mechanisms in stress-rupture.

The principal modes of mechanically induced damage in fibre reinforced composite materials are resin cracking, debonding (failure of interfacial adhesion between reinforcement and resin), delamination and fibre fracture. The mechanism of failure under a particular loading regime is however dependent upon the reinforcement geometry as well as the mechanical properties of resin and reinforcement.

In the stress-rupture of composites of mixed woven roving and chopped strand mat reinforcement transverse fibre debonding is immediately noted upon load application at loads in excess of 30% of the dry tensile strength. This debonding then propagates into the resin rich areas surrounding the reinforcement, resulting in matrix cracking. As the matrix cracks propagate they meet warp roving fibres and cause these to debond. Gradually the efficiency of load transfer between reinforcement and matrix deteriorates causing stress concentrations throughout the laminate. With a woven roving reinforced composite, crossover points between warp(0°) and weft(90°) rovings result in complex stress fields, high stress concentrations and frequent fibre fracture at these points. Another consequence of this

complex stress field can be the initiation of delamination between reinforcement layers as the kinks in the fibre tows gradually straighten following load application.

Comparisons of previous research on composite materials are usually restricted by variations in the types of reinforcement and resin formulations used. Mixed reinforcement polyester laminates of the type investigated in this thesis have however been considered recently by White[73] and Crowther.

White investigated a wide range of static loads and environments. He discovered that times to failure at static loads between 25 and 80% of the dry tensile strength of the material were very sensitive to the environment, showing shorter times to failure in an aqueous environment as opposed to dry. Since no transverse cracking was observed at static loads below 25% of the ultimate tensile strength he concluded that transverse cracking facilitates ingress of the aqueous environment and so accelerates fibre fracture. At static loads in excess of 80% of the dry tensile strength times to failure were considered to be too short to reveal the effect of the aggressive environment.

Crowther considered numerous different complex loading regimes which were described in section 3.1. Observations of the test specimens were made both during the test and

following failure. As in White's work, damage was noted very early in the lifetime of the test piece, with resin cracking and debonding evident after 20 minutes for a specimen subject to a static load 62% of its dry tensile strength. In all purely statically loaded specimens crack propagation and ultimate fracture resulted from the first damage site observed.

The viscoelastic nature of the polyester resin manifested itself in the form of dimples on the laminate surface. Matrix creep permits the kinks in the warp rovings to straighten. The combination of warp roving extension and the consequent increased constraint on the weft roving at cross over points results in dimpling. If the resin deforms plastically the dimples will be retained on unloading and this was evident in test pieces with times to failure in excess of 10^6s.

The superposition of any cyclic element upon the static load led to both more widespread sites and more varied types of damage. Greater degrees of warp roving delamination, gel coat cracking and debonding were all noted. The failure mechanisms due to the various cyclic loading regimes all followed similar trends. One anomaly was noted with a dramatic increase in the warp roving delamination in the specimens subjected to a rectangular loading pattern in addition to the static load. Crowther concluded that very

high loads, cyclic loading elements and large alternating stresses all lead to increased debonding.

Stress-rupture failure mechanisms of GFRP in aqueous environments illustrate several features. With static loading regimes one initiation and failure site is most common. Superimposed cyclic loading regimes are more deleterious due to the widespread damage resulting. In all cases any damage allows water ingress and transport. This facilitates two degradative effects of water, resin-glass interfacial breakdown and stress corrosion of glass fibres.

CHAPTER 6.

Summary of published work and plan of the investigation.

6.1 Materials.

The present material preferred by the CEGB is a mixed reinforcement chopped strand mat (CSM) and woven roving (WR) in a polyester matrix, and this was adopted for the experimental work. The lay-up used followed that of previous CEGB funded research programmes[33] (see Figure 7.1). Some vinyl ester matrix laminates were also fabricated and tested. Here the objective was to establish whether a matrix of a greater fracture toughness (the vinyl ester) afforded any beneficial properties to the material.

6.2 Modelling a water hammer event.

Section 4.0 illustrates that there is no one typical water hammer event. However, the type of water hammer event witnessed in service in CW systems is known. The load/time profile comprises a high rate of load application (strain rate in the order of 100%/s) to a stress about 6 times the design stress of the component, followed by an equally rapid unload, with the whole event lasting between 20 and 60ms. Present CW systems are designed to operate at stresses corresponding to 10% of the material UTUS, and therefore the peak magnitude of a water hammer event would be approximately 60% UTUS. The work of Harding and Welsh

discussed in section 4.3 shows that the material will exhibit an enhanced mechanical performance during the high loading rate phase of the water hammer. However, the literature does not include any work on the effects of a sub-critical event such as water hammer. As a result the initial task undertaken in the experimental programme was to apply a model water hammer event to small scale specimens (coupons) of material representative of that used in present CW system applications. The immediate effect of this model transient overload was then determined in terms of damage (if any) and residual short term mechanical properties. It is likely that several incidents resulting in water hammer events will occur throughout the 30 year lifetime of a component. Evidently the number of overloads is another variable. Some consideration was given to this variable in the experimental programme. A figure of 50 was adopted[51] as the number of overloads (including reflected pulses) occurring over 30 years of service.

6.3 Investigating the effect of the model water hammer event on long term material behaviour.

The large number of experimental studies of static and dynamic fatigue discussed in chapters 2 and 3 include several studies specific to CW system material type and load conditions. Although they greatly improved the data base available to the designer there are no accounts of material behaviour subsequent to a water hammer event. Bax[71] observed

reduced lifetime as a consequence of pre-loads, highlighting the need to discover if water hammer type loads have a similar effect, or whether the enhanced performance associated with high rates of load application would negate the effects of water hammer. In order to address this, part 2 of this thesis includes experimental work involving the application of both static and dynamic loads to coupons previously treated with the model water hammer event. The dynamic fatigue experimentation was carried out at a frequency of 23.15μHz, identical to service conditions, a frequency at which no data is available. CW system components are constantly in contact with warm water and sections 2.0-2.3 recount the detrimental effects of these service conditions. To take account of this all fatigue experimentation was carried out in an aqueous environment, at 40°C, the maximum service temperature. Previous studies using nominally identical materials to those used in this project have generated stress-rupture curves on virgin material. As a result, any effect of the model water hammer event on coupon lifetime can be established.

6.4 Applying a real water hammer event to a model component.

The experimental programme so far outlined provides information on both immediate and long term effects of model water hammer events. The value of this depends on the model event being realistic, and the coupons and test techniques being representative of service conditions and structures.

Part 3 of the programme, where GFRP pipes were tested, was designed to address this question, as well as providing basic design information and permitting assessment of the success of the model event. To facilitate comparisons pipes were fabricated from very similar material to that used in the coupon testing programme. A water hammer event of similar profile to the model event was propagated through a piping system incorporating some GFRP test pipes. Comparing the event profile, material response and post-event material condition for pipe and coupon test pieces, revealed how well the coupon model reflects a real event.

6.5 Investigating the validity of using coupon test data in the design of real components.

The pipe testing programme parallelled the coupon testing programme, with stress-rupture tests on pipes subjected to water hammer events as well as virgin pipes. Comparing pipe test results in isolation reveals the effect of water hammer upon component lifetime. Considered together, pipe and coupon test programmes generate other comparisons. With both types of test performed on very similar material and loaded in an identical mode (static fatigue), the validity of coupon tests as a guide to the behaviour of a real structure could be assessed. A comparison of the failure modes of pipes and coupons is also important. This allows the definition of failure in coupons (from which component

lifetimes are predicted) to be compared with a service component failure criterion.

PART 2

COUPON TESTING PROGRAMME.

CHAPTER 7.

Materials and testing.

7.1 Fabrication of material and test pieces.

The objectives of the material fabrication were as follows;

(i) To fabricate material resembling that used in power station cooling water system components presently in service.

(ii) To fabricate material comparable to that used in previous research thus facilitating comparison with results from such research.

(iii) To achieve a glass:resin ratio in chopped strand mat (CSM) of 1:1 and of 2:1 in the woven roving (WR).

(iv) To produce laminates with minimum void content.

(v) To produce laminates with a nominal thickness of 2.5mm.

After some experimentation the following technique was adopted;

Sufficient resin to provide a 1:1 glass:resin ratio was poured evenly over the melinex® covering the mould surface. The first layer of CSM was then placed on top of the resin. This was then left for 5 minutes after which the CSM was usually found to be totally impregnated with resin. In a few cases a limited amount of stippling with a paint brush was necessary around the edges of the CSM. Sufficient resin for

both the WR and CSM layers was then poured over the working area and the WR reinforcement placed in position. In applying each layer of reinforcement the natural curvature resulting from storage on a roll was used to the advantage of the fabricator. This was achieved by positioning the layer of reinforcement concave upwards in the centre of the working area. The weight of the reinforcement and the action of the gradually impregnating resin then flattened the reinforcement. Working with brushes or rollers was avoided as in many cases this introduces voids.

Five minutes was usually sufficient to achieve full impregnation of the WR layer. The final layer of CSM was then positioned and impregnated as above. Finally a sheet of melinex was rolled over the laminate. To avoid entrapment of air a line of resin was poured along one edge of the laminate. The sheet of melinex was then rolled up and positioned in contact with the resin. The roll of melinex was then unrolled over the laminate pushing the line of resin in front of the melinex/resin interface, preventing the inclusion of air at the surface. The top glass plate was then positioned with 2.5mm spacers between the glass plates. The load frames were then left overnight after which time laminates were removed for post cure. Laminates of glass fibre reinforced polyester and vinyl ester were fabricated following this procedure.

Glass fibre reinforcement geometry for both vinyl ester and polyester laminates was identical. The reinforcement geometry selected was scaled down from present CEGB service components. Laminate construction is illustrated in Figure 7.1. Test pieces of the dimensions given in Figure 7.2 were then machined from the GFRP laminates. The cut edges of the test pieces were polished prior to any mechanical treatment.

7.2 Quasi-static tensile testing.

Quasi-static tensile tests were carried out at a crosshead speed of 0.5 mm/minute using an Instron 1195 tensile testing machine. Gauge length extension was measured using a Wallace optical extensometer. 10 coupons of both the polyester and vinyl ester matrix materials were tested. The ultimate tensile unit strength (UTUS) and the modulus (calculated from-the initial linear portion of the load extension plot) were determined.

7.3 Application of overload to test pieces.

The type of overload profile originally specified[51] by the CEGB is illustrated in Figure 4.10. Data from tensile tests indicated that the peak load required would be approximately 6kN. To apply loads in the order of 6kN in 3-4ms requires servo-hydraulic load application. A high hydraulic fluid flow rate was essential to give the required rapid crosshead movement. A Schenk 1136 servo-hydraulic fatigue machine with a hydraulic fluid flow rate of 80 Litres/min, located at the

CEGB, Bedminster Down, was the most suitable machine available, and was used for overload application. Load/time profiles were generated using an input signal from a DC "pulser", as the function generator on the Schenck 1136 could not provide a suitable function. The controls of the pulser enabled both rise time to peak load, and the duration of hold, to be varied. The peak load to be achieved was selected using the conventional Schenk 1136 load amplitude potentiometer. It was found that the pre-selected value of peak load was not usually achieved and hence preliminary experiments were carried out to establish a relationship between nominal and true applied load. This was facilitated by a digital display of peak load on the Schenk 1136 control panel. A load output signal was also provided. This signal was recorded using a Gould 1421 20 MHz digital storage oscilloscope, permitting an observation of the true load profile achieved.

Although the D.C. pulser was capable of generating signals identical to the profile illustrated in Figure 4.10, the hydraulic flow of the machine was insufficient to achieve a rise time to peak load of 3-4ms. After some experimentation the minimum rise time to peak load was found to be 8ms. The nominal overload profile which was adopted is illustrated in Figure 7.3. In order to apply this type of load to the test piece an input signal of shorter rise time and greater peak magnitude was necessary. The requisite input signal,

determined by experiment, is illustrated in Figure 7.4. The true load profile applied to the test piece was then recorded using the storage oscilloscope and a representative load/time trace is illustrated in Figure 7.5. The maximum strain achieved was measured using Micro-Measurements EP-08-250BG-120 metal foil strain gauges, a Measurement Group P-3500 bridge completion/amplification unit and recorded on the storage oscilloscope.

CEGB data suggested that a component might be subjected to many overloads during its 30 year life, and hence 50 overloads of the profile illustrated in Figure 7.5 were applied to each test piece. Any reference to "overloaded test pieces" in this report implies test pieces subjected to this treatment.

7.3.1 Investigation of the effect of number of overloads and overload magnitude on GFRP.

The rise-time, duration, magnitude and number of repetitions of a water hammer event are all variables which depend upon the system and the event causing the water hammer. Many complex combinations of event are possible, but an exhaustive experimental investigation was not the objective of this study. Some consideration of two of the variables, number of repetitions and magnitude, was carried out.

50 was adopted as the number of overloads a component would be subjected to in service. However, the effect of the number of overload repetitions was considered to be of interest. A short programme applying different numbers of overloads, of peak magnitude equivalent to 60% material UTUS, was carried out. Ten overloads were applied to each of 10 coupons of polyester material. A further group of 10 coupons recieved 30 overload repetitions, and then 50 overloads were applied to a 10 further coupons. These coupons were then retained for damage investigation and short term mechanical property tests.

The effect of overload magnitude was investigated with the overload duration [25 (±3)ms] and number of overloads (50) held constant. Groups of 10 coupons were treated with 50 overloads of peak magnitudes 30% and 60% UTUS. Polyester matrix material coupons were treated in this manner and retained for damage investigation and mechanical tests.

Summarising the various coupon pre-loads;

(i) 10 repetitions, magnitude-60%UTUS, 10 coupons.

(ii) 30 repetitions, magnitude-60%UTUS, 10 coupons.

(iii) 50 repetitions, magnitude-60%UTUS, 10 coupons.

(iv) 50 repetitions, magnitude-30%UTUS, 10 coupons.

(v) 50 repetitions, magnitude-60%UTUS, 10 coupons.

7.4 Residual strength of overloaded coupons.

The residual strength and residual modulus of coupons treated to the range of overloads described below were determined using an Instron 1195 testing machine fitted with a Wallace optical extensometer. Summarising the coupon pre-loads;

(i) 10 repetitions, magnitude-60%UTUS, 5 coupons.

(ii) 30 repetitions, magnitude-60%UTUS, 5 coupons.

(iii) 50 repetitions, magnitude-60%UTUS, 5 coupons.

7.5 Investigation of overload induced damage.

7.5.1 Reinforcement damage.

Sections, of coupon width and 50mm long, were cut from the coupons. The resin was then burnt-off in an oven at 550°C for 4 hours. The three layers of reinforcement were then separated with tweezers. The chopped strand mat (CSM) layers were first surveyed with a hand lens and then gradually teased apart by hand in a search for fibre breakages. Various methods of assessing fibre damage in the woven roving (WR) reinforcement have recently been considered by Bushby[74]. After considerable experimentation he developed the following technique. After separating a bundle of fibres from an individual roving it is subdivided into individual filaments by gently pulling filaments out of the bundle by hand. The length of the filament is compared with the sample length, and the number of short filaments or breaks counted. This method was adopted in this study. For each section of

roving at least 750 filaments were observed, and the number of broken filaments and any incidence of multiple breakages noted. The coupons observed in this manner had been subjected to the same overload pre-treatments as those described in section 7.3.1, allowing the effects of number and magnitude of overloads upon reinforcement integrity to be investigated. Two rovings from each of five coupons were observed for each type of overload pre-treatment. Five virgin coupons were also observed. Throughout this section only polyester matrix coupons were investigated.

7.5.2 Polished sections.

Two types of polished section were taken from polyester coupons as follows;

(i) Longitudinal section:-parallel to the 0° fibres (direction of applied tensile load), perpendicular to the plane of the laminate.

(ii) In-plane section:-parallel to the plane of the laminate.

Sections of this nature were taken from coupons previously loaded as follows;

(i) No pre-load, i.e. virgin material (for comparative purposes).

(ii) One overload of the type illustrated in Figure 7.5.

(iii) Fifty overloads of the type illustrated in Figure 7.5.

7.6 Effect of overload profile on reinforcement damage.

The load/time profile of an overload event has three components, rise time, time at peak load and time to return to zero load. In most cases the time to return to zero load and rise time are almost the same. In this section the effect on reinforcement integrity of a very slow rate of load application was compared with the high loading rate model water hammer event applied to the overloaded coupons. The effect of a dwell at peak load was also investigated. Three different load profiles were applied to five polyester matrix coupons as follows;

(1) Peak load applied: 60% UTUS, Load up and unload rate equivalent to a crosshead speed of 0.5mm/min on Instron 1195, dwell time at peak load: zero seconds. One repetition.

(2) Peak load applied: 60% UTUS, Load up and unload rate equivalent to a crosshead speed of 0.5mm/min on Instron 1195, dwell time at peak load: 10 seconds. One repetition.

(3) Overloaded coupons, i.e. Fifty repetitions of the load/time profile illustrated in Figure 7.5.

A 50mm section was then cut from each coupon, the resin burned off and the number of fibre breaks determined in an identical manner to that described in section 7.5.1.

7.7 Stress-rupture.

Stress-rupture testing was carried out in a themostatically controlled water bath at a temperature of 40°C. Static loads

were achieved by first order levers and dead weights. Test piece failure was defined as separation of test piece into two halves. This was detected by a microswitch activated by the excessive lever arm movement resulting from test piece failure. The microswitch then deactivated the electronic timer dedicated to that load station. Two stress-rupture curves were compiled;

(i) Glass fibre reinforced polyester test pieces previously subjected to fifty repetitions of the overload specified in figure 7.5.

Range of loads applied: 20-80% of the Ultimate Tensile Unit strength (UTUS) of the material, as determined in section 7.2.

(ii) Glass fibre reinforced vinyl ester test pieces previously subjected to fifty repetitions of the overload specified in Figure 7.5.

Range of loads applied: 40-70% material UTUS.

7.8 Low frequency fatigue testing.

Cooling water system components may be subjected to a low frequency sinusoidal fatigue load associated with tidal variations. The effect of this type of load on virgin glass fibre reinforced polyester laminates has been adressed in an earlier study[33], but neither the true service frequency nor the effect on overloaded test pieces were considered.

The apparatus used to apply this cyclic fatigue load is illustrated in Figure 7.6. The system consisted of a thermostatically controlled water tank with twenty loading stations. Load application was by pneumatic means with a separate pneumatic actuator at each loading station. Load was transferred to the test piece from the actuator by a system of first order levers. The load cycle was controlled by a four channel pressure controller and software run on a Commodore PET microcomputer. The four different pressure channels could be programmed separately providing four separate pressure profiles. Load stations could be connected to any of the four channels. Consideration of lever arm ratio, pneumatic diaphragm size and channel selection allowed several different load profiles to be applied amongst the twenty available load stations.

In this study test pieces were subjected to sinusoidal fatigue loads with an R ratio of 0.67 at a frequency of 23.15 μHz. This could be considered as a static load with a superimposed sinusoidal fatigue load of ±20% of the static load (see Figure 7.7). Both the R ratio and the frequency, equivalent to two cycles per day, exactly imitate the stress pattern arising from tidal variations.

Three sets of data were compiled using laminates of the reinforcement geometry illustrated in Figure 7.1 and of the test piece dimensions given in Figure 7.2. The three sets of

data differ in matrix type and mechanical pre-treatment as follows;

(i) Virgin vinyl ester matrix test pieces.

Mean load: 45% material UTUS.

(ii) Matrix: vinyl ester. Test pieces previously subjected to fifty repetitions of the overload illustrated in Figure 7.5.

Mean load range: 45-70% material UTUS.

(iii) Matrix: polyester. Test pieces previously subjected to fifty repetitions of the overload illustrated in Figure 7.5.

Mean load range: 30-70% material UTUS.

Failed coupons were observed and any trends in failure mode with load or time were noted.

CHAPTER 8.

RESULTS.

8.1 Quasi-static Tensile testing.

Load-extension plots for the virgin polyester matrix material illustrated a discontinuity or "knee" in the plot. This discontinuity was found to occur at strains of between 0.3 and 0.5% for the coupons tested. The values of unit modulus quoted below were determined from the initial linear portion of the plot. The ultimate tensile unit strength (UTUS) and unit modulus of the polyester matrix material were found to be 233.15(±21) N/mm per kg/m^2 and 19026 (±2793) N/mm per kg/m^2 respectively. The UTUS and unit modulus of the vinyl ester matrix material were found to be 237.16(±18) N/mm per kg/m^2 and 18501 (±1071) N/mm per kg/m^2 respectively.

8.2 Application of overload to coupons.

Following the first three or four load cycles the integrity of strain gauge to coupon surface adhesion was in doubt and hence measurements were limited to the strain achieved for the first overload. The mean maximum strain achieved for the first load application for the five coupons tested was found to be 0.77(±0.12)%. The modulus of the material during this dynamic loading phase was calculated to be 21801 N/mm per kg/m^2.

The type of macroscopic damage resulting from this type of load application was identical in both the vinyl ester and polyester resin matrix materials. Following the first load application transverse resin cracking and debonding were both evident as illustrated in Figure 8.1. Cracks were noted associated with the edges of the coupon but also in the bulk of the material. The transparent nature of the material allowed other observations of damage which could not be recorded photographically. For example cracking was always associated with the transverse fibre tows and usually at, or very close to, the centre of the tow. Material quality was very good and nearly all coupons were void free. In the very rare case of a macroscopically visible void, no cracks were observed to be associated with it.

During the subsequent overload applications existing cracks and debonds propagated. New sites of similar damage were also formed. After one overload cracks were not surface breaking but as these cracks progressed numerous sites of surface breaking cracks became evident. The propagation of damage in the first ten overloads was further confirmed by readily audible acoustic emissions. The total macroscopic damage after fifty overload applications was very similar to that after approximately ten overloads. Far fewer audible acoustic emissions were noted after the first ten overloads. In some cases damage was confined to distinct bands along

the gauge length (see Figure 8.2). These appeared to be associated with the transverse fibre tows of the woven roving mat. Other test pieces illustrated a more uniform distribution of damage (Figure 8.3).

The vinyl ester matrix material was more resistant to the propagation of damage. This is illustrated in Figure 8.4 which shows a comparison of two coupons, both having been subject to fifty overloads of 60% UTUS but of different matrix material. The amount of transverse damage exhibited by the vinyl ester matrix coupon is far less than that of the polyester matrix one. Damage propagation was clearly better resisted by the vinyl ester matrix material.

Figure 8.5 shows the effect of overload magnitude on transverse damage in polyester matrix material. The sequence of 30% UTUS overloads resulted in far fewer, and shorter, cracks than the 60% overloads. A similar effect was observed for the vinyl ester matrix coupons. In general the vinyl ester matrix material sustained less damage than its polyester counterpart.

8.3 Residual strength of overloaded coupons.

Values of residual UTUS and residual unit modulus for the polyester matrix material subjected to the various numbers of overloads described in Section 7.4 are summarised in Table 1. Results are also given for virgin material for

comparison. All of the coupons which had been treated with a number of overload cycles (minimum of ten cycles) exhibited continuous load-extension plots without the knee observed for the virgin material.

8.4 Investigation of overload induced damage.

8.4.1 Fibre break investigation.

Fibre fracture was not discovered in any of the overloaded coupons investigated, irrespective of the magnitude or number of overloads applied. The only fibre damage was found in one of the 5 virgin coupons. 6 fractured filaments were observed in a filament bundle from the very edge of the coupon. These were noted prior to any attempts at separation and were thus attributed to damage as a consequence of specimen preparation in the routing procedure. Virgin coupons were investigated as a control, to test the technique. As the only damage witnessed was explained by procedures prior to resin burn off, and no fractured fibres were found amongst the overloaded coupons, it was concluded that the technique detected fibre fractures due to pre-loading and not as a consequence of the technique itself.

8.4.2 Resin damage.

(i) Longtudinal section through polyester matrix coupon that had been subjected to one 60% UTUS overload.

A typical region of a polished longitudinal section is shown in Figure 8.6. All the cracks visible were associated with

the transverse fibre rovings and propagated into the matrix. The cracks were not associated with fabrication flaws such as voids as sections from virgin material were free of voids. A region of cracking within the transverse roving is shown in Figure 8.7.

(ii) In-plane section of polyester matrix coupon that had been subjected to one 60% UTUS overload.
Figure 8.8 shows the a region from the layer nearest the coupon surface. Cracks did not pass through the bundles of fibres associated with the CSM reinforcement. This was further evident after polishing down through the CSM layer of the same section.

(iii) Longitudinal section of polyester coupon subjected to fifty repetitions of the 60% UTUS overload.
A typical region of this section is shown in Figure 8.9. This shows extensive cracking originating from a transverse glass roving.

(iv) In-plane section of polyester coupon subjected to fifty repetitions of the 60% UTUS overload.
An optical micrograph is illustrated in Figure 8.10. Here a crack similar to that depicted in Figure 8.8 has propagated into the resin around, and within, a CSM fibre bundle. It is noteworthy that individual filaments appear undamaged.

8.5 Effect of overload profile on reinforcement damage.

The percentage of broken fibres found in each of the five coupons subjected to each of the three different load profiles described in section 7.6 are shown in Table 2. This table indicates that overloaded coupons suffer no fibre breakages, the slow rate load up and unload results in 16% of the fibres being fractured, and the additional dwell time of 10s after the slow rate of load up resulted in 32% of the fibres observed being fractured.

8.6 Stress-rupture.

Stress-rupture test results are plotted on graphs of $\log_{10}$ time to failure against load (represented as a percentage of the UTUS) and are illustrated in Figures 8.11-8.13. Figure 8.11 illustrates a linear regression analysis of all the failed overloaded polyester matrix coupons. At the conclusion of the project some test pieces were still under load ("runouts") and figure 8.12 includes four such coupons at 20% UTUS. Figure 8.13 is a similar plot for overloaded vinyl ester matrix coupons including both failed coupons and runouts. A "best-fit" to these data was also obtained by linear regression analysis. The stress coordinate corresponding to a time to failure of thirty years and the correlation coefficient of the linear regression for each of the stress-rupture "curves" are compiled in Table 3.

8.6.1 Observed features of failed coupons.

(1) Polyester matrix material coupons.

At stresses above or equal to 50% UTUS failed coupons appeared very similar with large areas of delamination between CSM and WR layers associated with the fracture zone. Fracture surfaces also exhibited large amounts of fibre pull-out from the longitudinal WR reinforcement. Two, representative, failed coupons from the 50% UTUS stress level are shown in Figure 8.14. Little difference was exhibited from coupon to coupon irrespective of the time under load. Some difference was seen at the 40% and 30% UTUS stress levels where far less delamination or fibre pull-out were evident for the groups as a whole, in comparison to the 50% load level. This effect was further emphasised at the 20% UTUS stress level and two coupons are shown in Figure 8.15. These coupons have clearly distinguishable fracture surfaces with little delamination behind the fracture surface and exhibit greatly reduced fibre pull-out in comparison to the 50% UTUS failed coupons.

(2) Vinyl ester matrix material coupons.

Similar trends and features were noted to those reported for the polyester material. Figure 8.16 shows vinyl ester matrix coupons from the 55% UTUS load level exhibiting extensive delamination and fibre pull-out. Two coupons from the 40% load level are shown in Figure 8.17. The appearance of the fracture surfaces are somewhat different from Figure 8.16,

with a more clearly evident fracture surface, less delamination and far less fibre pull-out.

8.7 Low frequency fatigue tests.

Fatigue data are plotted as mean stress against number of cylcles to failure (S\N curves) with $\log_{10}$ time to failure also on this axis. Figure 8.18 includes runouts for overloaded polyester matrix coupons. Figure 8.19 shows results and runouts for both virgin vinyl ester and overloaded vinyl ester coupons. Failed coupons at all load levels were similar in appearance with extensive fibre pull-out and delamination bewteen WR and CSM layers.

CHAPTER 9.

DISCUSSION OF RESULTS.

9.1 Quasi-static tensile tests.

The results from this section demonstrate that the material fabricated is of comparable tensile strength to that used in previous studies[33] which are used for comparison in the data analysis.

9.2 Overload application.

The load profile adopted (Figure 7.5) does not exactly match that which was originally specified (Figure 4.10). However, the profile of a water hammer event is greatly dependent upon the system dimensions and operating parameters. Consultation with CEGB engineers[75] established that water hammer events of the profile adopted are plausible in power station cooling water systems.

9.2.1 Macroscopic damage resulting from overload application.

Consider the damage occurring after one repetition of the 60% UTUS overload cycle. The type of damage in both vinyl ester and polyester matrix materials was almost identical, always being associated with the transverse fibre tows of the woven roving reinforcement. In most cases this was found at the centre of the roving. Cross over points between warp

and weft rovings are regions of considerable roving distortion and result in a high stress concentration arising when then longitudinal tow straightens under load application. The centre of a tow is most affected by this, which may explain the prevalence of cracks at the centre of the transverse rovings.

Manufacturers data indicate that the elongation at break of cast vinyl ester and polyester resins are 5.0 and 2.5% strain respectively. Both these values are in excess of the 0.77(±0.12)% achieved in the overload application. Consequently it would not be expected for resin cracking to occur as a result of overload application. Damage therefore appears to be associated with the transverse reinforcement and may occur as a consequence of the phenomenom of strain magnification. This occurs where a laminate is loaded perpendicular to the fibre direction. The difference in moduli of fibre and matrix result in a non-uniform strain distribution and consequently a non-uniform stress distribution. The polished sections further confirm that cracking initiates at or within the transverse reinforcement. Figure 8.6 illustrates that after one overload cycle cracks have initiated at the transverse rovings. Several cracks originate from one tow and then act as a sharp notches from which cracks propagate into the surrounding matrix. Cracks were also seen (for example see Figure 8.7) within the bundles of fibres which constitute

the tow after one overload cycle, further evidence associating damage initiation with the transverse rovings.

Both polyester and vinyl ester matrix materials behaved in a similar manner in regard to damage type. The vinyl ester material, however, sustained less total damage after the sequence of fifty overloads. The vinyl ester resin has a greater fracture toughness than the polyester resin, and therefore has more resistance to crack propagation under identical load conditions. Irrespective of the initiation of a crack, which is likely to be very similar in both laminates, the vinyl ester matrix affords greater resistance to crack growth within the resin.

Not surprisingly the overload cycles at 30% UTUS had a less detrimental effect than those at 60% UTUS. However, damage type was identical and readily evident on a macroscopic scale. Both the number of sites of cracking and the extent of crack growth were less at the 30% UTUS overload level. This suggests that the stress, or energy, to initiate transverse damage is different at different places in the laminate. As a result fewer initiation sites are activated at lower load levels. Crack growth and therefore total damage after fifty overload cycles is therefore reduced due to the reduction in initial damage and a reduced driving force for crack propagation. One can only speculate as to the nature of the sites of initial cracks. If initial cracks

were the consequence of poor wetting it would be expected that all sites would require the same energy (ie same stress) to initiate a crack. This was not found to be the case with fewer sites of transverse cracking at the lower stress level (30% UTUS). Also, poor wetting or fabrication flaws were not observed during the microscopic investigation.

If the nature of the bonding between the fibre and resin was chemical[76] and involved covalent bonds across the interface, a plausible explanation may be as follows; The orientation of fibre-coupling agent-resin bonds will not be exactly the same along the length of a given fibre or bundle of fibres. When a stress is applied the stress applied to interfacial bonds oriented parallel to the maximum applied stress will be be equivalent to the maximum stress. Bonds at other angles will witness components of this maximum stress of a magnitude dependent upon their orientation. This chemical bond will have a finite strength and therefore at a given stress some of these bonds will be broken. At lower stresses fewer bonds will be orientated such that the component of the applied stress they witness is in excess of the bond strength and fewer bonds will be broken, consequently fewer sites of cracking would be initiated. A similar explanation may be possible on a basis of the strain limit of the interfacial bond, which will also depend on the orientation of the applied stress to the bond.

Two types of transverse crack distribution were observed, banded (Figure 8.2) and uniform (Figure 8.3). In effect they differ in crack spacing and crack density per unit area. Garrett and Bailey[77] have found that increasing the thickness of the transverse ply resulted in an increase in transverse crack spacing when 0/90 GFRP material was loaded and unloaded at quasi-static loading rates. There is no equivalent tranverse ply in the coupons used in this project as all the transverse continuous reinforcement is found in the one layer of woven roving. All coupons were nominally identical, although some variation in the degree of crimp in a given sheet of WR reinforcement may account for the variation between banded and uniform crack distributions. It is also worth noting that in the subsequent static and dynamic fatigue tests on overloaded coupons, no pattern emerged relating either damage mode to short or long times to failure.

9.2.2 Overload induced microscopic damage.

Referring to Table 2 it is evident that no fibre breakages were found in coupons subjected to the full fifty repetitions of the 60% UTUS high rate overload. There are two possible explanations for this. Firstly, that this was due to the enhanced mechanical properties of glass fibres at high loading rates as reported in chapter 4. Secondly, it could be argued that the maximum stress was not great enough

to cause any fibre fractures. The latter cannot be true because a single application of the very low strain rate overload, identical in magnitude to the high rate overload, caused 16% of the fibres to be fractured.

The strain rate applied to the coupons in the high loading rate overload was in the region of 60%/s, above the 8%/s at which Armenakas et. al.[53] encountered increased breaking strengths for glass fibres. This rate also falls within the regime for which enhanced breaking strengths of glass fibre composites were reported in Chapter 4[58,60]. Therefore, it is probable that the absence of fibre fractures was a consequence of the enhanced failure strength exhibited by glass fibres at high rates of load application.

Of interest here is also the dynamic modulus measured for the first coupon overload. Much of the literature discussed in Chapter 4 reports an increase in modulus for glass fibre composites at high loading rates. The dynamic tensile modulus calculated from the load up phase of the overload event was estimated to be 21801 N/mm per kg/m^2. This lies within one standard error of the modulus calculated from the quasi-static tests, 19026 (±2793) N/mm per kg/m^2. Therefore, the load up phase of the overload event did not result in an enhancement of the modulus. The most informative and relevant of the studies taken from the available literature, carried out by Harding and Welsh[63], used woven roving

reinforced polyester material similar to that considered in this thesis. In tests to failure they found increases in tensile modulus with increasing strain rate as shown in Figure 9.1. The graph shows that discernable increases in modulus were only evident at strain rates above 100%/s. This provides evidence that the rate of load application in the coupon overload was just below the level at which increased modulus would have been exhibited. In summary the loading rate was high enough to stimulate enhanced strength in the reinforcement, but not quite high enough to induce an enhanced tensile modulus.

The 10s dwell at peak load following the slow load up also had an effect with 32% of the fibres fractured, twice as many as had fractured as a consequence of a slow rate of load application. Evidently maintaining a constant stress in addition to the slow load up rate (in the order of 0.01%/s) is even more damaging to reinforcement integrity.

Although it was only possible to examine the extremes of overload profile parameters two trends are evident. Firstly long load up times (in the order of seconds) result in greater reinforcement damage than load up times in the order of milliseconds. This has some consequences for the designer of a CW system component. It implies that transient overloads other than water hammer with slower rates of load

application may be more detrimental than the short duration dynamic events with which this thesis is mainly concerned.

The increased reinforcement damage as a consequence of the dwell at peak load also requires consideration. The time at this peak load for a given water hammer event is dependent upon how far the pressure pulse has to travel before being reflected (see section 4.1). This is a function of the system design and although dwell times of 10s would be unusual it seems advisable to minimise the time at peak load of any possible water hammer events by design.

9.2.3 Post-overload residual mechanical properties.

The data shown in Table 1 (polyester matrix material only) demonstrate that irrespective of the number of overloads or overload magnitude the residual UTUS of the overloaded coupons was the same as the UTUS of virgin material (i.e lay within one standard error of the UTUS of virgin material). Tests to ultimate strengths upon this sort of material depend upon the strength and amount of the reinforcement. A reduction in this ultimate property would be produced only by damage to the reinforcement. The transverse resin cracking and debonding are damage states which a virgin coupon will pass through en route to failure and will thus have no effect upon the ultimate breaking load of a coupon in a quasi-static test. The burn off experimentation discussed in section 9.2.2 revealed that an overloaded

coupon sustained no fibre breakages and therefore it is not surprising that the residual UTUS of an overloaded coupon was the same as one of virgin material.

The unit modulus of the overloaded coupons has however been reduced in comparison to the virgin material. The load-extension curves of virgin and overloaded coupons were clearly different. The virgin material exhibited a two component curve, with the so called "knee" evident at strains of betwween 0.3 and 0.5%. This behaviour has been discussed by several authors[78-81] and it is generally accepted that the knee corresponds to the point at which transverse debonding occurs in both woven roving and 0/90 reinforced GFRP laminates.

The data in Table 2 also shows that both thirty and ten repetitions of the overload result in modulus reduction. In fact the residual unit moduli of overloaded coupons treated with ten, thirty and fifty overload cycles are the same (to one standard error). This suggests that most of the damage occurs during the first ten overload cycles or perhaps even fewer. The impression is confirmed both by macroscopic damage observations and by the occurrence of most of the audible acoustic emmissions in the first ten overloads. The implication is very significant. One or two water hammer events, generating 10 overload cycles of this nature, will generate as much damage, and have as deleterious an effect

upon the component performance, as would a sequence of many events which might intuitively be thought to be worse.

9.3 Stress-rupture.

9.3.1 Polyester matrix coupons.

Stress-rupture data for coupons subjected to the overload described in section 7.3 are plotted in comparison to data for virgin material, of identical reinforcement geometry and matrix, from the work of Crowther in Figure 9.2. This illustrates that overload application results in reduced test piece lifetime as compared with virgin material. Applying a simple linear regression analysis to the overloaded coupon data illustrates that static loads in excess of 10% material UTUS would result in component failure prior to the designated thirty year ($\log_{10}$=8.97) lifetime (without any safety/design factor).

The reduced time to failure for overloaded coupons may be attributed to two factors, one being the damage occurring as a result of overload application, and the other being the degradative effect of the environment.

First consider the damage resulting from the overload application. Transverse resin cracking and debonding have been noted as stages in the damage accumulation process en route to static fatigue failure by Crowther[33], amongst others. Crowther carried out in-situ observations and

documented the progression of macroscopic damage under static load up to the point of failure. In all test pieces transverse damage was noted prior to failure, providing evidence for the theory that overload application simply reduces coupon lifetime at a given load by the time it would have taken to reach that state of damage at that load. This is likely to be the case at loads above or equal to 50% UTUS where the time under load is shorter than the time necessary for the environment to diffuse into contact with, and chemically degrade, the reinforcement. Support for this idea is provided by the nature of failed coupons at 50% UTUS (see Figure 8.14) and above, which resemble quasi-static failures with large areas of delamination and long fibre pull-outs and show no evidence of environmental damage.

Secondly consider the combined effect of the environment and the damage occurring as a consequence of overload application. It is plausible that such damage may provide a rapid path for water ingress and accelerate the onset of chemical degradation of the reinforcement. This would result in a two fold failure mechanism, comprising mechanical damage and environmental attack.

The basis of such a mechanism is simple. At high loads (for example 50% UTUS and above as discussed) the reduction in time to failure as a result of overload is purely a

consequence of the overload induced damage and is unrelated to the environment in which tests are being carried out.

At lower loads the environment will have penetrated the matrix and will start to degrade the reinforcement earlier than would be normally expected at this load. In such circumstances environmental attack of the fibres will commence earlier than in tests on virgin material. Figure 8.15 shows some failed 20% UTUS load level coupons. In all cases the fracture surface is planar and exhibits practically no delamination or fibre pull-out. This is a result of environmental attack with many fibres degraded prior to test piece failure.

9.3.2 Vinyl ester matrix coupons.

Figure 9.3 shows a linear regression analysis of the overloaded vinyl ester matrix coupons in comparison to some data from a previous study[82] on virgin material of very similar reinforcement geometry and identical matrix resin. As with the polyester matrix material the overload has a detrimental effect reducing the predicted failure stress for thirty years from 40% UTUS in virgin material to 36% UTUS for overloaded coupons. The nature of failed coupons at short lifetimes is very similar to the polyester matrix materials. For example Figure 8.16 illustrates failed coupons from the 55% load level which exhibit extensive delamination and fibre pull-out. At the lowest load level

investigated in this study, 40% UTUS, the failure follows the environment dominated mode described earlier as illustrated in Figure 8.17. The discussion concerning failure modes and environment, expanded above for polyester matrix material, evidently holds true for the vinyl ester matrix coupons.

9.3.3 Comparing overloaded vinyl ester with overloaded polyester.

Having established that the model overload applied to coupon test pieces results in a reduction in time to failure compared to virgin material, attention is now turned to the effect, if any, of the different matrices upon the long term behaviour of the laminate under constant tensile load. Figure 9.4 shows the two linear regression lines for overloaded vinyl ester and overloaded polyester coupons. The two lines intersect and it appears that polyester coupons exhibit longer lifetimes at high loads. At such short lifetimes (< 3hours) the scatter in times to failure has its greatest and most misleading effect. If the region after the intersection is considered the vinyl ester material clearly performs better than the polyester material. There may be three reasons for this. Firstly, the vinyl ester coupons were reported to have sustained less damage following the sequence of fifty overloads than the polyester coupons. If only a dry damage accumulation mechanism was in action, the vinyl ester coupons could be considered to have sustained

less damage en route to failure than polyester coupons following the same failure mechanism. Consequently, an overloaded vinyl ester coupon would have a greater portion of its life remaining, and hence exhibit longer times to failure, than an overloaded polyester coupon under the same static load.

Secondly, it was suggested in the discussion of overload induced damage progression, that the tougher vinyl ester resin affords a greater resistance to crack growth than the less tough polyester resin. This is also relevant here, as under constant load a driving force is present for overload induced cracks to propagate. A tougher resin whilst not resisting damage initiation should however resist crack propagation. Babic, Dunn and Hogg[83] found this to be the case in a series of impact tests on glass reinforced composites with various matrices. They found that residual short term mechanical properties were unaffected by increased resin toughness. However, the tougher resins resulted in a reduced area of visible damage, demonstrating that tough resins resist damage propagation. This should be the case for virgin as well as damaged material. Data reported by Heppell and Phillips[82] provides evidence that virgin vinyl ester matrix material survives to longer lifetimes than virgin polyester matrix material of identical reinforcement geometry loaded at the same stress levels.

Thirdly, there is the effect of the environment. The vinyl ester material sustained less damage following overload application. Therefore,the reinforcement, which ultimately must be damaged for coupon failure, is better protected from the degradative effects of the environment. The tougher matrix may also afford some resistance to crack proapagation occurring due to the combined effect of stress and environment, commonly known as stress-corrosion cracking. Evidence to support this is reported by Hogg, Hull and Price[84]. In tests carried out in an aqueous acidic environment the material with the toughest resin matrix was found to exhibit the lowest rate of crack growth.

In summary the vinyl ester matrix material offers three advantages over its polyester counterpart as follows:

(1) Greater resistance to crack growth under constant load.

(2) Greater resistance to overload induced damage propagation under constant load.

(3) Provides reinforcement with more post overload protection from environment as a consequence of sustaining less damage during overload application.

9.4 Low frequency fatigue testing.

9.4.1 Polyester matrix material.

Overloaded coupons tested under this load regime have been subjected to all components of a cooling water system load profile except periodic unloads and are therefore of

particular interest. Linear regression analysis of data plotted in terms of maximum stress are illustrated in Figure 8.18. This indicates that the load corresponding to thirty years service is 31% UTUS, somewhat in excess of the 10% UTUS adopted as the design load in present CEGB applications. In the absence of data from tests at this frequency on virgin material, the effect of low frequency fatigue loading upon the overload induced damage cannot be determined.

A comparison of the effect of a static load, the low frequency fatigue load and their interactions with the damage resulting from the overload, is possible as in both cases identical overloaded polyester coupons were used. The first problem is to decide upon what stress level to compare the two sets of data. For the static load scenario there is only one load, whereas under a sinusoidal load regime there are three options. Figure 9.5 shows the three methods of plotting the fatigue data and a regression line for statically loaded coupons. Evidently there is no "correct" method to compare static and cyclic fatigue data. In this study, a given static load (stress-rupture) will be compared with the maximum load occurring under the low frequency fatigue regime. This treats the cyclic load regime as if it were a series of unloads from a maximum load, which is equal to the static load applied under stress-rupture loading conditions.

Having adopted this as the method of comparison, it is evident from Figure 9.6 that at times beyond $\log_{10}$=1.75 the fatigue loading regime results in longer lifetimes at a given load. Such results imply that at high stresses the fatigue loading regime results in a greater rate of damage (resulting from the overload) propagation than the monotonic stress-rupture load. Conversely, at low loads, the damage propagation by creep alone is more detrimental than the cyclic fatigue mechanism. This is the opposite effect to that reported by Crowther, Wyatt and Phillips[34]. Their study followed similar lines to that described in this section using identical material but on virgin, non-overloaded coupons and carrying out their fatigue tests at a frequency of 0.0083Hz, low in comparison to most other studies but considerably higher than the 23.15μHz of tests described in this thesis. The two studies only differ in frequency of fatigue load and in overload application. The differences in results must therefore be a function of one, both, or a combination of the two.

9.4.2 Vinyl ester matrix material.

Results for both virgin and overloaded coupons are shown in Figure 8.19. Although a complete S/N curve was not generated for the virgin material a useful comparison between the behaviour of virgin and overloaded coupons under low frequency fatigue load conditions can be made. Consider the

45% UTUS load level where results for 5 virgin coupons are shown. Comparing these with the results for the 5 overloaded coupons it is obvious that the overload causes a reduction in coupon life at that load.

Also of interest here is a comparison of the overloaded polyester and vinyl ester coupons. Figure 9.7 shows results for polyester and vinyl ester materials plotted on the same axes. At the 60% and 47% UTUS load levels the vinyl ester material clearly survives to longer lifetimes than its polyester counterpart. At 45% UTUS the two sets of data merge. Evidently more tests at the lower load levels are necessary to make reasonable comparisons.

PART 3

PIPE TESTING PROGRAMME

CHAPTER 10.

Experimental.

10.0 Objectives.

The major aims of this part of the experimental programme were as follows;

(i) To design a model component (a pipe) of the type found in a cooling water system in GFRP and provide mechanical testing data on this reduced scale version of a real component.

(ii) To obtain stress-rupture data for the pipe test pieces.

(iii) To investigate the effect of a true water hammer event on the model GFRP pipe.

(iv) To determine the effect of a sequence of ten true water hammer events, peak magnitude 23(±1) bar, on the stress-rupture life of GFRP pipes.

10.1 Design and Fabrication of pipe sections.

Designing pipes of a specified pressure rating with a homogeneous material applies the formula for hoop stress. This calculation establishes the circumferential stress in the pipe wall material and depends upon the operating pressure, pipe diameter and pipe wall thickness. The value obtained can then be compared with the failure stress of the candidate materials and the pipe wall thickness adjusted

accordingly. With a composite material such as GFRP thickness is not exactly proportional to strength. Laminates of identical reinforcement content may vary in thickness and fibre volume fraction. It is more rigorous to consider strength of GFRP in terms of the amount of reinforcement present. This is accounted for in BS 4994 by the parameter U_Z, the design unit loading, defined as "the load permitted to be applied to a reinforcement type, per unit width, per unit mass of reinforcement." The unit of U_Z is the N/mm per kg/m^2 glass.

In accordance with CEGB practice the pipes for use in this section were designed in accordance with BS 4994. Although power station cooling water system pipes may be of the order of metres in diameter, test equipment limited the internal diameter of test pipes to 151mm. Various reinforcement geometries and densities were considered to achieve a pipe with a design operating pressure in the 3-4 bar region. This figure takes account of a safety or design factor which at present is taken as ten for CW system applications. Therefore, the theoretical burst pressure of a pipe designed to 3-4 bar would be 30-40 bar. A mixed wall composition was desirable to reflect present CEGB component construction. The arrangement selected is given in Figure 10.1. An additional advantage of adopting this reinforcement geometry and matrix resin type is evident if Figures 7.1 and 10.1 are compared. The laminate construction of both pipe and coupon

were very similar and this allowed a fair comparison of pipe and coupon tests.

The pressure rating of the pipe was calculated using equation 6 taken from BS 4994. Although this is analagous to a hoop stress calculation, the absence of a term for pipe wall thickness is noteworthy.

$$Q_m = pD_i/2 \qquad \text{(EQUATION 6)}$$

where, Q_m is the maximum circumferential unit load in N/mm, D_i the internal diameter in mm and p the total effective pressure in N/mm^2.

The parameter Q_m can be calculated from the minimum ultimate tensile unit strength for each of the types of reinforcement. This is designated by BS 4994 to be 200 N/mm width per kg/m^2 glass for CSM and 250 N/mm width per kg/m^2 glass for WR. The reinforcement cloth weights selected result in a pipe rated at a pressure of 42.4 bar (see Appendix B). Applying the design factor of 10, used by the CEGB, results in a pipe with a design operating pressure of 4.24 bar.

The longitudinal seam created when fabricating a pipe from discontinuous reinforcement was considered a potential problem, especially in the woven roving layer. To overcome

this each layer incorporated an overlap in the reinforcement. The three overlapped seams were also staggered around the pipe. Consultation with manufacturers confirmed this to be a common practice of little consequence.

Each pipe section required a method of attachment to the test equipment. Stub flanges of the dimensions stipulated in BS 4994 were adopted as the most universally compatible with the various rigs used. These were built into the pipe during the fabrication stage.

Fabrication of 0.75m pipe sections conforming to the specification given above was carried out by Plastics Design and Engineering Ltd. A summary of pipe design data and a photograph of a pipe are shown in Figure 10.2.

10.2 Determination of burst pressure of GFRP pipes.

Burst tests were carried out using the apparatus illustrated in figure 10.3. Initially pipes under test were filled with water prior to gaseous pressurisation, the so-called "hydro-pneumatic" method of pressurisation. However, this resulted in gasket "blow-out" before the pipe burst pressure. After some experimentation the most successful system incorporated full face rubber gaskets, end plate retaining bolts torqued to 13.6Nm and a purely gaseous method of internal pressurisation.

Six pipes were tested in total. The rate of internal pressurisation was set to the minimum value on the pressure regulator. The rate achieved was approximately 0.7 bar/s. The ambient temperature was measured for each test. On three pipes the hoop and axial strain were monitered using WFLA-6-IL-17 strain gauges, Fylde FE-492-BBS quarter bridge completion units, Fylde FE-251-GA amplification modules and a chart recorder. Strain gauge positioning is illustrated in Figure 10.4.

10.3 Development of a method for the application of a sequence of controlled water hammer events to GFRP pipes.

The aim of this section of work was to achieve a water hammer pulse of similar load profile to the overload applied to the coupon test pieces, and apply it to the GFRP pipe sections described in section 10.1.

10.3.1 Description of rig and control parameters.

The equipment used was located at the British Hydromechanics Research Association (BHRA). The major components of the rig are illustrated in Figure 10.5. Operating procedure was relatively simple. After bolting the test section(s) in position the system was filled with water and the valve at the downstream end closed. Water was then drained from the cavity section to create a region of free space (the cavity) of known volume. The air from this section was then

evacuated with a vacuum pump. The downstream valve was then opened resulting in a very rapid flow of water into the cavity section. This flow was halted on reaching the end of the cavity section resulting in the propagation of a pressure pulse along the length of the rig, through the test section, and reflecting at the surface of the reservoir at the upstream end.

The three parameters under the control of the operator were, the height of water in the reservoir at the upstream end, the volume of the cavity at the downstream end and the duration of time taken to open the valve ("valve opening time").

The height of water in the reservoir was monitored by a transparent sight tube. In this text values of the corresponding head of pressure are quoted.

The depth of water in the cavity (analagous to volume) was determined using a point gauge. Access to the cavity section was facilitated by a sealable inspection orifice approximately 20mm in diameter. The bottom of the pipe was set as the datum of the point gauge scale and water depth measurements made relative to this. The volume of free space above was then calculated from cavity section dimensions.

Prior to any experimentation it was evident that the following parameters influenced the profile of the pressure pulse achieved;

(i) Volume of cavity (monitored in experiments by depth of water in cavity).

(ii) Height of reservoir at upstream end.

(iii) Duration of downstream valve opening time.

(iv) Time for pressure pulse to traverse system (i.e. Length of system and wavespeed in steel and GFRP).

It was immediately apparent that the valve opening procedure, previously a manual operation, could introduce variabilty into experiments requiring more than one pressure pulse. A hydraulic actuator was therefore fitted to ensure repeatable valve opening times. The actuator selected permitted valve opening times between 100 and 500 ms and the hydraulic control valves were set to produce a minimum valve opening time. Although the exact valve opening time was not determined, it was sufficient for it to be the minimum possible and most importantly repeatable.

10.3.2 Development of a sequence of controlled water hammer events.

Section 10.3.1 summarises the mode of operation and the parameters under the control of the operator. It was now necessary to manipulate these parameters to achieve a sequence of water hammer events approaching the required profile as closely as the equipment permitted. Results from

previous work[85] on GFRP pipes carried out with this rig were available, but provided little assistance. Developing a sequence of suitable events was therefore an involved process and some consideration is given to it in the following sections.

Initially the following points required clarification;
(i) Whether pressure pulses of the requisite magnitude and load profile could be produced repeatably.
(ii) Whether two test sections connected in series would be subjected to the same pressure pulse (i.e. that there was no attenuation of the pressure pulse as it traversed the rig).

Some pilot experiments were therefore necessary to address these points. To this end a four phase sequence of experimentation was carried out as follows;
Phase 1: Installation of hydraulic valve actuator and commissioning of rig with steel test section. This stage was principally concerned with the assessment of the effectiveness of the valve actuator, gaining experience of control parameters and looking at any attenuation of pressure magnitude as the pulse passed through the test section. All of these points could be quickly assessed with a steel test section and thus this was adopted for phase 1.
Phase 2: Tests with GFRP test sections. Following the initial experimentation with the steel test section some development work was required using GFRP pipes to ensure

that the system worked in practice and that events of the desired type could be produced.

Phase 3: Tests with instrumented GFRP test sections. In applying controlled water hammer events to the GFRP pipes prior to stress-rupture, pressure was to be monitored in the steel sections adjacent to the GFRP pipes. This required a knowledge of the relationship between the pressures measured in GFRP and steel. It was also necessary to determined strain and pressure response in the GFRP pipe wall.

Phase 4: Applying a sequence of controlled water hammer events to the GFRP pipes prior to stress-rupture.

10.3.3 Commissioning rig with steel pipe section.

Following the installation of the hydraulic valve actuator the rig was operated with a steel T-piece test section incorporating four Data Instruments SA PSIS pressure transducers as illustrated in Figure 10.6. The objective here was to observe the shape and duration of the pressure pulse produced, determine its reproducibility and establish the effect of the parameters under the operators' control, such as cavity volume and reservoir height, upon the pressure pulse profile. The positioning of the pressure transducers was selected in order to observe the variation in pressure pulse profile along the test section and from top to bottom of the pipe. Data from the pressure transducers was recorded using an Amstrad PC1640 HD20 computer. The data acquisition software permitted

observation of both pressure/time traces and numerical pressure values.

10.3.4 Investigation of the reproducibility of a pressure pulse at constant reservoir height and constant cavity volume.

After filling the rig with water, cavity volume and reservoir height were set to known values. The downstream valve was then opened allowing a pressure pulse to traverse the system. This procedure was then repeated several times using the same cavity volume and reservoir height. Typical pressure as a function of time profiles recorded at the four pressure transducers are illustrated in Figures 10.7-10.10, with a summary of the contents of each Figure in Table 4. The data in Table 4 demonstrate that there is very little variation in the peak pressure recorded as the pressure pulse traverses the test section. The peak magnitude achieved for 5 consecutive events, resulting from nominally identical cavity volumes and reservoir heights are illustrated in Table 5. This shows that reproducible events of peak pressure 21.68(±0.32) bar can be produced. Important here is the variation from the mean of less than 0.5 bar.

In Figures 10.7-10.10 the profile of one pressure pulse recorded at each of the four pressure transducers is depicted. Each figure illustrates the processed data from two pressure transducers. Figure 10.7 shows a comparison

between the two pressure transducers along the the top of the test section, illustrating that the profile of the pressure pulse changes little as it travels along the test section. Figure 10.8 illustrates the pressure pulse profiles obtained from the two pressure transducers positioned on the underside of the test pipe which are also very similar. Figures 10.9 and 10.10 illustrate the pressure pulse profile obtained from two pressure transducers at the same point (i.e. distance along the test pipe), but comparing the pressure transducers on the top and the underside of the pipe. Not surprisingly these two traces were almost identical.

The general shape of the pressure pulse was also of interest with no clearly defined flat top region in evidence. The total event time was approximately 50-60ms with a rise time to peak load in the order of 20-30ms. It was considered that the pressure pulse achieved approached the original specification (see Figure 4.10) in terms of event duration and magnitude. Although the event duration was approximately double that applied to the coupon test pieces, the events were comparable in terms of magnitude. Comparisons were therefore possible between coupon and pipe test programmes.

10.3.5 Investigation of the effect of cavity volume on pressure pulse profile.

The reservoir height was then maintained at a constant value and pressure pulses recorded as a function of cavity volume. The variation in peak pressure with increasing cavity volume, at constant column height, is shown in Figure 10.11 illustrating that peak pressure is approximately proportional to cavity volume over the range investigated.

10.3.6 Investigation of the effect of reservoir height on pressure pulse profile.

Cavity volume was then held constant and pressure pulses recorded as a function of reservoir height. The data from this experiment are plotted in figure 10.12. The graph illustrates that the peak pressure achieved at constant cavity volume is almost independent of reservoir height. This is not surprising when the Joukowski water hammer equation is considered;

$$\Delta H = -\delta V a/g \qquad \text{[Equation 5]}$$

where; ΔH = change in pressure, δV = change in fluid velocity, a = acoustic speed in pipe wall and g = the acceleration due to gravity.

This equation (derived in appendix A) illustrates that the magnitude of the pressure pulse is dependent upon the change

in velocity of the water and the acoustic velocity in the pipe wall material, but not the initial head of pressure.

Reservoir height would however be expected to affect the profile, or more specifically the dwell time at peak load, of the pressure pulse. Larger heads of pressure effectively increase the length of the system. The pressure pulse will therefore have a longer uninterrupted water system to traverse and hence the duration of time at the peak pressure would be increased by larger reservoir heights. However, the range of column heights considered in this study have a negligible effect on event duration.

10.3.7 Preliminary tests with GFRP pipe sections.

In the application of pressure pulses to the GFRP pipe sections it was proposed to connect two pipes in series in the test section. The test section was positioned between two immovable steel pipe sections with full face flanges. The two GFRP pipes were joined using two pairs of split rings. Two, 3mm thick, neoprene rubber gaskets smeared with petroleum jelly were positioned between the two pipes to achieve an adequate seal. One end of the GFRP pipe assembly was then attached to the full face flange at one end of the test section using split rings. Double gaskets were again used at the flange-GFRP pipe interface. The GFRP pipe assembly was supported throughout this, and subsequent assembly operations. Separate steel mating pieces were then

attached to free ends of the GFRP pipe assembly and the rig. A Viking-Johnson coupling (see Figure 10.13) which fitted over the mating pieces in a sleeve like manner, was used to make the final connection. The arrangement is shown in figure 10.14. It was thought that the Viking-Johnson coupling might apply some tensile load to the test section when tightened, and this was checked as described below.

Initially two pipes without instrumentation were set up in the test arrangement. The calibration curve obtained with the steel test section (Figure 10.11) was consulted and a cavity volume selected corresponding to a pressure of 24 bar (60% of pipe design pressure). A sequence of nine water hammer events were applied to the GFRP pipes. The results are shown in Table 6 and demonstrate that seven or eight events were required to achieve the expected peak pressure. This was caused by entrapped air. After considerable effort it was found possible to reduce this problem, but not eliminate it.

10.3.8 Instrumented GFRP pipe tests.

The instrumented GFRP pipe tests needed to address the following points.

(i) Record the pressure pulse in the steel pipe immediately before and after the GFRP sections, to measure any attenuation in pressure resulting from the GFRP section or the couplings.

(ii) Record the pressure pulse in both the GFRP test sections and the steel mating pieces thus establishing a relationship between the two.
(iii) Measure the static strain in the GFRP pipes due to the experimental arrangement (i.e. measure any effect of the Viking-johnson coupling).
(iv) Measure the strain achieved in the GFRP pipes during the passage of a pressure pulse of known magnitude.
In order to address these points the test section was set up with the arrangement of pressure transducers and strain gauges illustrated in Figure 10.15. A general view of the experimental arrangement is given in Figure 10.16.

Pressure transducers could not be attached directly to the GFRP pipe sections and necessitated the attachment of an aluminium boss. Research[75] at Marchwood Engineering Laboratories (MEL) had demonstrated that side branches leading to the pressure transducer can result in spurious pressure measurements. Although efforts were made to minimise the side branch length, reducing it to zero was precluded by the nature of the transducer, which incorporated a recessed transducer diaphragm. Engineers at CEGB-MEL have established that spurious signals exhibit a smooth sinusoidal form. Genuine water hammer event signals are less smooth, with high frequency components superimposed on the main pressure as a function of time event. It was considered most expedient to run a set of preliminary tests

using the same model of pressure transducers used in the commissioning with the steel test section, record and observe the shape and form of some pressure pulses, and establish whether genuine signals had been recorded.

The strain gauge instrumentation consisted of WFLA-6-IL-17 metal foil strain gauges, Fylde FE-492-BBS quarter bridge completion units and Fylde FE-251-GA amplification modules. Dynamic strain information was recorded using two Racal "Store 4" tape recorders, and analysed using a Spectral Dynamics SD380 signal analyser.

The instrumented pipe sections were bolted in position and filled with water. The values of strain recorded along the test section at rest (empty of water) are illustrated in Figure 10.17. The maximum values of hoop (0.05%) and axial (0.18%) strain resulting from the experimental set up are acceptable, corresponding to levels below the strain (0.3-0.5%) at which first damage occurred in the tensile tests reported in section 8.1. Any detrimental effects of the Viking-johnson coupling were therefore deemed to be negligible.

A sequence of water hammer events similar to those described for the uninstrumented GFRP pipes (see Table 7) were then applied. Pressure as a function of time data from the four pressure transducers recorded during the application of a

sequence of typical water hammer events are illustrated in Figures 10.18-10.21 with a summary of the contents of each Figure in Table 8. Each Figure shows a pressure/time plot for two pressure transducers. Consider Figures 10.18 and 10.19 which show the pressure pulses recorded for all four pressure transducers during the passage of one pressure pulse. Immediately evident are the similarities in the shape of the four pressure/time profiles shown. The peak pressures recorded were; (Downstream PT1, steel)-23.5 bar, (PT2, GFRP)-22.5 bar, (PT3, GFRP)-23.0 bar, and (Upstream PT4, steel)-22.5 bar. The attenuation of peak pressure as the pressure pulse travelled through the rig and the couplings was therefore very small. This was confirmed by the pressure pulses recorded for the other water hammer events illustrated in Figures 10.20-10.25.

In comparison to the set of pressure pulses resulting from the first water hammer event, the observation of subsequent water hammer events illustrated a gradual change in the profile of the pressure pulse from event to event. The first pulse achieved immediately after filling the rig was composed of multiple peaks (3-4). After the fifth water hammer event, the pressure pulse profile exhibited a single sharper peak, but of similar event duration. This was considered to be a consequence of the air in the system. The passage of each successive water hammer event gradually expels more of the free air. This gradual change has a

significant effect on the pressure pulse profile. After several water hammer events nearly all of the free air has been expelled and air dissolved in the water contained within the rig begins to be removed which also affects the profile of the pressure pulse to some extent.

The positions and orientations of the strain gauges attached to the GFRP pipes are ilustrated in Figure 10.15. The numbers (1-8) associated with each gauge are merely for reference with gauge 1 situated at the downstream end of the GFRP test sections and gauge 8 the upstream. Dynamic strain data were successfully recorded for the passage of several separate water hammer events. The strain/time histories illustrated several features. After the first pressure pulse four further significant pulses could be distinguished, with other negligible pulses faintly in evidence, as the pressure wave rapidly attenuated. The first pulse, recorded at the gauges oriented in the hoop direction, indicated mainly tensile strains, but also exhibited a region of compressive loading as the reduced pressure wavefront travelled back through the system (see chapter 4). Small compressive strains were recorded at the two axial gauges, demonstrating that compressive stresses were induced along the pipe axis in response to the passage of the pressure pulse.

Considered as a whole, the plots for the six gauges oriented parallel to the hoop direction (gauges 1,2,4,5,6 and 8)

showed very similar behaviour, with little variation in the peak strain recorded along the test sections. This is in agreement with the pressure/time histories, which exhibited little or no attenuation in peak pressure with distance along the test section.

Consideration was then given to the shape of the strain/time plot by observing an event at a higher resolution. Following a rapid rise time the peak was widely spread with a second broad peak like region in evidence. The event considered was the fourth following filling the rig and this broad peak is attributed to the free air still present in the system. The peak strain achieved was approximately 0.9%. The dynamic modulus, calculated from the initial linear portion of the strain/time history and the corresponding region of the pressure/time history, was found to be to be 19420 N/mm per kg/m^2.

The nature of the strain/time plots during the passage of the fifth water hammer event following filling the rig were then considered. Here the pulse was not as broad, or fluctuating, as that for the fourth event. Evidently, as more free air is expelled the event profile becomes more well defined.

10.3.9 Review of pilot experimentation and refinement of the sequence of water hammer events.

At this stage an assessment of the suitability of the rig was necessary. Of the points of concern prior to this experimentation the following had been addressed;

(i) The system of pipes and couplings worked in practice and the Viking-johnson coupling placed only a small and tolerable stress on the test pipes.

(ii) The attenuation of the pressure wave as it traversed the test section was negligible.

(iii) The pressure/time profiles recorded at the pressure transducers were a genuine reflection of the event and not a spurious consequence of the transducer attachment method.

(iv) The pressure measured in the steel mating pieces could be regarded as the same as that witnessed by the GFRP pipes.

(v) Water hammer events of a magnitude selected and controlled by the operator could be achieved, but only after all the free air had been expelled from the apparatus.

Since the main requirement of the programme was to subject 25 GFRP pipes to the same sequence of 10 water hammer events, of known magnitude and duration, prior to the determination of their time to failure under constant internal pressurisation, further development work was undertaken, and the following procedure adopted;

Three parallel calibration curves of peak pressure as a function of cavity volume were established:

(i) System following rig filling.

(ii) System following the application of one water hammer event of 1st pressure pulse magnitude approximately 18 bar at a known cavity volume.

(iii) System free of entrapped air (established with steel test section).

Using these three calibration curves it was possible to achieve a sequence of ten water hammer events with the first and second events of less than the 23 bar required, but of a repeatable magnitude from pipe to pipe. The following eight events achieved a controllable and reproducible nominal peak pressure of 23 bar. In practice it was found that only the first event need be less than 23 bar.

Within the limitations of equipment and project time scale, this procedure was deemed to approach the initial aims as closely as was possible. Therefore, it was adopted as the basis for the sequence of water hammer events applied to the pipes in the following section.

10.4 Application of water hammer events to GFRP pipes prior to stress-rupture.

Two GFRP pipes, connected in series, were positioned in the test section. Pressure transducers were positioned in the steel mating pieces immediately adjacent to the test

section. Ten repetitions of a pressure pulse with a nominal peak magnitude of 23.15 bar (60% burst pressure) were then applied. The cavity volume adopted, and the magnitude of peak pressure achieved, for a typical sequence are summarised in Table 9. Observations of pipe integrity were made after the passage of each pressure pulse. The peak pressure recorded at each of the two pressure transducers was also noted. The mean water temperature measured prior to each water hammer event for each pair of pipes tested was found to be 24.4(±1.0)°C.

10.5 Stress-rupture of pipe sections.

Stress-rupture testing of GFRP pipes was carried out in a thermostatically controlled water tank at a temperature of 40°C. The apparatus is illustrated in Figure 10.26 with the pipe end closure method shown in Figure 10.27. Internal pressurisation was by hydro-pneumatic means with the gaseous pressure provided by a stabilised compressed air supply. To overcome the possible problem of air leakage at the end closures, or reduction in pressure due to a permanent deformation of the pipe, a Haskel MAA-4 air pressure amplifier was incorporated in each pressure line. This device amplifies a source pressure up to a multiple of four, and operates so as to maintain a constant output pressure which was its major function here. It was positioned in the pressure line between the source of compressed air and the

three-way valve situated at the pressure inlet to the pipe (see Figure 10.26).

The procedure for pressurising a pipe was quite simple. The compressed air supply was gradually increased until it was just below the value required (measured on the gauge dedicated to that air line), this having been determined from the desired pipe test pressure and the amplification setting of the air amplifier. A pressure gauge was then attached to the three-way valve and the pipe pressure measured. The compressed air supply was then adjusted until the desired test pressure was achieved. The air amplifier then maintained the pipe at this pressure by pumping in additional air if necessary. Pipe pressures were also monitored daily. In practice up to five pipes were connected to one pressure line.

This method also overcame the problem of achieving accurate pressure measurements at each pipe. The accuracy of the pressure gauges dedicated to the compressed air supply was considered inadequate. However, by incorporating a three-way valve in each pressure line only one high quality pressure gauge was required to perform all the pressure measurements.

Pipe Failure was defined as "leak or break". Each pipe had an electrode positioned within it. An electrode was also situated in the water tank outside the pipes. Any leakage

resulted in electrical conduction between the electrodes and caused the timer and pressure supply to that pipe to be deactivated. Following pipe failure the region of leakage was located and marked. Failed pipes were then dissected with an angle grinder to facilitate the examination of the inner surface of the pipe wall. In a few cases the failure zone was isolated, cut out, the resin burnt off for four hours in a muffle furnace at 550°C, and the integrity of the reinforcement examined.

Two sets of data were compiled using pipes of the material composition described in Section 10.1;

(i) Virgin pipes.

(ii) Pipes subjected to the series of water hammer events described in section 10.4.

In both cases 25 pipes were tested, 5 pipes at each of 5 internal pressures corresponding to 40, 45, 50, 60 and 70% of the mean burst pressure determined in section 10.2.

CHAPTER 11.

Results.

11.1 Burst tests.

Severe problems were encountered in achieving a satisfactory seal between end plate and pipe flange for the first two pipes tested. In both cases a sequence of loads were applied before burst was achieved. The results given below are confined to the four pipes where an adequate seal was achieved and failure occurred during the first and only pressure application. For these pipes internal pressurisation was by purely gaseous (N_2) means. The failure pressures and strain data are summarised in Table 10.

The following observations were made from an inspection of the failed pipes. Pipe three was tested under water and hence pressurisation ceased immediately the bubbling created by the escaping gas became evident. The nature of the failure was leakage from a small delaminated disc approximately 50mm in diameter. A general view of the failed pipe is illustrated in Figure 11.1. The region marked with a black circle corresponds to the main failure zone. Whitening (delamination) and resin cracking on the surface of the delaminated area were evident. A band where the woven reinforcement appeared to be tearing apart is also illustrated in Figure 11.1. This band was evident down the entire length of the pipe. Internal and external resin

cracking were noted along the length of the pipe, parallel to the pipe axis.

Pipe four was pressurised by purely gaseous means and was therefore located at some distance from the operator. In this test a true burst failure was achieved with the pipe separating into three parts (see Figure 11.2). Extensive fibre pull-out and delamination were observed. Several other sites of delamination were also evident which were not associated with a fracture surface. Resin cracking at approximately 45° to the longitudinal axis is illustrated in Figure 11.3. This was prevalent over the entire surface of the pipe. The failure mode exhibited by pipes five and six was very similar to that described for pipe four. The mean burst pressure for these four pipes was calculated to be 38.58(±1.79) bar, very close to the design value of 42.4 bar.

11.2 Application of water hammer events to GFRP pipes prior to stress-rupture.

Each water hammer event resulted in four significant pressure pulses of gradually attenuating magnitude. Following an initial peak of 23 bar the peak magnitude of subsequent pressure pulses were approximately 15, 8.5 and 5 bar. All pipes illustrated multiple sites of axial debonding (see Figure 11.4) and axial resin cracking following the first water hammer event. Initial sites of this damage were

apparent throughout the entire test section. After each subsequent water hammer event new damage sites evolved and existing areas propagated. The spread of axial debonding resulted in the inter connection of poorly wetted zones along individual tows. Some resin cracks propagated along the entire length of the pipe. Later examination revealed some cracks to be surface breaking although "through-thickness" cracks were not observed. Macroscopic damage parallel to the circumferential reinforcement was not apparent.

One pipe burst during the application of the fourth water hammer event. The maximum pressure recorded was 17.41 bar. A general view of the failed pipe is illustrated in Figure 11.5. The fracture surface was associated with the overlaping region of the woven roving reinforcement. The cut edges of the fibre mat were clearly evident. Multiple sites of delamination at the cross over points of the fibre tows in the woven roving mat were also noted (see Figure 11.6).

11.3 Pipe stress-rupture.

11.3.1 Virgin pipes.

A plot of stress, expressed as a percentage of the mean burst stress, against time to failure for the virgin pipes is shown in Figure 11.7. Two pipes, where the failure was associated with particularly severe fabrication flaws, were excluded from this set of results. The nature of these flaws

is shown in Figures 11.8 and 11.9. Figure 11.8 depicts an inclusion and Figure 11.9 a region where the alignment of the reinforcement was very poor. Both of these flaws had an extremely detrimental effect on the times to failure of the pipes. The pipe with the inclusion failed after fifteen minutes at 70% burst pressure. The pipe with the poor alignment was pressurised at 45% burst pressure and failed after two-hundred and twenty minutes, significantly less than the one thousand six-hundred and sixty hours recorded as the lowest time to failure of the four other pipes tested at this pressure level. In both cases the failure (i.e. leakage) occurred at the precise location of the flaw. Whilst pipes with such flaws were not considered to be representative of virgin material, they do highlight the adverse effects of fabrication flaws on thin walled structures of this type.

The majority of the virgin pipes exhibited the same failure mode with leakage occurring at one site, a "pinhole" type of failure. In nearly all cases the region of failure was not identifiable unless a small pressure was applied to the pipe whilst still full of water, and the point of leakage located. Surface breaking cracks in the resin, approximately 20mm long (see Figure 11.10), were witnessed on two pipes. However, the crack did not pass straight through to the other side of the pipe wall. The inside of the pipe wall at the same point as the point of leakage exhibited a region of

delamination associated with the crack shown in Figure 11.10. For many of these pinhole failures any associated delamination or resin cracking were completely absent.

To permit examination of the reinforcement, a section of pipe wall, including the location of leakage for a pinhole type failure, was heated to burn off the resin. The outer layer of chopped strand mat (CSM) reinforcement exhibited a region of fibre bundle fractures which formed a clear crack, approximately 20mm long, through the CSM layer (Figure 11.11). The crack was oriented perpendicular to the hoop stress, with the mid point corresponding to the point of leakage located after failure. Upon removing this layer of CSM it became evident that the crack was directly in line with the edge of the overlap in the outer CSM layer. After removing the CSM reinforcement from the overlap the woven roving reinforcement was examined. The position of the crack in the CSM was easily distinguishable as the egression of water had led to some deposits of insoluble matter. Macroscopic damage of the WR reinforcement at this point was not observed. However, a roughly circular area of approximately 50mm diameter, positioned adjacent to the crack in the CSM layer, exhibited multiple fibre fractures (see Figure 11.12). These fibre breakages were clearly visible without any optical aid with the majority, but not all, occurring in the circumferential rovings (i.e. the plane of fibre fractures was perpendicular to the hoop

stress). In all cases numerous fractured fibres were noted across an entire roving. All fibre fractures occurred at the point where one roving met another perpendicular roving prior to passing under it. Examination of the underside of this WR region revealed similar damage to WR fibres but confined to a much smaller area of approximately 20mm diameter (see Figure 11.13). The inner CSM layer exhibited a crack approximately 35mm in length again oriented perpendicular to the hoop stress. The crack was positioned in the centre of the region of WR damage about 30mm along the pipe circumference from the crack observed in the outer CSM layer. Figure 11.14 illustrates the relative positions of the damage in each layer.

11.3.2 Pipes previously subjected to the sequence of controlled water hammer events.

A plot of stress, expressed as a percentage of the mean burst stress, against time to failure for pipes subjected to water hammer events is shown in Figure 11.15. Failure modes for these pipes were of three forms. A few pipes exhibited the type of failure noted for the virgin pipes with a pinhole which could only be distinguished as the the point of leakage with the aid of low level internal pressurisation following pipe failure. In all cases such failures were associated with an axial crack which had resulted from the sequence of controlled water hammer events.

The majority of failed pipes exhibited a small failure zone with some delamination (see Figures 11.16 and 11.17). Again all failures were associated with water-hammer induced axial cracking. Two pipes failed by through thickness cracks with the major failure surface perpendicular to the hoop stress. Both of these corresponded to water-hammer induced axial cracks associated with the region of overlap in the WR reinforcement (see Figures 11.18 and 11.19).

A failure region from one pipe was cut out of the pipe wall and the resin burnt off to allow reinforcement damage examination. Macroscopically the failure was of the pin hole type with a small region of delamination centered about the pin hole and an axial crack which had resulted from the water hammer events. Overall, similar features to those described for the failed virgin pipes were observed with fibre fractures noted in all three reinforcement layers in line with the overlap in the WR mat (see Figure 11.20). However, the overloaded pipes differed in the severity of damage to the fibres on the inner side of the WR and the inner CSM layers. On the inner surface of the WR reinforcement a line of fibre fractures were observed perpendicular to the hoop stress (Figure 11.21). In each case the fibre fractures covered the width of a roving but did not pass through its thickness. Damage of this nature was evident in one line, along the entire section, some 120mm in length. This line of fibre fracture corresponded

exactly to the water hammer event induced crack observed prior to resin burn off. The inner most layer of CSM also exhibited a crack approximately 120mm in length (Figure 11.22). This crack was in line with the crack in the outer layer of the CSM, the line of WR fibre fractures, and the position of the water hammer induced crack.

CHAPTER 12.

Discussion of results.

12.1 Pipe burst testing.

The mean burst strength of 38.58(±1.79) bar was slightly lower than the 42.67 bar theoretical burst pressure calculated from BS 4994. Although data from only four tests were available, the coefficient of variation for ultimate material strength determined in the pipe burst tests of 4.6% was lower than the 9.0% arising from the coupon tests. This indicates that wider test pieces without edges give more consistent results for ultimate properties than coupon type test pieces.

The failure mode was identical in pipes 4, 5 and 6 where a true burst occurred resulting in a great deal of damage. Pipe 3 provided an insight into the progression of damage towards failure. This test was conducted under water allowing the first sign of failure to be noted (leakage resulting in bubbling) thus permitting the internal pressurisation to be halted prior to catastrophic failure. The failure zone exhibited resin cracking associated with a disc of damage where the woven roving had become delaminated from the chopped strand mat layer. Also of note was the apparent separation of the overlapping region in the woven roving reinforcement. This indicates that there was

insufficient overlap resulting in a band of weakness along the axis of the pipe. It seems likely that had further presurisation continued that another major failure zone would have occurred in this band. This was further borne out by the appearance of pipes 4, 5 and 6 which exhibited an axial fracture surface corresponding to the overlapping region. Although the overlapping region will always be a site of potential weakness efforts must be made to mitigate its detrimental effects. At present neither the amount of overlap required nor the effect of staggering the overlap in adjacent layers are documented. Experimental data relating these factors to the mechanical properties of a material or structure are therefore necessary.

12.2 Application of water hammer events to GFRP pipes prior to stress-rupture.

The occurrence of three reflected pulses per event is not surprising, as all the energy and momentum associated with the water hammer will not be dissipated by the first pressure pulse. The original specification of ten water hammer events of 23 bar magnitude has clearly been exceeded, but the result is more realistic in the sense that ten water hammer events produced forty pressure pulses, with ten each of 23, 15, 8.5, and 5 bar being applied to each pipe. This sequence is comparable to the fifty overloads applied to the coupon samples. Fifty pressure pulses could occur from twelve or thirteen water hammer events, the equivalent of

one pump failure, incorrect valve closure or operator error every few years. This demonstrates that such a number would not be conservative for a system in service for thirty years.

The damage resulting from the controlled water hammer event was very similar to that achieved by overload application to the coupon samples. Initial damage was associated with the fibre tows oriented perpendicular to the maximum applied stress, the axial tows in the case of the pipes. Many sites of damage were evident after the first water hammer event and unlike the coupon samples none of these could have originated from a cut edge resulting from test piece preparation. Damage occurred throughout the bulk as a consequence of the hoop stress alone. This damage also propagated into the resin rich regions resulting in surface breaking resin cracks. Poorly wetted areas were joined by transverse debonds, increasing the deleterious effect of previously isolated fabrication flaws. The damage reduced the efficiency of load transfer throughout the material.

The premature failure of one pipe during the application of a water hammer event is readily explained by the nature of the fracture surface (see Figure 11.5). The cut edges of the fibre mat were clearly evident where little or no overlap in the joint region of the woven roving reinforcement had been achieved. In the region where failure occurred, mechanical

properties of the pipe were therefore reduced to those of the matrix resin. This further emphasises the need for sufficient reinforcement overlap to allow hoop loads to be transferred between layers by shear forces.

The dynamic modulus of 19420 N/mm per kg/m^2 is very similar to both the quasi-static and dynamic moduli measured for the coupon test pieces. This indicates that the strain rate achieved in the load up phase of the controlled water hammer event (approximately 100%/s) was insufficient to stimulate the material to exhibit enhanced modulus behaviour. A similar observation was made for the coupon overload and was discussed in section 9.2.2.

12.3 Pipe stress-rupture.

Stress-rupture data for virgin pipes are plotted in Figure 11.7. Immediately evident are the considerable scatter and the poor fit of the linear regression analysis. These are also features of the stress-rupture data for the pipes which had been treated with the sequence of water hammer events ("overloaded pipes") although the regression analysis achieved a better fit to these data.

12.3.1 Failure modes.

As the pipe wall was exposed to water on both sides it is likely that water will have diffused into the outer side as well as the inner side of the pipe wall. However, the

internal pressure will have provided a greater driving force for water to penetrate the pipe wall from the inside. This is borne out by the fibre damage observed, with a longer crack in the inner CSM layer than the outer.

As water egressed from the inside of the pipe into the CSM reinforcement the CSM fibres will have become subject to the simultaneous effects of stress and environment. The clear zone of CSM fibre bundle fractures, oriented perpendicular to the maximum applied stress (hoop stress), is consistent with stress corrosion cracking. Once a crack existed in the CSM layer the environment was in contact with the WR reinforcement. The combined action of stress and water were again evident from the numerous fibre fractures. The fibre fractures in the WR layer were located exclusively at the point where one roving begins to pass under another (i.e at the edge of the cross-over region). However, Crowther[33], investigating the uniaxial stress-rupture of virgin glass/polyester coupons, found that a large proportion of fibre fractures occurred in the centre of the roving in the cross-over region. This difference may be a consequence of the different stress systems. In biaxial (e.g. unrestrained, closed-end pipes) stress-rupture tests, both hoop and axial rovings are in tension. The stress in the axial roving may cause a greater constraint on the hoop roving than the unstressed transverse roving causes in the longitudinal roving in a uniaxial coupon test.

The outer layer of CSM examined after resin burn-off also exhibited a clearly defined crack. This was aligned with the overlap in the outer CSM layer, a probable region of stress concentration, and therefore a likely site for the combined action of stress and environment. Water will have almost certainly have penetrated this and other regions from the outside of the pipe wall prior to pipe failure, and some reinforcement damage may have occurred as a result. Aqueous diffusion, from the water bath providing the constant temperature environment, cannot be quantified. In pipes with such thin walls this may not be insignificant, and may result in artificially pessimistic times to failure at a particular pressure.

On the whole, a combination of stress enhanced diffusion and stress corrosion damage to the reinforcement created a path through the pipe wall, causing the leakage which was defined as failure. The path was not straight through the pipe wall, and no identifiable through thickness crack was present. A similar effect was observed by Jones and Hull[86], who concluded that "weepage failures" in filament wound GFRP pipes under biaxial stresses resulted from the occurrence and intersection of transverse cracks.

The failures of overloaded pipes fell into three categories: pinhole failures, pinhole failures with associated

delamination and in two cases a through thickness crack. All points of pipe failure were associated with an axial crack resulting from the sequence of water hammer events.

The pinhole failures probably followed the same failure mode as was described for the virgin pipes with an inner pipe wall axial crack providing an immediate site of water ingress, and an additional stress concentration. Evidence for this is provided by the observations of reinforcement integrity in the region of a pinhole failure from an overloaded pipe, described in section 11.3.2. Figure 11.22 shows the inner most CSM layer with a region of fibre fracture directly in line with the position of the water hammer induced crack. It is unlikely that this damage will have occurred as a consequence of the water hammer events as similar damage was found in the virgin pipes. Also, in the coupon tests, the sequence of overloads had no effect on the CSM reinforcement. It is therefore reasonable to assume that the CSM fibre fracture occurred as a result of stress corrosion cracking. As in the case of the virgin pipe, WR fibre damage was observed. Figure 11.21 shows a line of fibre fractures which coincided with the water hammer induced crack and the crack zone in the CSM fibres. The axial crack will act to cause a stress concentration and a region of easy water ingress. The combination of these two resulted in stress corrosion damage to the WR fibres. Further separation of the layers of reinforcement revealed

the line of cracking and fibre damage to coincide with one edge of the WR fabric in the overlap region (see Figure 11.20). It seems likely that this may have contributed to the location of the water hammer induced crack, and the point of environmental attack on the outer CSM layer. The outer CSM also exhibited a zone of stress corrosion damage in line with the damage described above.

The mechanism of failure in the overloaded pipes was evidently very similar to that observed in the virgin pipes. In the overloaded pipes the water hammer induced crack provided both a zone of stress concentration and a point/line of easy access for the environment. The reduced lifetime results from a reduced initiation time for first damage, and an easier, shorter path for water to penetrate the pipe wall.

In both virgin and overloaded pipes the initiation of damage was a crack in the inner CSM laminate with the crack oriented perpendicular to the maximum stress. In this study damage was often found to be associated with an overlap in one of the reinforcement layers. In the virgin material, the overlap in the outer CSM layer corresponded to the point of fluid leakage. The CSM overlap is generally considered to be less detrimental than the WR overlap as the nature of the CSM reinforcement allows the overlap to merge. Also the CSM reinforcement does not carry as much load as the continuous

WR fibres. Here, however, it has been demonstrated that the CSM overlap can provide a preferential site of damage development, and as result should be considered more carefully in design. Time to failure also depends upon the ease with which water can find a path through the pipe wall. According to Jones and Hull this depends upon transverse cracks intersecting. In this study transverse cracks have been found to be associated with overlap regions of the reinforcement, further emphasising the need to stagger these regions, which may be numerous in a service structure.

12.4 Consideration of the effect of water hammer on time to failure of pipe under constant internal pressure.

The two sets of data are plotted on the same axes for comparison in Figure 12.1. Evidently there is considerable scatter in both sets of data, and comparing linear regression lines would have been meaningless. As the tests were carried out on nominally identical pipes, at nominally identical stress levels, the safest comparison to make is at individual stress levels. Figure 12.1 depicts both virgin and overloaded pipe stress-rupture data. The individual test data are summarised in Table 11. At the 70, 60 and 45% burst pressure stress levels the groups of data are clearly distinguishable, with overloaded pipes exhibiting shorter times to failure than virgin pipes at the same internal pressure.

At the 50 and 40% burst pressure levels, the virgin and overloaded data sets overlap. Although the general trend was of reduced lifetime for overloaded pipes, a measure of the difference between the two data groups was necessary. Therefore, a significance test was carried out for the overlapping data. In both cases a two-tailed t-test was applied. Details of the statistic and calculations are given in Appendix C. At 50% of burst presssure the difference in the mean values of time to failure for virgin and overloaded pipes was significant at the 20% level and hence the "difference is not established". At 40% of pipe burst pressure, the difference in mean times to failure of virgin and overloaded pipes was significant at the 10% level. Such a value is said to indicate a "possible difference". However, the virgin pipe data group at this stress level includes two runouts which further complicate analysis. Evidently, further testing at all stress levels, particularly the lowest, is necessary.

Overall it has been demonstrated that the series of water hammer events results in reduced times to failure at the stress levels considered in this project.

PART 4.

DISCUSSION AND IMPLICATIONS FOR FUTURE DESIGN.

CHAPTER 13.

Comparing the pipe and coupon results.

Parts 2 and 3 describe parallel research programmes on the most widely used test piece configuration, a coupon, and on pipes modelling real CW system components. Commonly, design is based upon coupon test data, but it is open to question how well such tests reflect the behaviour of service structures. Despite this, the published literature contains no experimental studies to correlate the two. This thesis considers for the first time the validity of using coupon test data for design, by comparing the behaviour of a glass/polyester laminate in pipe and coupon forms.

13.1 Virgin pipes and coupons.

In order to establish the effect of test piece configuration on time to failure, the results for virgin material are examined first. The first step is to find a basis upon which to compare stress in the uniaxial coupon test with the biaxial stress system in a pipe. The material UTUS determined from the coupon tests was 233(±21) N/mm per kg/m^2. In the pipe burst tests the hoop stress at burst was found to be 208(±11) N/mm per kg/m^2. If a maximum-stress failure criterion is adopted for the pipe, it is reasonable to regard these two measurements as being equivalent. Since they agree to within one standard error they will be

regarded as being the same in the following analysis. The hoop stress at which pipes were loaded is expressed as a percentage of the material UTUS.

Figure 13.1 shows a stress-rupture plot of virgin pipe and virgin coupon[33] test data. If the comparison is based upon the regession lines it would appear that at higher loads pipes exhibit longer times to failure than coupons and at lower loads the times to failure of pipe and coupon tests tend towards agreement. In addition, comparisons of individual data groups can be made at the 70%, 60% and 45% load levels. At both 70% and 60% pipes exhibit longer lifetimes than coupons. However, at the 45% load level the pipe and coupon data overlap with all pipe data at the longer lifetime end of the data group as a whole. Caution is necessary here as each of the 40% and 45% pipe load levels includes a pair of runouts and may, if the times to failure were known, extend the virgin pipe data group to far longer times to failure than the coupons at an identical stress level.

Another consideration in this comparison is the definition of failure in the pipe and coupon tests. In coupon tests the time to failure is recorded when both halves of the coupon have separated. In the pipes, failure was defined as leak or break, and was almost exclusively a very small leakage. The virgin pipe failure investigation revealed that failure

resulted from the passage of water through the pipe wall, with a small zone of fibre fracture but no well defined hole. Certainly there was no through thickness crack 25mm long, to which the coupon failure might be said to correspond. It seems likely that a path for leakage would form in the coupon some time before separation occurred. If the failure criterion in the coupon tests was the same as for the pipes the recorded times to failure would have been much shorter. This effect would be most prevalent at longer times to failure, rendering the above comparison open to criticism. In service components, the failure criterion would be leakage and not separation. Since it is impossible to set up a "leakage criterion" for the coupon test pieces, one can only assert that life would certainly be less than that recorded for coupon separation. Thus, on a comparable basis, and taking into account runouts, material tested in pipe form exhibits longer times to failure than material tested in coupon form at identical stress levels.

13.2 Overloaded pipes and coupons.

Before comparing the overloaded pipe and coupon stress-rupture data the transient overloads applied to pipe and coupon need to be compared. Consider the model water hammer applied to the pipes (Figure 7.5) and a typical water hammer pulse (Figure 10.18). The coupon event duration is approximately half that of the pipe event. However, the strain rates in pipe and coupon, 100%/s and 60%/s

respectively, are within the range giving enhanced properties as described in section 4.3. Neither event has a "flat-top region" and in both, peak stresses correspond to approximately 60% material UTUS, the expected service maximum. In general the event applied to coupons is a reasonable model of a real water hammer pulse. Evidence for this conclusion was provided by the damage resulting from each overload. In both cases damage comprised resin cracking associated with the transverse reinforcement, oriented perpendicular to the applied stress. Therefore, it is reasonable to compare stress-rupture data for overloaded pipes and coupons.

Stress-rupture data for overloaded pipes and coupons are shown in Figure 13.2. At all stress levels pipes exhibit longer times to failure than their coupon counterparts at the same stress level. This is clearly the case at the lowest stress level in the pipe testing programme (40% UTUS) where the pipe and coupon data groups are clearly distinguishable without any overlap.

CHAPTER 14.

Designing from pipe and coupon data.

In part 1 of this thesis research upon which design codes are based was reported. The vast majority of the experimental studies involving stress-rupture were performed with coupon type test pieces. The discussion of pipe and coupon results in chapter 13 casts doubt on the validity of this practice. Two main points emerged from chapter 13. Firstly, when using coupon stress-rupture data it is important to define the failure criterion for the service structure and to ensure it coincides with the failure criterion of the coupon test. For CW systems leakage would doubtless be defined as failure. If so, it would be incorrect to use coupon tests failing by separation as a basis for design, because coupons would have "leaked" some time before they fractured.

The second conclusion from chapter 13 was that at a given stress level pipes exhibit longer times to failure than coupons. This is very significant and implies that designing on the basis of coupon tests is in fact pessimistic. This will result in over-designed and therefore financially unattractive structures. Little criticism can be made of the pipe testing technique in defining a time to failure at a given load as the failure criterion is leakage. The pipe is described as a model component, but if a 151mm diameter pipe

were required in a CW system, an item of this wall thickness and laminate constitution would fulfill present CEGB design criteria. In effect, therefore, these tests were carried out on a real component.

Evidently tests on model components, reflecting service conditions, are required to design in GFRP correctly. An understanding of the failure mechanism is also important, as is a well defined failure criterion. Failure as a consequence of leakage, resulting from diffusion, chemical degradation of the matrix, interface and reinforcement, and overload induced damage is complicated. It requires a path between the various laminae for the water to follow, and may be different in thicker laminates. Intuitively it seems likely that it would be harder (take longer) for water to find a path in a thicker laminate. This suggests that design involving scaling up from test data on thin walled samples may be incorrect, and possibly lead to over design. Evidently there is a need for experimentation on pipes to investigate the effect of material thickness and component size on leakage failures.

Some of the problems and considerations of designing CW system components from pipe and coupon data have been discussed above. Attention is now given to the existing design codes, discussed in section 2.0, to consider how

successful they appear in the light of experimental results reported in this thesis.

14.1 BS 4994.

The design factor, calculated from BS 4994, for a CW system with a constant pressure reservoir (non-coastal) is 9.9. This is represented graphically in Figure 14.1 by a broken horizontal line below which design is safe according to BS 4994. The linear regression analysis of the overloaded coupon data is also shown on this graph and intersects with the BS 4994 design line at or very close to a point corresponding to a time of 30 years, the desired lifetime of CW system components. This does not allow any room for error. This comparison involved the extrapolation of coupon data from 20 months to 30 years, and coupon failures were based upon complete material separation, which has been identified as an optimistic criterion. Therefore, it would be reasonable to assert, based upon these overloaded coupon tests, that BS 4994 had not properly addressed the design requirements of a CW system which might be subject to water hammer events.

The overloaded pipe stress-rupture data are also illustrated in Figure 14.1. Once again comparison with the design factor calculated from BS 4994 requires an extrapolation of the regression line. At the designated component lifetime of thirty years, the predicted constant stress causing failure

is approximately 27% UTUS, over 2.5 times the design stress calculated from BS 4994. This would appear to be a significant margin and indicates that BS 4994 is adequate and does provide safe design of real structures. However, the extrapolation was made from only 25 results and from tests of a maximum duration of 75 days. Clearly more data are required at lower stress levels. The indication from the overloaded pipe stress-rupture data is that although BS 4994 takes no account of transient overloads, applying the code to CW system components results in safe design. However, this is still unsatisfactory as much depends upon the validity of the extrapolation procedure.

BS 4994 does address the added complication of dynamic fatigue, although any variation in frequency is ignored. The dynamic fatigue data compiled for overloaded polyester coupons is shown in Figure 14.2 and is compared with the design stress arising from the factor of 13.86, calculated from BS 4994 for the conditions prevailing at coastal power stations. Extrapolating the linear regression to thirty years reveals a predicted mean stress level causing failure of approximately 27% UTUS, considerably in excess of the calculated safe design stress, 7.21% UTUS. Again the basis of this conclusion is an extrapolation, which casts doubt on the predicted material behaviour after 30 years. However, the indication here is that BS 4994 is conservative, and that more experimentation is required in the area of very

low frequency dynamic fatigue of overloaded material, preferably in pipe form.

14.2 CEGB Code.

The CEGB design code discussed in section 2.0 is mainly based upon BS 4994 and therefore the previous discussion is relevant to this code. The major point to note is that the CEGB code considers the effect of transients on long term material performance to be negligible and both pipe and coupon experimentation demonstrate that this is not the case.

14.3 ASTM D-2992.

The other design code considered was ASTM D-2992. It differs from BS 4994 in that instead of predicting a safety factor it instructs the designer how to carry out stress-rupture tests on pipes, how to plot the data and to extrapolate to the desired component lifetime. A comparison with predictions from the code and experimental data cannot be made. The pipe stress-rupture test method adopted in this thesis closely resembles the requirements of this code. Data are represented as stipulated in ASTM D-2992 in Figure 14.3. The plot is of log stress against log time to failure (hours). Non SI units are used, to conform with the instructions within the code. The extrapolation of the plot shows that present CEGB design factor (K=10) is conservative and therefore safe. Although this conclusion can be made

after following ASTM D-2992, designing from 25 tests and a maximum test time to failure of 1800 hours for service life of 30 years is questionnable. Evidently a greater number of tests at longer lifetimes are advisable to check the validity of the extrapolation procedure.

When compared with predictions made from the the overloaded pipe stress-rupture data, both BS 4994 and ASTM D-2992 appear to achieve safe design. In both cases this conclusion could only be made after a dubious extrapolation procedure. The success of BS 4994 should be kept in perspective and the criticisms discussed in chapter 2 considered. Transient overloads have been demonstrated to reduce component lifetime and whilst BS 4994 achieves safe design it is despite, and not because of, rigorous assessment of such events. The experimentally based ASTM D-2992 appears a better option although it also omits to address the proven detrimental effect of transient overloads on material lifetime.

CHAPTER 15.
Conclusions.

(1) The application of model water hammer events to coupon samples of GFRP result in transverse resin cracking but no fibre fractures. A vinyl ester matrix offers greater resistance to crack propagation than a polyester matrix.

(2) The loading rates occurring during a water hammer event induce enhanced mechanical properties in the reinforcing glass fibres.

(3) Up to fifty model water hammer events cause no reduction in coupon UTUS. However, tensile modulus is decreased after ten events.

(4) Coupons subjected to a service-life equivalent number of water hammer events exhibit reduced lifetimes under constant stress in comparison to virgin material.

(5) Applying service-type water hammer events to GFRP pipes causes multiple resin cracks perpendicular to the hoop stress.

(6) Insufficient overlap in pipe wall reinforcement can result in pipe failure during water hammer.

(7) Pipes subjected to ten service-type water hammer events exhibit reduced stress-rupture lifetimes in comparison to virgin pipes.

(8) The reduced lifetime of pipes subjected to water hammer events is a consequence of enhanced stress corrosion cracking at the site of a water hammer induced crack.

(10) At nominally identical stresses, laminates tested in pipe form exhibit longer lifetimes than those in coupon form. Therefore, designing from coupon test data leads to the over-design of service components.

(11) It is incorrect to design pressure vessels, where failure is defined as leakage, from test data accumulated in coupon tests, where failure is defined as material separation.

(12) BS 4994 does not adequately address the design of pressure vessels which may be subject to water hammer.

CHAPTER 16.

Suggestions for further work.

(i) Investigation of the effect of water hammer event profile on damage. It has become evident from this thesis that water hammer events are detrimental to both material integrity and long term material performance. Further experimentation is necessary to determine which components of a water hammer event load/time profile (rise time, hold time, peak load and event magnitude) are most damaging. Such experimentation could be carried out on coupon test pieces. This might allow the definition of a "safe" water hammer event profile.

(ii) Further stress-rupture testing on virgin and overloaded GFRP pipes. This project has indicated that to design pressure vessels such as pipes requires data compiled on model structures. The existing data base of pipe stress-rupture is very small and needs expanding, especially at longer lifetimes. It has also been illustrated that tests should take account of the failure mode in service, which is facilitated by pipe tests. Further to this, realistic tests should confine an aqueous environment to the inside of the pipe. This would represent service conditions more accurately and allow a better understanding of the stress corrosion failure mechanism.

Specifically pipe stress-rupture tests could assess the effect of the following on lifetime;

(a) Resin type. Experimentation has shown a tougher resin, vinyl ester, to offer some beneficial properties. Further attention should be given to matrix resin selection in an attempt to reduce water hammer induced resin cracking and increase the lifetime under constant stress.

(b) Pipe wall thickness and component size (pipe diameter). In service components are far larger and have thicker walls than the pipe tested in this thesis. Failure in both virgin and overloaded pipes involved water diffusing along a relatively short path. It is unknown whether a similar effect would occur as readily in a thicker structure and this requires investigation.

(c) Reinforcement geometry/nature and position of overlap in reinforcement. Post failure damage assessment revealed that environment induced reinforcement damage occurred preferentially at the sites of overlap in both the woven roving and chopped strand mat layers. Attempts to mitigate, or reduce, the effect of the overlap, of which there may be many in larger service structures, must be made.

In both overloaded and virgin pipes the chopped strand mat layer was severely damaged by the environment, providing a site for environmental attack on the major reinforcement,

the woven rovings. Experimentation with different reinforcement geometries may make aqueous penetration more difficult and hence prolong the lifetime of a component.

(iii) Low frequency fatigue tests on GFRP pipes incorporating the assessments highlighted in (ii). The experimentation on overloaded coupons tested at very low frequencies has indicated that such a load regime is less detrimental than stress-rupture loading at a comparable stress level. This suggests that efficient design of coastal plant CW systems require data accumulated at the in-service operating frequency. Evidently such tests should be carried out on pipes to imitate service structures.

(iv) A more detailed study of the failure mechanism occurring in virgin and overloaded pipes under stress-rupture load conditions. The study of this area reported in this thesis is not extensive. Further analysis could investigate:

(a) Pipes prior to failure, to assess damage propagation.

(b) Reinforcement damage in failed, thicker structures, to determine what path water followed to achieve a leakage.

(c) Whether other sites of reinforcement damage occur in the pipe wall remote from the point of leakage.

REFERENCES.

1. British standard specification for the design and construction of vessels and tanks in reinforced plastics. BS 4994, 1987.

2. Bryan-Brown, M.H., Walker, D.M. and Wyatt, R.C. CEGB Report No. SSD/SW/80/R352, 1980.

3. ASTM D2992-71. Standard method for obtaining hydrostatic design basis for reinforced thermosetting resin pipe and fittings.

4. Code of practice for the use of glass-fibre reinforced plastics (GRP) in cooling water (CW) systems, CEGB Scientific and Technical Branch, Bristol, 1989.

5. Thomas, W.F. Physics and Chemistry of Glasses, Vol. 1, No. 1, Feb. 1960, pp. 4-18.

6. Ashbee, K.H.G., Frank, F.C. and Wyatt, R.C. Proc. Roy. Soc. A, Vol. 300, Sept. 1967, p.p 415-9.

7. Abeysinghe, H.P., Edwards, W., Pritchard, G. and Swampillai, G.J. Polymer, Vol. 23, Nov. 1982, pp. 1785-1790.

8. Ashbee, K.H.G. and Wyatt, R.C. Proc. Roy. Soc. A, Vol. 312, 1969, pp. 553-564.

9. Pritchard, G. and Taneja, N. Composites, Vol. 4, No. 5, July 1973, pp. 181-183.

10. Pritchard, G. and Taneja, N. Composites, Vol. 4, No. 5, Sept 1973, pp. 199-202.

11. Pritchard, G., Swampillai, G.J. and Taneja, N. Trans. Inst. Chem. Eng., Vol. 56, 1978, pp. 96-100.

12. Sharp, W.H. and Weber, M.K. Corrosion, Vol. 12, Feb. 1956, pp. 71-78.

13. Springer, G.S.,"Effects of temperature and moisture on sheet moulding compounds", in Environmental effects on composite materials, Vol. 2, edited by Springer, G.S., Technomic Publ. Co. Ltd, Pennsylvania, 1984.

14. Ellis, B. and Found, M.S. Composites, Vol. 14, No. 3, July 1983, pp. 237-243.

15. Springer, G.S., Sanders, B.A. and Tung, R.W.
"Environmental effects on glass fibre reinforced polyester and vinylester composites", in Environmental effects on composite materials, Vol. 2, edited by Springer, G.S., Technomic Publ. Co. Ltd, Westport, 1981.

16. Pritchard, G. and Speake, S.D.
Composites, Vol. 18, No. 3, July 1987, pp. 227-232.

17. Zhurkov, S.N.
Int. J. Fracture Mech., Vol. 1, 1965, pp. 311-322.

18. Boller, K.H.
U.S. Forest Products Laboratory Report No. 2039, U.S. Department of Agriculture, Sept. 1958.

19. Steel, D.J.
Trans. J. Plastics Inst., Oct. 1965, pp. 161-7.

20. Bershtein, V.A. and Glikman, L.A.
Soviet Physics-Solid State, Vol. 5, No. 8, Feb. 1964, pp. 1651-1656.

21. Dixon, R.H., Ramsey, B.W. and Usher, P.
Royal Inst. of Naval Architects, Symposium on GRP ship construction, Oct 1972, Paper 1.

22. Cameron, J.B.
Trans. J. Plastics Inst., Vol 35, Oct. 1967, pp. 681-7.

23. Schumacher, G.
Materialprufung, Vol. 10, No. 7, July 1968, pp. 231-7.

24. Holland, N.H. and Turner, B.F.
CEGB Report No. RD/SW/R42, Jan. 1966.

25. Menges, G. and Schwartz, O.
Kunstoffe, Vol. 59, No. 11, Nov. 1969, pp. 775-9.

26. Chiao, T.T, Lepper, J.K., Hetherington, N.W. and Moore, R.L.
J. Composite Materials, Vol. 6, July 1972, pp. 358-370.

27. Wright, D.C.
RAPRA confidential report No. 1908, Oct. 1975.

28. Bryan-Brown, M.H. and Walker, D.M.
"Power station condenser waterboxes in GRP", British Plastics Federation, 11th Reinforced Plastics conference, Brighton, Nov. 1978.

29. Wyatt, R.C., Norwood, L.S. and Phillips, M.G.
"The stress-rupture behaviour of GRP laminates in aqueous environments", 1st International conference on composite structures, Paisley, September 1981.

30. Wyatt, R.C., Norwood, L.S. and Phillips, M.G.
CEGB Report No. SSD/SW/82/N161, Nov. 1982.

31. Phillips, M.G., Heppell, N., Wyatt, R.C. and Norwood, L.S., "Creep rupture behaviour of glass fibre composites in aqueous environments", Ann. Conf. Reinforced-Plastics/Composites Institute, Houston, Texas, Feb. 1983.

32. Sims, G.D. and Gladman, D.G.
Plastics and Rubber: Materials and Applications, May 1978, pp. 41-48.

33. Crowther, M.F.
Ph.D. Thesis, Bath University, 1987.

34. Crowther, M.F., Wyatt, R.C. and Phillips, M.G.
Composites Science and Technology, Vol. 36, 1989, pp. 191-210.

35. Owen, M.J. and Found, M.S.
J. Phys. D:Appl. Phys., Vol. 8, 1975, pp. 480-497.

36. Owen, M.J. Griffiths, J.R. and Found, M.S.
"Biaxial stress fatigue testing of thin walled GRP cylinders", in Proc. of the 1976 Int. Conf. on Composite Materials, New York, USA, 1976, pp. 917-941.

37. Owen, M.J. and Griffiths, J.R.
J. Mats. Sci., Vol. 13, No. 7, July 1978, pp. 1521-1537.

38. Owen, M.J. and Rice, D.J.
Composites, Vol. 12, No. 4, Jan. 1981, pp. 13-25.

39. Norris,C.B.
"Strength of orthotropic materials subjected to combined stress", Forest Products Report No. 1816, Forest Products Laboratory, Madison, Wisconsin, U.S., May 1962.

40. Pagano, N.J. and Whitney, J.M.
J. of Composite Materials, Vol. 4, July 1970, pp. 360-378.

41. Soden, P.D., Kitching, R. and Tse, P.C.
Composites, Vol. 20, No. 2, March 1989, pp. 125-134.

42. Highton, J., Adeoye, A.B. and Soden, P.D.
J. of Strain Analysis, Vol. 20, No. 3, 1985, pp. 139-150.

43. Koski, L.
Experimental evaluation of the long term strength of reinforced plastic (GRP) pipes", Technical Research Centre of Finland Report No. VTT 518, 1988.

44. Lieblin, S.
"Survey of long-term durability of fiberglass-reinforced plastic structures", NASA-CR-165320, 1981.

45. Lenain, J.C. and Bunsell, A.R.
Composites, April 1978, pp. 77-82.

46. Wylie, E.B. and Streeter, V.L.
"Fluid Transients", McGraw-Hill, USA, 1978.

47. Streeter, V.L. and Wylie, E.B.,
"Fluid Mechanics", McGraw-Hill, USA, 1975.

48. Streeter, V.L. and Wylie, E.B.
"Hydraulic Transients", McGraw-Hill, USA, 1967.

49. Engineering Sciences Data, Item No. 83046, Fluid mechanics-Fluid flow, Speed of propagation of pressure waves. Engineering Sciences data unit, London, 1985.

50. Kroon, J.R. Stoner, M.A. and Hunt, W.A.
J. American Water Works Association, Vol. 76, No. 11, Nov. 1984, pp. 39-45.

51. P. Tanner. Private communication, 30/10/87.

52. Williams, D.C. and Pulley, M.J.
CEGB SSD/SW/77/M6584, 1984.

53. Armenakas, A.E., Garg, S.K. and Sciammarella, C.A.
J. of Applied Physics, Vol. 41, No. 4, 1970, pp. 1657-1664.

54. O'Neill, K.B., Dague, M.F. and Kimmel, J.E.
"High Speed Tensile Testing of Tyre Textiles", in High Speed Testing, Vol. 5, Edited by Dietz, A.G.H. and Eirich, F.R., Interscience Publishers, New York, 1965.

55. McAbee, E. and Chmura, M.
SPE Journal, 1961, Section 13-D, pp. 1-10.

56. McAbee, E. and Chmura, M.
"Static and High Rate Tensile Behaviour of Various Resin-Reinforcement Combinations", in High Speed Testing, Vol. 5, Edited by Dietz, A.G.H. and Eirich, F.R., Interscience Publishers, New York, 1965.

57. Liftshitz, J.M.
J. Composite Materials, Vol 10. Jan 1976, pp. 92-101.

58. Harding, J. and Saka, K.
University of Oxford, Department of Engineering Science report No. OUEL 1602/85, 1985.

59. Harding, J. and Welsh, L.M.
J. Mats. Sci., Vol. 18, No. 6, June 1983, pp. 1810-1826.

60. Rotem, A. and Liftshitz, J.M.
"Longitudinal Strength of Unidirectional Fibrous Composite under High Loading Rate". Proc. of 26th Annual Technical conf., Reinforced plastics/Composites Division, The Society of the Plastics Industry, Section 10-G, Feb. 1971.

61. Daniel, I.M. and Liber, T.
"Testing of fibre composites at high strain rates", in Proc. of 2nd Int. Conf. on composite materials, ICCM/2, Toronto, Canada, April 1978, pp. 1003-1018.

62. Armenakas, A.E. and Sciammarella, C.A.
Experimental Mechanics, Vol. 13, Oct. 1973, pp. 433-440.

63. Welsh, L.M. and Harding, J.
"Effect of strain rate on the tensile failure of woven-reinforced polyester resin composites", In Proc. DYMAT 85, Int. Conf. on Mechanical and Physical behaviour of Materials under Dynamic Loading, Paris 2-5 September, 1985.

64. Kawata, K., Hondo, A., Hashimoto, S., Takeda, N. and Chung, H.L.
"Dynamic Behaviour Analysis of Composite Materials" in proceedings of the Japan-US conference on composite materials, Tokyo, Jan. 1981, pp. 2-11.

65. Pink, E. and Campbell, J.D.
J. Mats. Sci., Vol. 9, No. 4, April 1974, pp. 658-664.

66. Kumar, A.
Applied Polymer Symposia, No. 12, 1968, pp. 731-738.

67. Hall, I.H.
J. of Applied Polymer Science, Vol. 12, 1968, pp. 731-738.

68. Eirich, F.R.
"On the strength of Polymeric materials at high rates of strain", in High Speed Testing, Vol. 5, Edited by Dietz, A.G.H. and Eirich, F.R., Interscience Publishers, New York, 1965.

69. McAbee, E. and Chmura, M.
SPE Journal, Jan. 1963, pp. 83-90.

70. Nahas, M.N.
J. Mats. Sci., Vol. 22, No. 2, Feb. 1987, pp. 657-662.

71. Bax, J., Plastics and Polymers, Vol. 38, No. 133, Feb. 1970, pp. 27-30.

72. Jones, C.J., Dickson, R.F., Adam, T., Reiter, H. and Harris, B.
Proc. Roy. Soc. Lond. A 396, 1984, pp. 315-338.

73. White, R.J., Ph.D. thesis, Bath University, 1985.

74. Bushby, R.S.
"Evaluation of creep response for glass/phenolic composites", Final year project, University of Bath, 1989.

75. E.Curtis (CEGB-MEL), private communication, 13/2/89.

76. Pleuddemann, E.P.
"Mechanism of adhesion through silane coupling agents", in Composite Materials, Vol. 6, Ed. by Broutmann and Krock, Academic Press, New York, 1974. pp. 174-216.

77. Garrett, K.W. and Bailey, J.E.
J. Mats. Sci., Vol. 12, .No. 1, Jan. 1977, pp 157-168.

78. Dodds, R.
RAPRA Members Journal, May/June 1976, pp. 49-56.

79. Dodds R.
RAPRA Members Journal, July/August 1976, pp. 71-76.

80. Talreja, R.
J. of Composite Materials, Vol. 19, July 1985, pp. 355-375.

81. Krolikowski, W.
SPE Journal, Sept. 1964, pp. 1031-1035.

82. Heppell, N. and Phillips, M.G.
"The tensile stress-rupture behaviour of grp in aqueous environments", SWIRL Report No. 2451, Feb. 1983.

83. Babic,L. Dunn,C. and Hogg, P.J.
Plastics and Rubber Processing and Applications, Vol.12, 1989, pp. 199-207.

84. Hogg,.P.J., Hull, D. and Price, J.N.
"Stress Corrosion of GRP" in Proc. 39th Ann. Conf. Reinf. Plastics Inst., The Society of the Plastics Industry, New York, Jan. 1984.

85. Priddin, K.G.
BHRA Report No. RR1793 "Transient pressure testing of GFRP pipe", Feb. 1982.

86. Jones, M.L.C. and Hull, D.
J. Mats. Sci., Vol. 14, No. 1 Jan 1979, pp. 165-174.

87. Chatfield, C.
"Statistics for technology, A Course in Applied Statistics", 3rd edition, Chapman and Hall, London, 1985.

OVERLOAD TREATMENT		RESIDUAL UTUS	RESIDUAL MODULUS
No. of overloads	Overload magnitude	(N/mm per kg/m^2)	(N/mm per kg/m^2)
10	60% UTUS	209.79 (±15)	13770 (±396)
30	60% UTUS	218.18 (±17)	14238 (±302)
50	60% UTUS	216.62 (±14)	13387 (±840)
VIRGIN MATERIAL		233.12 (±21)	19026 (±2793)

TABLE 1

COUPON LOAD HISTORY	No. of coupons in sample	No. of rovings sampled per coupon	Fibre breaks (%)
Virgin coupons	5	2	0
50 repetitions of the model water hammer event.	5	2	0
Peak load: 60% UTUS Load/unload: crosshead speed=0.5mm/min. Dwell at peak load: 0s. 1 repetition.	5	2	16
Peak load: 60% UTUS Load/unload: crosshead speed=0.5mm/min. Dwell at peak load: 10s. 1 repetition.	5	2	32

TABLE 2

	Polyester matrix material	Vinyl ester matrix material
Predicted strength retention after 30 years (% mean UTUS).	11%	37%
Gradient	−7.35	−3.84
Correlation coefficient	0.85	0.77

TABLE 3 Data from linear regression analysis on overloaded coupon stress–rupture results.

FIGURE	TEST PIECE	PRESSURE TRANSDUCER DATA DEPICTED	PEAK PRESSURE RECORDED (Bar)
10.7	STEEL T-PIECE	PT 1	22.25
		PT 3	23.5
10.8	" "	PT 4	22.5
		PT 2	22.5
10.9	" "	PT 1	22.5
		PT 2	22.5
10.10	" "	PT 4	22.0
		PT 3	23.5

(The data given above were all recorded during the passage of the same pressure pulse).

TABLE 4

EVENT	CAVITY VOLUME (m^3)	RESERVOIR HEAD (Bar)	PEAK PRESSURE ACHIEVED (Bar)
1	0.0069	0.247	21.8
2	0.0070	"	21.9
3	0.0069	"	21.6
4	0.0069	"	22.0
5	0.0068	"	21.1

TABLE 5.

EVENTS AFTER FILLING RIG	CAVITY VOLUME (m^3)	PEAK PRESSURE ACHIEVED (Bar)
1	0.0072	2.5
2	0.0082	4.5
3	0.0082	8.0
4	0.0082	11.0
5	0.0082	12.6
6	0.0104	13.7
7	0.0122	20.5
8	0.0090	20.7
9	0.0090	20.5

All tests conducted at a reservoir head of 0.346 Bar.

TABLE 6.

EVENTS AFTER FILLING RIG	CAVITY VOLUME (m^3)	PEAK PRESSURE ACHIEVED (Bar)
1	0.0142	10.8
2	0.0142	17.3
3	0.0142	18.3
4	0.0173	19.4
5	0.0144	23.8
6	0.0111	23.7
7	0.0111	21.2
8	0.0111	24.8
9	0.0111	25.7

All tests conducted at a reservoir head of 0.346 Bar.

TABLE 7.

FIGURE	TEST NUMBER	PRESSURE TRANSDUCERS DEPICTED	PEAK PRESSURE ACHIEVED (Bar)
10.18	206	PT 1	23.5
		PT 2	22.5
10.19	206	PT 3	23.0
		PT 4	22.5
10.20	207	PT 3	20.0
		PT 4	20.0
10.21	207	PT 1	21.0
		PT 2	20.5
10.22	208	PT 1	24.5
		PT 2	23.5
10.23	208	PT 3	23.5
		PT 4	23.5
10.24	209	PT 1	25.5
		PT 2	24.5
10.25	209	PT 3	24.5
		PT 4	24.5

TABLE 8

CAVITY VOLUME (m^3)	PEAK PRESSURE ACHIEVED (Bar).
0.0387	16.7
0.0344	23.0
0.0199	22.0
0.0148	23,7
0.0117	23.0
0.0090	23.2
0.0082	22.9
0.0078	23.0
0.0080	23.3
0.0073	23.8

(Reservoir head = 0.346 Bar).

TABLE 9.

Pipe	Failure pressure (Bar)	Limit of linearity in strain (%)		Maximum strain recorded (%)	
		Hoop	Axial	Hoop	Axial
4	38.33	0.56	0.34	0.86	0.47
5	36.33	0.71	0.34	0.75	0.34
6	41.33	0.9	0.37	0.9	0.41

TABLE 10 GFRP pipe burst test data.

HOOP STRESS (% MEAN VALUE AT BURST)	Log TIME TO FAILURE (seconds) VIRGIN PIPES					OVERLOADED PIPES				
40	6.39	6.49	7.03	►7.18	►7.19	6.22	6.22	6.41	6.48	6.81
45	6.78	6.86	►7.15	►7.15	—	4.78	5.78	5.25	5.38	6.32
50	6.48	5.87	6.72	6.14	5.68	4.81	6.08	5.10	6.40	5.70
60	6.64	6.76	6.11	6.66	6.64	3.26	5.11	5.81	2.95	5.68
70	4.78	5.72	5.72	5.68		3.56	3.65	3.73	4.21	4.23

(► Denotes a "runout")

TABLE 11 Pipe stress-rupture data.

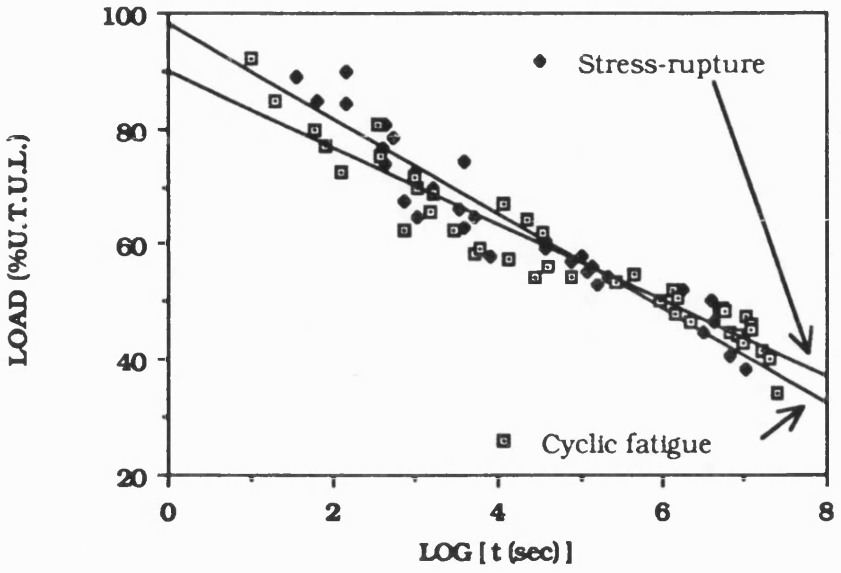

Test life as a function of applied load for GRP under two loading regimes, static and cyclic fatigue.

FIGURE 3.1 (from Ref. 34)

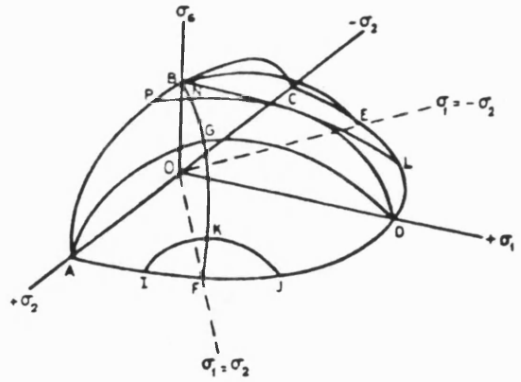

Failure surface in $\sigma_1, \sigma_2, \sigma_3$ space.

FIGURE 3.2 A theoretical failure envelope (from Ref. 37).

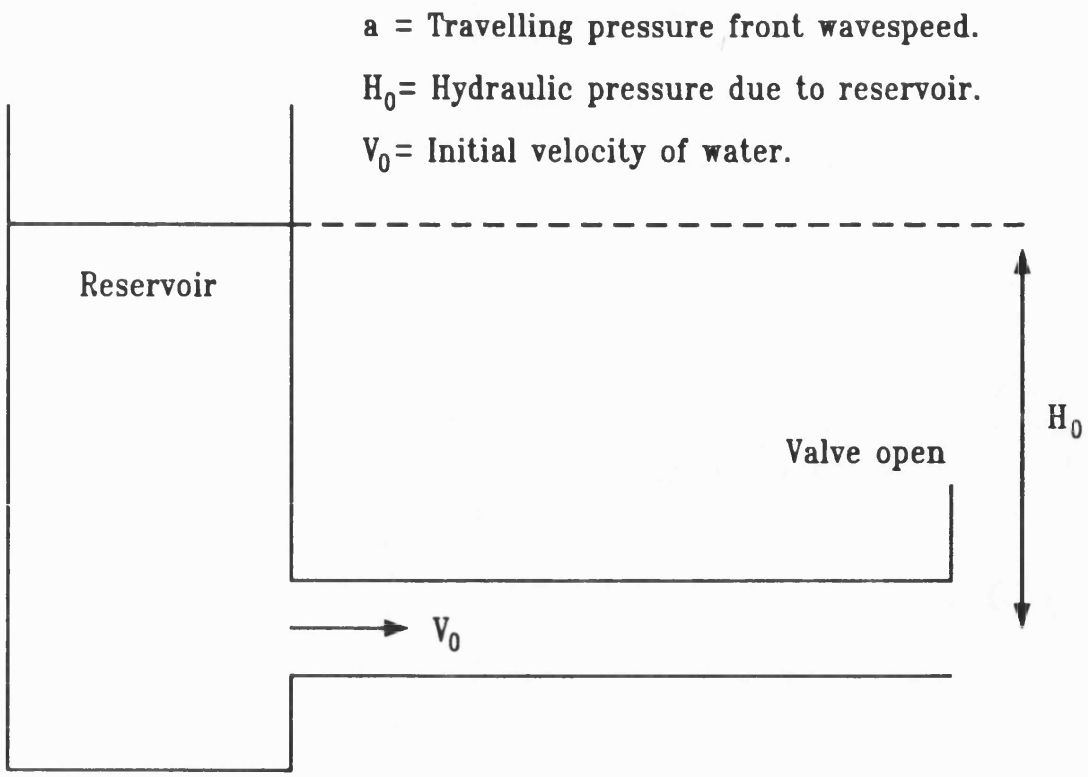

FIGURE 4.1

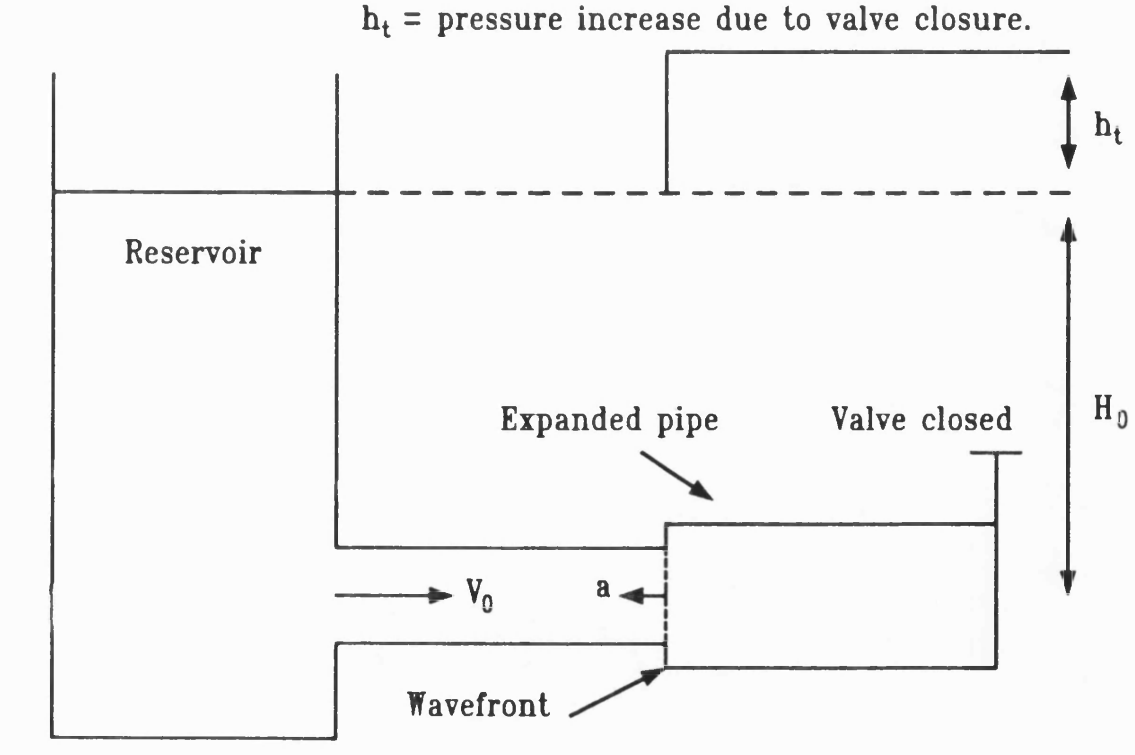

FIGURE 4.2

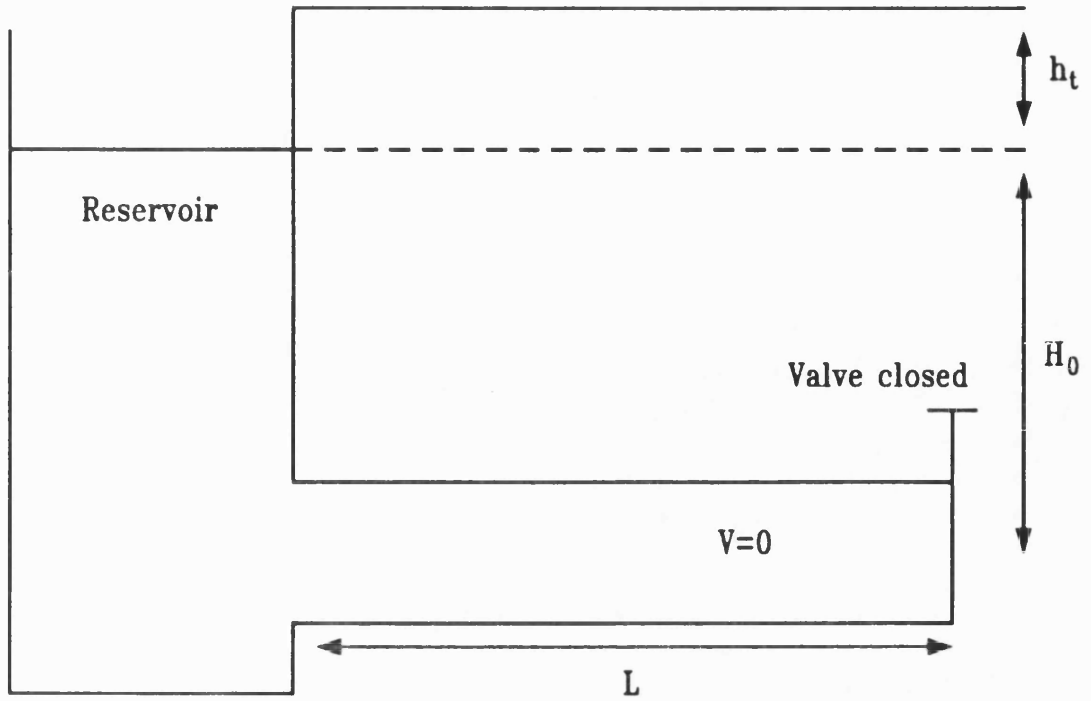

FIGURE 4.3 System conditions after L/a seconds.

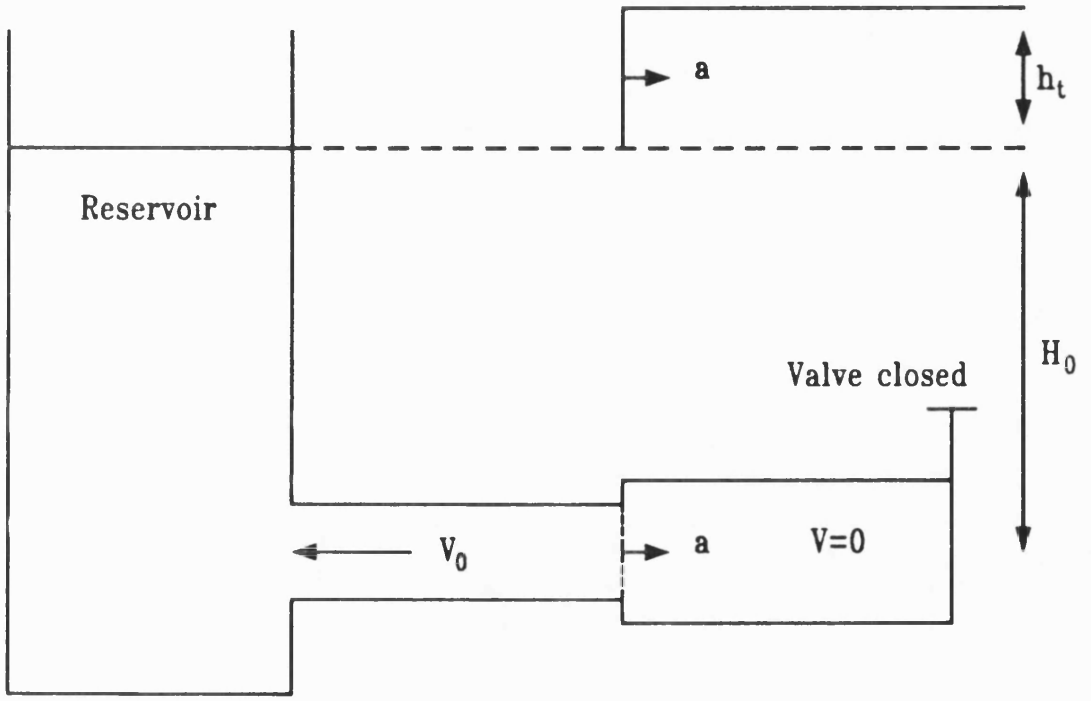

UPSTREAM DOWNSTREAM

FIGURE 4.4

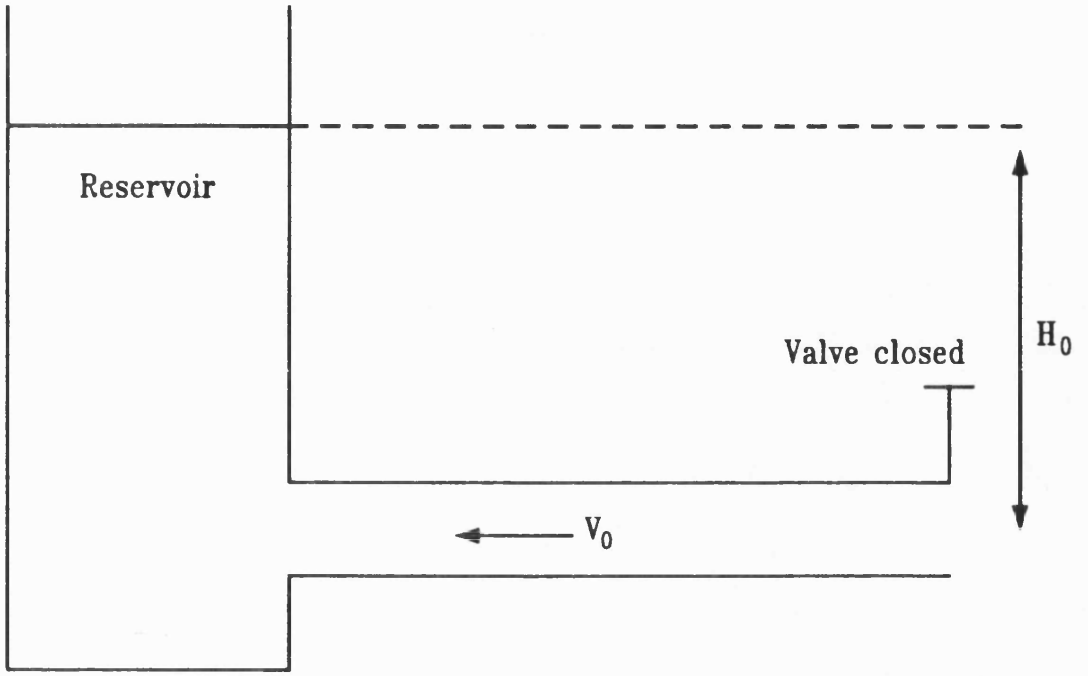

FIGURE 4.5

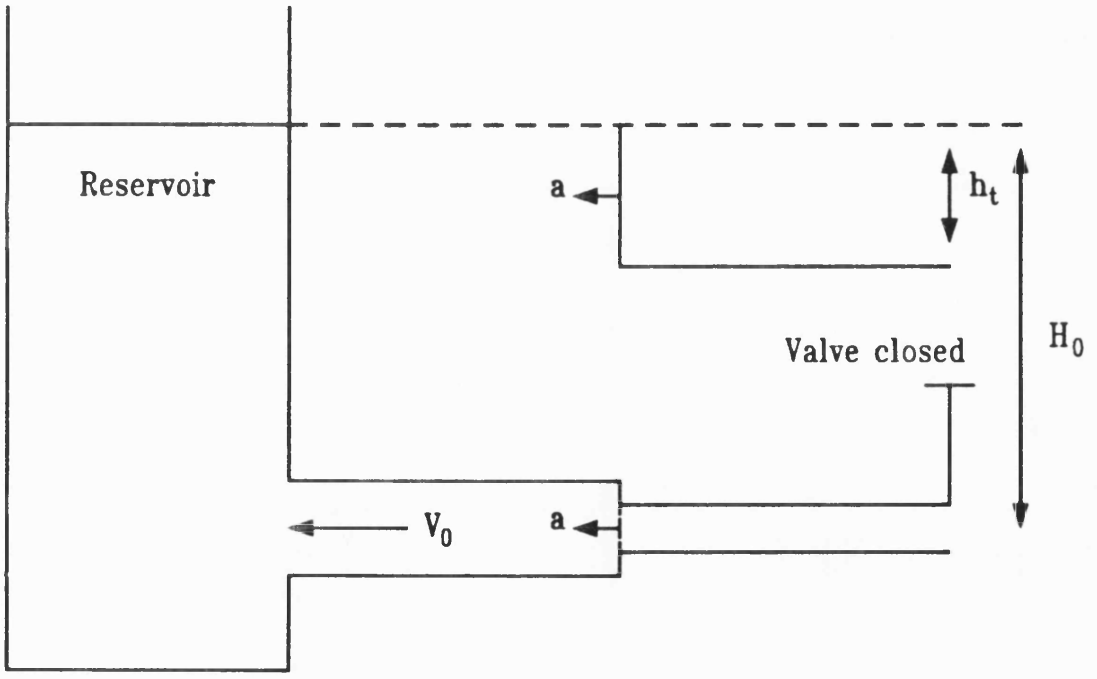

FIGURE 4.6

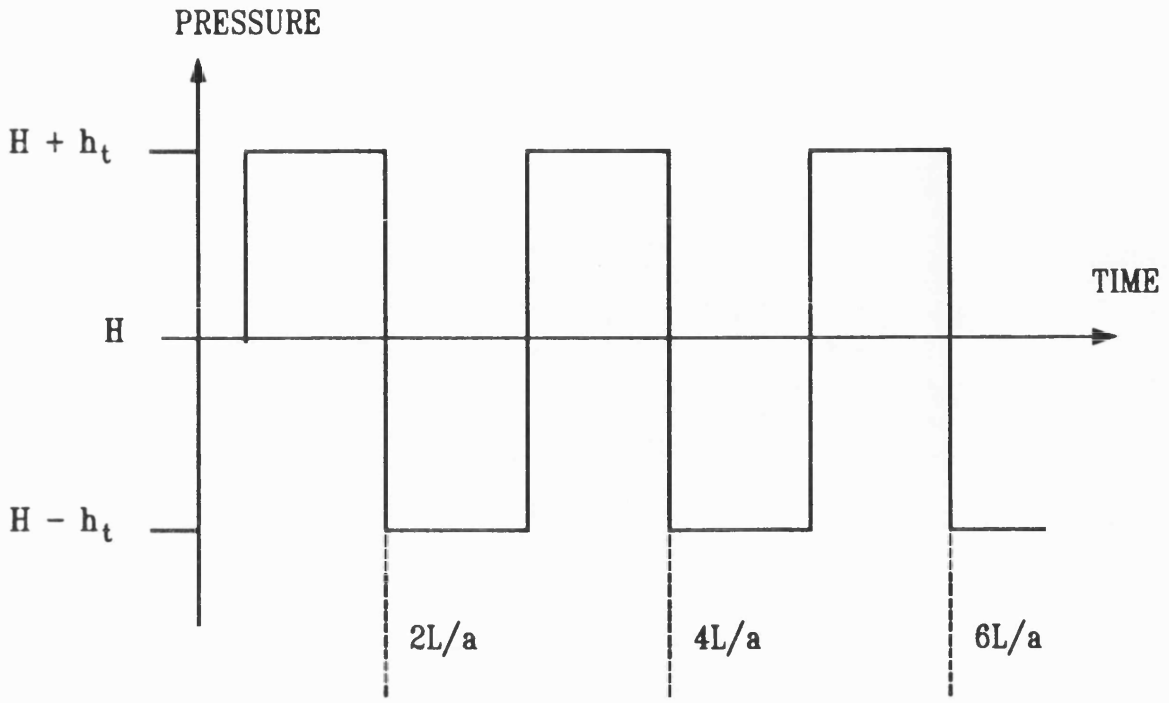

FIGURE 4.7 Pressure profile at valve.

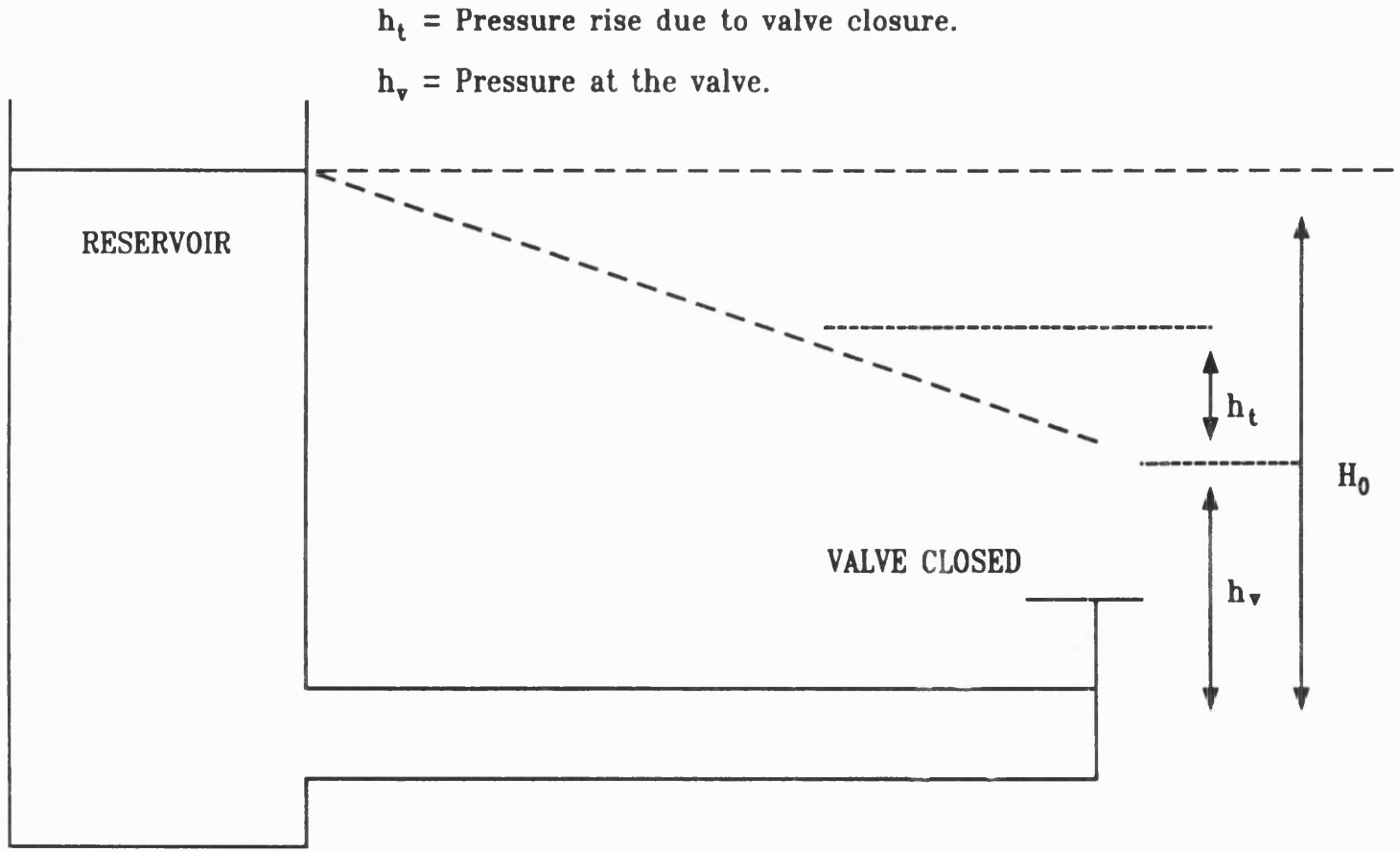

FIGURE 4.8 Simple piping system with friction.

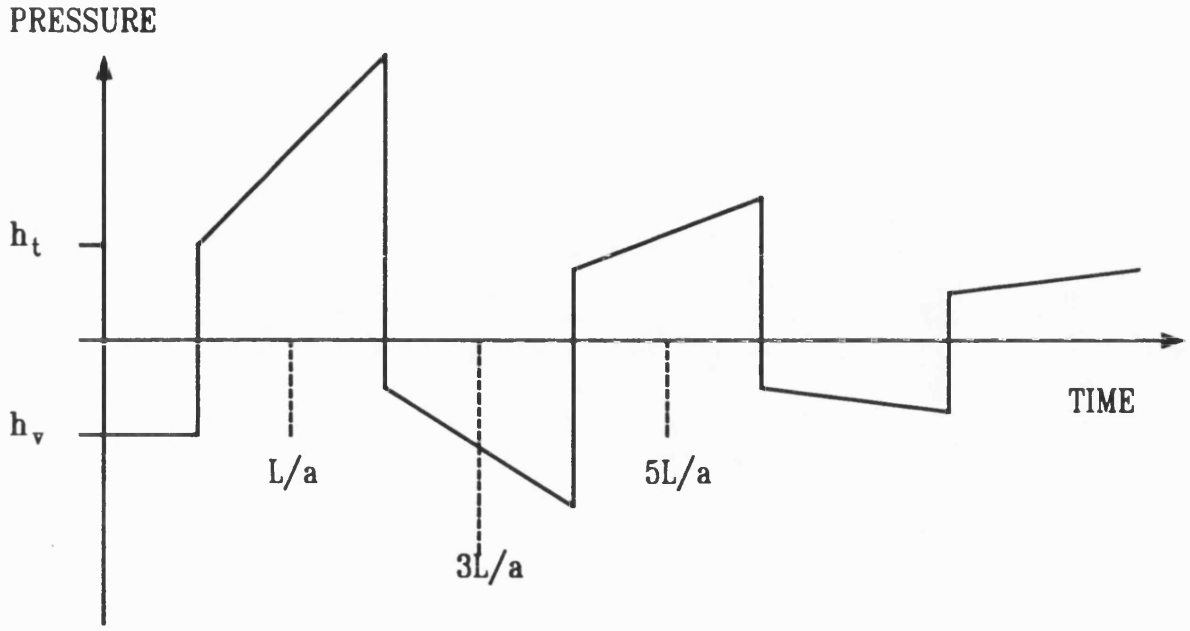

FIGURE 4.9 Pressure profile at valve for piping system with friction.

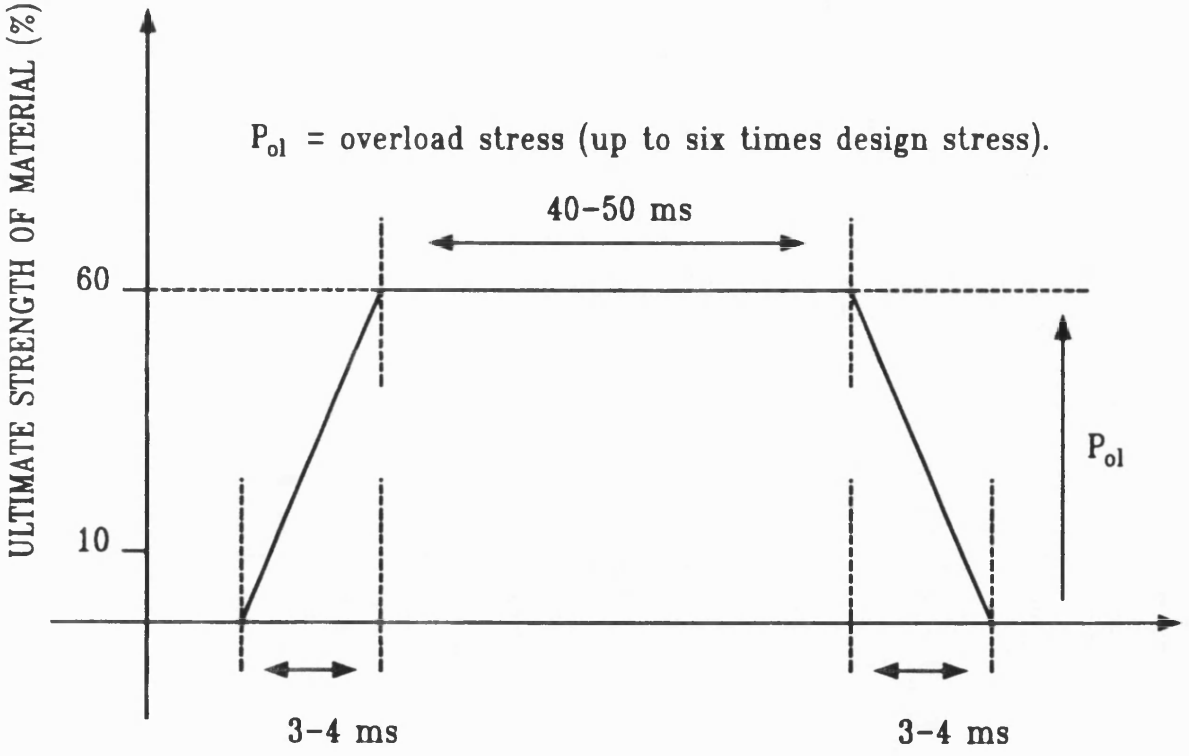

FIGURE 4.10 Transient overload specified by CEGB.

RESIN: Scott Bader Crystic 625 (Polyester)
or Dow Derakane 411-45 (Vinyl ester)

REINFORCEMENT:

Multemat chopped strand mat (CSM) by Fibreglass Ltd.
Type ECK 25 bi-directional woven roving (WR) by TBA Ltd.

CONSTRUCTION.

1×300 gms/m^2 CSM
1×830 gms/m^2 WR
1×300 gms/m^2 CSM

CURE: 5 hours at 40^0C.

FIGURE 7.1 Coupon material specification.

[DIMENSIONS: mm]

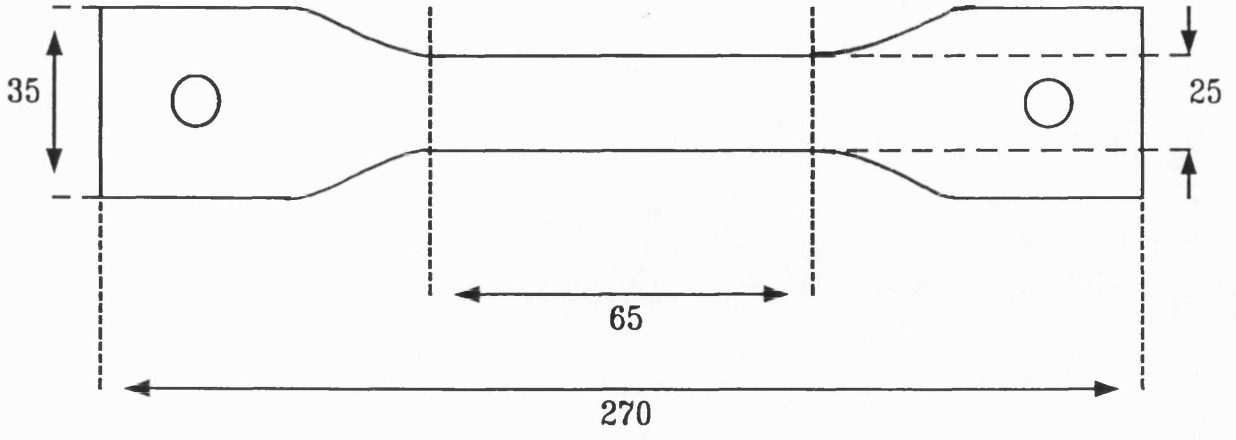

FIGURE 7.2 Coupon Dimensions.

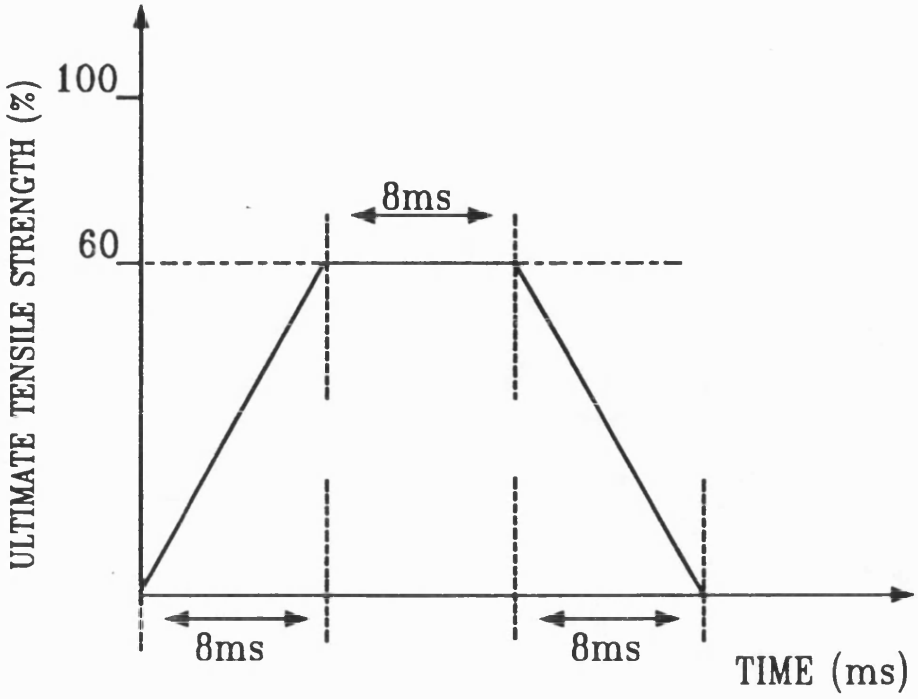

FIGURE 7.3

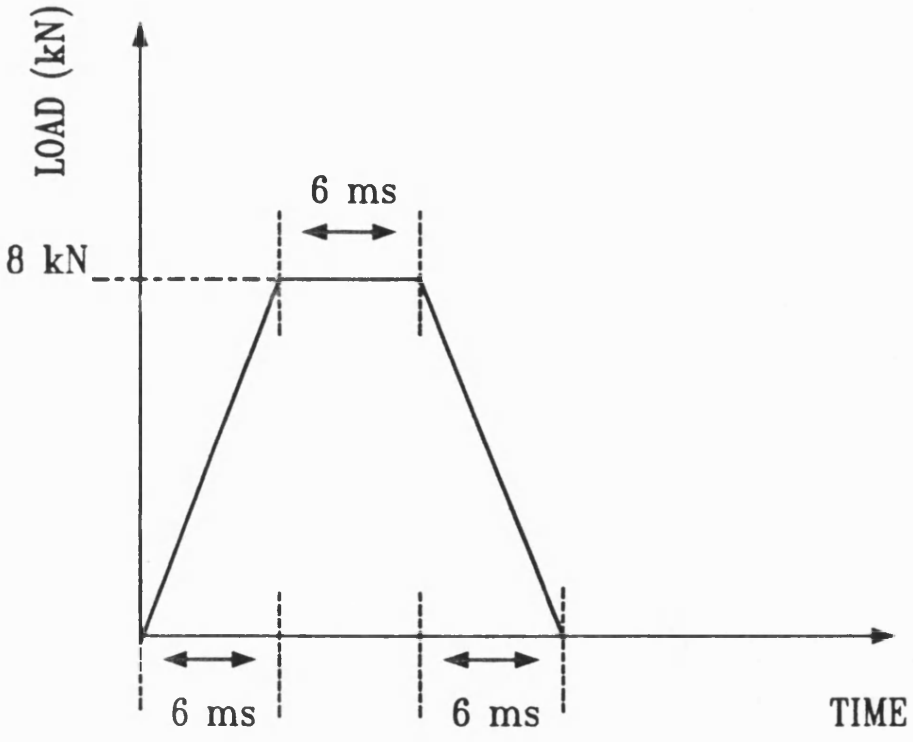

Input signal for overload of coupon test pieces.

FIGURE 7.4

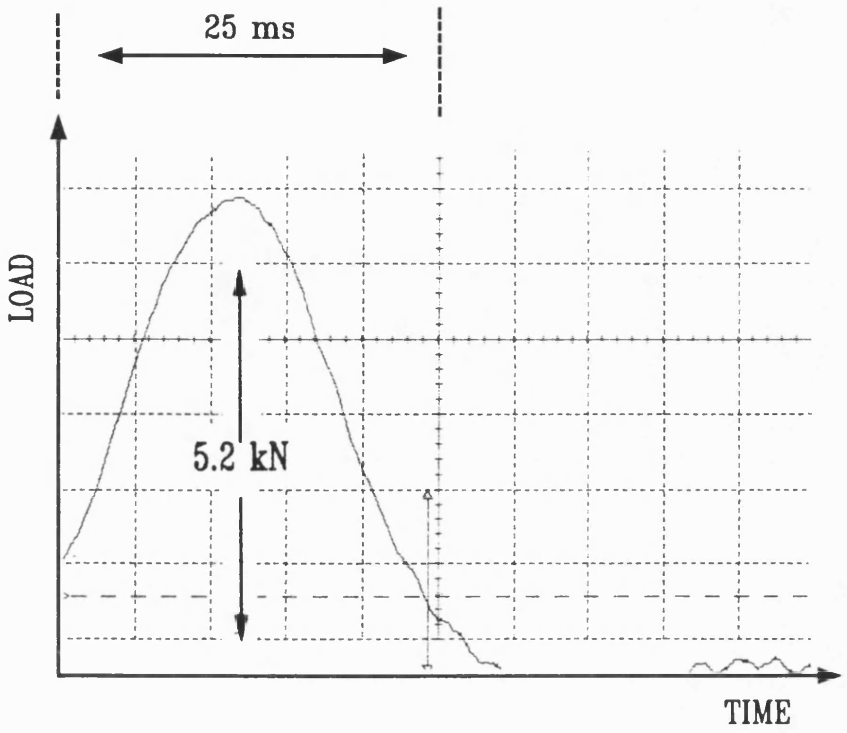

FIGURE 7.5 Profile of a single overload event.

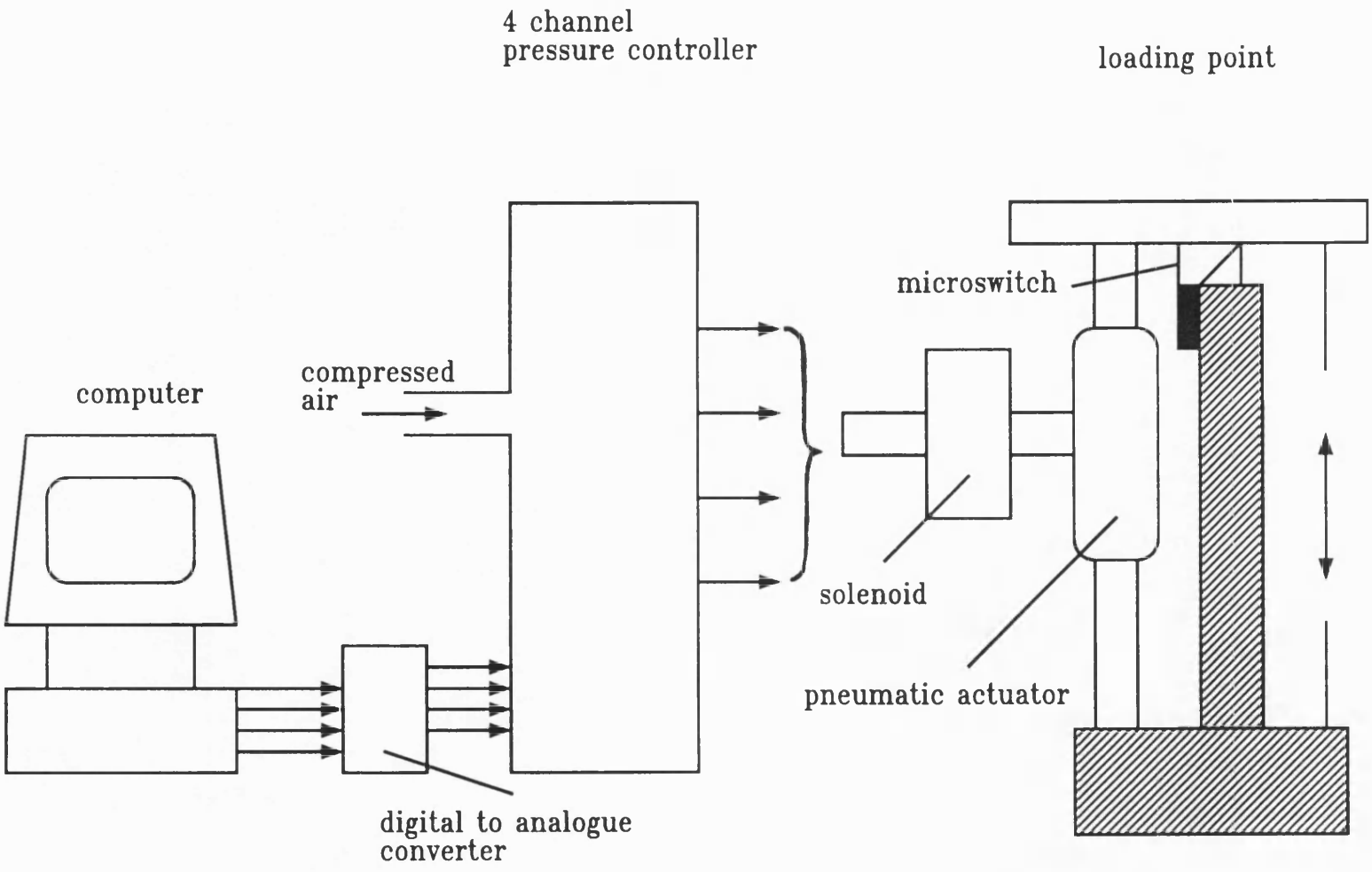

FIGURE 7.6 Schematic representation of pneumatic loading rig.

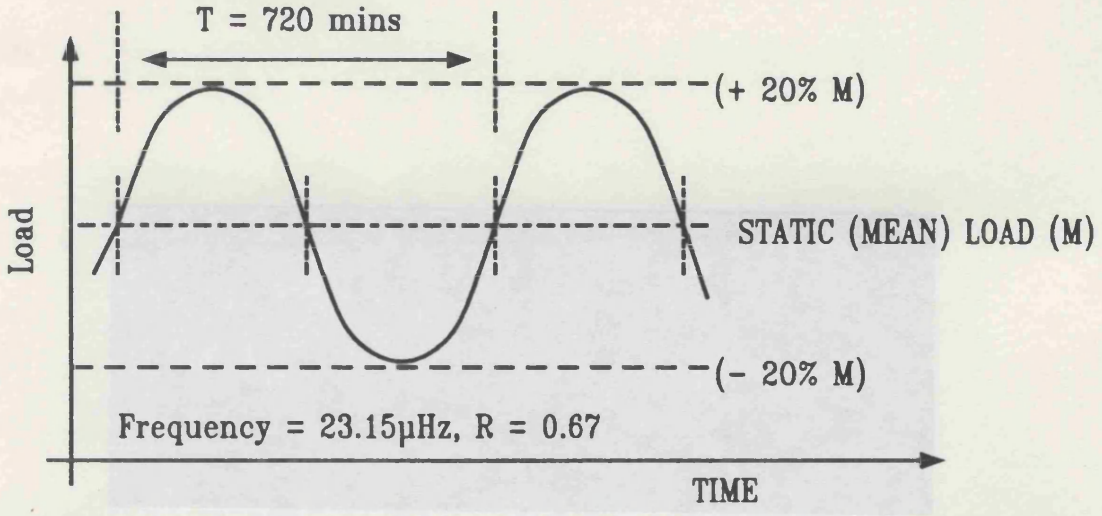

Load profile for stress-rupture with superimposed sinusoidal load.

FIGURE 7.7

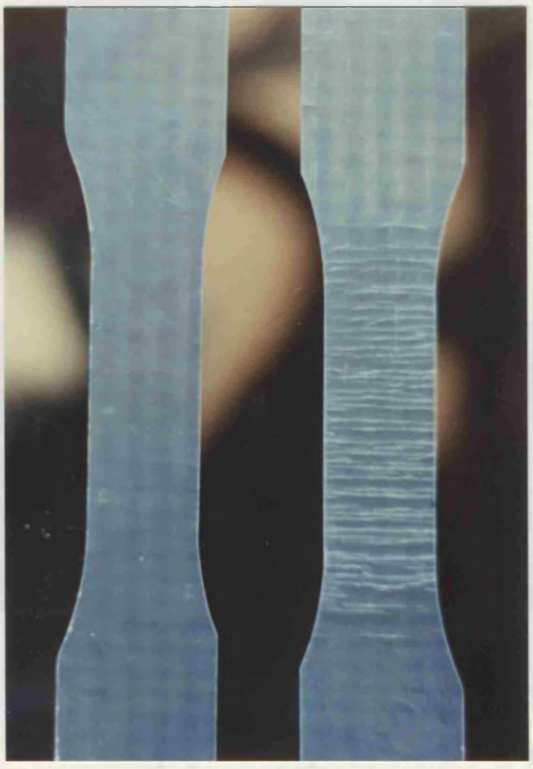

(i) (ii)

FIGURE 8.1 (i) Virgin material.
(ii) Coupon after one overload application.

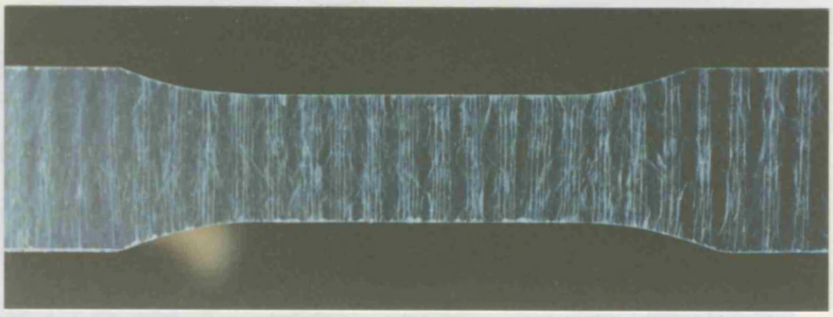

Overloaded polyester coupon, banded damage type

FIGURE 8.2

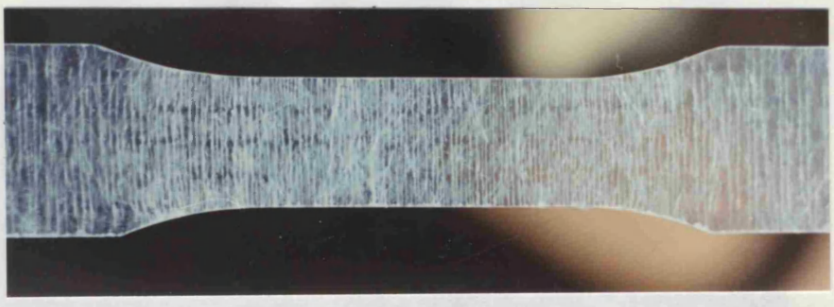

Overloaded polyester coupon, uniform damage type

FIGURE 8.3

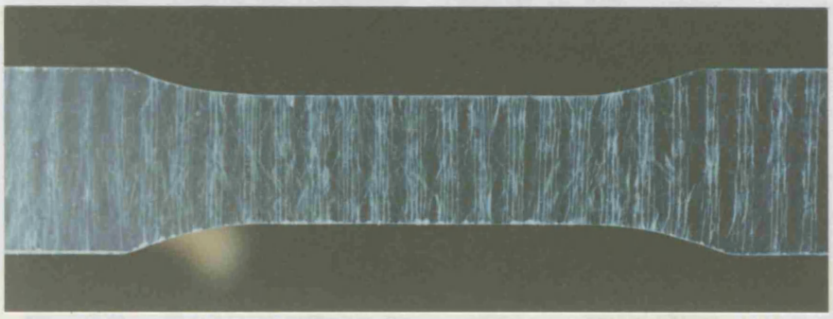

Polyester coupon: 50 repetitions
60% UTUS overload.

Polyester coupon: 50 repetitions
30% UTUS overload

FIGURE 8.5

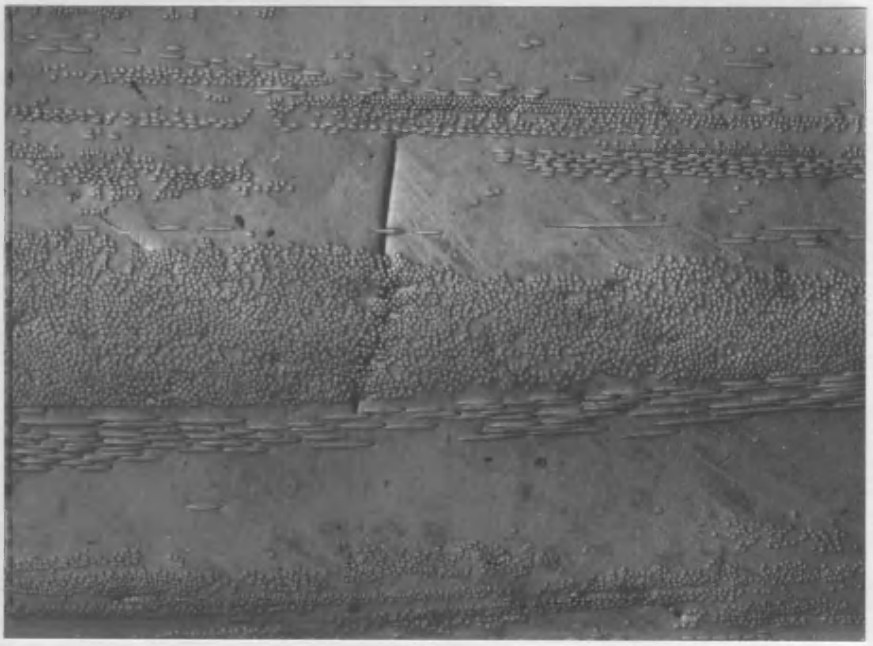

Optical micrograph showing resin cracking originating from a transverse roving bundle after one 60% UTUS overload cycle. Magnification: 50.

FIGURE 8.6

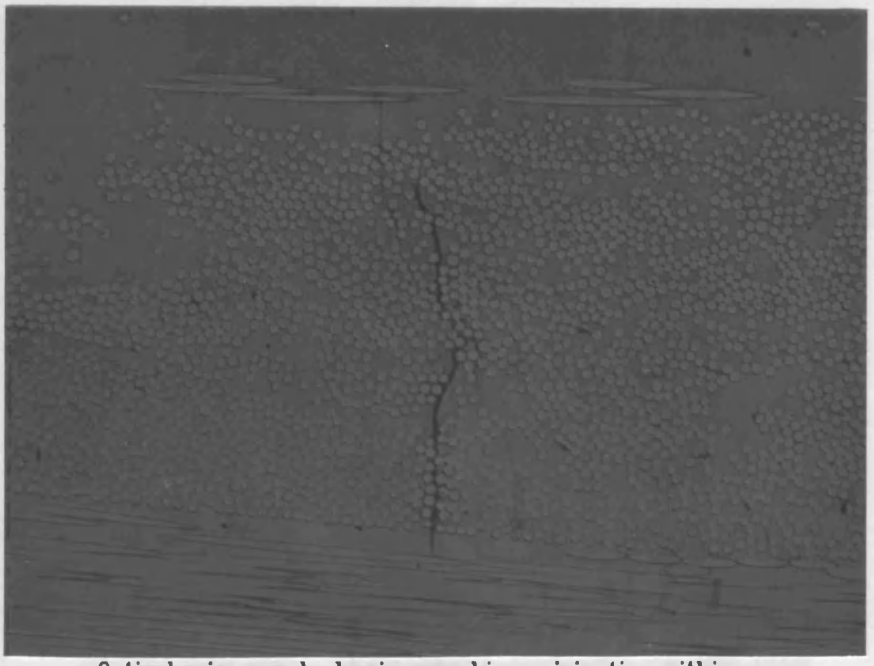

Optical micrograph showing cracking originating within a transverse roving bundle after one 60% UTUS overload cycle. Magnification 100.

FIGURE 8.7

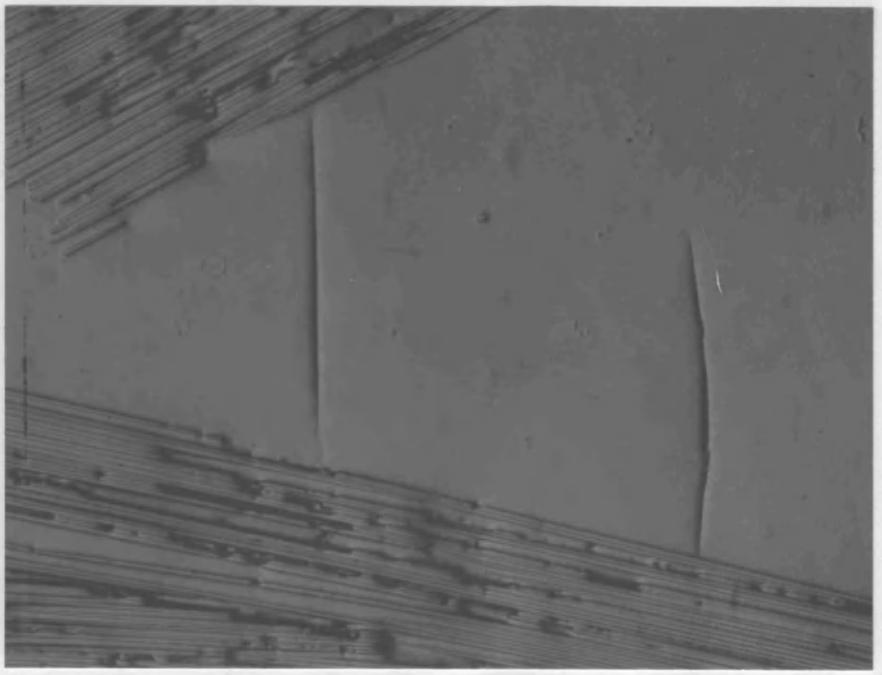

In-plane section from a polyester coupon after one 60% UTUS overload cycle.
Magnification: 50.

FIGURE 8.8

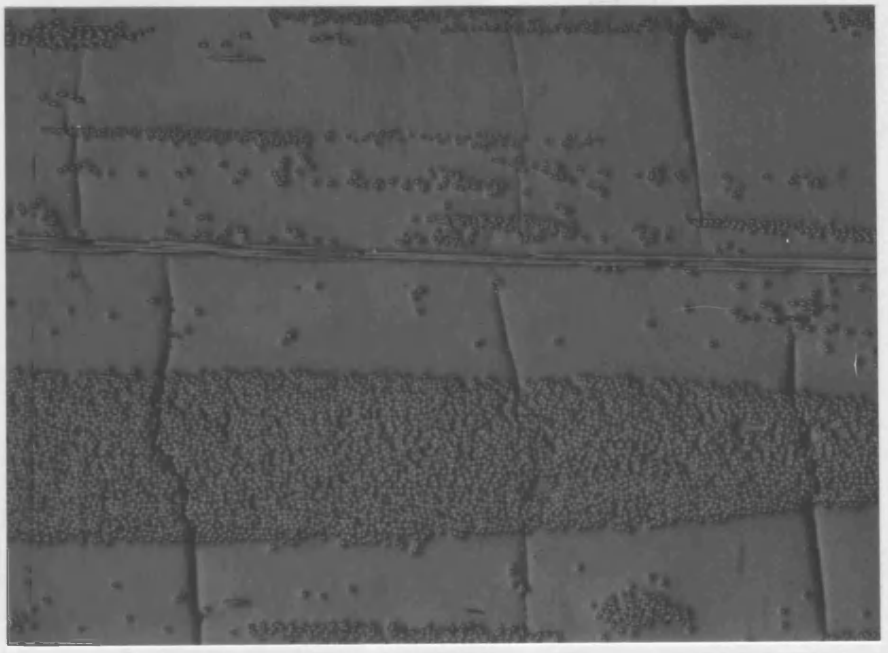

Longitudinal section of polyester coupons after fifty 60% UTUS overload cycles.
Magnification: 50.

FIGURE 8.9

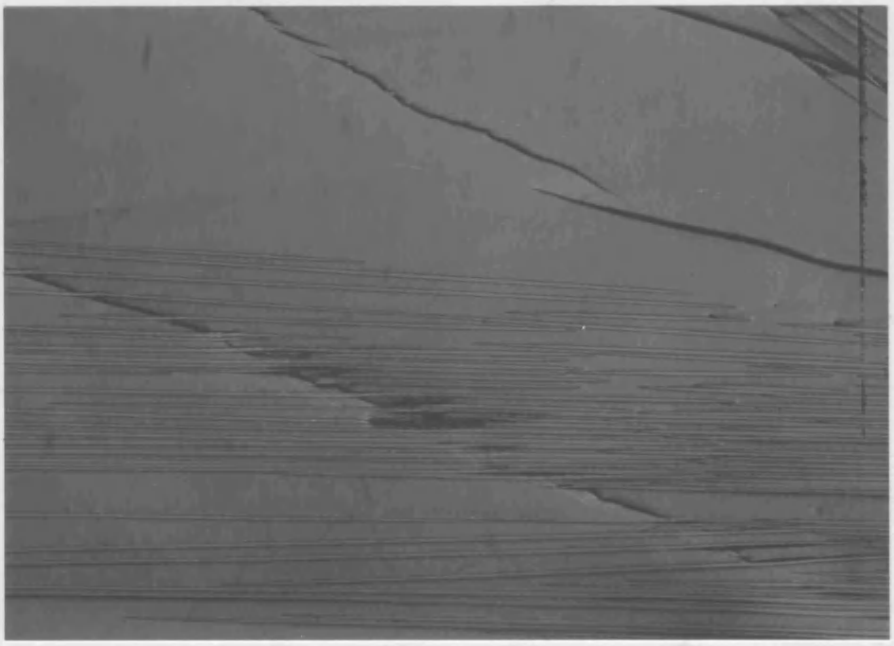

In-plane section of polyester coupon after fifty 60% UTUS overload cycles.
Magnification: 50.

FIGURE 8.10

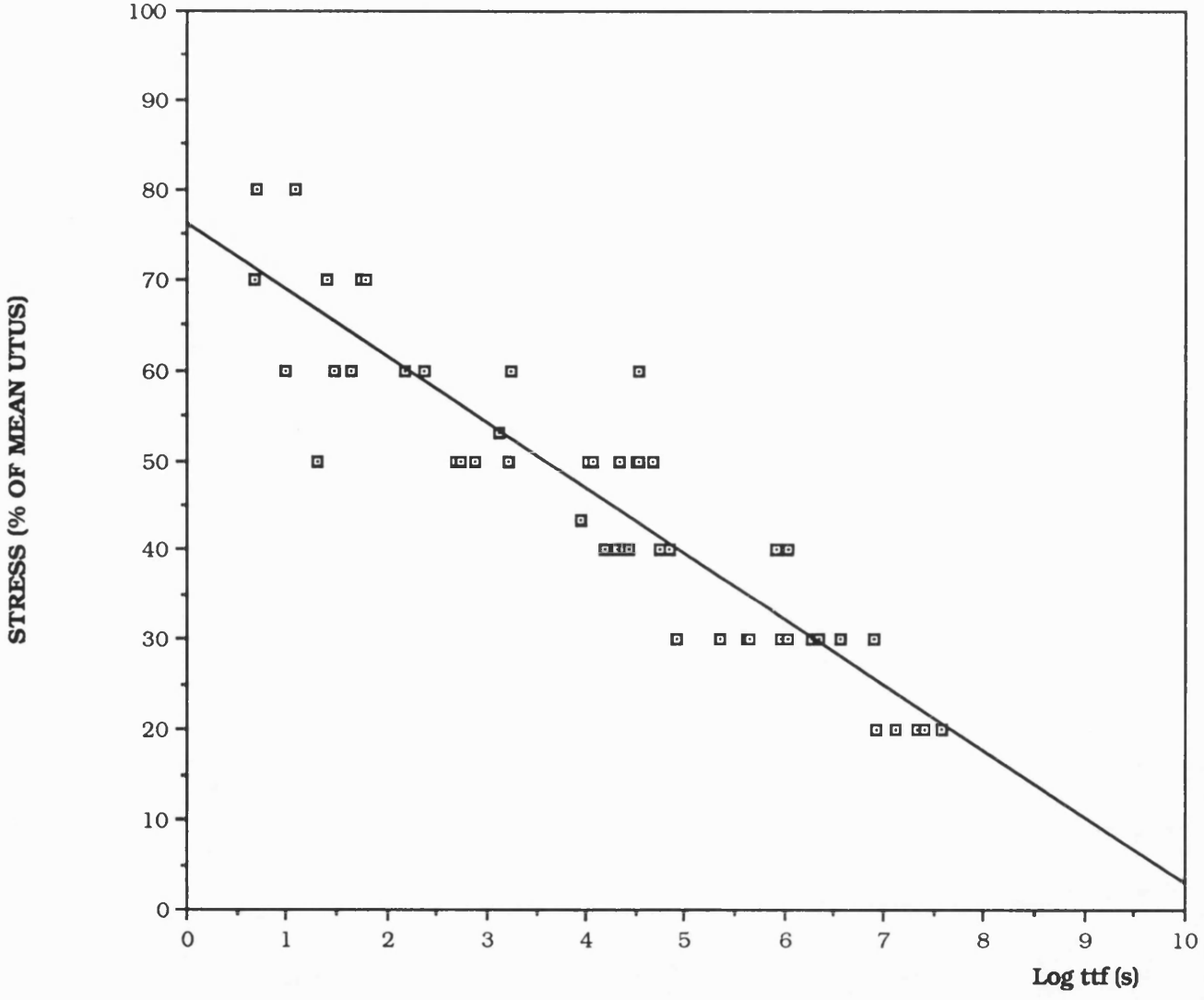

FIGURE 8.11 STRESS-RUPTURE DATA FOR FAILED OVERLOADED POLYESTER COUPONS.

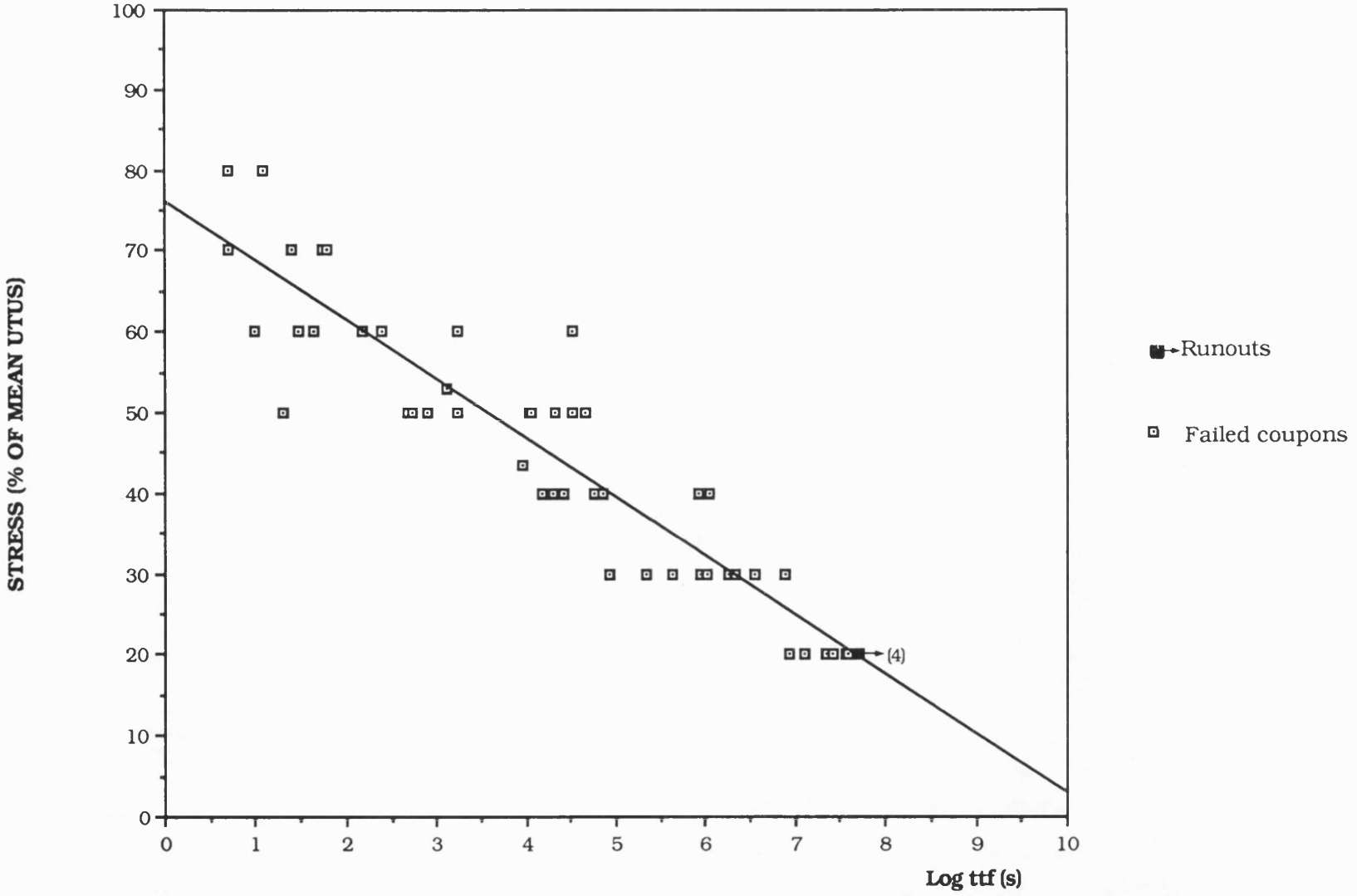

FIGURE 8.12 PLOT OF STRESS-RUPTURE DATA FOR OVERLOADED POLYESTER COUPONS.

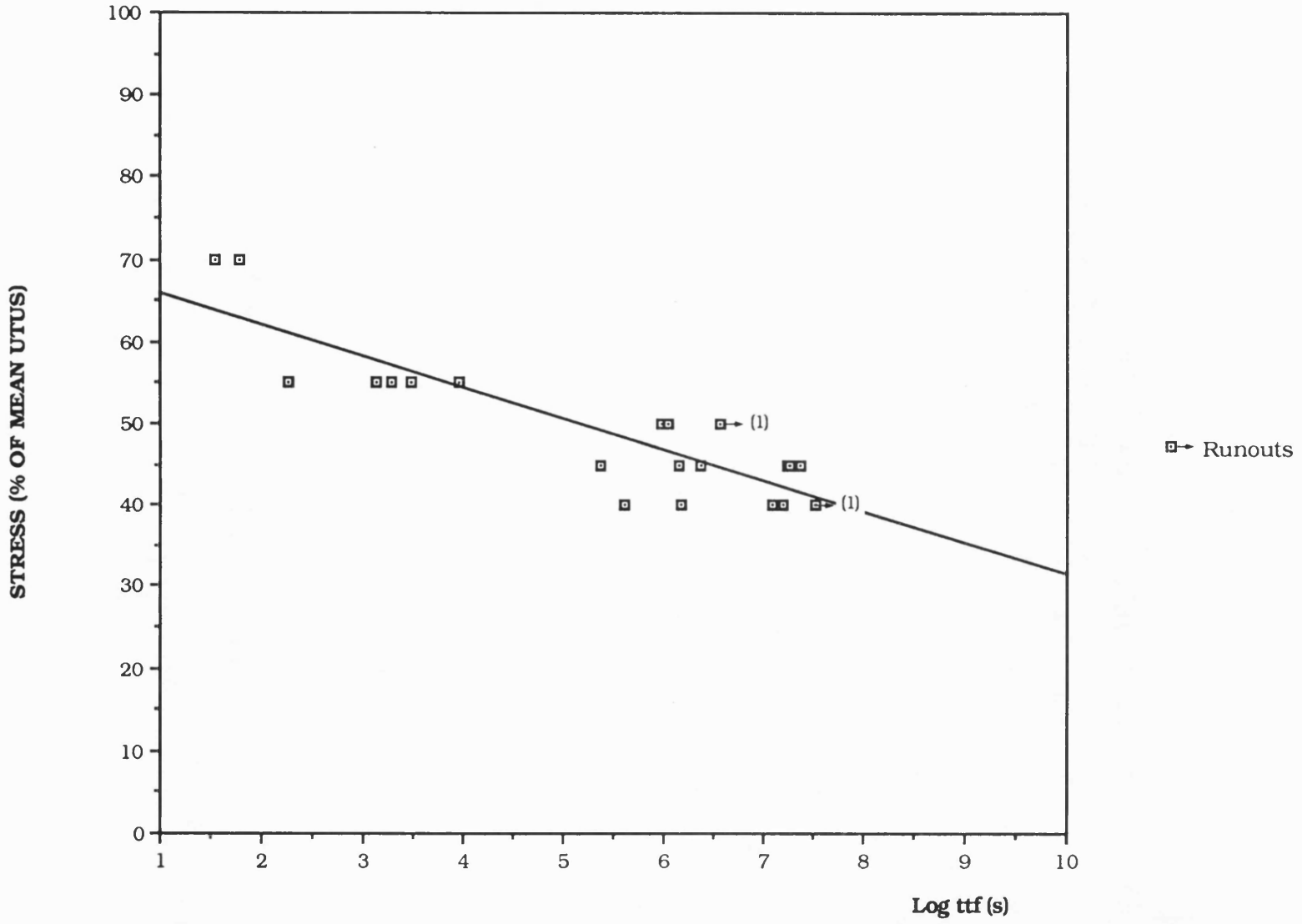

FIGURE 8.13 PLOT OF STRESS-RUPTURE DATA FOR OVERLOADED VINYL ESTER COUPONS.

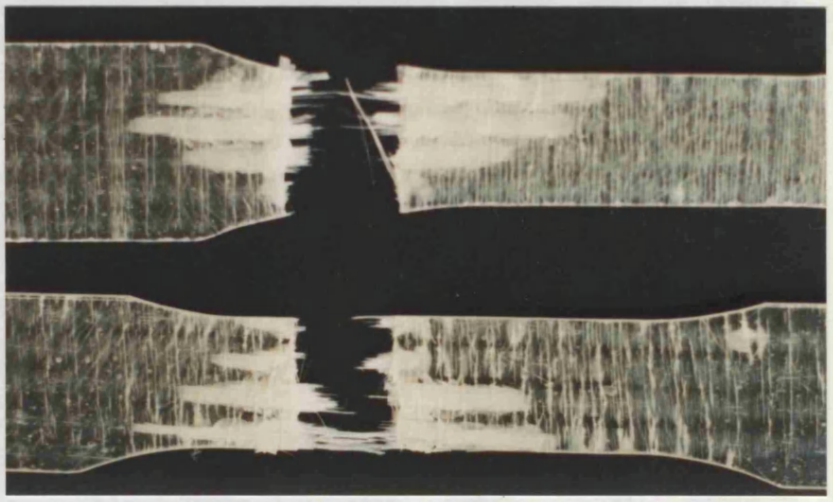

Overloaded polyester coupons.
Stress-rupture failures at the 50% UTUS load level.

FIGURE 8.14

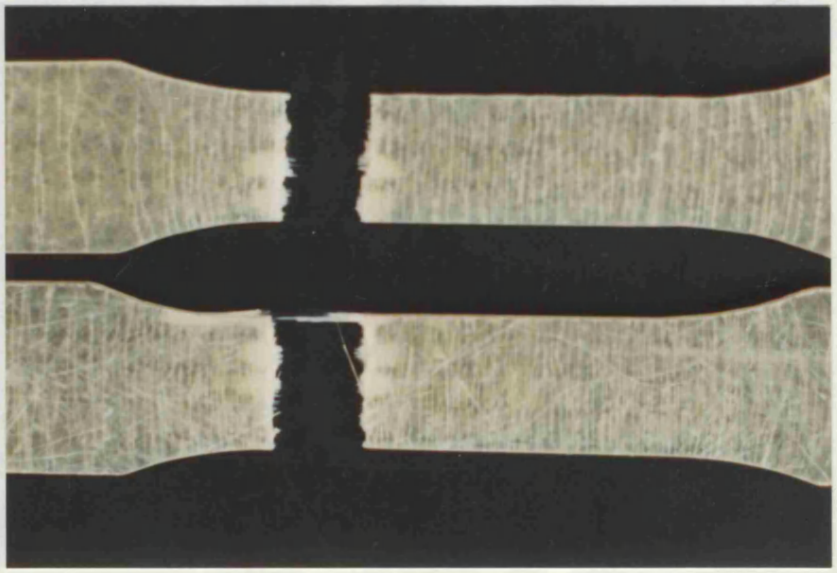

Overloaded polyester coupons.
Stress-rupture failures at the 20% UTUS load level.

FIGURE 8.15

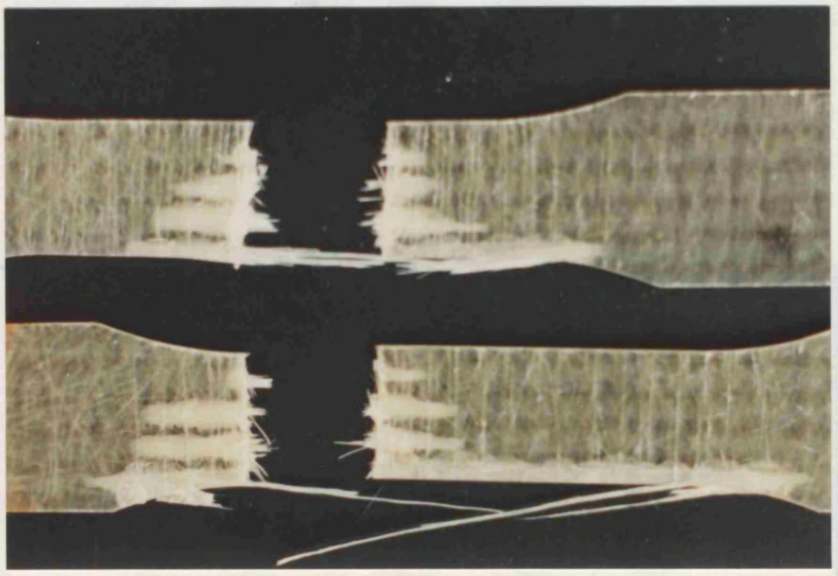

Overloaded Vinyl ester coupons.
Stress-rupture failures at the 55% UTUS load level.

FIGURE 8.16

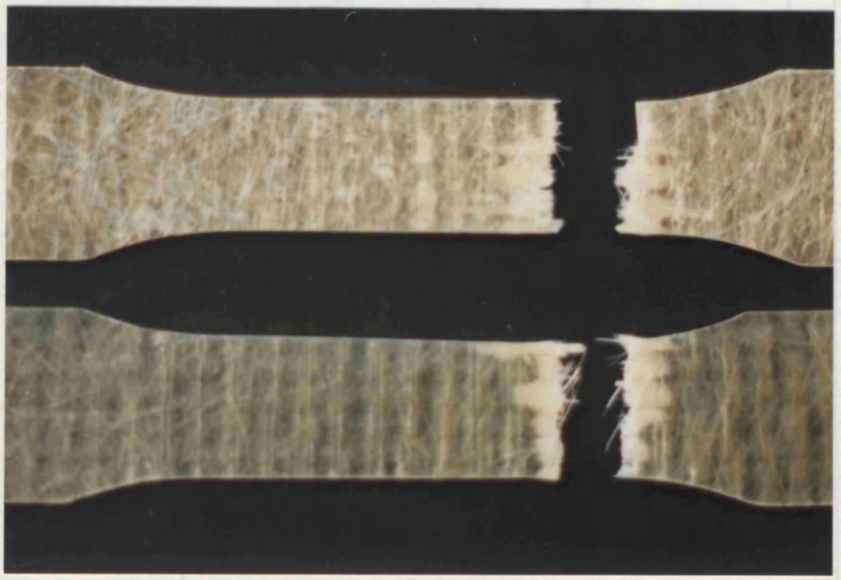

Overloaded Vinyl ester coupons.
Stress-rupture failures at the 40% UTUS load level.

FIGURE 8.17

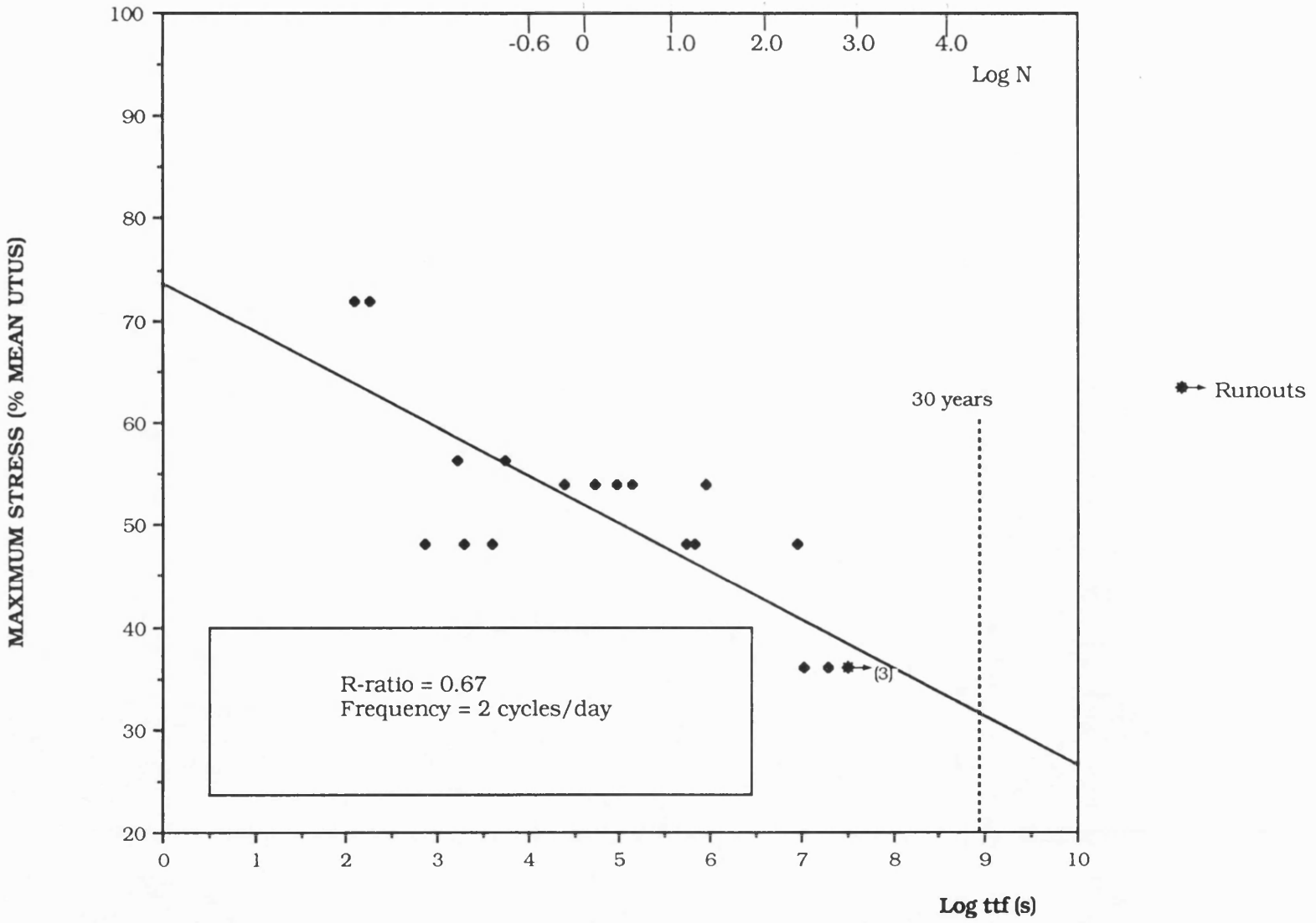

FIGURE 8.18 DYNAMIC FATIGUE DATA FOR OVERLOADED POLYESTER COUPONS.

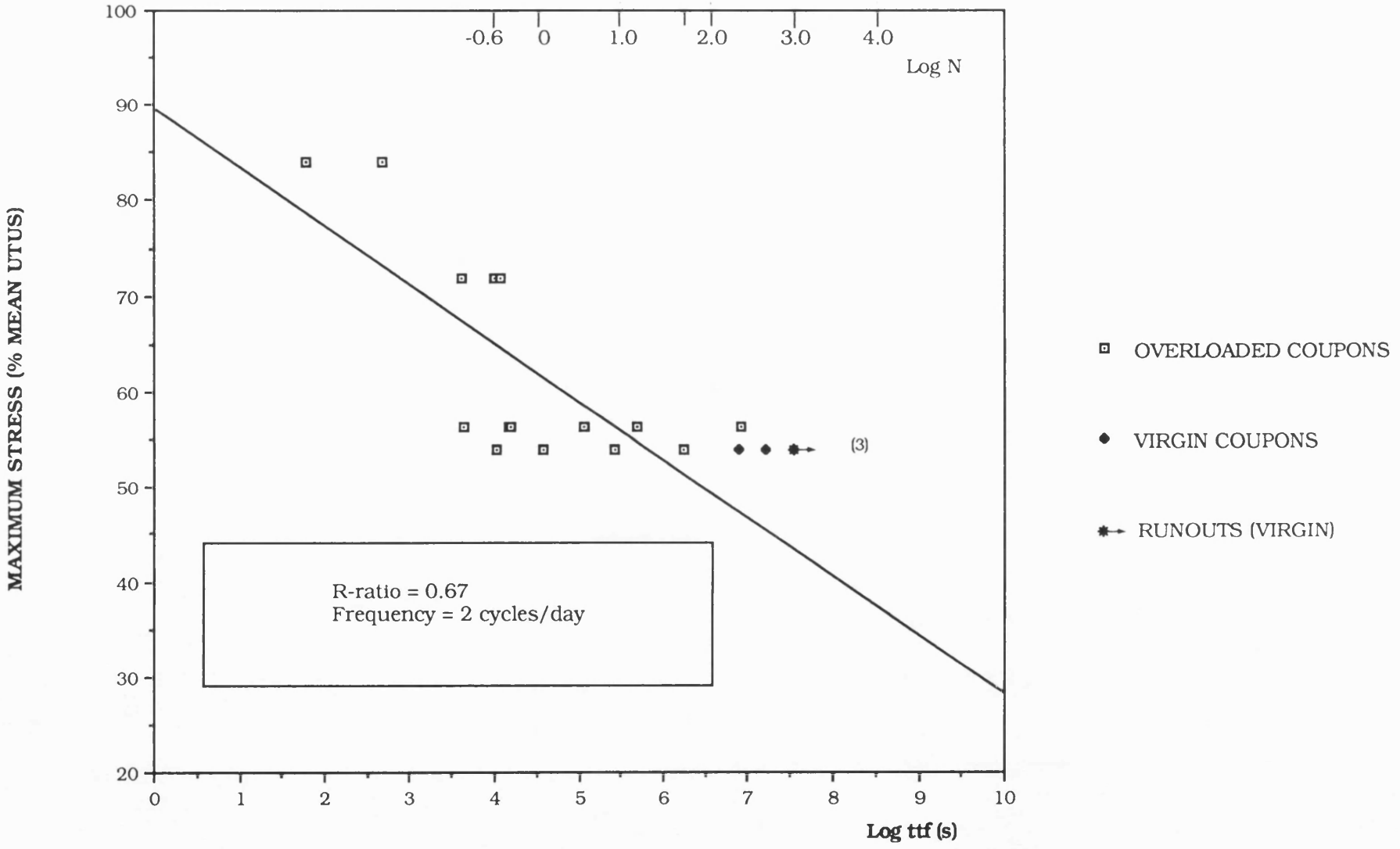

FIGURE 8.19 DYNAMIC FATIGUE DATA FOR VIRGIN AND OVERLOADED VINYL ESTER COUPONS.

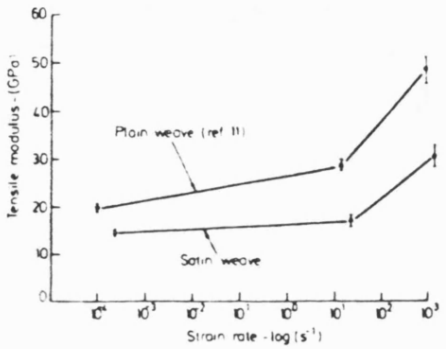

FIGURE 9.1 Strain rate dependence of tensile modulus (woven GFRP specimens) [From Ref. 63.]

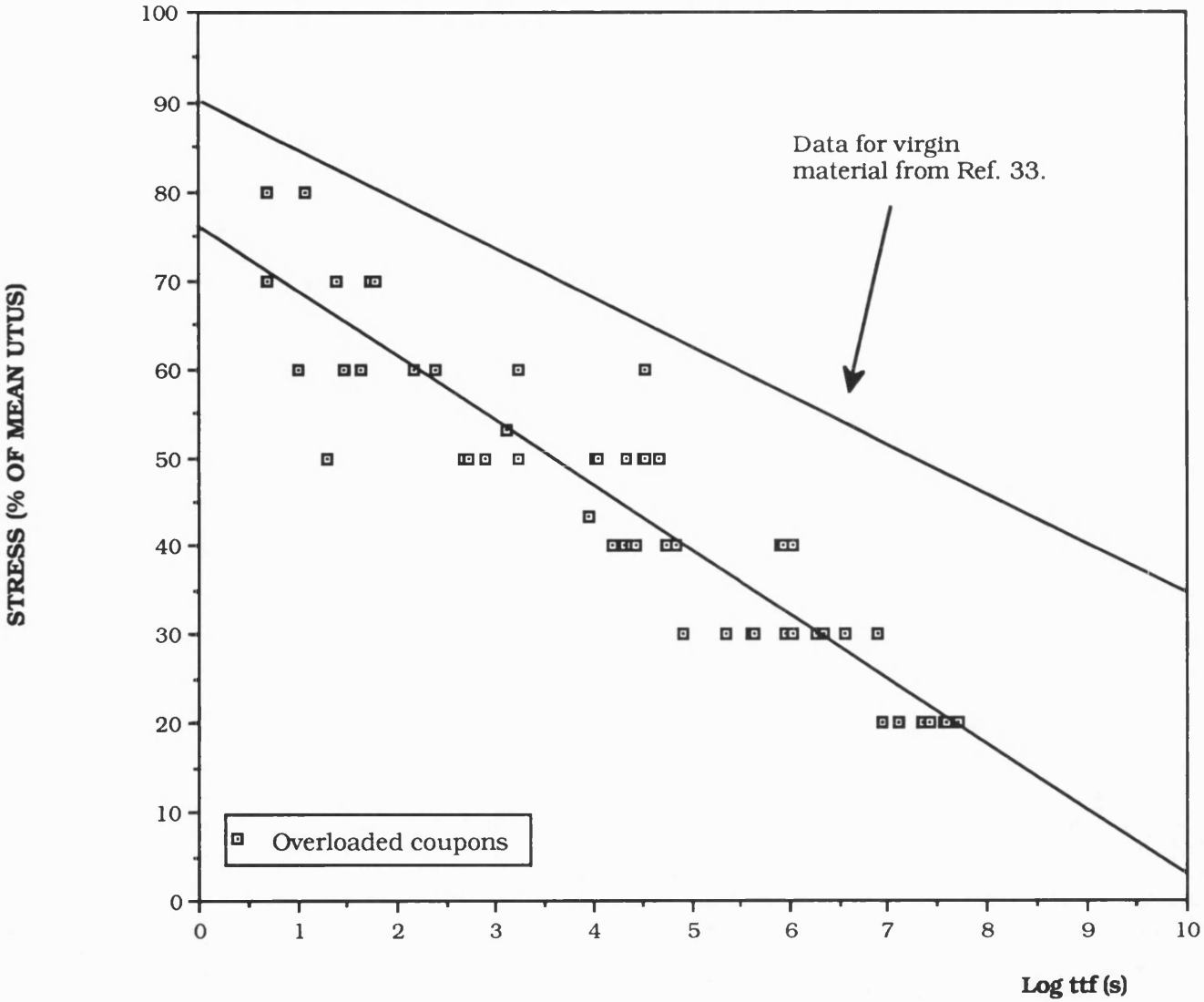

FIGURE 9.2 COMPARISON OF STRESS-RUPTURE DATA BETWEEN VIRGIN AND OVERLOADED POLYESTER COUPONS.

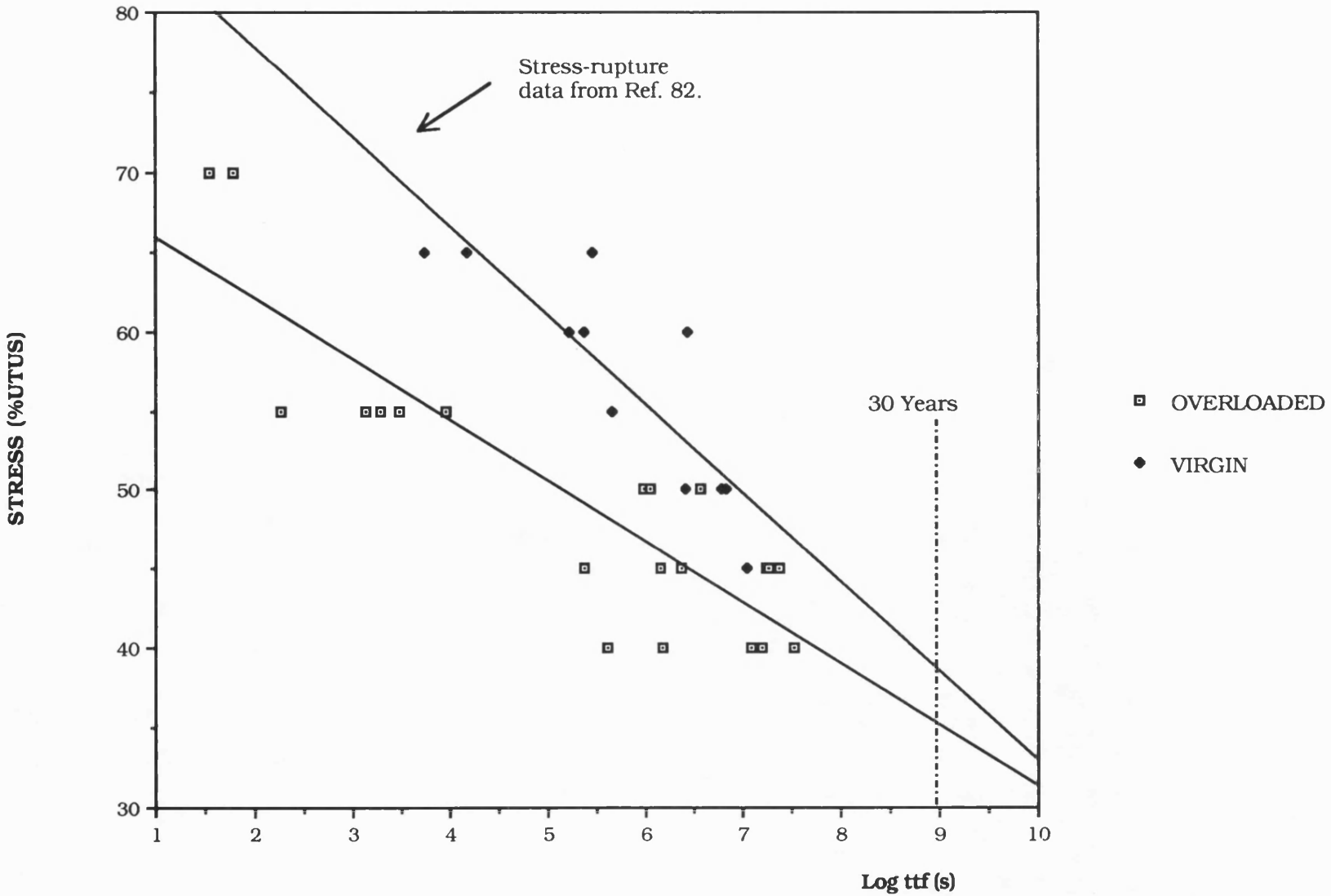

FIGURE 9.3 COMPARISON OF STRESS-RUPTURE DATA FOR VIRGIN AND OVERLOADED VINYL ESTER COUPONS.

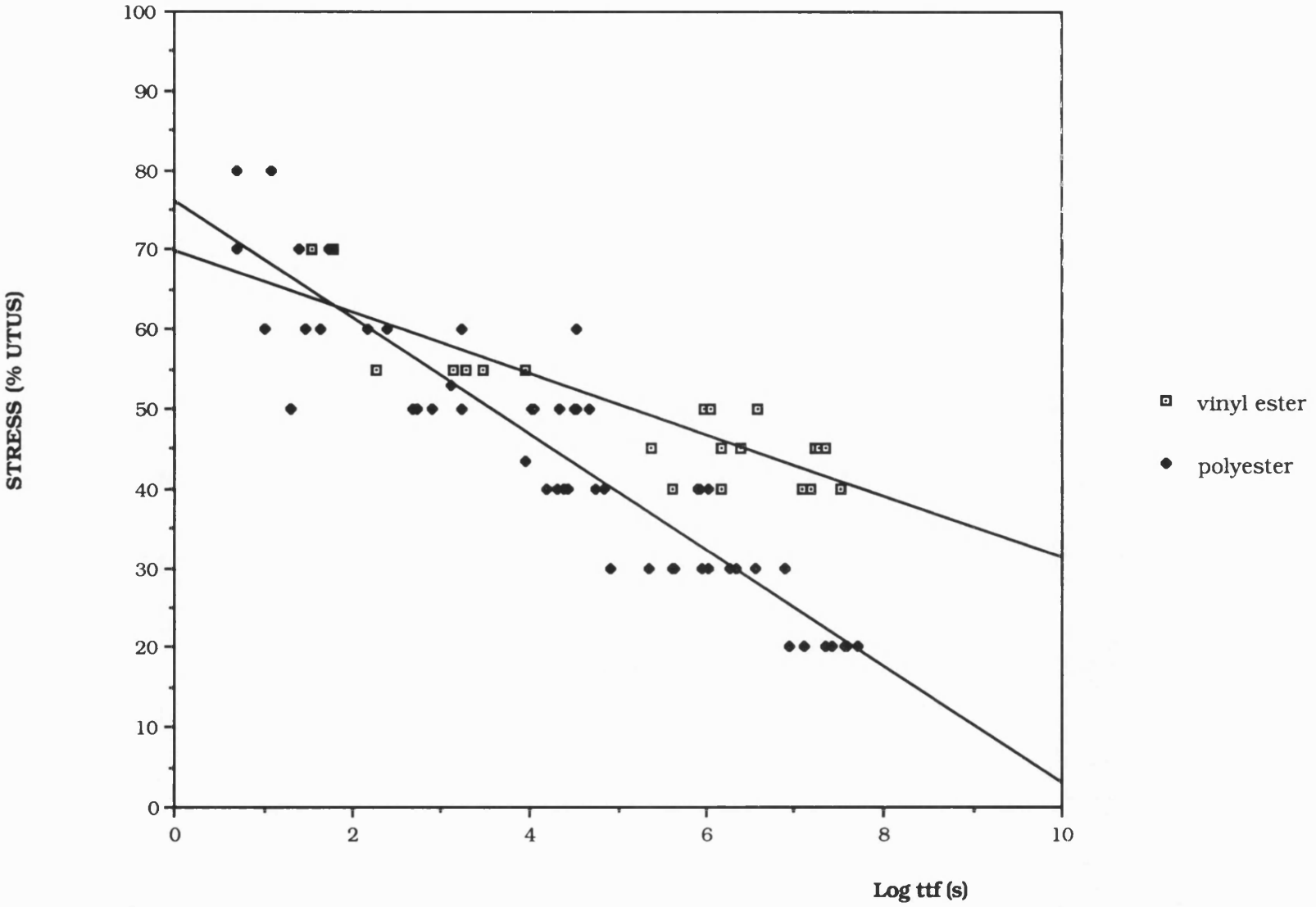

FIGURE 9.4 COMPARISON OF OVERLOADED POLYESTER AND VINYL ESTER COUPON DATA.

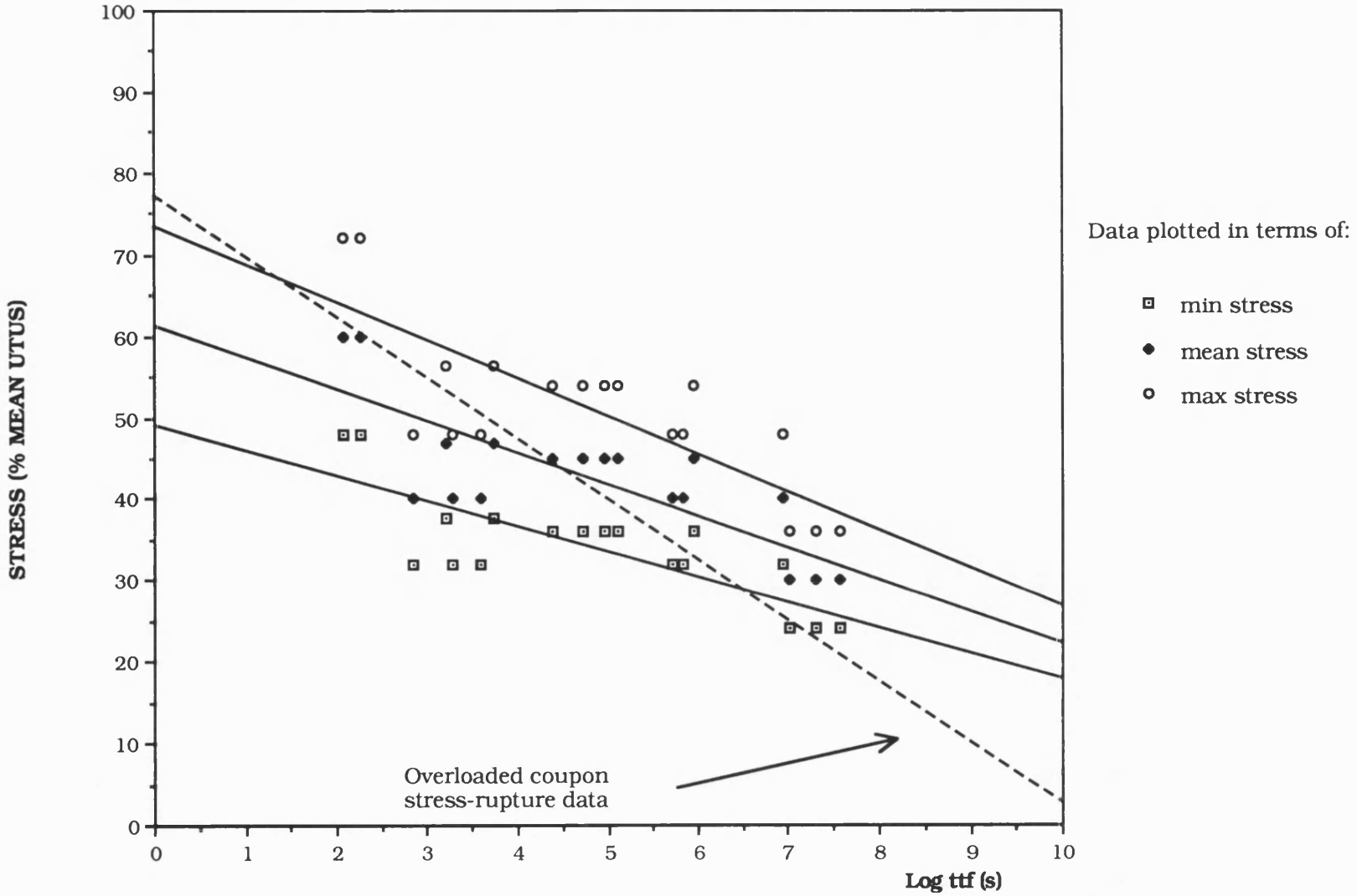

FIGURE 9.5 COMPARISON OF DYNAMIC AND STATIC FATIGUE DATA FOR OVERLOADED POLYESTER COUPONS.

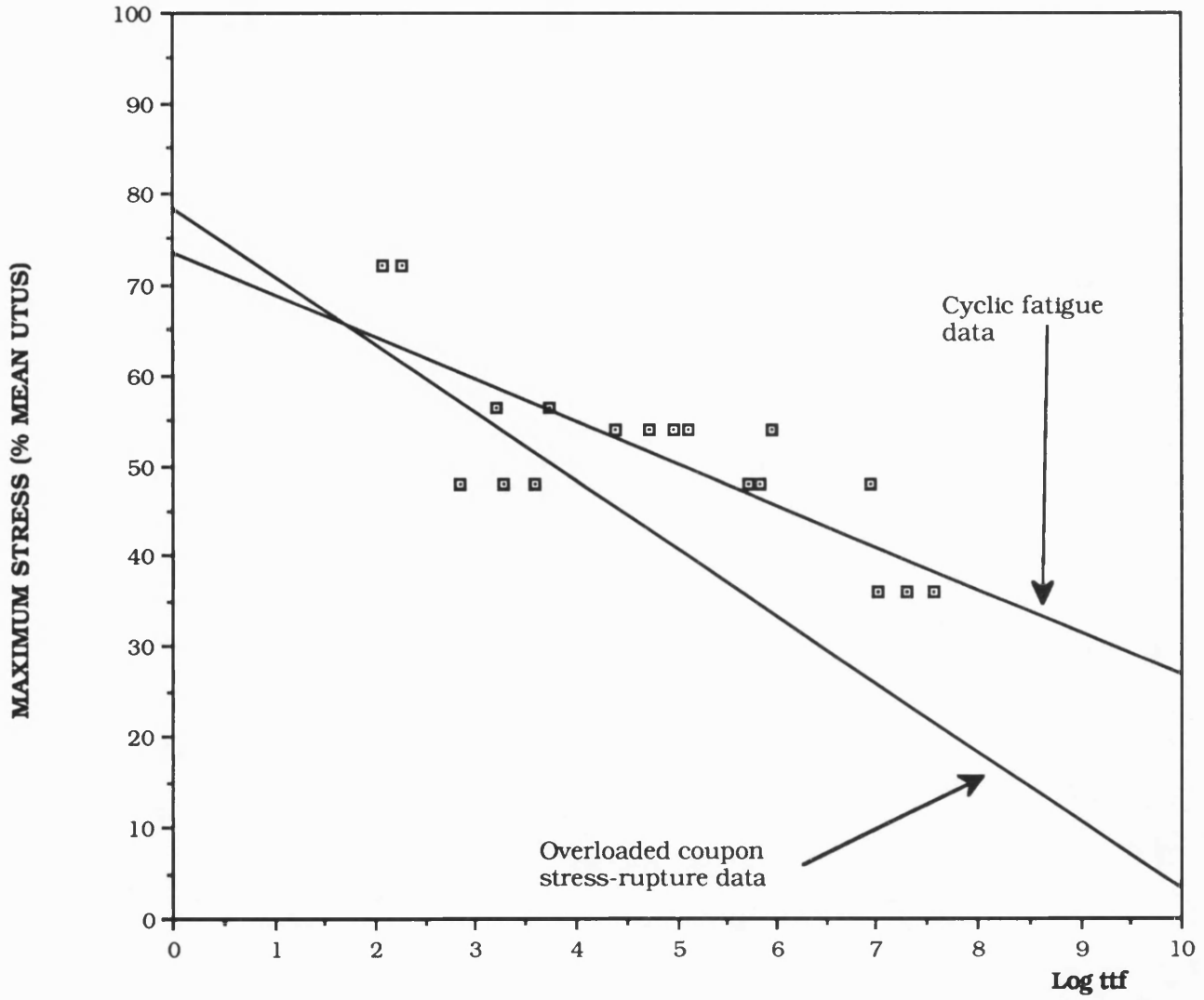

FIGURE 9.6 COMPARISON OF DYNAMIC AND STATIC FATIGUE DATA FOR OVERLOADED POLYESTER COUPONS.

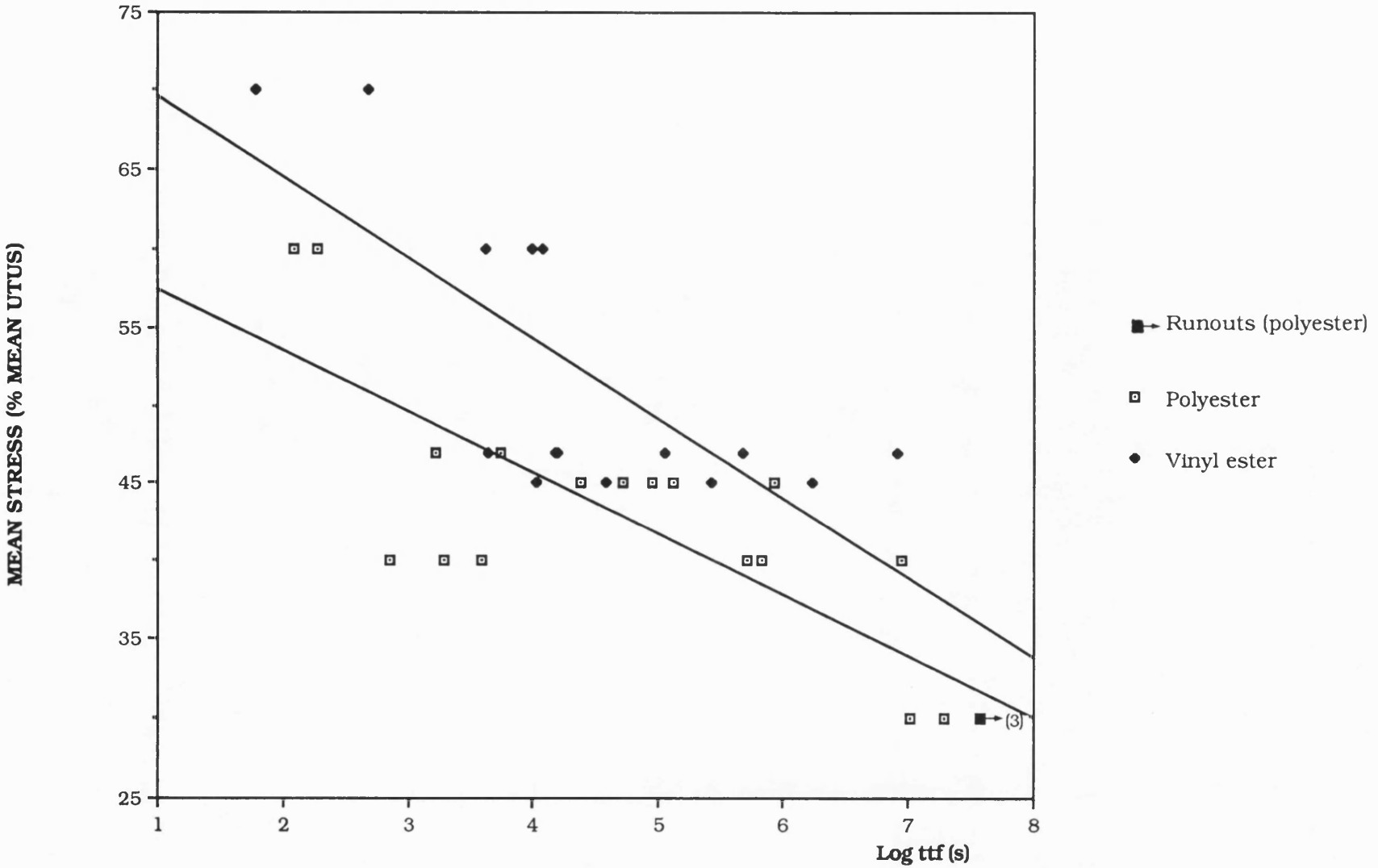

FIGURE 9.7 COMPARISON OF DYNAMIC FATIGUE DATA FOR OVERLOADED POLYESTER AND VINYL ESTER COUPONS.

RESIN: Scott Bader 625 TV.

REINFORCEMENT: 1×300 gms/m^2 Chopped strand mat.
1×800 gms/m^2 Woven roving.
1×300 gms/m^2 Chopped strand mat.

CURE: 5 Hours at 40^0 C.

FIGURE 10.1 Summary of pipe wall composition.

INTERNAL DIAMETER = 151mm

PIPE LENGTH = 750mm

STUB FLANGES DESIGNED
TO BS 4994 (1987)

BURST PRESSURE CALCULATED
FROM BS 4994 = 42.4 Bar.

FIGURE 10.2 Summary of pipe design information.

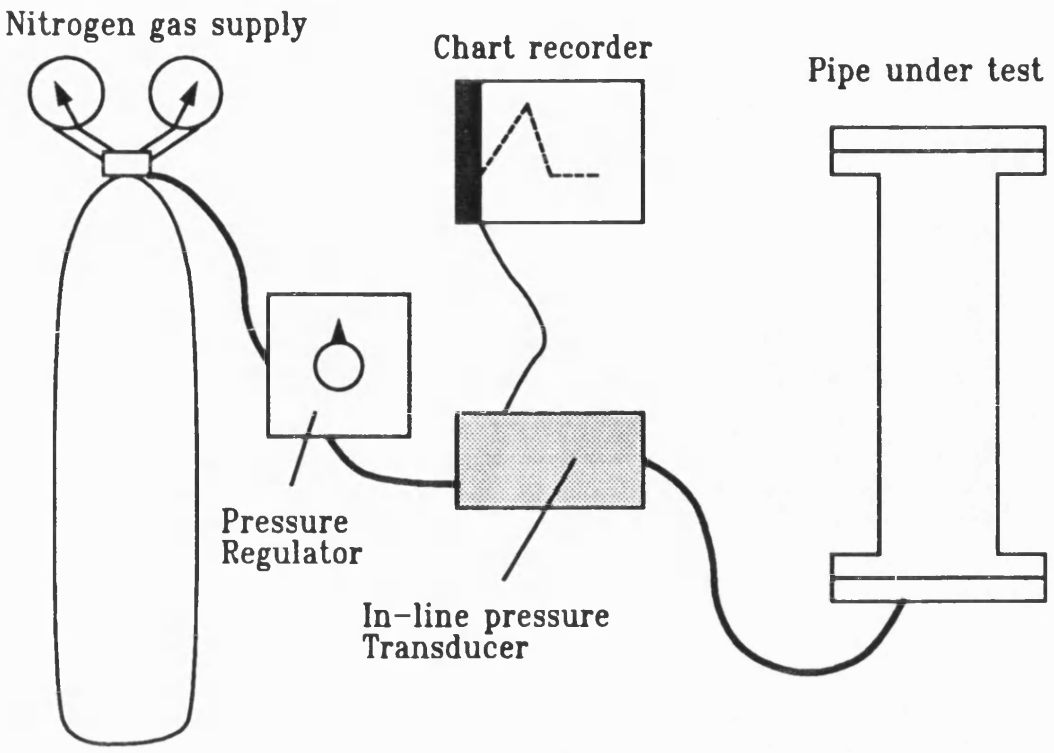

FIGURE 10.3 Pipe burst apparatus.

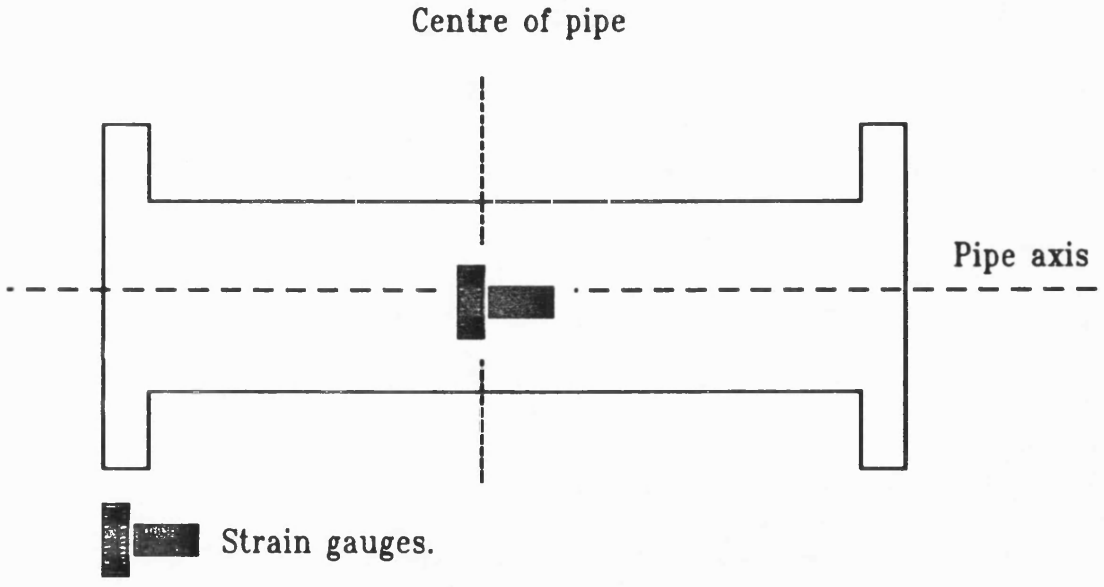

FIGURE 10.4 Positioning of strain gauges for burst tests.

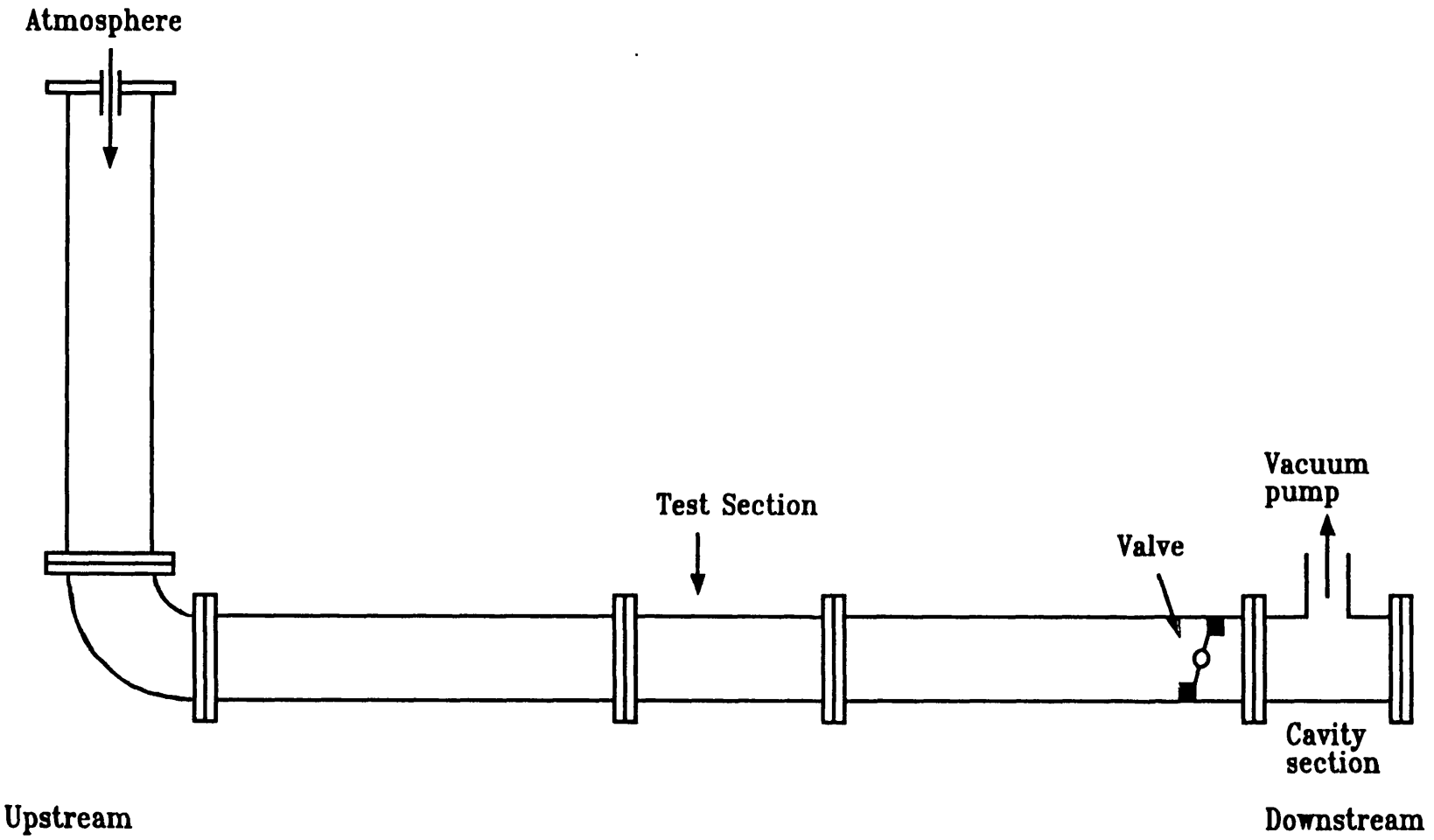

FIGURE 10.5 Rig used for the application of controlled water hammer event to pipes.

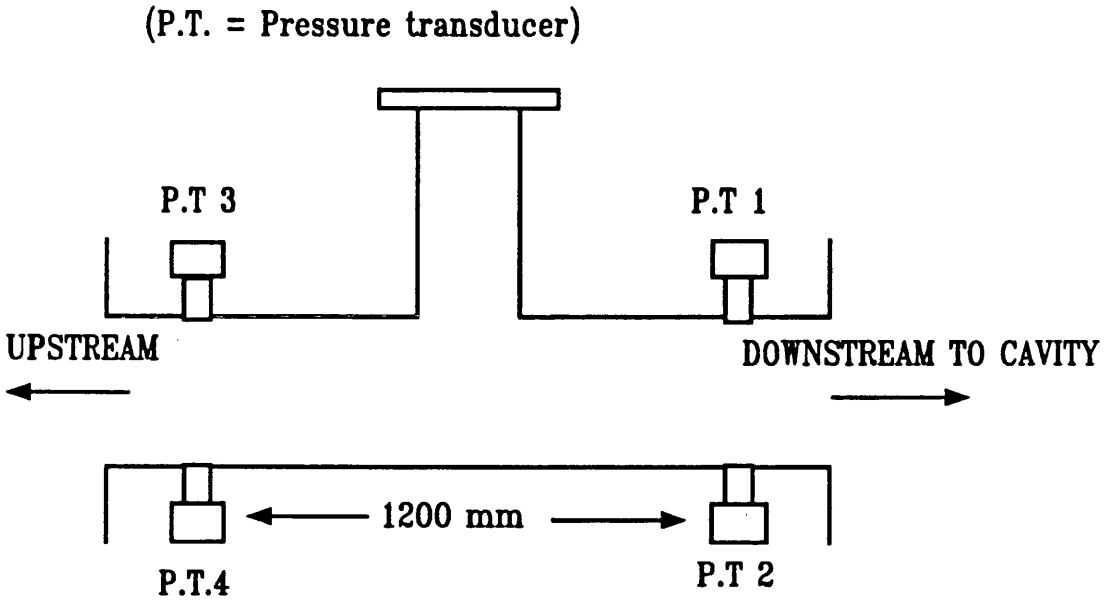

FIGURE 10.6 Arrangement of pressure transducers on steel test section.

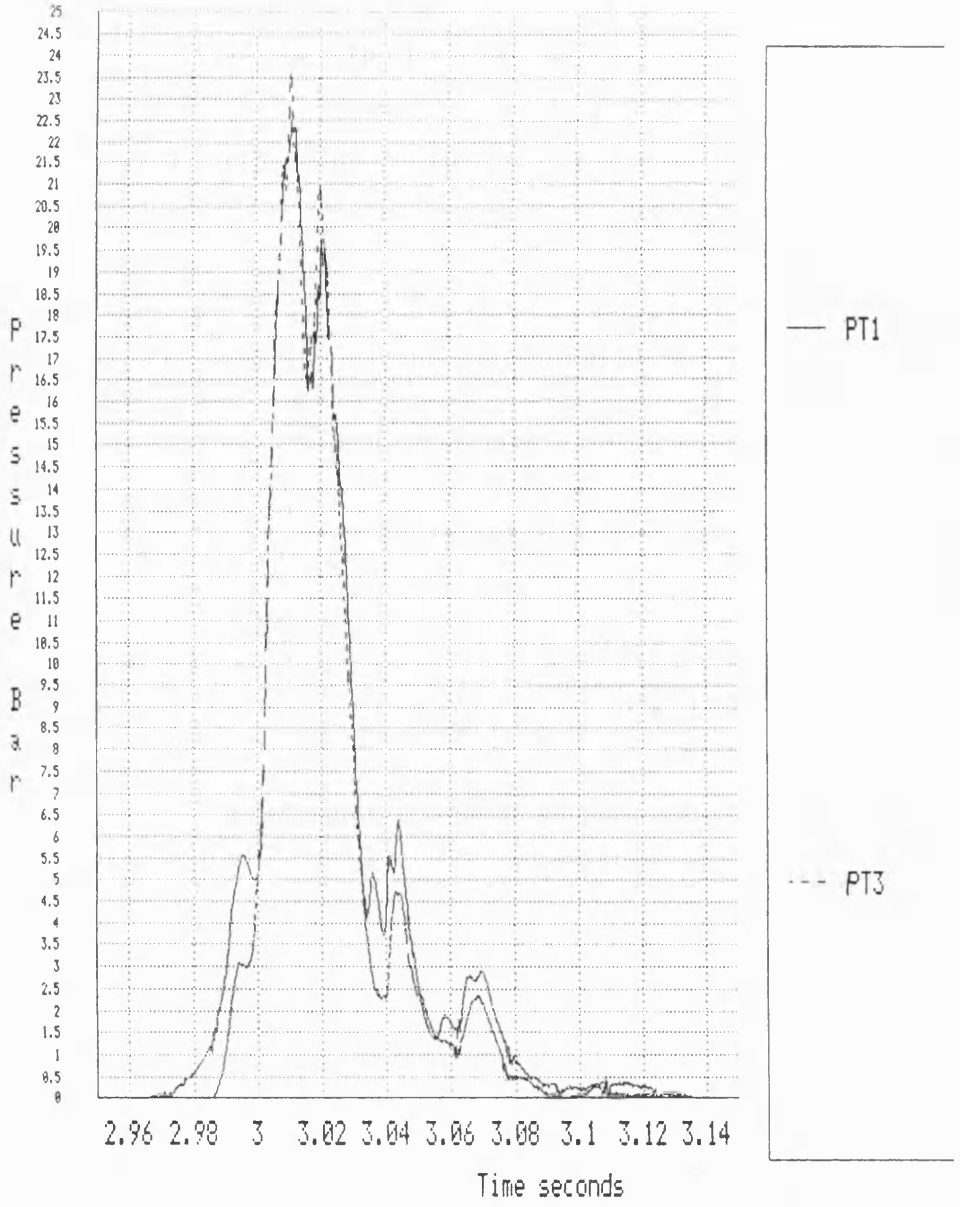

FIGURE 10.7

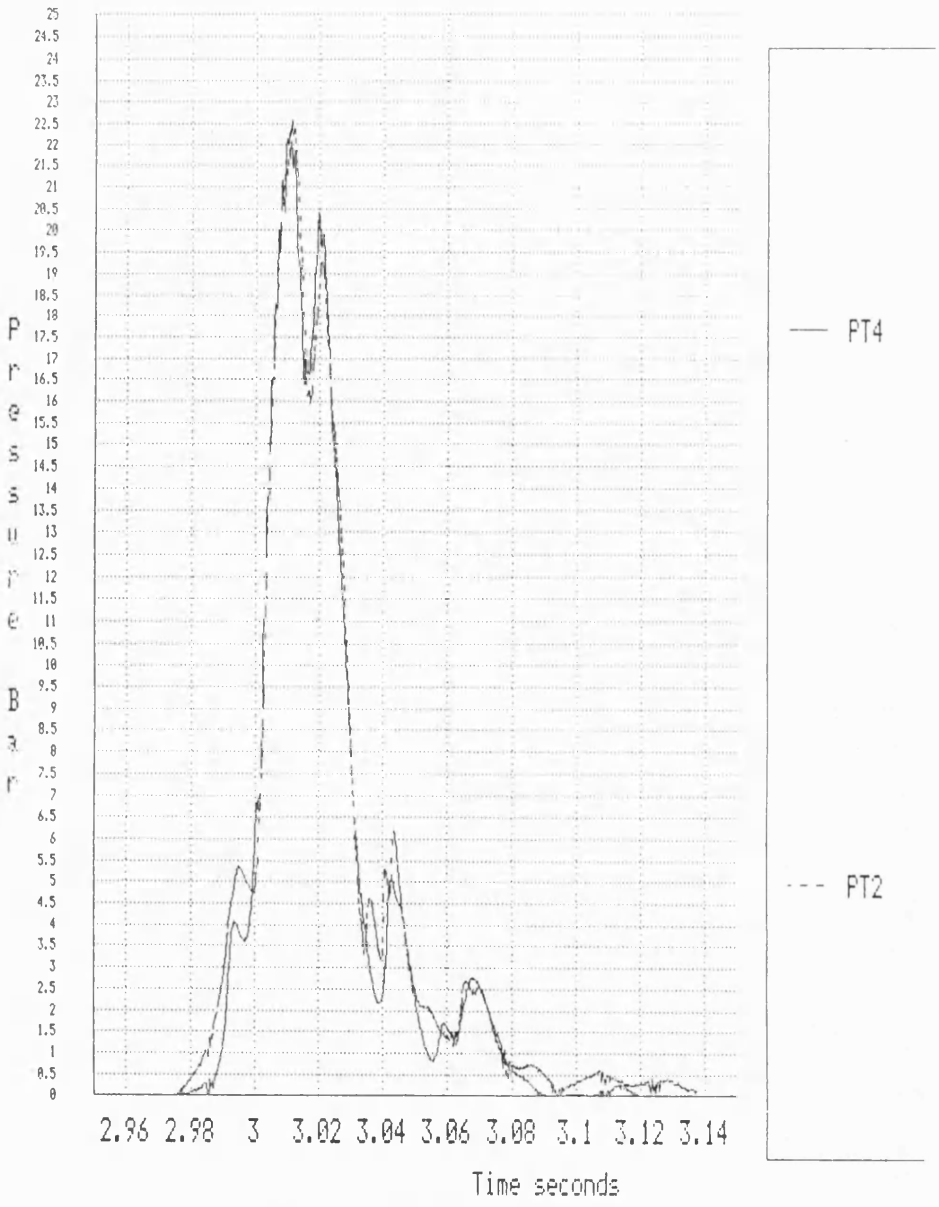

FIGURE 10.8

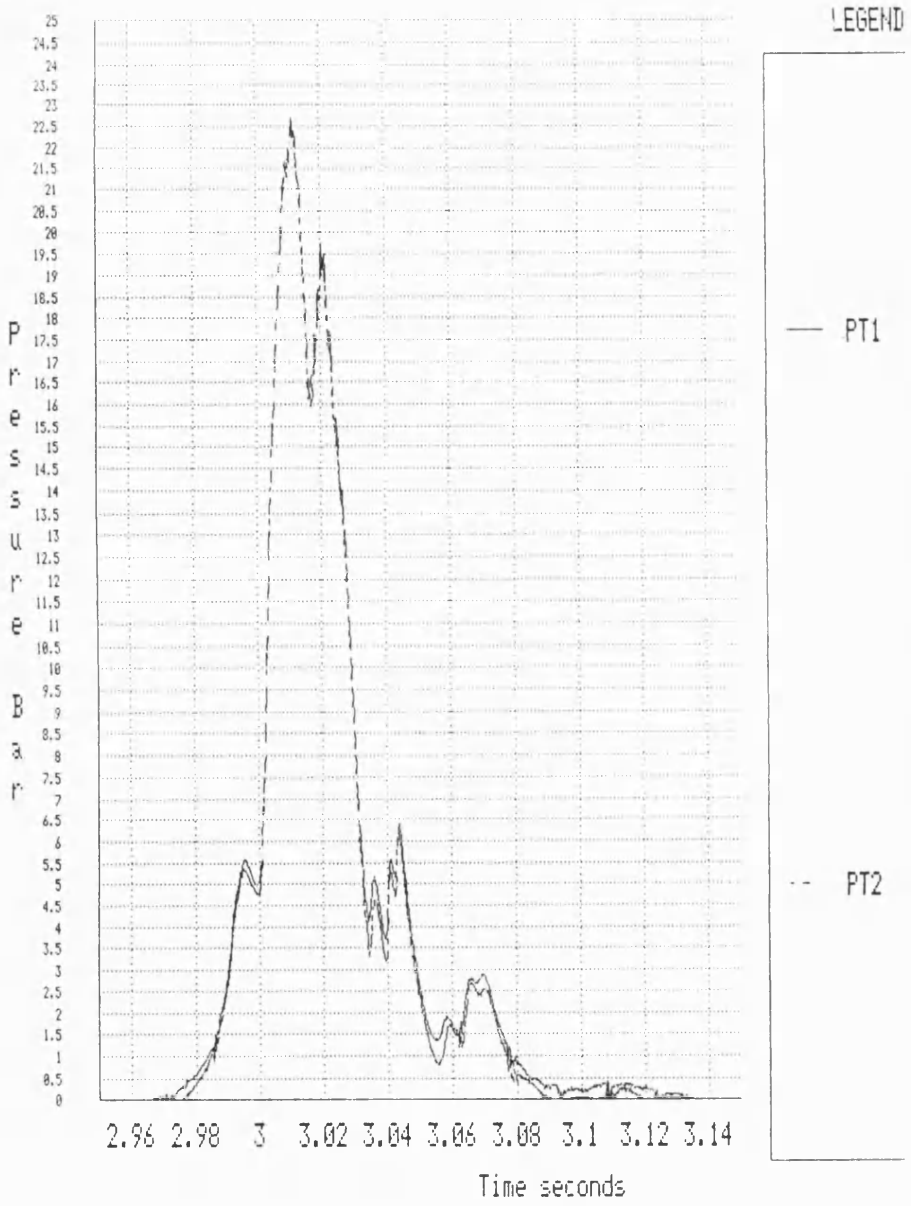

FIGURE 10.9

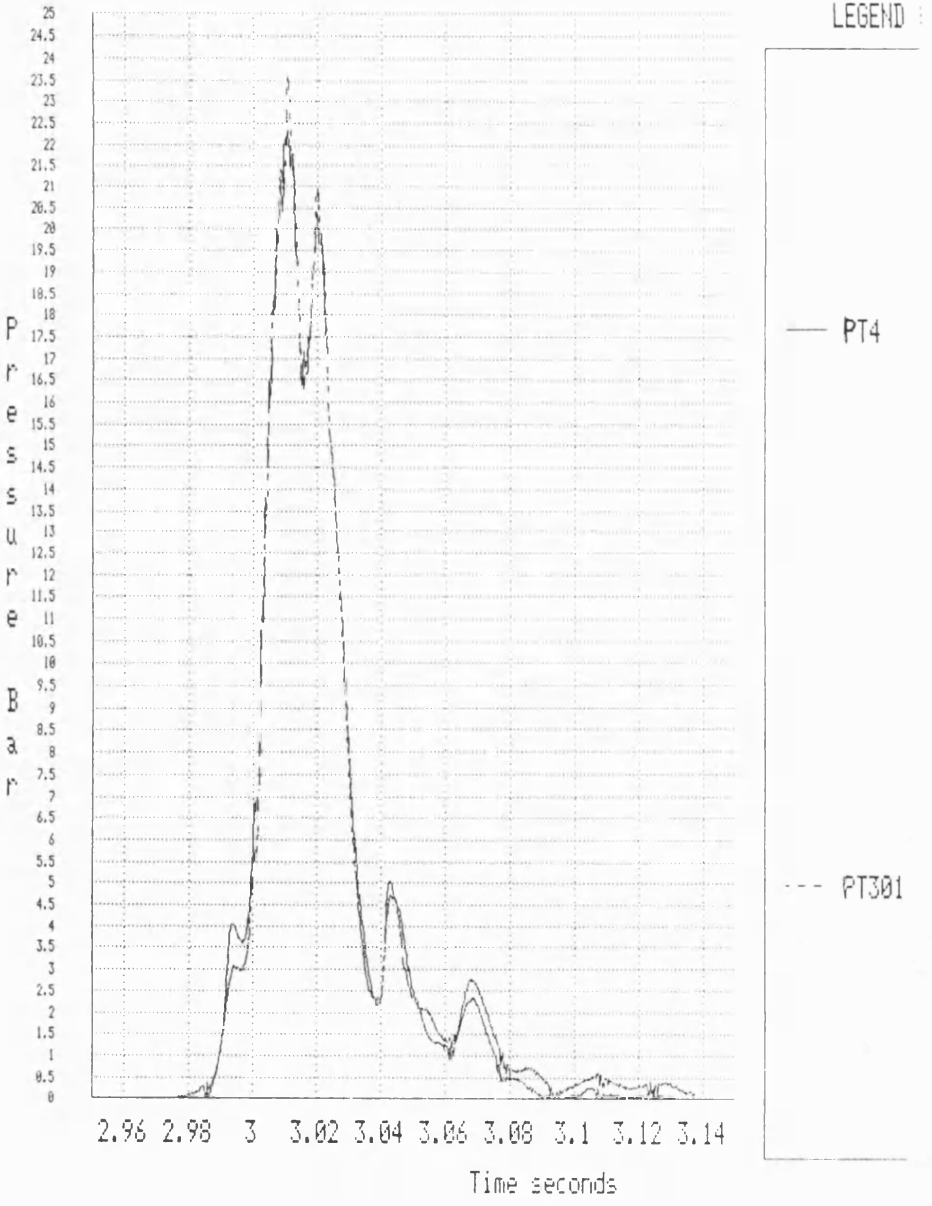

FIGURE 10.10

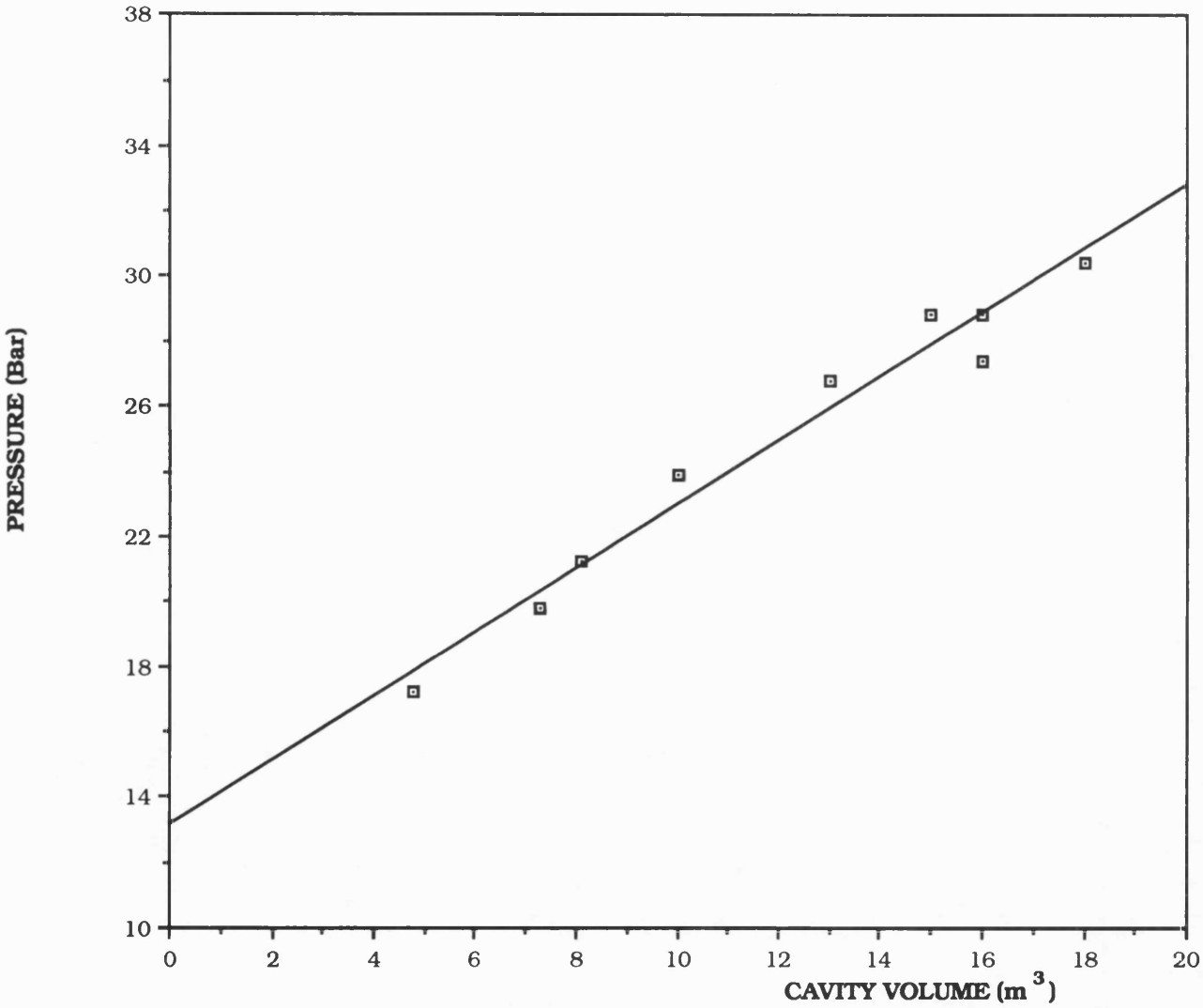

FIGURE 10.11 RIG CALIBRATION: PEAK PRESSURE AS A FUNCTION OF CAVITY VOLUME.

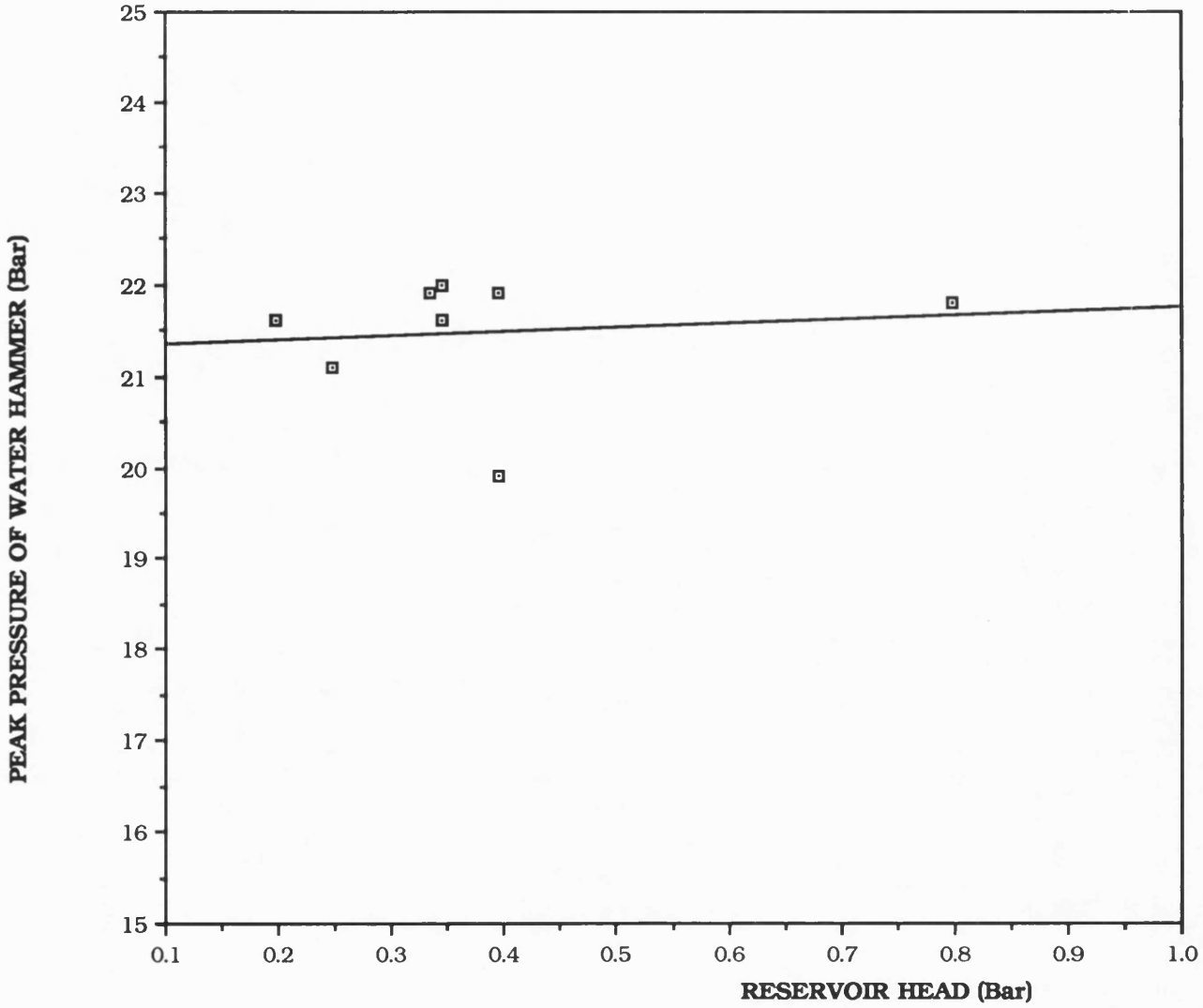

FIGURE 10.12 RIG CALIBRATION: PEAK PRESSURE OF WATER HAMMER AS A FUNCTION OF RESERVOIR HEAD.

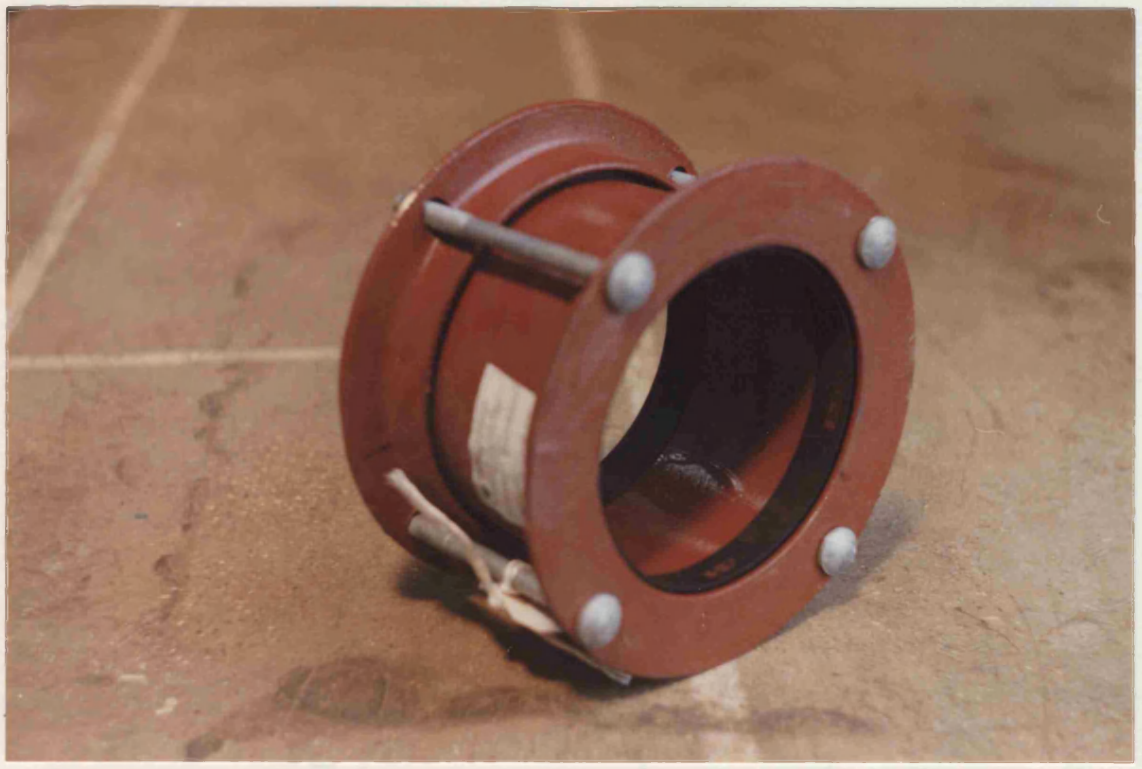

FIGURE 10.13 Viking–Johnson coupling.

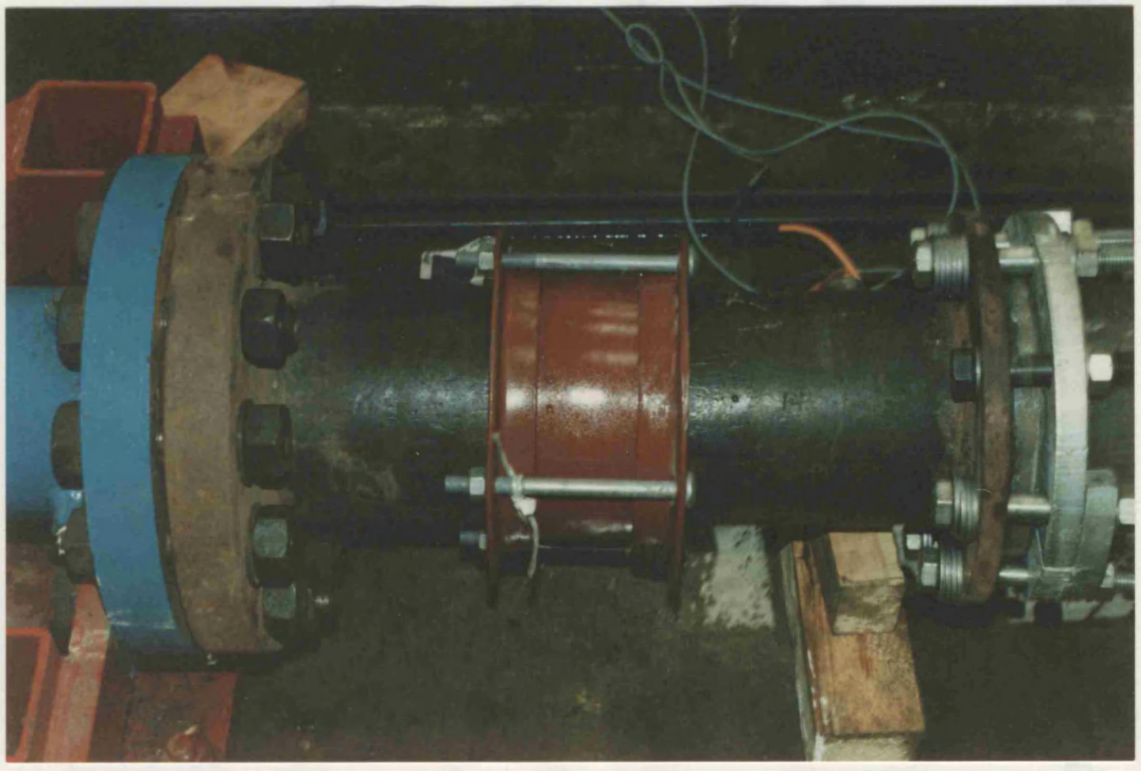

FIGURE 10.14 Viking–Johnson coupling in position on rig.

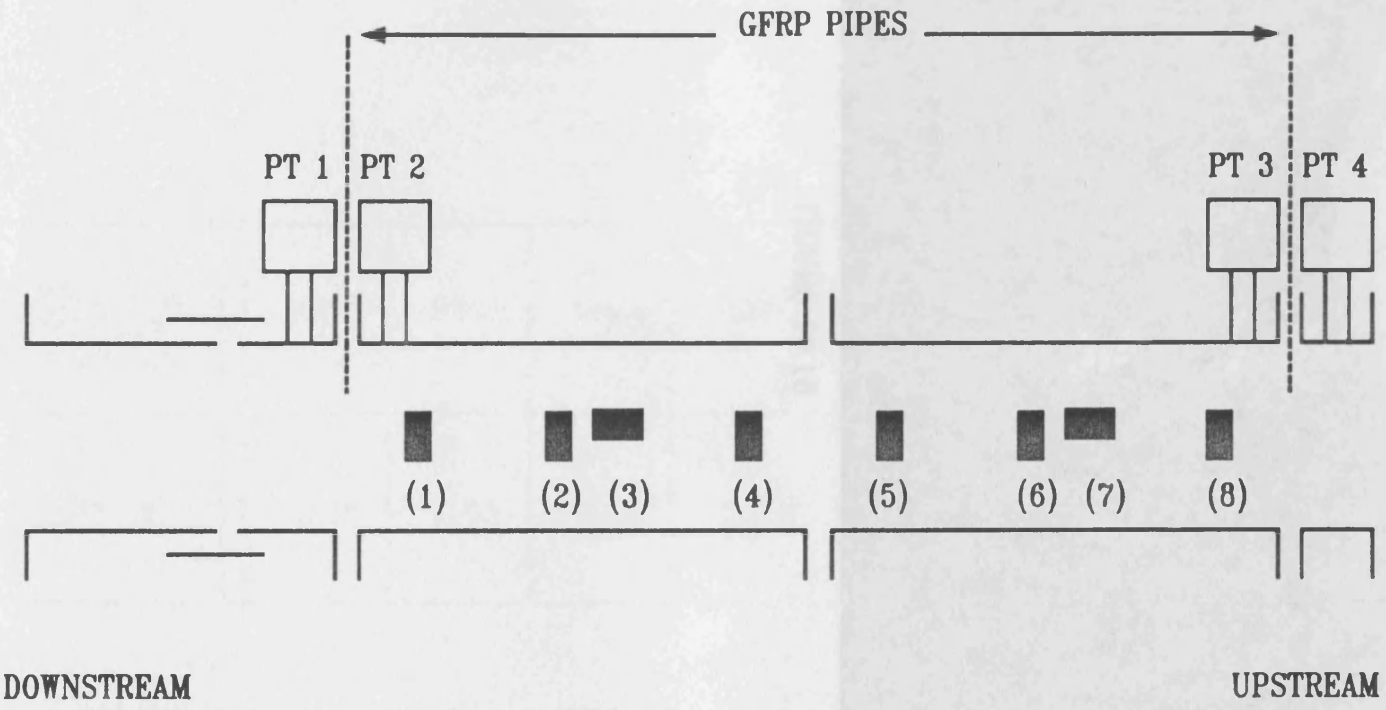

ARRANGEMENT OF PRESSURE TRANSDUCERS AND STRAIN GAUGES FOR TESTS ON INSTRUMENTED GFRP PIPES.

FIGURE 10.15

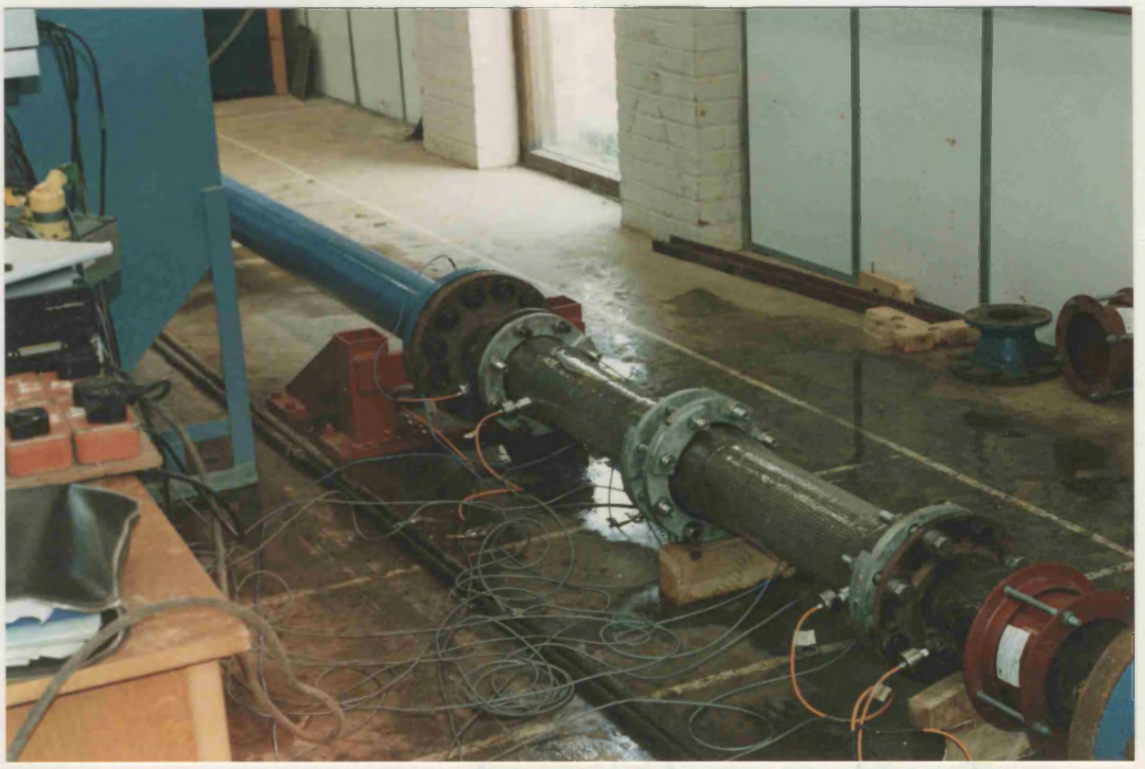

FIGURE 10.16

CAVITY ← RESERVOIR →

STRAIN GAUGE ORIENTATION AND POSITION	HOOP	HOOP	AXIAL	HOOP	HOOP	HOOP	AXIAL	HOOP
STRAIN (%)	0.03	0.02	0.15	0.03	0.05	0.07	0.18	0.03

FIGURE 10.17 Static strain on GFRP test pipes prior to filling rig with water.

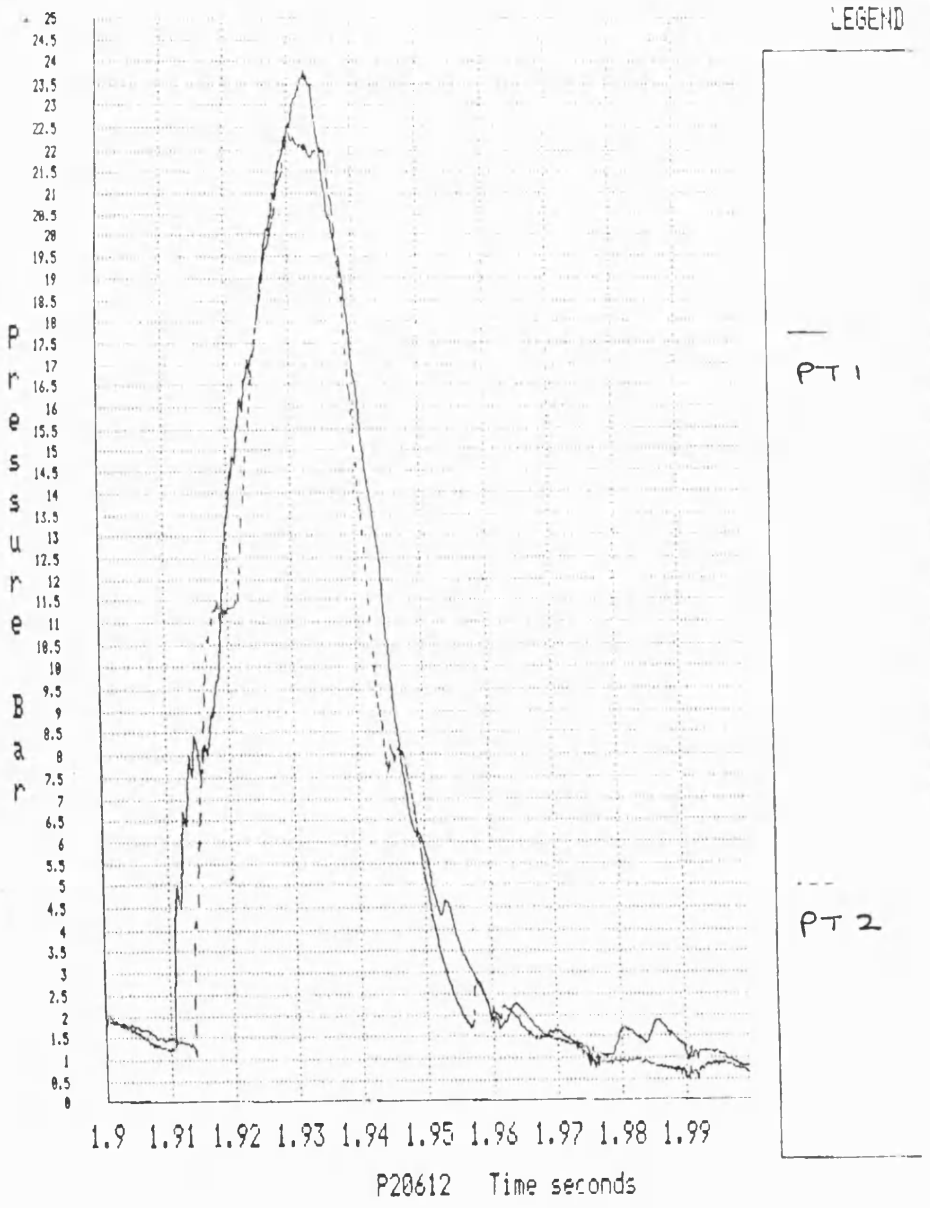

FIGURE 10.18

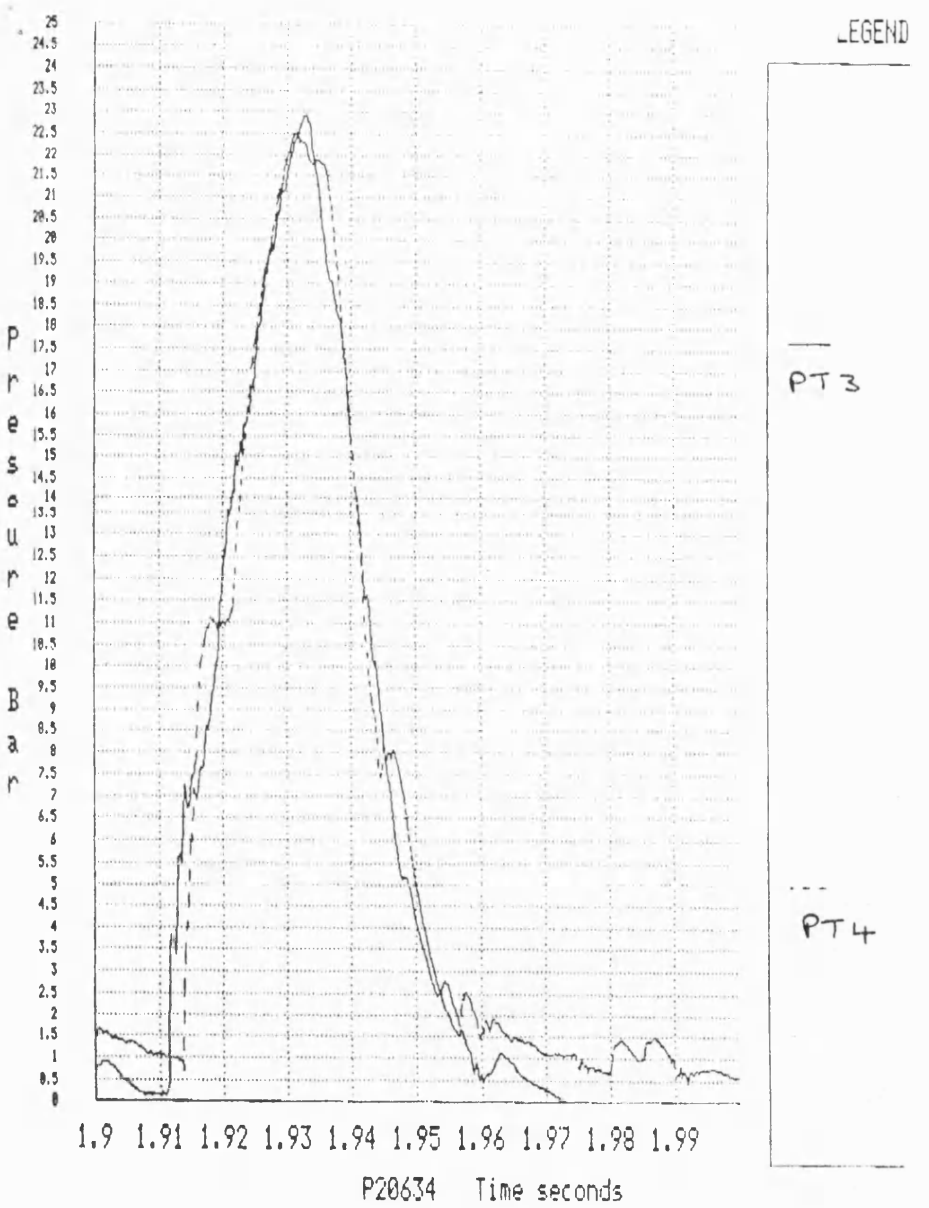

FIGURE 10.19

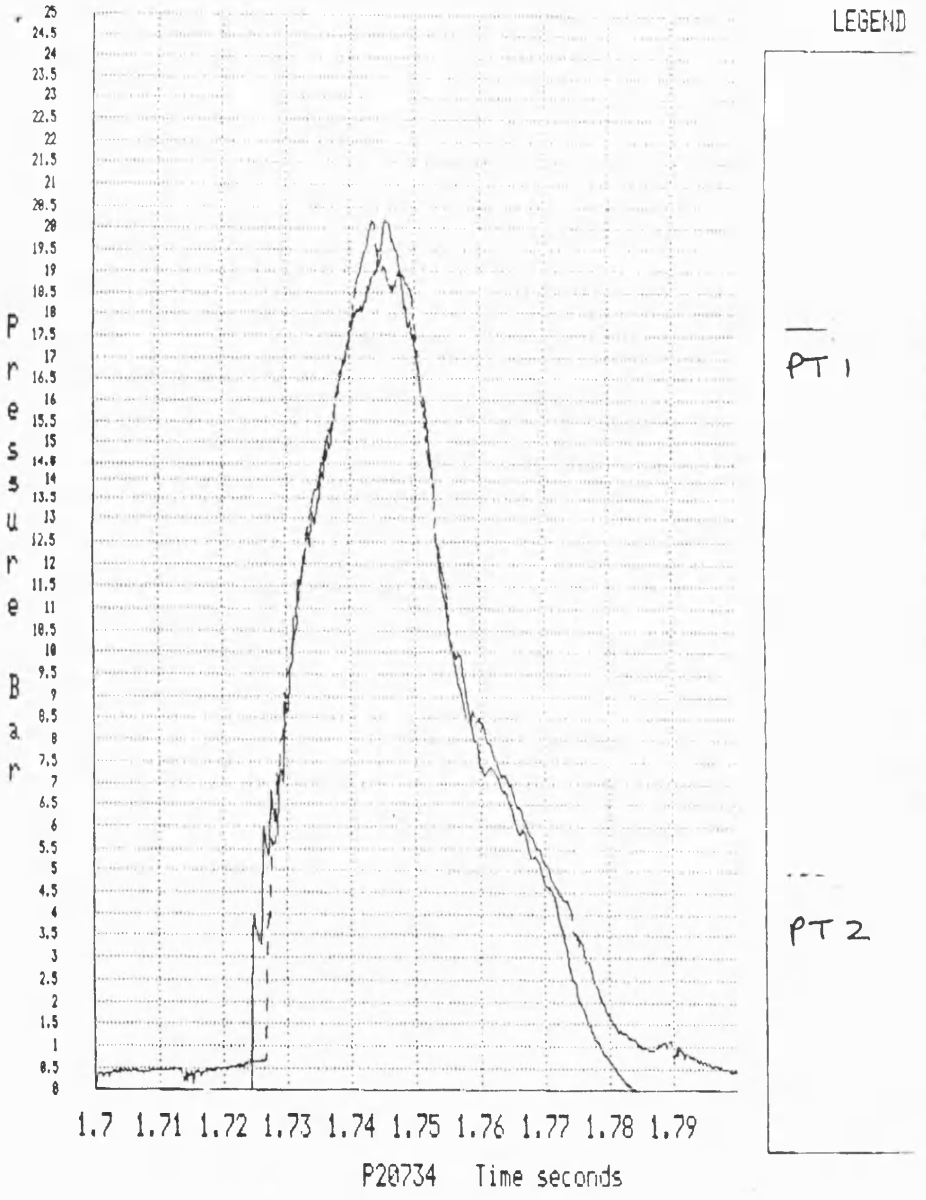

FIGURE 10.20

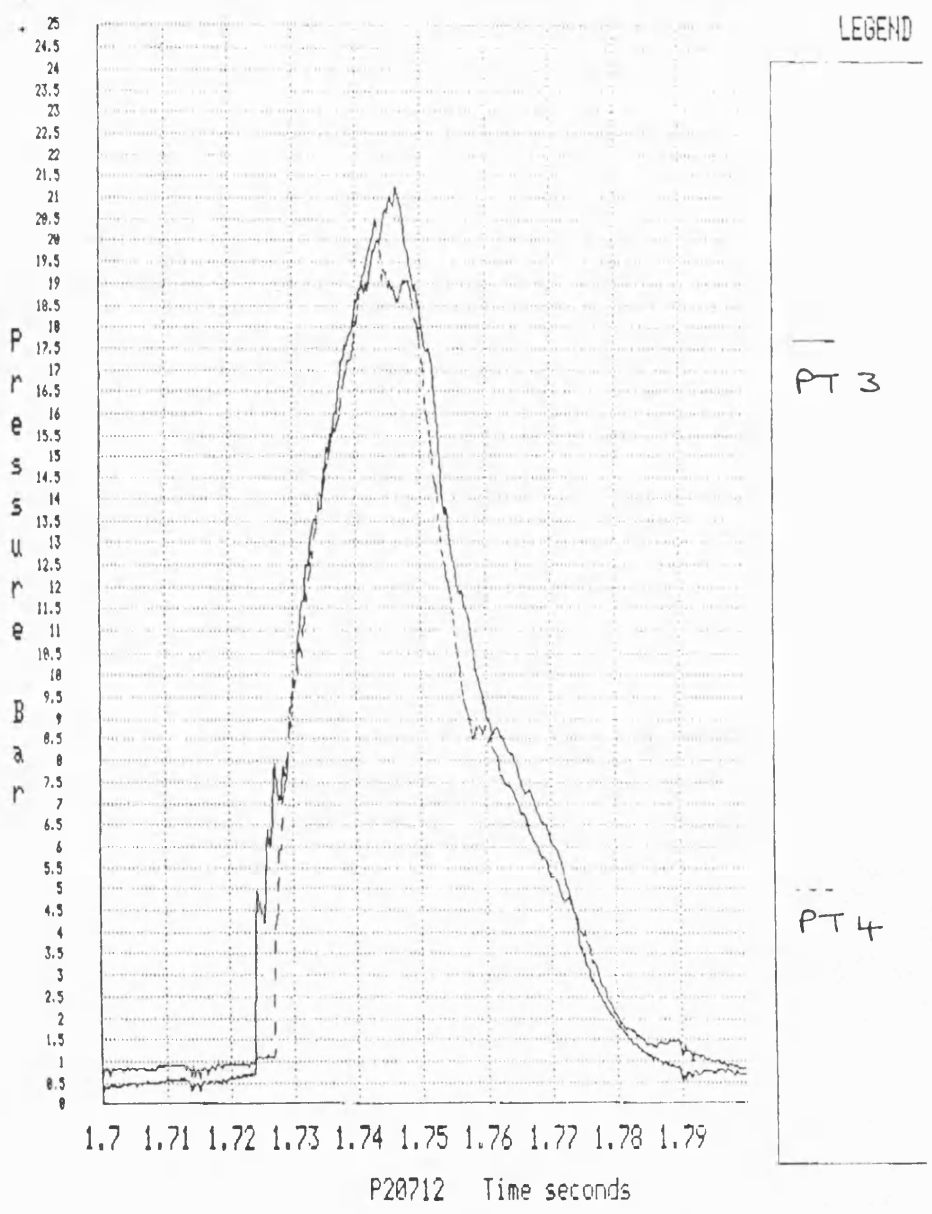

FIGURE 10.21

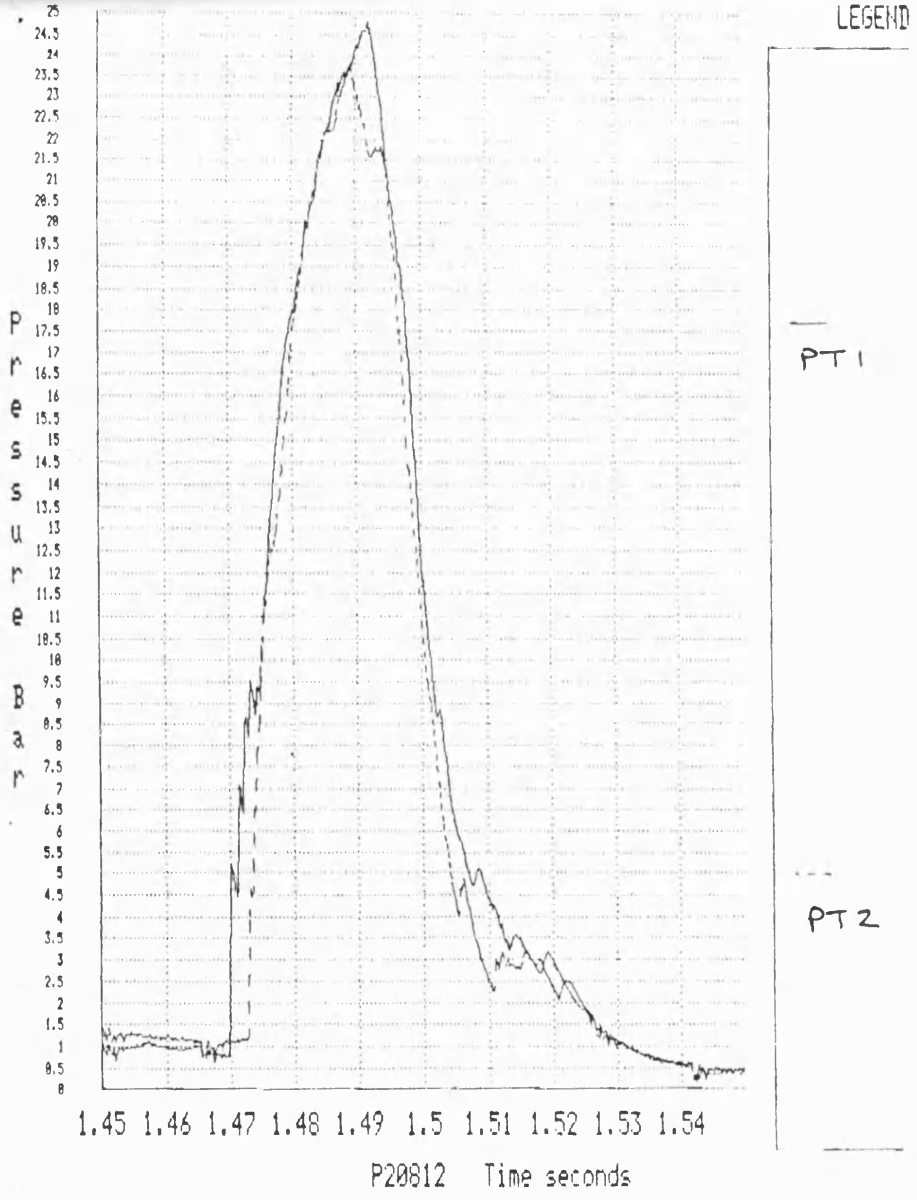

FIGURE 10.22

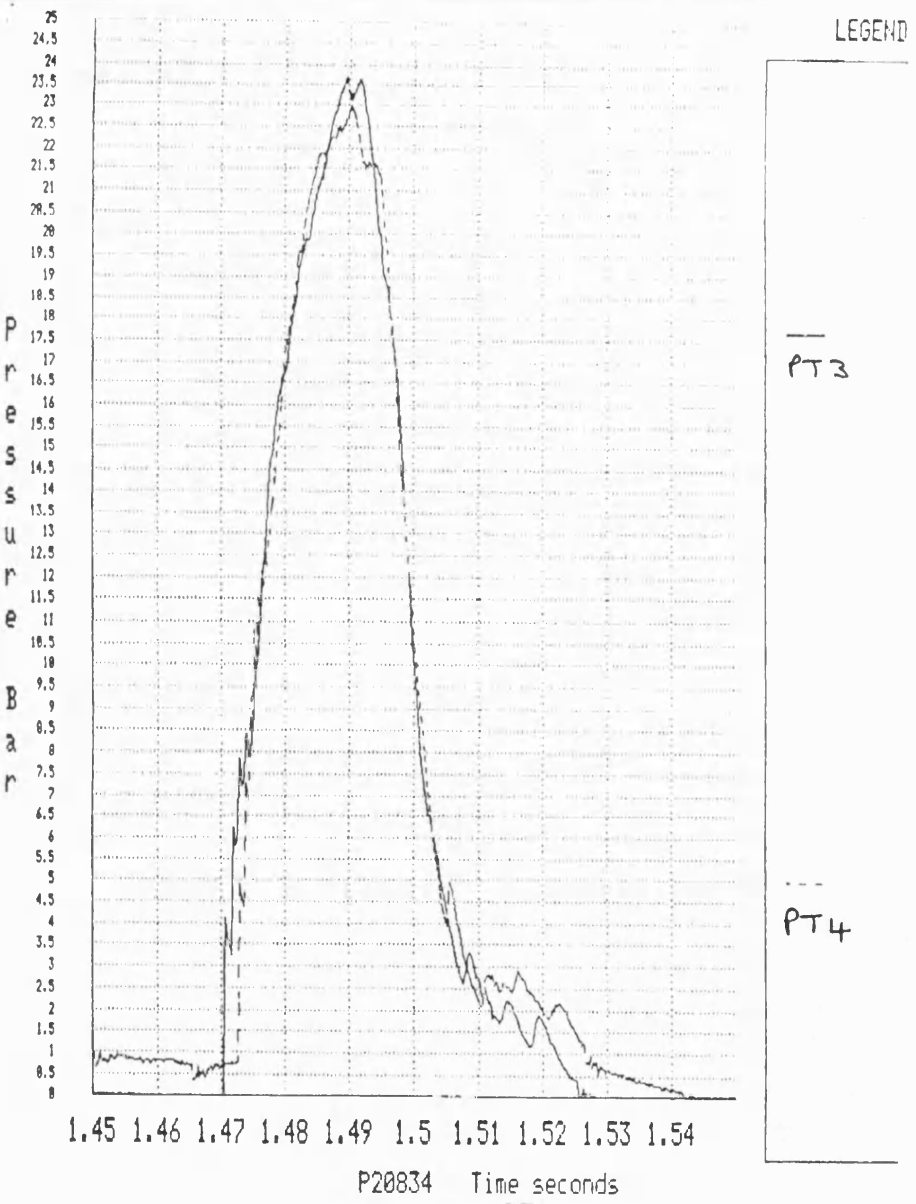

FIGURE 10.23

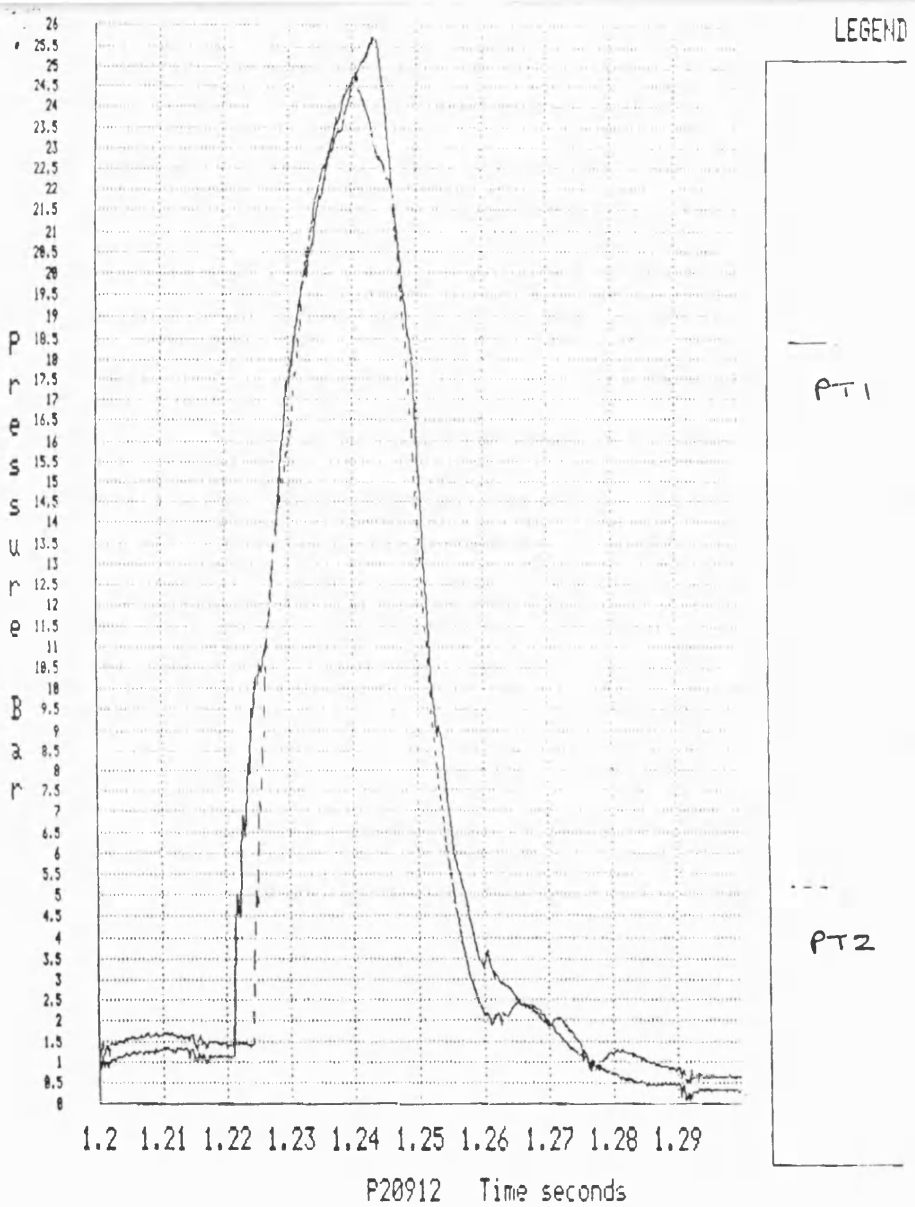

FIGURE 10.24

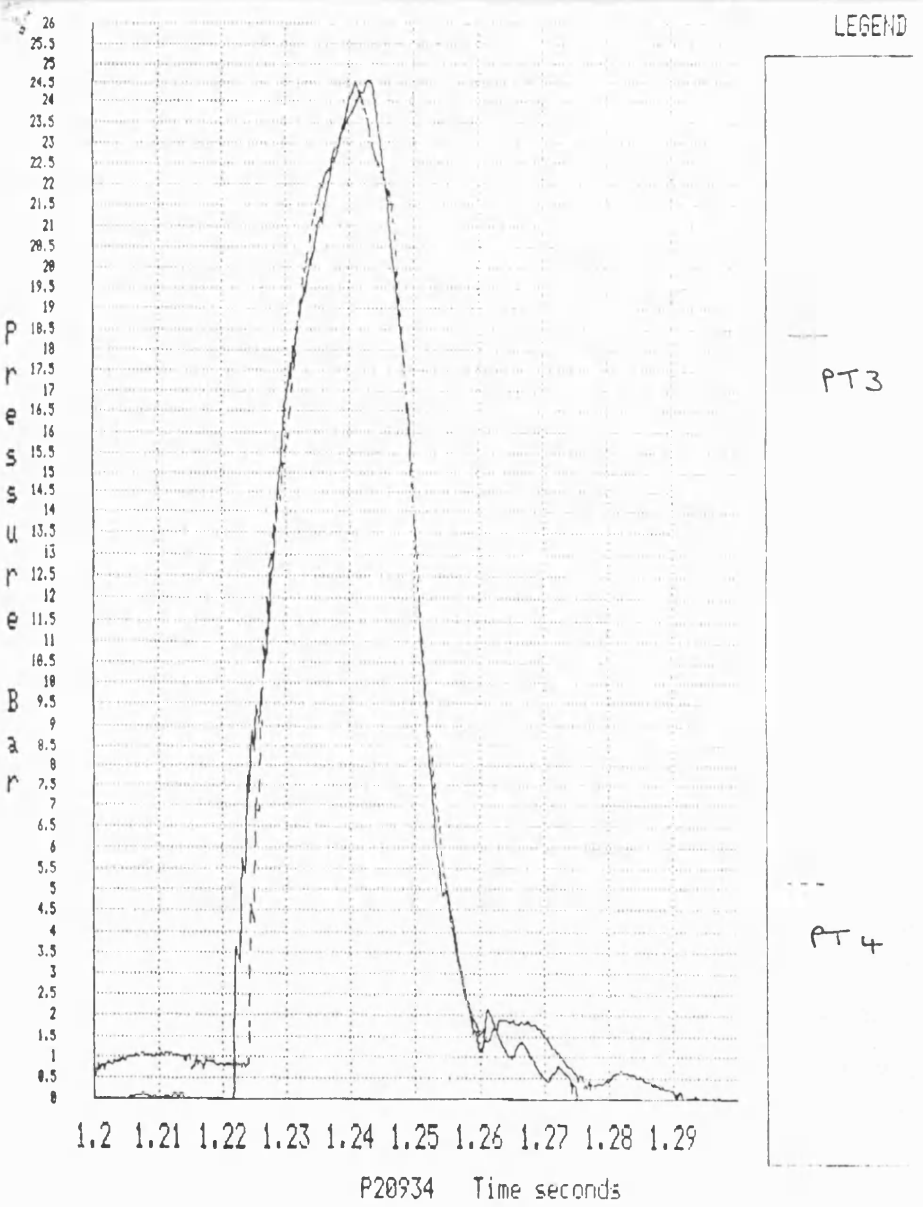

FIGURE 10.25

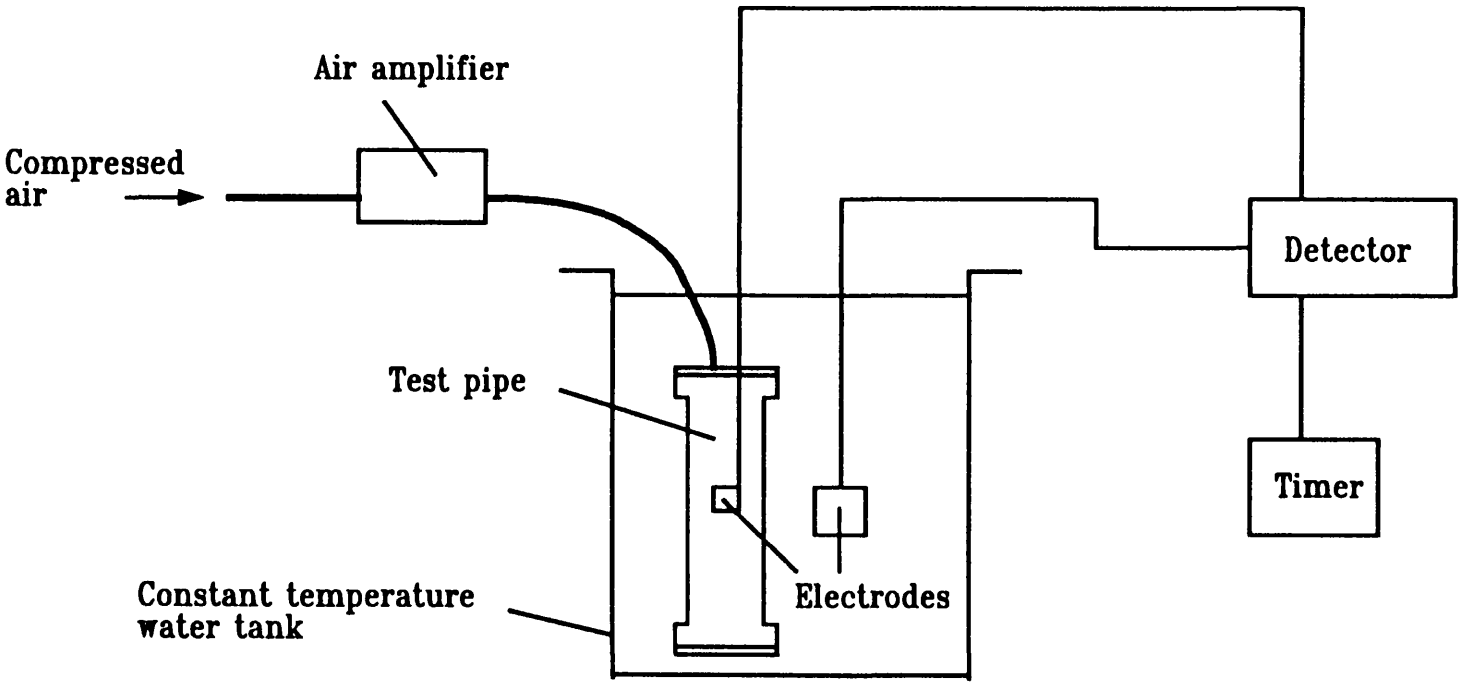

FIGURE 10.26 PIPE STRESS-RUPTURE APPARATUS.

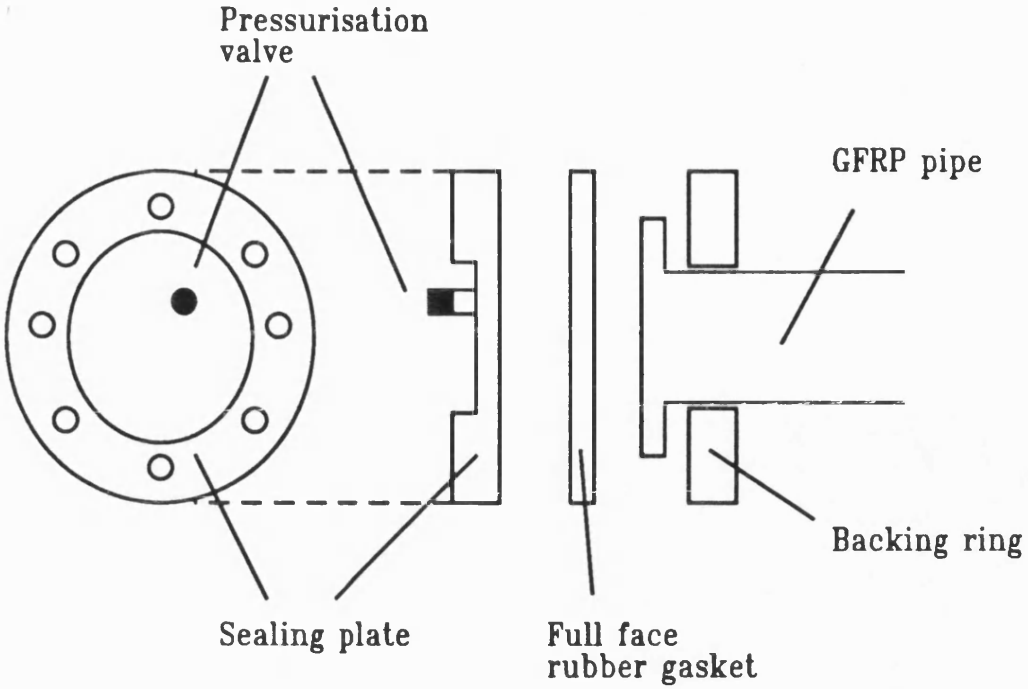
Pressurisation valve
GFRP pipe
Backing ring
Sealing plate
Full face rubber gasket

FIGURE 10.27

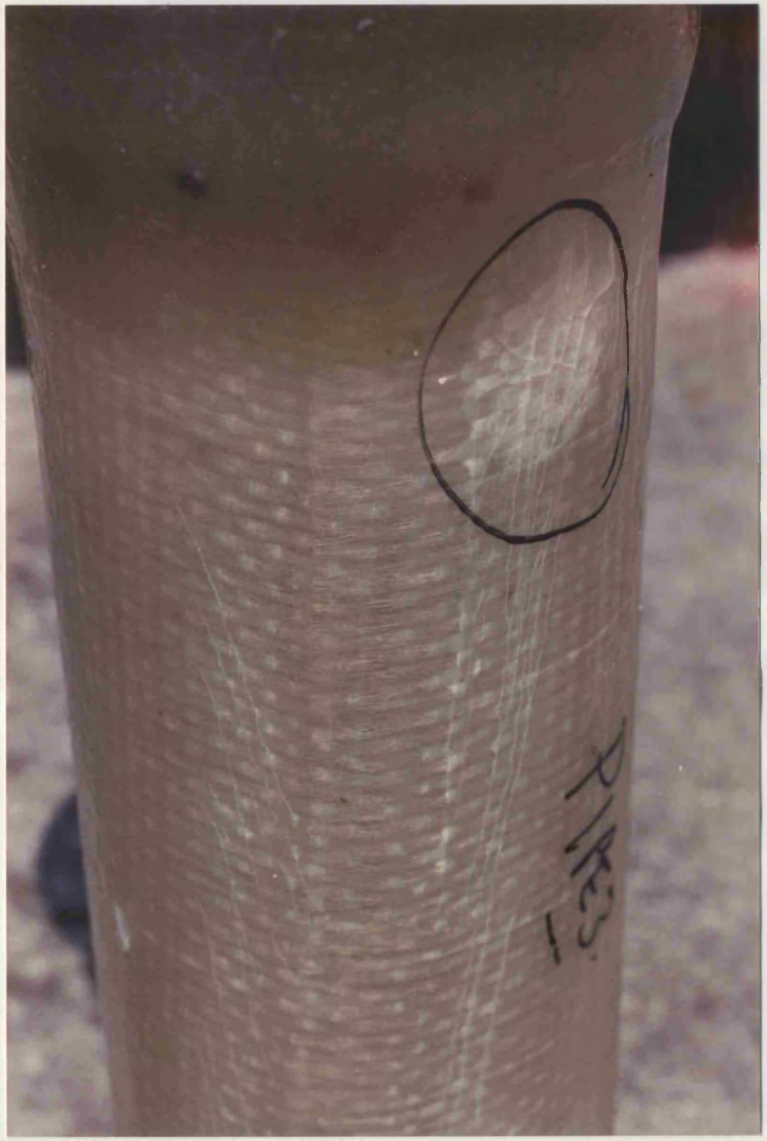

FIGURE 11.1

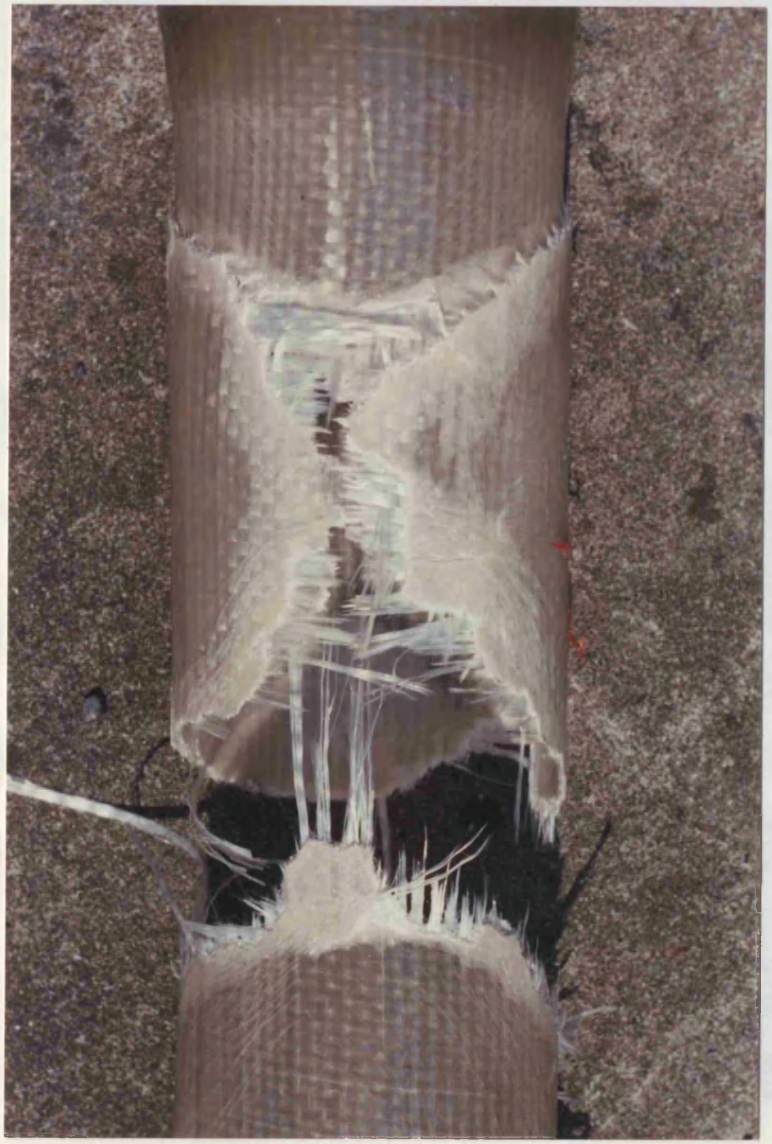

FIGURE 11.2

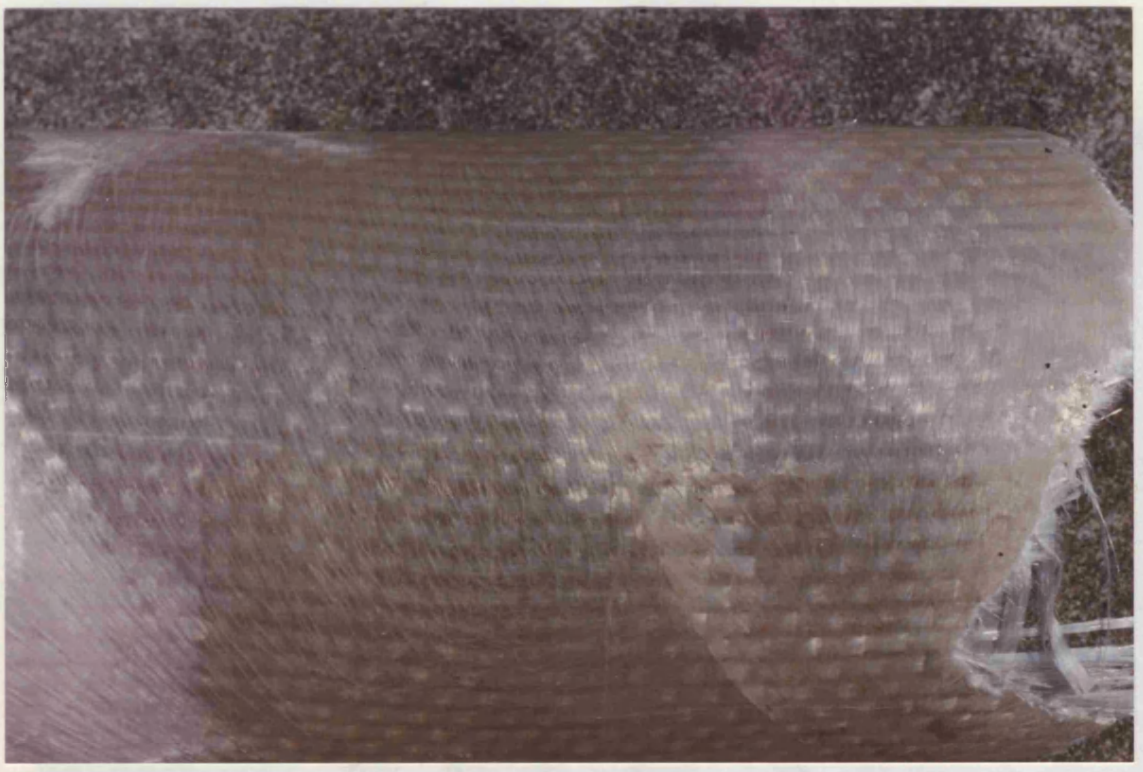

FIGURE 11.3

Longitudinal axis of pipe ⟶

Band of axial debonding/resin cracking.

FIGURE 11.4

FIGURE 11.5

FIGURE 11.6

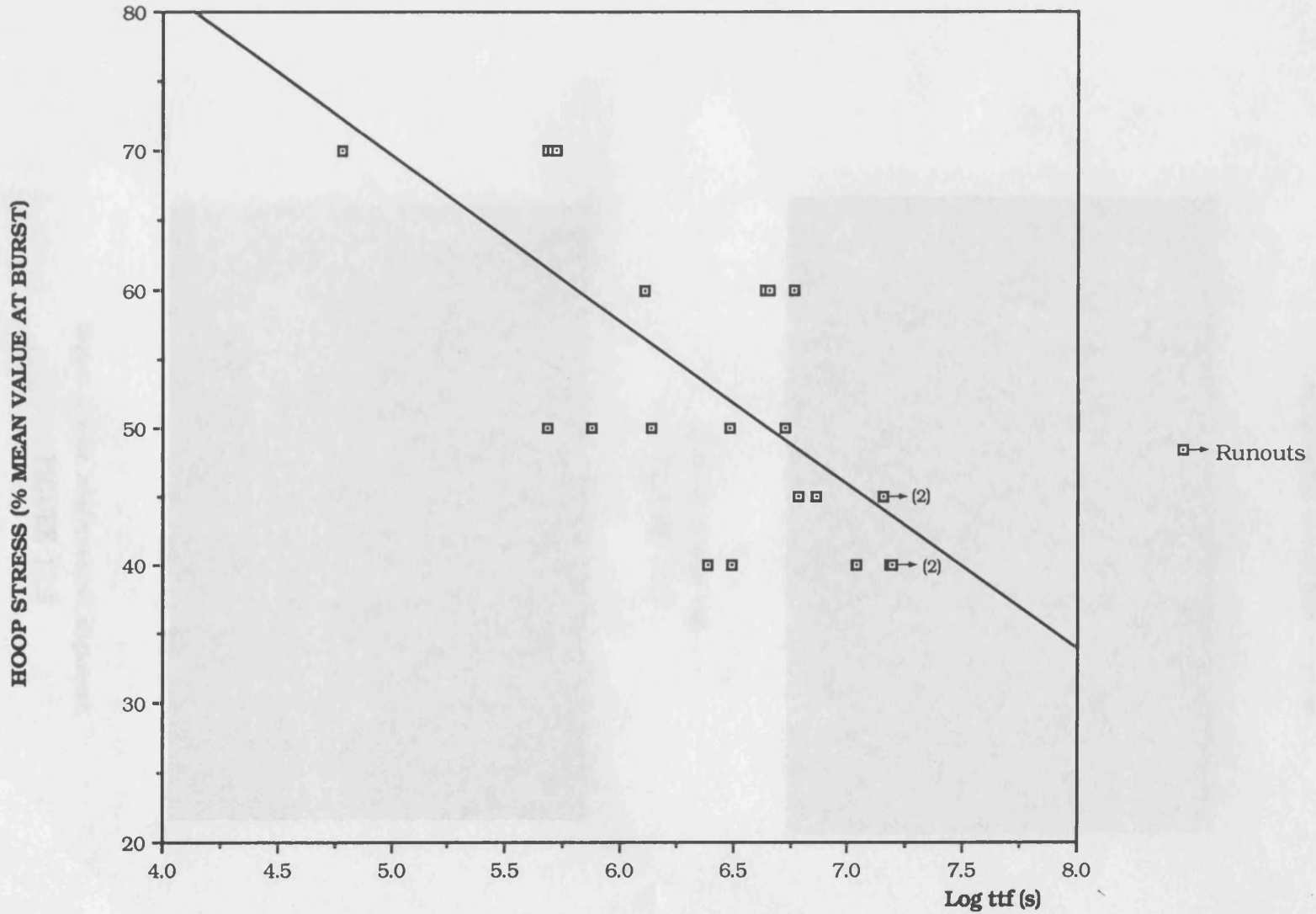

FIGURE 11.7 VIRGIN PIPE STRESS-RUPTURE DATA.

Longitudinal axis of pipe ⟶

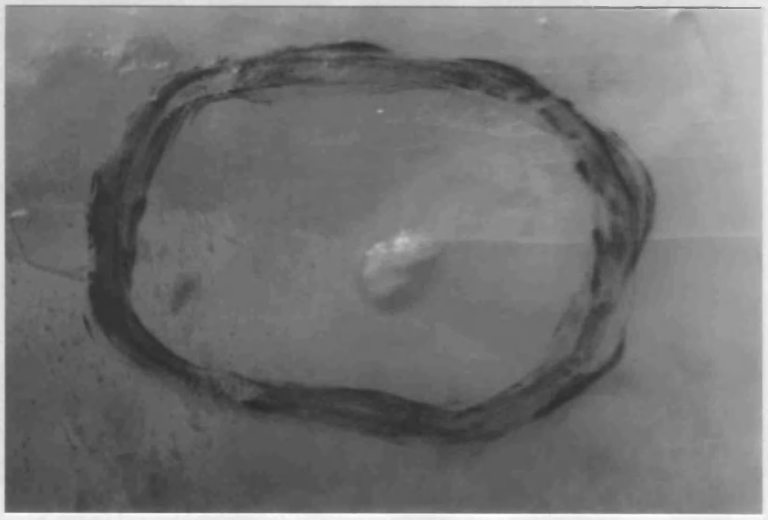

Inclusion in pipe wall

FIGURE 11.8

Region of poor reinforcement alignment.

FIGURE 11.9

Longitudinal axis of pipe ⟶

Point of leakage in a failed virgin pipe.

FIGURE 11.10

Longitudinal axis of pipe ⟶

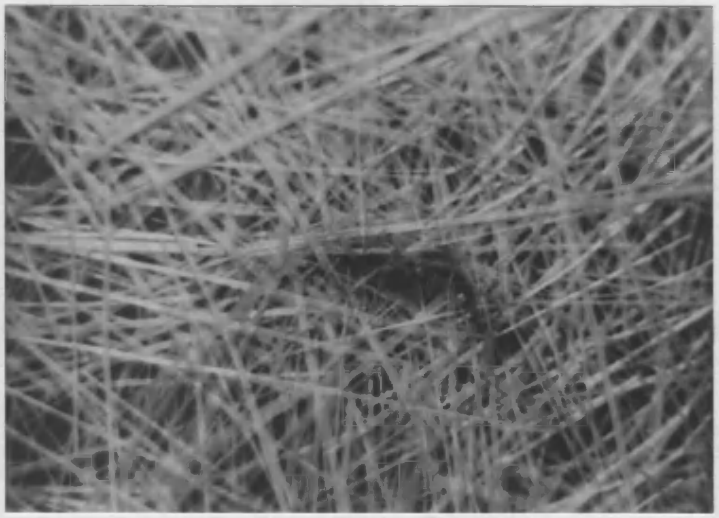

Region of fibre fractures in CSM at point of leakage (virgin pipe).

FIGURE 11.11

Longitudinal axis of pipe ⟶

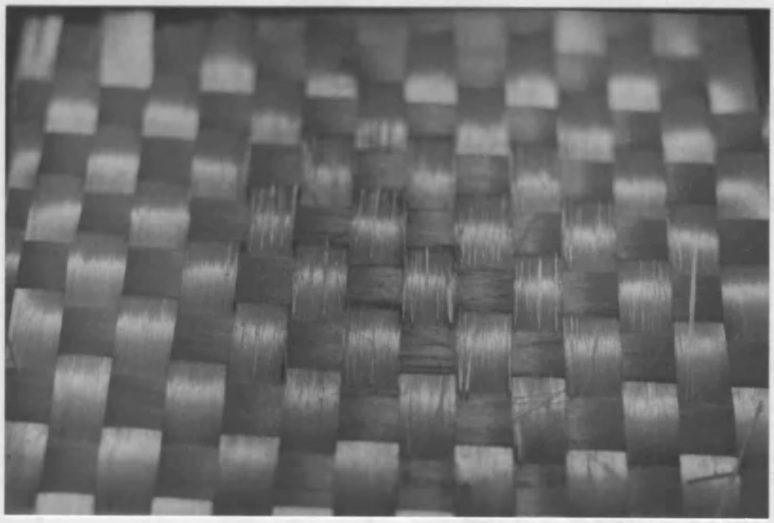

Zone of fibre fractures on outer pipe wall side of WR cloth (virgin pipe).

FIGURE 11.12

Longitudinal axis of pipe ⟶

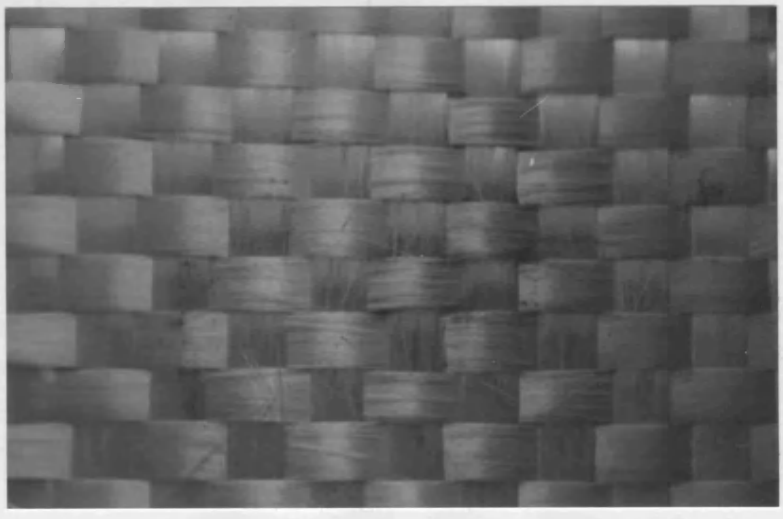

Zone of fibre fractures on inner pipe wall side of WR cloth (virgin pipe).

FIGURE 11.13

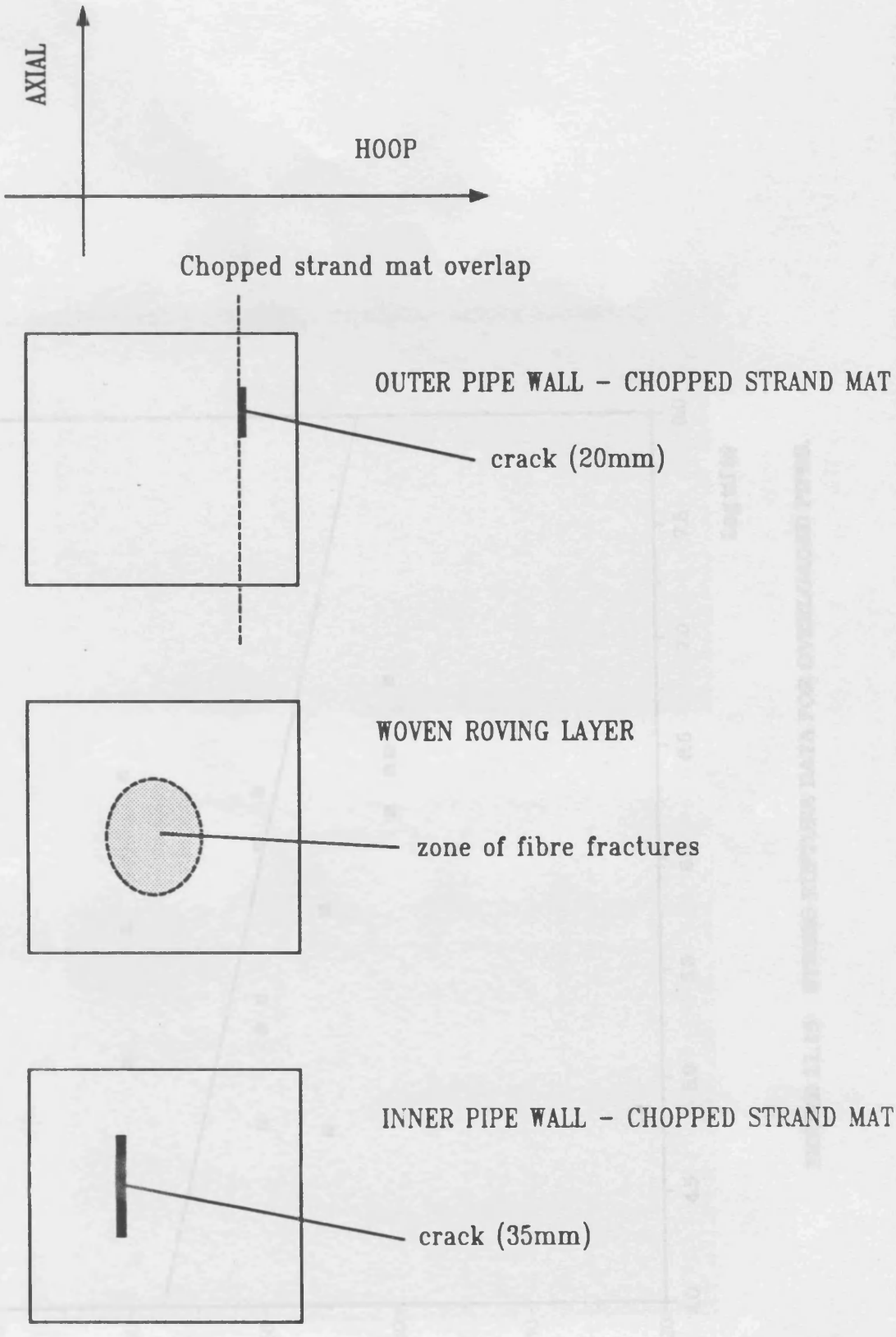

FIGURE 11.14 SCHEMATIC OF REINFORCEMENT DAMAGE AT POINT OF LEAKAGE IN VIRGIN PIPE WALL.

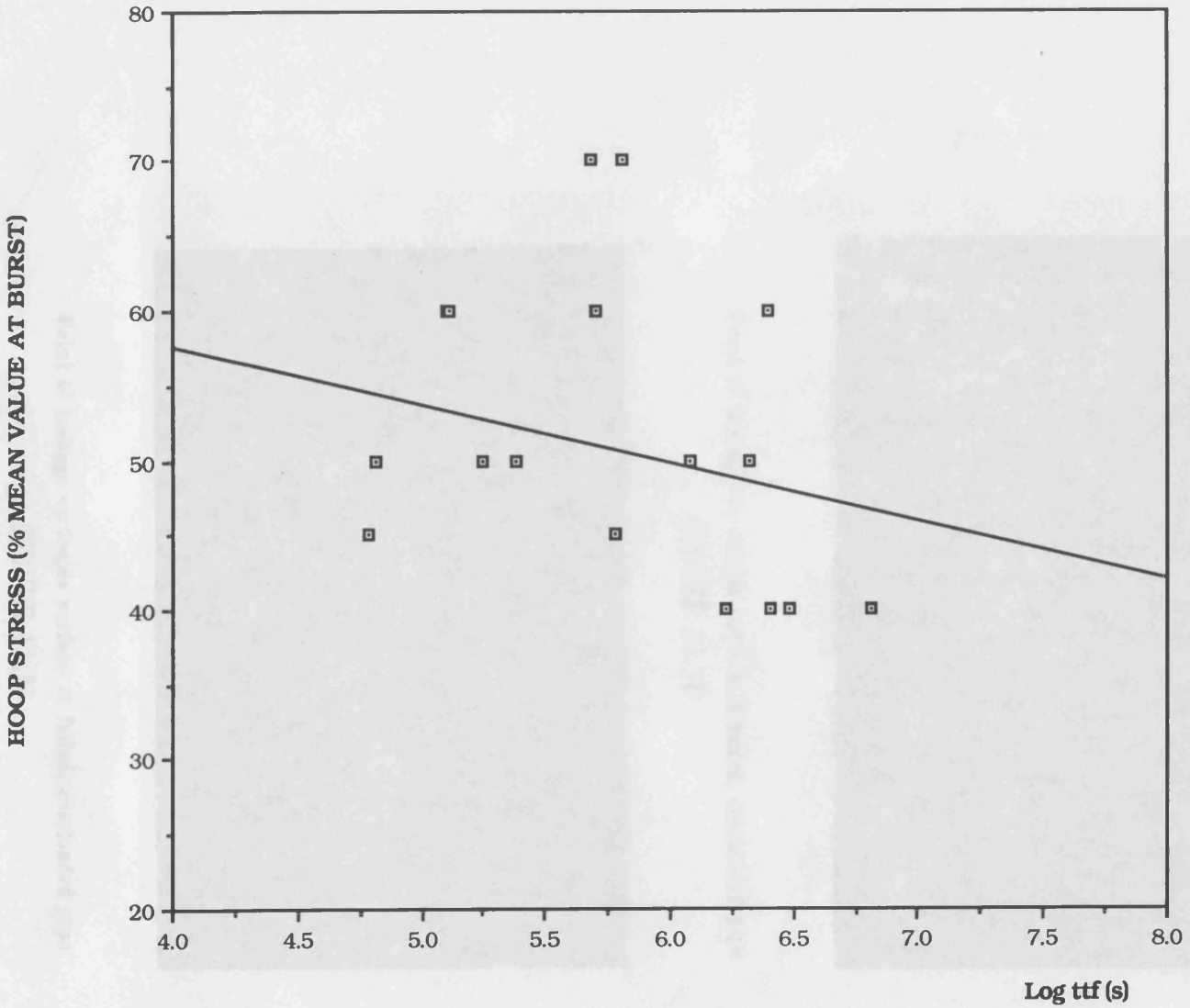

FIGURE 11.15 STRESS-RUPTURE DATA FOR OVERLOADED PIPES.

Longitudinal axis of pipe ⟶

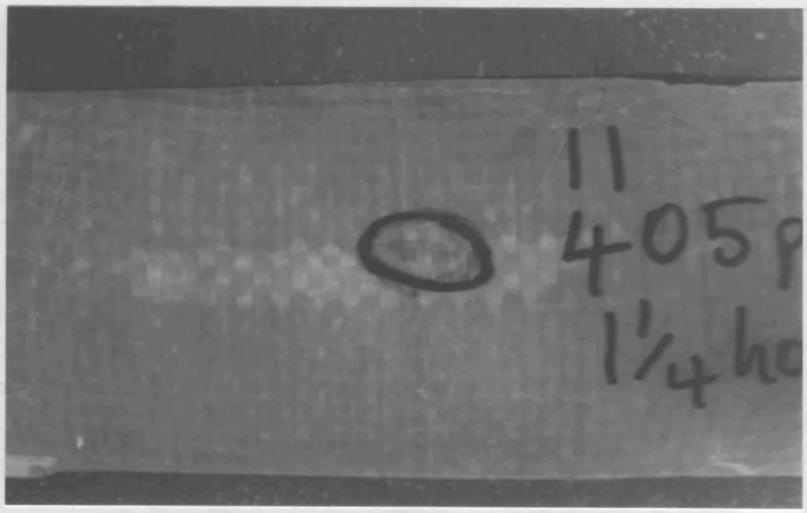

Point of leakage on outside surface of failed, overloaded pipe

FIGURE 11.16

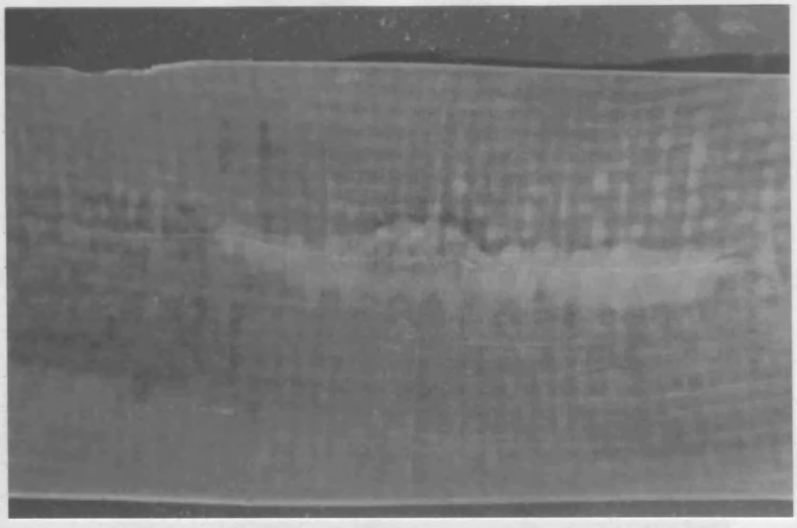

Point of leakage on inside surface of failed, overloaded pipe

FIGURE 11.17

Longitudinal axis of pipe ⟶

FIGURE 11.18

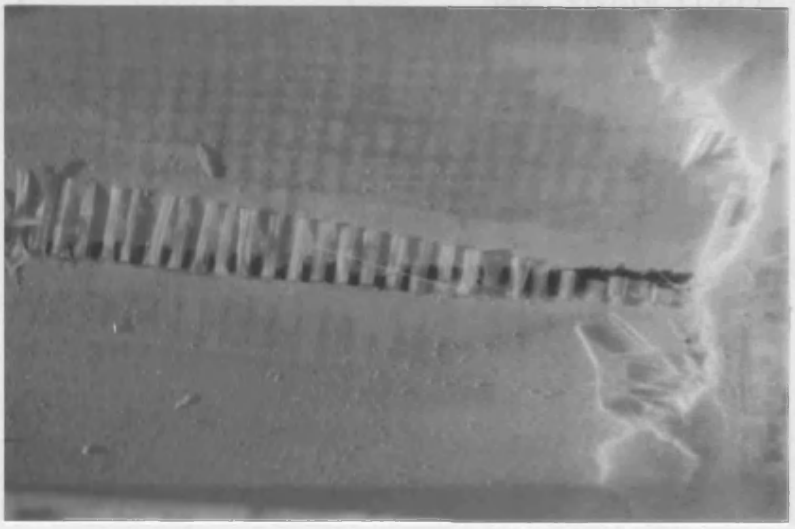

FIGURE 11.19

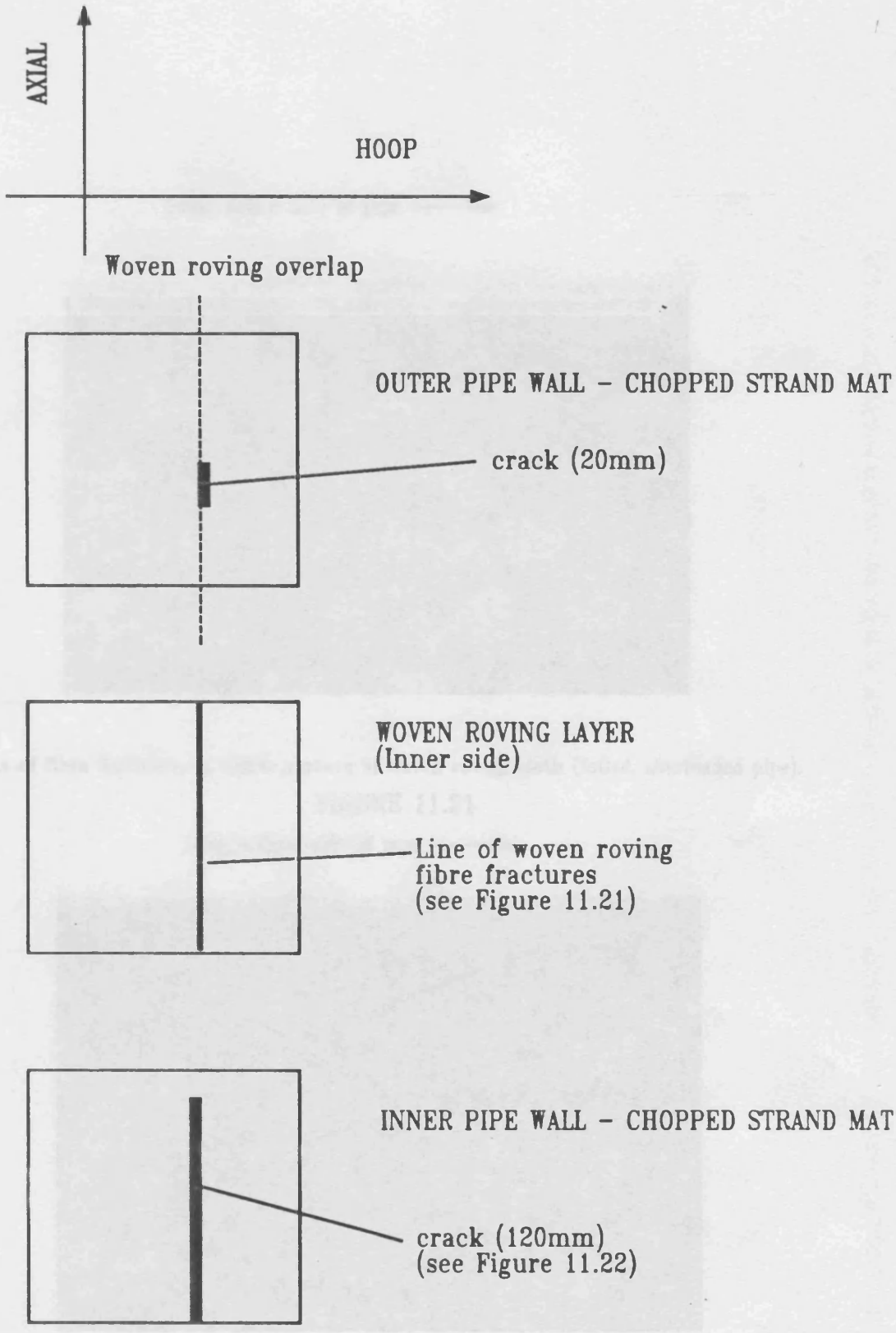

FIGURE 11.20 SCHEMATIC OF REINFORCEMENT DAMAGE AT POINT OF LEAKAGE IN OVERLOADED PIPE WALL.

Longitudinal axis of pipe ⟶

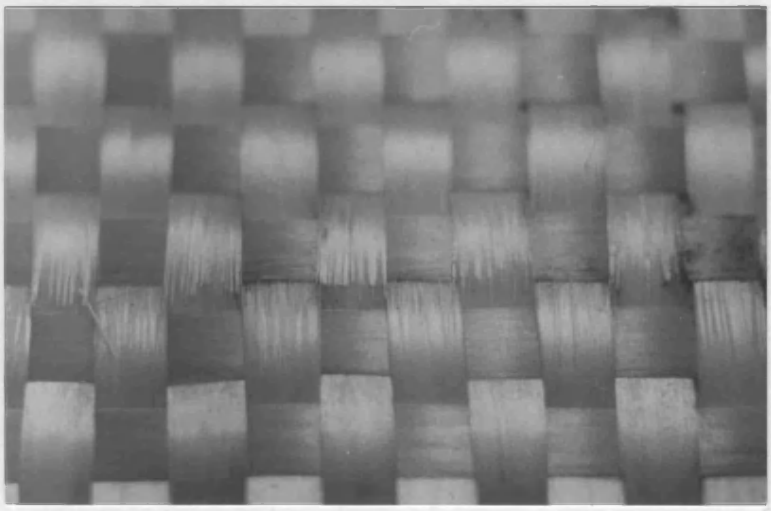

Line of fibre fractures on inside surface of woven roving cloth (failed, overloaded pipe).

FIGURE 11.21

Longitudinal axis of pipe ⟶

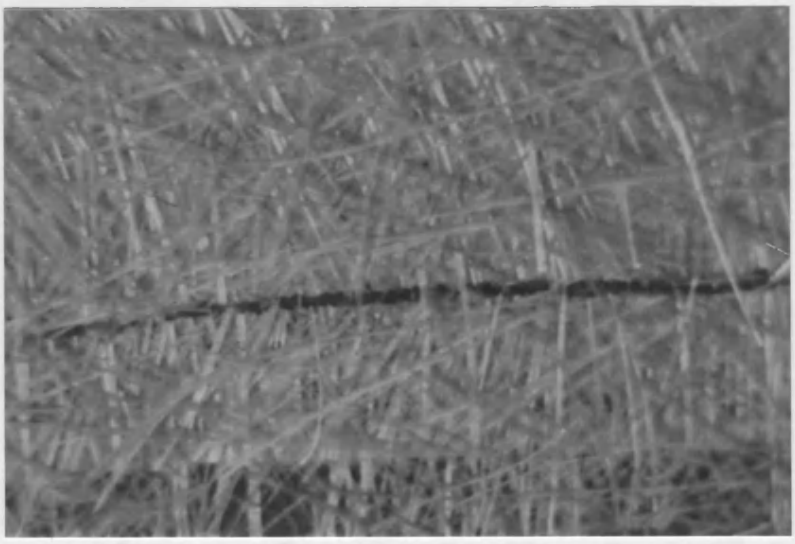

Fibre fractures in CSM in line with water hammer induced resin crack.

FIGURE 11.22

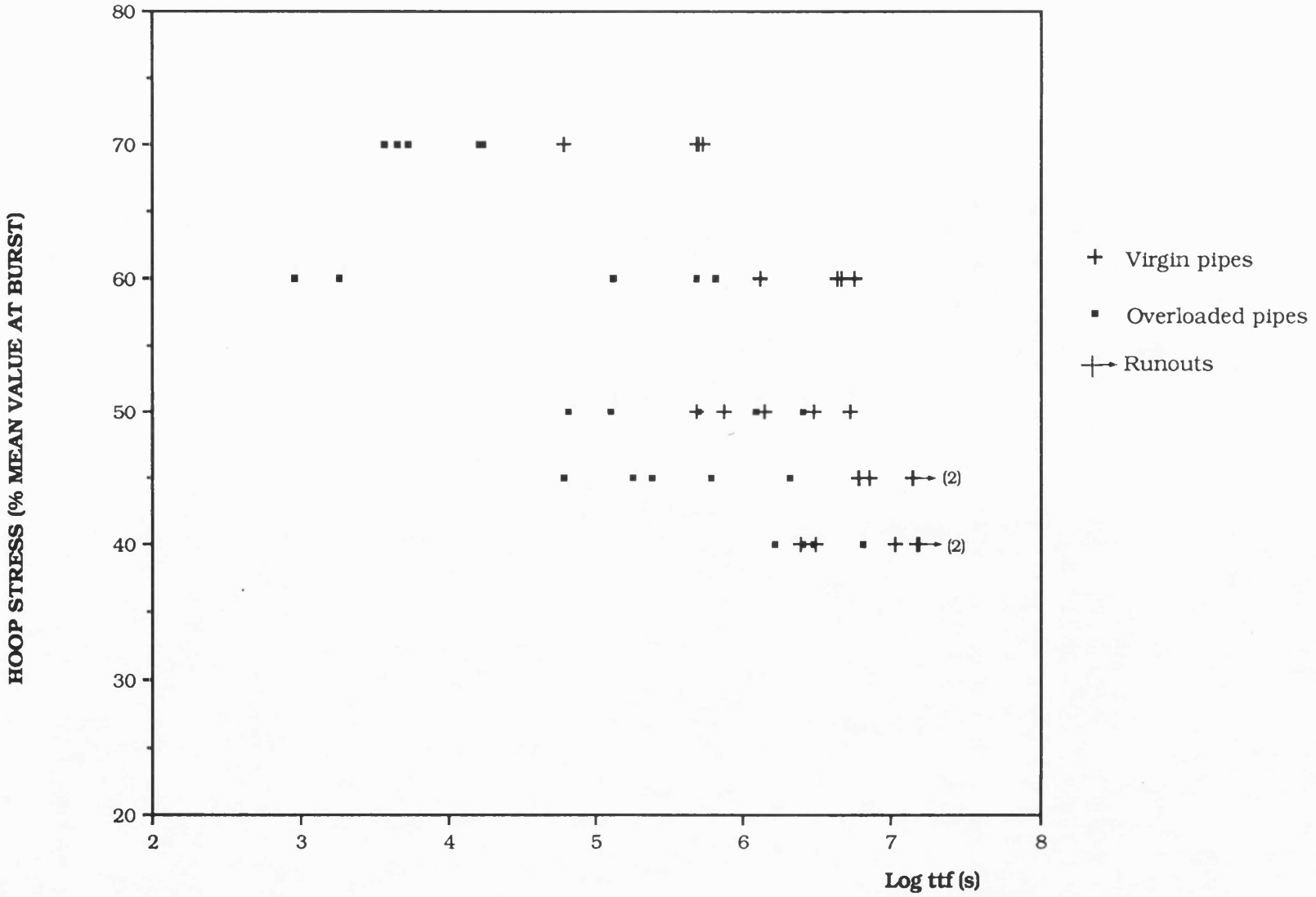

FIGURE 12.1 COMPARISON OF STRESS-RUPTURE DATA FOR VIRGIN AND OVERLOADED POLYESTER PIPES.

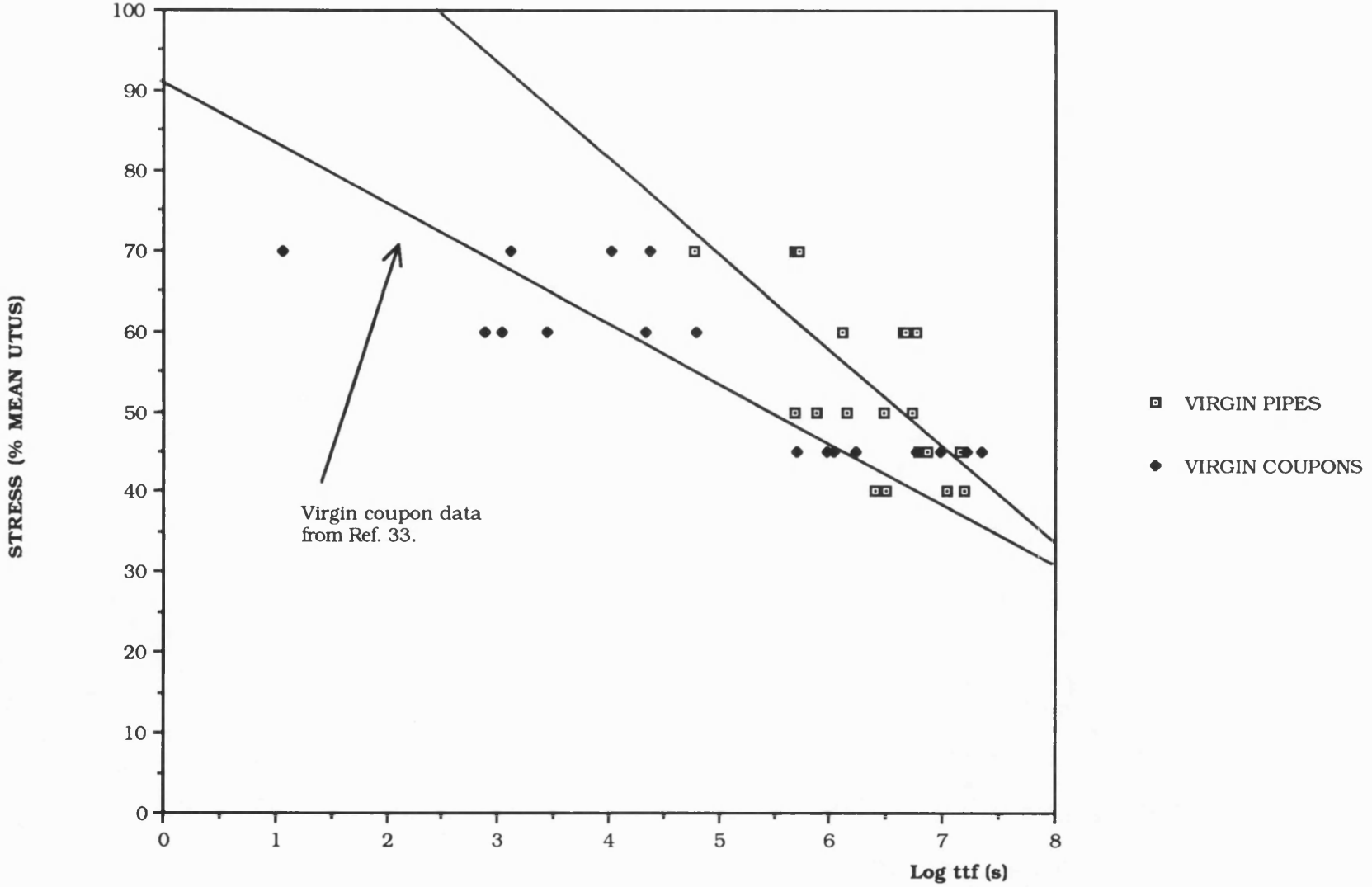

FIGURE 13.1 COMPARISON OF VIRGIN POLYESTER PIPE AND COUPON STRESS-RUPTURE DATA.

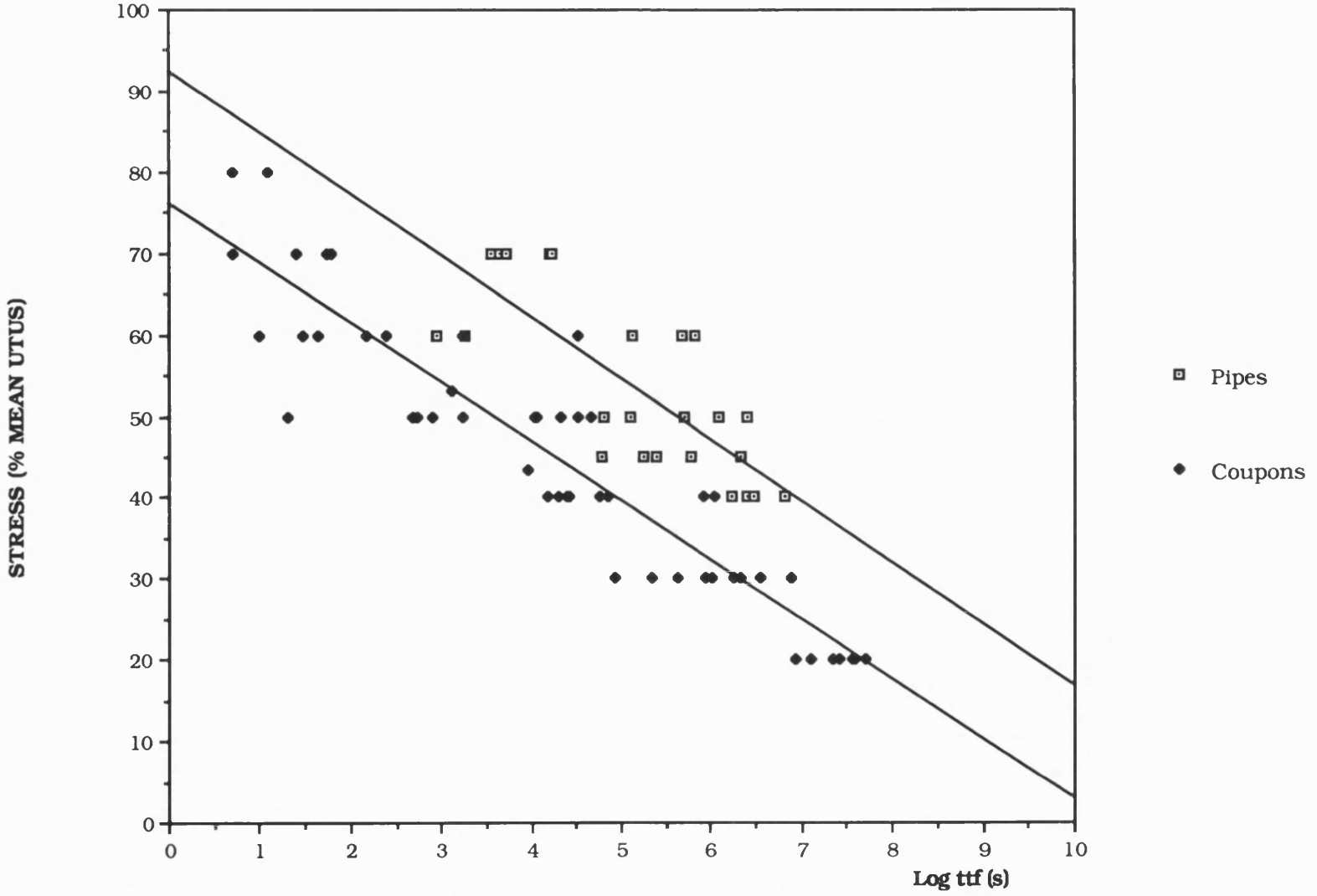

FIGURE 13.2 COMPARISON OF OVERLOADED PIPE AND COUPON STRESS-RUPTURE DATA

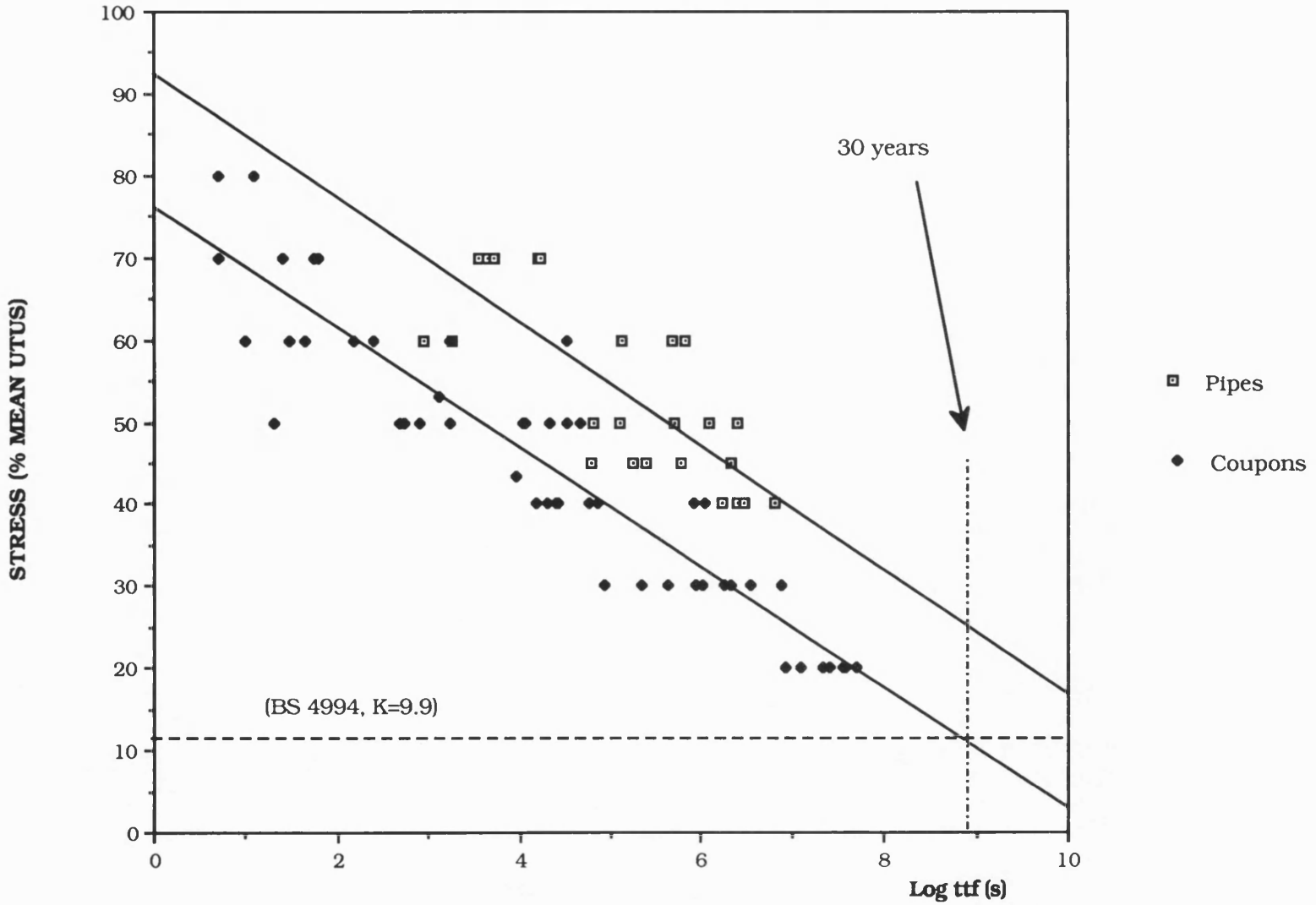

FIGURE 14.1 RELATIONSHIP BETWEEN OVERLOADED COUPON STRESS-RUPTURE DATA, OVERLOADED PIPE STRESS-RUPTURE DATA, BS 4994 AND DESIGN LIFETIME OF A COMPONENT.

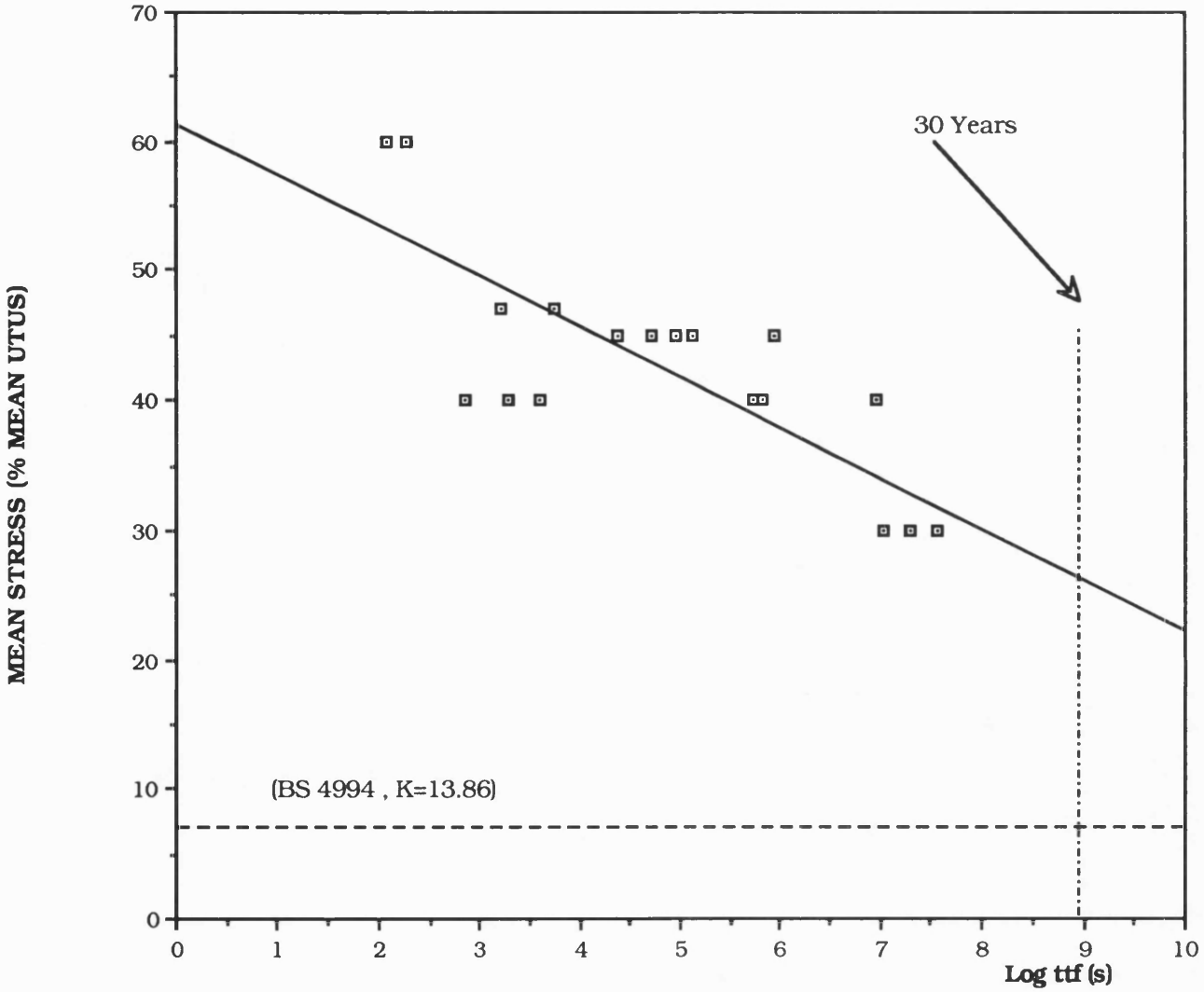

FIGURE 14.2 COMPARISON OF DYNAMIC FATIGUE DATA FOR OVERLOADED POLYESTER COUPONS WITH DESIGN FACTOR FROM BS 4994.

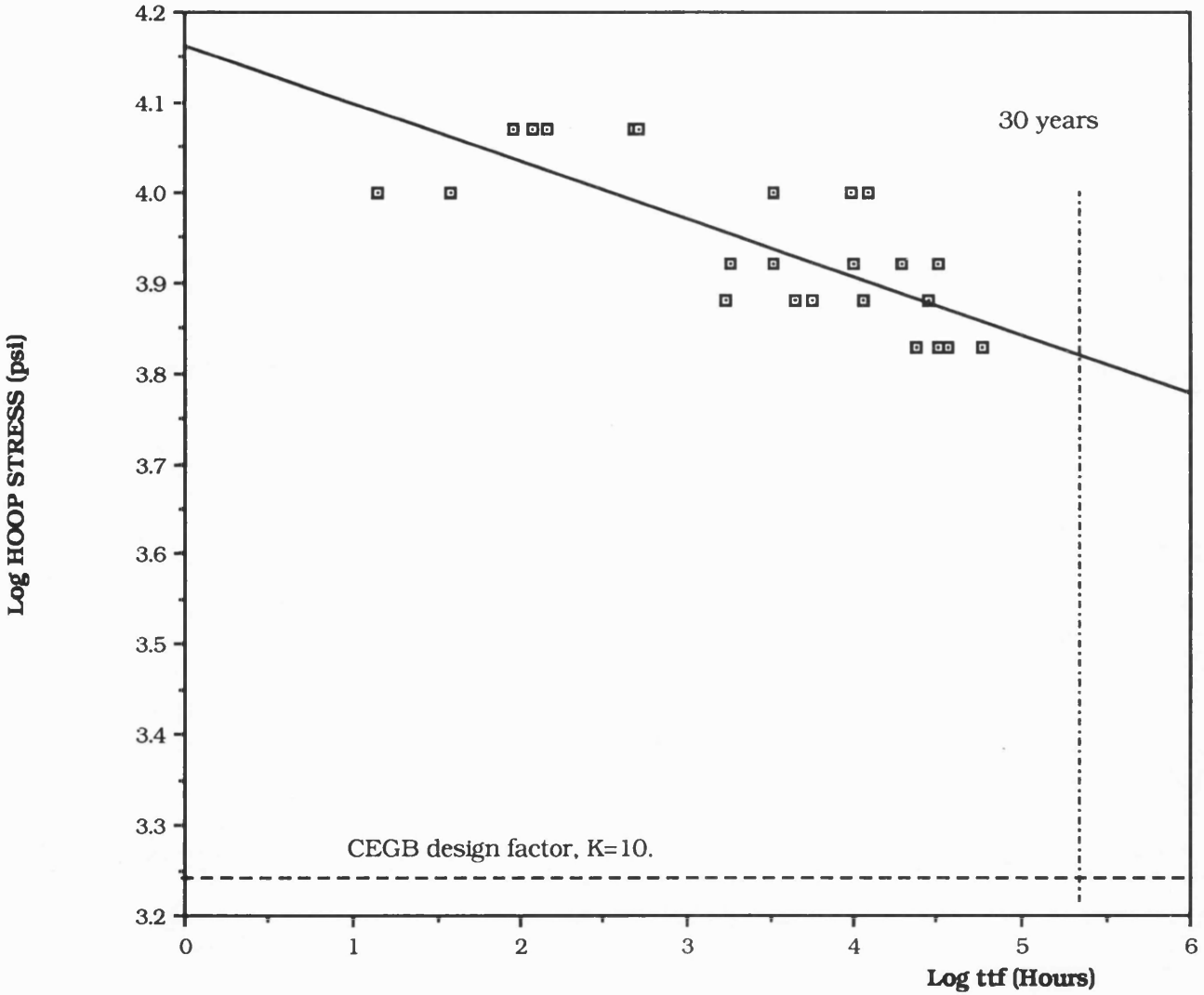

FIGURE 14.3 PLOT OF OVERLOADED PIPE STRESS-RUPTURE DATA IN ACCORDANCE WITH ASTM D-2992.

APPENDIX A.

BASIC EQUATIONS OF WATER HAMMER.

Momentum equation.

Consider a fluid flowing in a frictionless pipe of cross-sectional area, A, initially with a flow velocity of V_o m/s. After sudden valve closure and the passage of a pressure pulse of absolute velocity $(a-V_o)$ m/s the fluid velocity will have changed by δV m/s. The volume subject to this velocity change in one second will be $A(a-V_o)$ m^3, henceforth known as the "control volume". Figure A1 illustrates this concept. The resultant force acting on this control volume is equal to the change in momentum of the control volume following valve closure.

Change in momentum per second = [momentum of volume $A(a-V_o)$ after passage of pressure wave] - [momentum of volume $A(a-V_o)$ before passage of pressure wave].

$$= \rho A(a-V_o)(V_o-\delta V) - \rho A(a-V_o)V_o$$

$$= \rho A(a-V_o)\delta V$$

i.e. The mass of fluid $\rho A(a-V_o)$ is having its' velocity changed by δV in one second.

The momentum change is equal to the force exerted and relates to the increase in pressure, δH, as follows;

$$\text{Impulse} = \delta Ha = \rho A(a-V_o)\delta V + \rho A(V_o+\delta V)^2 - \rho AV_o^2$$

$$\delta H = [\delta VA/g][V_o/(a-1)] \quad \text{(Equation 6)}$$

Figure A1 Diagram illustrating the application of conservation of momentum to the volume $A(a - V_o)$.

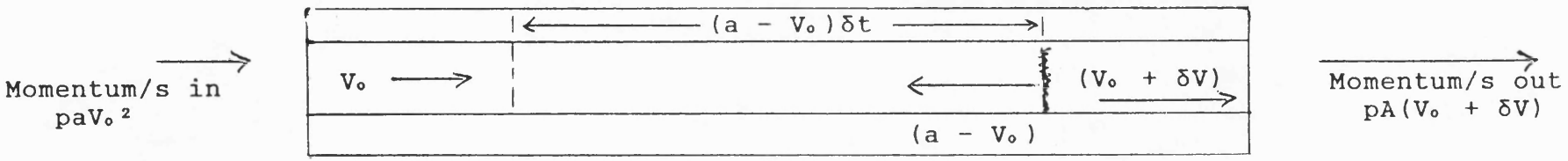

[δt = Time interval after valve closure, A = cross sectional area of pipe and p = density of fluid].

V_o is usually very small reducing equation 6 to,

$$\delta H = -\delta VA/g \qquad \text{(Equation 7)}$$

If this equation is then applied to CEGB data appropriate to fluid flow in a power station CW system a value for δH can be calculated.

Power station cooling water system data.

Flow velocity, V_o = 3-4 m/s.

Operating pressure, H = 3-4 bar (30.5-40.7m head).

A value of the speed of propagation of the pressure wave, a, is also required. This is dependent upon the physical properties of the fluid and the elastic properties of the pipe carrying the fluid. Additionally the method of fixation of a pipeline may affect the wavespeed.

The wavespeed, a, in a fluid, in a thin walled pipe of circular cross-section may be estimated using equation 8.

$$a = [\rho(1/K + \{D\phi/tE\})]^{-1/2} \qquad \text{(Equation 8).}$$

where; ρ = density of fluid (1000kg/m^3).

K = bulk density of fluid (2.15 GN/m^2).

D = Internal diameter of pipe (2.75m).

ϕ = a factor relating to the method of fixing and hence restraint on the pipe (taken as unity).

t = nominal thickness of pipe wall (0.1m).

E = Elastic modulus of pipe wall material (15GPa).

Using the figures in brackets a value of 660 m/s is calculated. Substituting this value into equation 7, and assuming that flow is completely halted, indicates a value for δH of 268m ($\approx$26.3 bar).

N.B. Operating pressure = 4bar ($\approx$40.7 bar).

APPENDIX B.

TEST PIPE DESIGN CALCULATIONS.

Specification.

Operating pressure = 3-4 bar.

Burst strength = 10 times operating pressure.

Internal diameter, D_i = 151mm.

Reinforcement: mixed wall construction, alternate layers of chopped strand mat (CSM) and woven roving (WR).

Applying equation 6 (see page 108) from BS 4994 requires the calculation of Q_m, the maximum circumferential load. This is dependent upon the minimum ultimate tensile strength for the reinforcement, designated by BS4994 to be 200 and 250 N/mm per kg/m^2 for CSM and WR respectively.

Selected reinforcement geometry and densities.

CSM------ 0.3 kg/m^2.

WR------ 0.8 kg/m^2.

CSM------ 0.3 kg/m^2.

$$Q_m = 2[200\{0.3\}] = [0.8\{250\}]$$

$$= 320 \text{ N/mm}.$$

$$Q_m = PD_i/2$$

Therefore the pipe pressure rating , P = 42.4 bar.

Applying the CEGB design factor of 0.1 results in a pipe operating pressure of 4.24 bar.

APPENDIX C.

Summary ot t-test calculations.

In the comparisons between the overloaded and virgin pipe stress-rupture data the data groups at the 40% and 50% mean hoop stress at burst stress levels overlapped. Was there a significant difference in the means of the two sets of data?

40% Mean hoop stress at burst.

		$\log_{10}$ time to failure (s)				
VIRGIN PIPES	(n_1)	6.39	6.49	7.03	7.17	7.17
OVERLOADED PIPES	(n_2)	6.22	6.22	6.41	6.48	6.81

	VIRGIN PIPES	OVERLOADED PIPES
Σx_i	34.25	32.14
$\Sigma (x_i)^2$	235.19	206.83
$\Sigma (x_i)^2 - (\Sigma x_i)^2/5$	0.578	0.234

Hence

$\bar{X}_1 = 6.85$ $\bar{X}_2 = 6.428$

$(S_1)^2 = 0.578/4 = 0.1445$ $\therefore S_1 = 0.380$

$(S_2)^2 = 0.234/4 = 0.0585$ $\therefore S_2 = 0.242$

The combined estimate of variance is given by;

$S^2 = \{(S_1)^2 + (S_2)^2\}/2 = 0.1015$ $\therefore S = 0.3186$

If the true means of the two data groups are given by μ_1 and μ_2, the null hypothesis is given by $H_o: \mu_1 = \mu_2$, and the alternative hypothesis is given by $H_1: \mu_1 \neq \mu_2$. Thus a two tailed test is appropriate.

The test statistic is given by, $t_o = \dfrac{\bar{x}_1 - \bar{x}_2}{s\sqrt{(1/n_1 + 1/n_2)}} = 2.094$

If H_o is true then the sampling distribution of t will be a t-distribution with eight degrees of freedom, as the estimate of s is based on eight degrees of freedom.

From t-tables (see Chatfield[87]) we find $t_{0.05,8} = 1.86$ so that probability $(|t|>1.86) = 0.10$

Thus the difference in the means of the two data sets is significant at the 10% level.

50% Mean hoop stress at burst.

		$\log_{10}$ time to failure (s)				
VIRGIN PIPES	(n_1)	5.68	5.87	6.14	6.48	6.72
OVERLOADED PIPES	(n_2)	4.81	6.40	5.10	6.08	5.70

	VIRGIN PIPES	OVERLOADED PIPES
Σx_i	30.89	28.09
$\Sigma (x_i)^2$	191.57	159.56
$\Sigma (x_i)^2 - (\Sigma x_i)^2/5$	0.73	1.75

Hence

$\bar{X}_1=6.18$ $\bar{X}_2=5.62$

$(S_1)^2 = 0.73/4 = 0.183$ $\therefore S_1=0.428$

$(S_2)^2 = 1.75/4 = 0.438$ $\therefore S_2=0.662$

The combined estimate of variance is given by;

$S^2 = \{(S_1)^2 + (S_2)^2\}/2 = 0.3105$ $\therefore S=0.557$

If the true means of the two data groups are given by μ_1 and μ_2, the null hypothesis is given by $H_o:\mu_1=\mu_2$, and the alternative hypothesis is given by $H_1:\mu_1\neq\mu_2$. Thus a two tailed test is appropriate.

The test statistic is given by, $t_o = \dfrac{\bar{x}_1 - \bar{x}_2}{s\sqrt{(1/n_1 + 1/n_2)}} = 1.59$

If H_o is true then the sampling distribution of t will be a t-distribution with eight degrees of freedom, as the estimate of s is based on eight degrees of freedom.

From t-tables (see Chatfield[87]) we find $t_{0.10,8} = 1.397$ so that probability $(|t|>1.86 = 0.20$

Thus the difference in the means of the two data sets is significant at the 20% level.